Fine structure of the HIV-1 glycan shield

by

Anna-Janina Behrens

Glycobiology Institute, Department of Biochemistry
Corpus Christi College, University of Oxford

A thesis submitted for the degree of *Doctor of Philosophy*
Hilary term 2017

Supervised by
Dr Max Crispin and Prof. Nicole Zitzmann

Declaration

The work presented in this thesis was undertaken in Dr Max Crispin's laboratory at the Oxford Glycobiology Institute, Department of Biochemistry, University of Oxford between 2014 and 2017. I, Anna-Janina Behrens, hereby declare that all the work presented is my own with the following exceptions. Recombinant proteins were provided by a number of different laboratories as listed in Table 2.1. Pseudovirus neutralization experiments in Chapter 4 were performed by Katie Doores' laboratory (King's College London, UK). MALDI-TOF mass spectrometry experiments were performed at Ludger Ltd. (Oxford, UK) with the help of Dr Daniel Spencer. Orbitrap QE LC-ESI mass spectrometry experiments were performed with the help of Dr Abhinav Kumar (University of Oxford). Ion mobility mass spectrometry experiments were performed with the help of Prof. David Harvey (University of Oxford). This work has not been submitted for any other degree at this university or any other institute of learning. The introduction of this thesis is based on my first-author book chapter 'Targeting glycans of HIV Envelope glycoproteins for vaccine design' in 'Chemical biology of glycoproteins' (Appendix G). Furthermore, this thesis includes text excerpts and figures of my first-author articles published throughout my DPhil as listed in Appendix G. Where required, permission from individual journals was obtained.

Acknowledgements

I am deeply grateful to a large number of people who have helped and supported me throughout my DPhil. Firstly, I would like to thank Dr Max Crispin for welcoming me into his laboratory and providing me with the opportunity to work on this interesting project. I greatly appreciate his continuous support, guidance, passion for glycans and confidence in me that has helped me to become the independent scientist I am today. I would also like to thank Corpus Christi College for supporting my thesis with the Chris Scanlan Memorial Scholarship. It is an honor to work in the memory of such an excellent scientist.

Special thanks to Prof. Raymond Dwek, who always lends an ear and has an endless repertoire of advice and interesting stories to tell. I would also like to thank Prof. Nicole Zitzmann for the co-supervision of my thesis. I enjoyed working in the supportive environment of the Glycobiology Institute very much. Especially, I would like to thank all members of our lab – past and present – for creating a pleasant working atmosphere (Gemma, Snezana, Iona, Lan, Kirstin, Joel, Yasa, and Mia). In particular, I would like to mention Laura for her indispensable help in getting started with this project and sharing her vast knowledge about HIV-1 glycans and glycoanalytics; Prof. David Harvey for being the most patient ion mobility mass spectrometry teacher with an inimitable expertise on glycan fragmentation and also Dr Weston Struwe for all his mass spectrometry support and advice. Alex, thanks for making our (too) short (a) time in the lab last year a very special one.

Furthermore, I am grateful to the people at Ludger Ltd., especially Dr Daniel Spencer, who helped me to perform initial site-analysis experiments and whose input was crucial in getting started with all this. Many thanks to Dr Holger Kramer and Dr Abhinav Kumar for their expertise and their help with performing mass spectrometry experiments. I would like to thank all our collaborators, in particular Prof. John Moore, Dr Katie Doores, Prof. Rogier Sanders, and Dr Anita Sarkar for many joint projects and helpful discussions.

There are many people outside work who have made my time in Oxford very special. My current and former flat mates and the whole flat dinner team, I won't forget our uncountable cooking evenings. Loic, thanks for being a very good friend and wonderful training partner in every imaginable type of sport. Anna and Kim, I can't put into words how happy I am about all the time we spent together and all the things we share(d). I also need to thank all my friends I found during school and university in Peine, Lübeck, and Münster. Despite the distance, our friendships have lasted and I am convinced they will continue to do so long into the future.

Finally, I couldn't have done this without the support of my family, who have always been there for me. Mama, thanks for being as caring and worrying as a mother should be, and Papa, thanks for the boxes full of postcards over the last decade. Eike, sometimes I don't understand how, but I am extremely happy that we managed to overcome 1000 km apart. Thanks for sticking with me, I can't wait for the next chapter to start.

Abstract

The HIV-1 envelope glycoprotein trimer (Env) is covered by an extensive array of glycans that shield it from immune surveillance. The high density of glycans on the trimer surface imposes steric constraints that limit the actions of glycan processing enzymes, such that multiple under-processed structures remain on specific locations. These oligomannose-type glycans are recognized by broadly neutralizing antibodies (bNAbs) that are not thwarted by the glycan shield but, perhaps paradoxically, target it. In multiple studies, bNAbs have been shown to be capable of providing passive protection from viral challenge, making Env a focus of antibody-mediated vaccine design.

Here, the development of a workflow for the semi-quantitative, site-specific N-glycosylation analysis of a soluble recombinant, native-like trimer mimic (BG505 SOSIP.664) is reported. The resulting data reveal a mosaic of dense clusters on the outer domain of Env and allow mapping the extremes of simplicity and diversity of glycan processing. Although individual sites usually minimally affect the global integrity of the glycan shield, examples are identified of how deleting certain glycans can subtly influence neutralization by bNAbs that bind at distant sites.

Env is a trimer of heterodimers of gp120 and gp41, which is generated by cleavage of an endogenous protease. In this thesis, the detailed effect of protease cleavage on glycan processing is examined by comparing the site-specific N-glycosylation profiles of the native-like trimer mimic to the corresponding uncleaved pseudotrimer and the matched gp120 monomer. Trimer-associated glycan remodeling forms a localized subdomain of the native mannose patch.

Furthermore, the glycosylation analysis of further Env immunogens – a glycan-depleted trimer and a flexibly-linked, uncleaved trimer (both based on BG505 SOSIP.664) – provides important insights into the robustness of the HIV-1 glycan shield and the Env maturation pathway. Overall, this thesis reveals how structural constraints shape Env glycosylation and the network of bNAb-targeted glycans that should be preserved on recombinant vaccine candidates.

Table of contents

1 Introduction

1.1 The Human immunodeficiency virus

The human immunodeficiency virus (HIV) causes acquired immunodeficiency syndrome (AIDS) and remains one of the major health challenges worldwide. It is estimated that 37 million people were living with HIV in 2015, most of them in sub-Saharan Africa [1]. Incidents of infection, however, are continuously growing in Eastern Europe and Central Asia. Although there have been huge developments in antiviral therapy, a vaccine is likely to be an essential component in the control of the epidemic [2].

HIV research began in 1981, when Michael S. Gottlieb observed and linked five clinical cases of homosexual men contracting a rare lung infection (*Pneumocystis carinii* pneumonia) in Los Angeles [3]. In June 1981, the Center for Disease Control and Prevention (CDC) in Atlanta published the first public report of clinical observations of what would later be known as AIDS [4]. Since then, over 35 years of intense HIV research have led to an increasing understanding of the virus and significant advances in the development of an effective treatment. What was once a lethal infection, has been described as a 'manageable chronic disease' [5]. UNAIDS states that in 2015 more than 17 million people were receiving antiretroviral treatment [1]. Despite this achievement, more than half the people living with the virus still do not have access to medication, thus, there is a need for the development of an effective vaccine in order to bring the HIV/AIDS pandemic under control.

There are two distinct types of human immunodeficiency virus, HIV-1 and HIV-2, which share about 60 % amino acid sequence identity [6]. Both types originate from zoonotic (animal to human) transmission of simian immunodeficiency viruses (SIVs), and both are capable of causing AIDS [7]. HIV-2 is generally associated with a longer asymptomatic stage, lower virus titers and a lower transmission rate compared to HIV-1 [7]. Being only endemic in West Africa, HIV-2 is currently not the main focus of attention of the HIV research community. HIV-1 is classified into

four groups (M, N, O and P), all of which emerged from different zoonotic infections [8,9]. About 90 % of all HIV-1 infections are caused by infections of the 'major' group M, which is the only group that has established a pandemic spread. It comprises nine genetically distinctive clades (A, B, C, D, F, G, H, J and K), which vary in their geographical prevalence across the world. Clade A, B and C are the most prevalent genetic forms, with clade C being responsible for about half of all HIV-1 infections [8]. Clade A is common in Eastern and Central Africa as well as in Eastern Europe [8]. Clade B is the dominant form in Western and Central Europe, USA, Thailand, Australia and Japan, whereas clade C is dominant in Southern and Eastern Africa and India [8].

1.1.1 Structure, genome and viral lifecycle

HIV-1 is a single-stranded, enveloped RNA retrovirus belonging to the genus *Lentivirus* (Figure 1.1). The virus particles are 100-120 nm in diameter and contain two copies of the positive-stranded RNA genome [10]. The viral genome encodes three major gene products (gag, pol and env). All of them are translated as polyproteins, with Gag providing the structural lattice of the viral particle (the viral matrix, the capsid and the nucleocapsid) and Pol the viral enzymes (protease, reverse transcriptase and integrase). The enveloped virus is surrounded by a lipid bilayer gained while budding from the host cell. The surface transmembrane protein, envelope (Env), is embedded into this bilayer (Figure 1.1B). Env is a trimer of heterodimers of gp120 and gp41, which is generated by protease cleavage, usually furin, of the pro-protein gp160. It is one of the most heavily glycosylated proteins with about half of the mass of gp120 being composed of N-linked glycans [11]. Env initiates host cell infection and displays the main target for an antibody-mediated immune response. The structure and function of Env will be discussed in detail in Section 1.2.2.

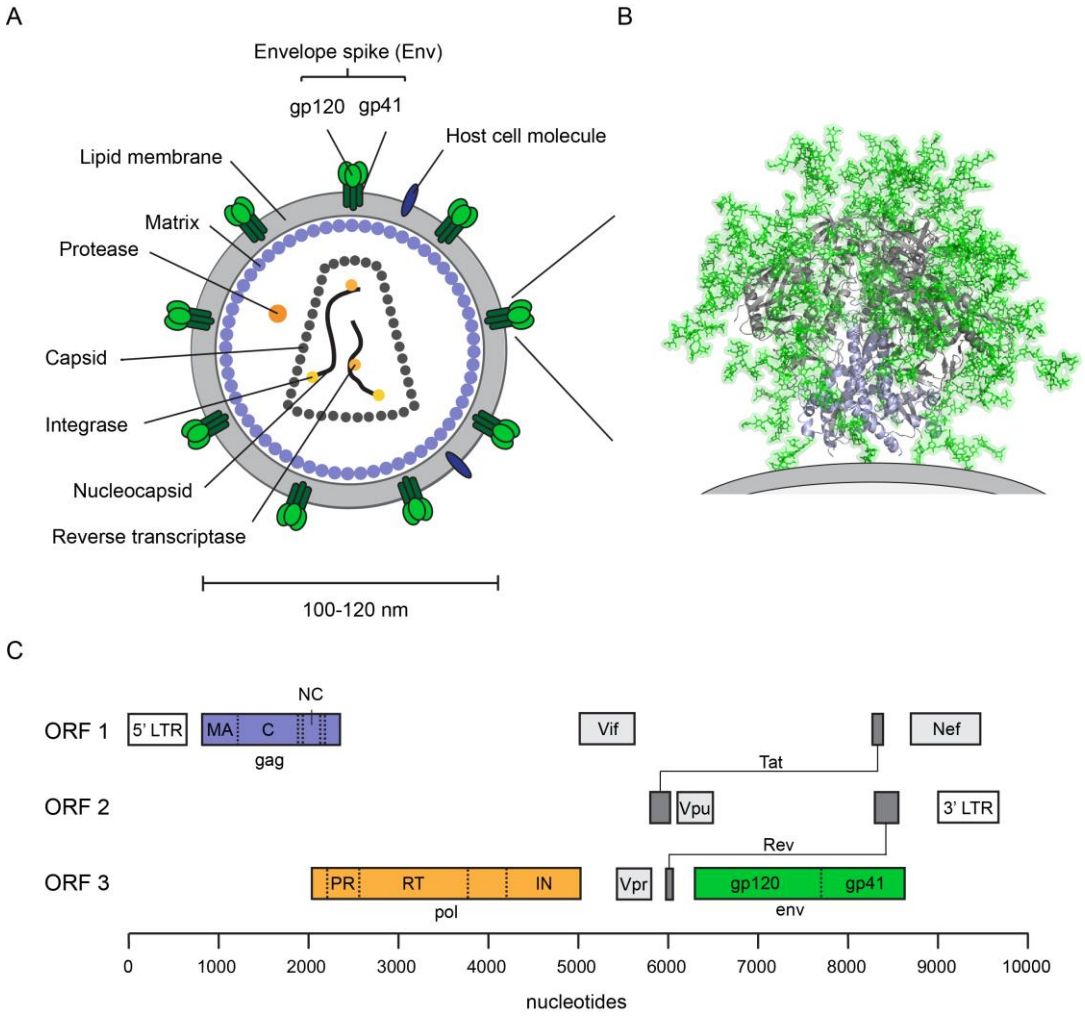

Figure 1.1: Structure and genome of the HIV-1 virion
(A) Virions assemble into spherical particles about 100-120 nm in diameter [10]. The two copies of the positive sense, single-stranded RNA genome are surrounded by nucleocapsid proteins and the enzymes integrase and reverse transcriptase. The genome is enclosed by a conical capsid, which itself is surrounded by a matrix ensuring structural integrity. The envelope spike (Env), composed of a trimer of heterodimers of gp120 and gp41, is embedded into the host cell-derived lipid membrane. Around 14 Env molecules are incorporated into each virion [12]. (B) Fully glycosylated model (glycans in green sticks) of Env based on PDB ID 5ACO [13]. Env is a trimer of heterodimers of non-covalently associated gp120 and gp41. (C) The RNA HIV-1 genome of approximately 9.8 kb is transcribed in multiple open reading frames (ORFs). The structural matrix (MA), capsid (C) and nucleocapsid (NC) proteins are encoded by gag (blue) and cleaved by the viral protease (PR). PR also cleaves itself and the viral enzymes (encoded by pol, orange) reverse transcriptase (RT) and integrase (IN). Env (green) encodes the envelope glycoproteins gp120 and gp41. Dark grey, regulatory proteins Tat and Rev; accessory proteins Vpr, Vpu, Vif and Nef are shown in light grey. The long terminal repeats (LTRs) have a function in transcription regulation. Sequence information were extracted from the Los Alamos HIV sequence database [14].

The tropism of HIV-1 is defined by the presence of its main receptor, cluster of differentiation 4 (CD4), which is expressed on the surface of macrophages, dendritic cells and

T helper cells ($CD4^+$ T lymphocytes), as well as its co-receptors, C-C chemokine receptor 5 (CCR5) or CXC-chemokine receptor 4 (CXCR4) [15-18]. The majority of HIV-1 infections are established by CCR5-tropic viruses [19,20]. Viral binding to CD4 receptors is mediated through the gp120 subunit of the envelope spike. Upon binding, conformational changes in Env are initiated, particularly in gp41, which allow subsequent co-receptor binding and fusion of the viral and host cell membranes (Section 1.2.2). The viral capsid is now released into the host cell cytoplasm and uncoated. In the cytoplasm, the viral reverse transcriptase (RT) produces double-stranded DNA from the exposed, viral RNA. As an intermediate, a double-stranded hybrid of RNA/DNA is formed, whose RNA strand is degraded by the Ribonuclease H domain of RT [21] and replaced by a second DNA strand synthesized by RT. The precise timing of these events is still not completely clear. A newer model suggests that the completion of reverse transcription is required before uncoating can occur and that the capsid has a crucial role for transport towards the nucleus [22]. The pre-integration complex, consisting of the double-stranded DNA associated with the viral protease, integrase, matrix and accessory protein Vpr, is imported into the nucleus, where the viral integrase integrates the DNA into the host cell genome. The host cell's translation machinery then takes over protein production, i.e. transcription (with the help of transcriptional activator Tat) and translation of viral genes, and thus enables the formation of new virions, which bud from the host cell membrane. The viral protein Vpu counteracts the human plasma membrane protein tetherin (CD317) in inhibiting the release of viral particles [23]. Viral particles are non-infectious until the viral protease cleaves the Gag proprotein and thus allows the maturation of a condensed viral capsid core and nucleocapsid [24].

Alternatively, the integrated provirus DNA can latently persist in memory T cells where it replicates with the host cell genome, hence impeding the complete eradication of the virus by antiretroviral treatments [25-27]. It has recently been shown that replication-competent proviral reservoirs mainly derive from quiescent T cells, in contrast to those that undergo clonal expansion [28].

1.1.2 Transmission and pathogenesis

The major route of HIV-1 transmission is via entry through the vaginal or rectal mucosa during sexual intercourse. Thus, the virus needs to penetrate the mucosal and epithelial barriers covering the genital and gastrointestinal tracts in order to encounter host cells prone to infection. This is thought to be achieved by several means including transcytosis, endocytosis, or passing through small gaps within the epithelia [29,30]. It is still not clear if HIV-1 is transmitted in a cell-bound state or as a free virus. SIV, however, can be transmitted in both ways [31]. Interestingly, an infection with HIV-1 is in most cases established by one single transmitted/founder virus meaning that a successful vaccine needs to induce an immune response capable of eliminating this initial virus [32-34].

Following transmission, the virus spreads into lymphoid tissues (spleen, bone marrow and lymph nodes) and, in particular into the gut-associated lymphoid tissue (GALT), where numbers of $CCR5^+/CD4^+$ T lymphocytes are high, and where a grave depletion of T lymphocytes is observed during acute infection, independent of the route of transmission [35-38]. The migration and retention of the virus in the gut is thought to be mediated by the gut-homing receptor, integrin $\alpha_4\beta_7$, on the surface of lymphocytes that interacts with a tripeptide in the V2 loop of gp120 [39]. Engagement of gp120 rapidly activates production of the integrin LFA-1, which facilitates cell-to-cell transmission of HIV-1 through the initiation of virological synapses [39]. It has been hypothesized that the protective effects observed in the RV144 vaccine trial (described in Section 1.1.5) are partly attributed to a high titer of antibodies that target the V2 loop of gp120 and thus block the gut-homing receptor binding site [40]. In fact, antibody therapy targeting $\alpha_4\beta_7$ integrin has recently lead to promising results in sustained control of infection in macaque studies [41]. In early phases of infection, the virus primarily infects $CD4^+$ T cells [42,43] (although dendritic cells are among the first cells it encounters and are thus important for initial infection). Viral spread can generally occur in a cell-free manner or from cell to cell via virological synapses, whereas the latter is reported to be more effective [44]. During the course of infection dendritic cells and

macrophages become more significant for viral spread. Interestingly, infection of macrophages has been reported to potentially occur as a result of phagocytosis of infected T cells [45].

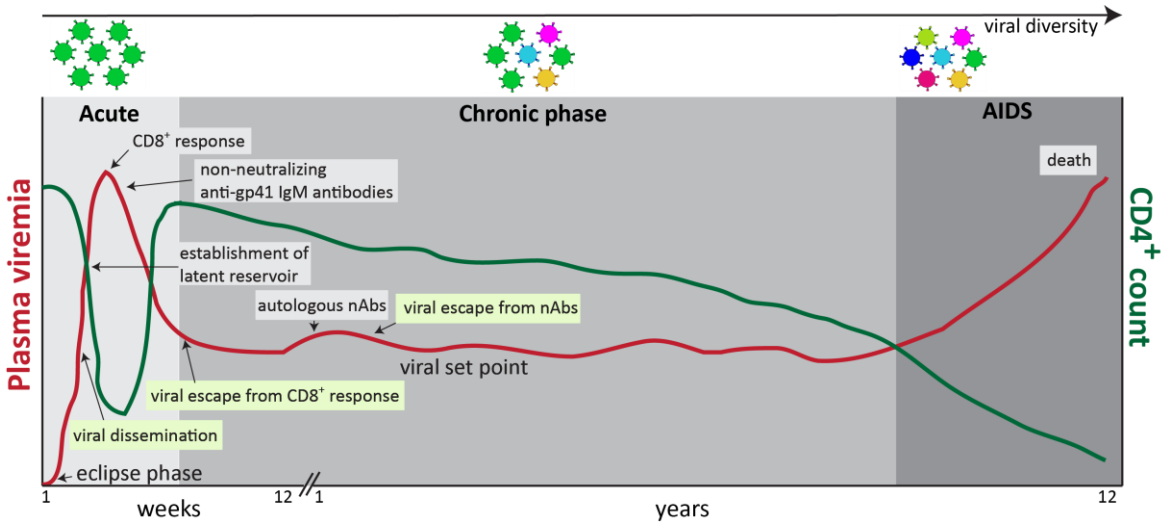

Figure 1.2: Course of HIV-1 infection
Plasma viremia and CD4⁺ T cell counts of a typical course of infection. See main text for details. nAbs, neutralizing antibodies. This figure was adapted from [46].

The phases and disease progression of an HIV-1 infection are illustrated in Figure 1.2. During the first ~10 days after infection, termed the *eclipse phase,* viral RNA in the plasma remains undetectable [47]. Following this initial phase virus levels increase exponentially, mainly due to dendritic cell-mediated dissemination, peaking between 21-28 days. In this *acute phase* CD4⁺ T cell numbers decrease, CD8⁺ T cells are activated, antibody production starts (seroconversion), and patients may present influenza like symptoms. Over the following weeks of infection, viral levels decrease to reach the *viral set point* under the pressure of a rising adaptive immune response [48-51]. CD4⁺ T cell counts in the blood then return to almost normal levels, although levels in the GALT remain low, in both HIV-1 and SIV [38,47,52,53]. HIV-1 is highly mutative and manages to repeatedly escape the adaptive immune system, e.g. by presenting non-neutralizing epitopes or by shifting the position of its surface glycans. The immune system itself is progressively weakened as a result of gradually decreasing CD4⁺ T cell counts (through apoptosis and pyroptosis [54]). In about half of HIV-1 infected individuals, the virus switches its co-receptor preference from CCR5 to CXCR4

in the course of infection [55]. It is hypothesized that this co-receptor switch accelerates $CD4^+$ T cell depletion and could thus be an important factor of viral pathogenesis [56]. Subsequently, the latter stage of the disease is marked by vulnerability to opportunistic infections, indicating progression to AIDS.

1.1.3 The viral envelope is the main target for a neutralizing antibody immune response

Assembled HIV-1 virions obtain the lipid envelope and the Env protein spikes as they bud from the host cell's plasma membrane. Env and Gag are both enriched in lipid raft microdomains in the plasma membrane, which very likely represent the location of virus assembly [24,57]. This is supported by the increased presence of sphingolipids, cholesterol, and phosphatidylinositol-4,5-bisphosphate in the viral envelope [58,59]. Although the glycan shield protects the highly mutative protein surface from the immune system and constantly evolves to escape antibody recognition [60-62], it is paradoxically itself a target for immune surveillance.

The shielding function is manifested by the host cell origin of the glycans that thus limit the freedom of action for B cell responses due to antigen self-tolerance. Furthermore, sialylated viral envelope glycolipids (termed gangliosides) have been described to interact with the cellular lectin receptor Siglec-1 (sialic acid-recognizing Ig superfamily lectins-1) on the surface of dendritic cells and therefore potentially enhance HIV-1 infection [63,64]. One notable exception can be observed during the transmission of primary virions, which can carry non-self ABO blood group antigens of the infected human. HIV-1 is able to incorporate host cell ABO carbohydrates into its membrane during budding, hence virus from A- or B-positive donors showed sensitivity to anti-A- or anti-B-antibodies from blood group-discordant recipients [65-67]. These blood group antigens possibly originate from glycolipids and/or membrane-bound glycoproteins present in the host cell's membrane and thus constitute a host mechanism for reduced viral infectivity. Nevertheless, the discovery and isolation of broadly neutralizing antibodies (bNAbs) from patients has established general consensus that the glycans on the HIV-1 surface not only offer protection but are also themselves a target for immune surveillance. Many of these Env-targeting bNAbs have glycan-

dependent epitopes [68-82]. Numerous studies have shown that bNAbs provide passive protection from viral challenge to non-human primates highlighting their potential for therapy and vaccine development [83-89]. The development of bNAbs and their glycan epitopes will be the focus of Section 1.3.

1.1.4 Immune response

Upon infection, invading pathogens are first challenged by the host's innate immune response. HIV-1 host cell entry occurs via interaction of Env with the entry receptors described above, but virions can also be captured via pattern recognition receptors (PRRs). Soluble and membrane-bound PRRs recognize viral pathogen-associated molecular patterns (PAMPs) and thereupon induce the expression of antiviral genes as well as inflammation e.g. by secretion of interferons and proinflammatory cytokines and chemokines [90]. Immune sensing mainly occurs in cells targeted by HIV-1, where exogenous viral particles, viral RNA, and intermediates of the reverse transcription process are recognized [91]. However, HIV-1 has evolved to limit detection by PRRs and to inhibit immune signalling e.g. by physically shielding viral nucleic acids in the cytoplasm before the dsDNA is translocated into the nucleus [91]. Moreover, the viral accessory protein Vpu inhibits nuclear factor kappa B (NF-κB) signalling and hence weakens antiviral gene expression [91]. The detailed processes by which the innate immune system senses HIV-1 and how the virus evades this response were reviewed recently in great detail [91-93].

Among the first immune cells that HIV-1 encounters are $CD4^+$ memory T cells, macrophages and dendritic cells (in particular Langerhans cells), which express various groups of PRRs, and vary in their response to HIV-1 invasion. Recognition of HIV-1 glycans through specific carbohydrate-binding PRRs, termed C-type lectin receptors (CLRs), plays a key role in HIV-1 transmission and replication. The CLR family shares a conserved structural motif in one or more carbohydrate recognition domains [94]. CLRs mediate pathogen internalization and endosomal degradation and induce antigen presentation and immune signalling cascades [95]. They display distinct carbohydrate specificities linked to their carbohydrate recognition domains [96]. The particularly

high content of oligomannose-type glycans on HIV-1 Env (Section 1.2.3) allows recognition by mannose-binding CLRs. Among the lectin receptors that recognize mannose residues on the HIV-1 surface are dendritic cell-specific ICAM3-grabbing non-integrin (DC-SIGN; expressed on dendritic cells and macrophages) and langerin (expressed on Langerhans cells) [97-99]. The outcome of glycan receptor recognition depends on the immune cells and the CLR [100]. Binding of HIV-1 to dendritic cells via DC-SIGN is thought to promote viral infection and transmission to $CD4^+$ T cells [101-104]. However, the role of Langerhans cells in infection and transmission through langerin expression is controversial. It is known that binding of gp120 to langerin leads to virus internalization into Birbeck granules, but opinions about whether or not this protects or promotes infection and transfer to T cells vary [97,105-109].

The complement system plays a diverse role in HIV-1 infection [110]. It exhibits a protective role upon HIV-1 infection by complement-dependent viral lysis and phagocytosis, which are mainly triggered through the classical pathway by HIV-1-specific antibodies [111-113]. Additionally, direct binding of complement factor C1q to gp41 as well as the interaction of gp120 glycans with the soluble PRR mannose-binding lectin (MBL) is reported to activate the complement system [110,114,115]. Although, as part of the lectin pathway, MBL only mediates low levels of HIV-1 neutralization, its binding can inhibit DC-SIGN uptake of virions and hence protect from viral infection [116,117]. The presence of regulators of complement activation in the viral envelope, such as the membrane-associated CD59 and soluble factor H, limits complement-dependent lysis of virions and infected cells [110,118,119]. In contrast, the complement system also plays a critical role in augmenting viral spread and promoting infection. For example, complement activation products like C3 fragments can be deposited on the viral surface which facilitates binding of HIV-1 to cells expressing complement receptors CR3 and CR4 (i.e. dendritic cells and macrophages) [110,120,121].

The adaptive immune response is triggered and regulated by interactions between HIV-1 and dendritic cells. Two distinct types of dendritic cell-mediated HIV-1 transmission have been

described termed *cis*- and *trans*-infection. During *cis*-infection, dendritic cells produce and release progeny virions that allow infection of target cells through viral-receptor-mediated entry. During *trans*-infection, transmission of endocytosed or surface-adhered virions occurs through the exosomal secretion pathway and via the formation of infectious synapses (under participation of DC-SIGN) with the target cell, respectively [122,123]. Of note is that macrophages are potentially also capable of both *cis*- and *trans*-infection to T cells [44].

The first $CD8^+$ T cell responses arise close to the peak of HIV-1 viremia (Figure 1.2), and peak around one to two weeks later. The earliest targets are very often Env and Nef [124]. The peak in cell count of specific $CD8^+$ T cells triggers the virus sequence to change dramatically and produce $CD8^+$ epitope escape mutants [47,125]. As $CD4^+$ T cells themselves are targeted by HIV-1, related immune responses are hard to verify and cell numbers gradually decline during infection [47,126]. The initial antibody response against HIV-1 Env starts around two weeks after transmission and is non-neutralizing, which is likely to be explained by the presence of non-functional Env displaying immunogenic surfaces usually not accessible in functional Env trimers [127-129]. An HIV-1-specific B cell response producing autologous neutralizing antibodies starts around 3 months after infection [61,130]. These antibodies also induce escape mutants of the virus. Antibodies that neutralize heterologous viruses to some degree can be identified in about 20-30 % of all infected people after several years of infection [131,132]. However, potent bNAbs targeting conserved regions of Env are relatively rare. In a recent longitudinal study on an HIV-1 infected cohort in Eastern and South Africa, only about 15 % of individuals developed an antibody response with more than 50 % neutralization breadth after 2 to 4 years of infection [133]. Additionally, acute HIV-1 infection leads to an early damage of the mucosal B cell generative microenvironments by inducing lysis and apoptosis [47,134]. In summary, unfortunately neither the innate nor adaptive immune responses are strong or fast enough to clear an HIV-1 infection before manifestation of a latent disease state.

1.1.5 Current therapies and steps towards a vaccine

The first antiretroviral drug against HIV-1 was Azidothymidine, which was launched only a few years after discovery of the virus [135]. As of 2016, there were 39 US Food and Drug Administration (FDA) approved drugs available, which can be divided into six distinct classes according to their mechanism of action: Nucleoside-analog RT inhibitors, non-nucleoside RT inhibitors, integrase inhibitors, protease inhibitors, fusion inhibitors and entry inhibitors. The large number of available drugs can be rationalized by the speed at which HIV-1 has evolved resistance to individual drugs [136]. The viral genome was shown to mutate with an extremely high *in vivo* rate of about 4×10^{-3} mutations per base per cell [137]. High mutation frequencies are the result of an error prone reverse transcriptase and induction of mutations through cellular cytidine deaminases combined with high viral replication rates [137-141]. This leads to the generation and selection of drug-resistant escape mutants – termed quasi-species [138,142]. The original mono-drug therapy was therefore replaced by a highly active antiretroviral therapy (HAART; or cART-combined antiretroviral therapy), which is a combination therapy of at least three different antiretrovirals targeting two or more distinct molecular targets [143]. HAART has significantly reduced the morbidity and mortality of infected patients; decreasing viral loads and increasing $CD4^+$ T cell counts [144-148]. In some parts the world, HAART has increased life expectancies to almost normal levels. It can also be used as a preventive measure for high risk groups such as relationships where one partner is infected or mother-to-child transmission during pregnancy [144,149].

Although the development of HAART has been a great success in fighting the HIV-1/AIDS pandemic, it isn't a cure. The combination of high side effects associated with antiretrovirals and very complex treatment regimens often leads to nonadherence, which can quickly result in an increase of viral load as HAART is unable to eliminate latent virus reservoirs [150,151]. Additionally, preventive measures such as condoms and male circumcision can significantly lower the risk of an HIV-1 infection, and trials of some vaginal microbicide creams have also yielded promising results [152,153]. However, all these preventative methods depend highly on personal behavior, and none

can fully eradicate the disease. The most hope lies in the development of a successful vaccine. In general, vaccines aim to provide adaptive immunity to a particular pathogen. As described above, most HIV-1 infections originate from one single transmitted/founder virus that needs to be stopped before reservoirs of latent virus are established in cells. This is thought to happen very early during infection, leaving only a window of a few days during which the virus could be eradicated [47,154].

Four vaccination approaches have been investigated during previous vaccine trials: Protein subunit vaccines, recombinant adenovirus vectors, canarypox vector prime followed by a protein subunit boost, and a DNA prime followed by a recombinant adenovirus vector boost [155]. The first two major trials, Vax003 and Vax004, explored the application of AIDSVAX, which contained recombinant gp120 and the adjuvant alum. Solely non-neutralizing antibodies were developed and no protection was observed [156,157]. The STEP trial and the Phambili trial investigated three recombinant, attenuated adenovirus type 5 vectors expressing Gag, Pol and Nef. A stimulated $CD8^+$ T cell response was observed, however no protection was achieved and the studies were stopped early due to concerns that the risk of an HIV-1 infection was actually increased [158-161]. During the RV144 trial in Thailand a canarypox viral vector (ALVAC) expressing gp120, Gag, and Pol was used to prime, followed by two booster injections of the AIDSVAX gp120 vaccine. This trial provided small protective effects for the first time, with ∼30 % fewer infections observed among vaccine recipients 3.5 years after vaccination [162]. It is not clear how exactly this protection was mediated, but the leading hypothesis is that the reduced risk of infection if associated with V1/V2-targeting antibodies [163]. One possibility is that part of the protective effect can be attributed to non-neutralizing, anti-HIV-1 Fc-mediated antibody effector functions [164]. The efficacy of a DNA prime (consisting of six plasmids encoding Env, Gag, Pol and Nef from different strains) and adenovirus type 5 vector boost (expressing a Gag-Pol fusion protein and Env from different strains) was investigated during the HVTN 505 trial [165]. This trial was also terminated before completion, again due to no protection being observed and concerns of adenovirus vectors increasing the risk of infection [166]. Adenoviral vectors are currently still the most promising $CD8^+$ T cell response-

generating vectors, but as clear explanations for the potential increase in susceptibility to HIV-1 infections are lacking, both additional human safety tests and the simultaneous development of alternative vector systems are required [167].

Currently, follow-up trials building on the promising results of the RV144 study are being developed and are under investigation, testing for example redesigned vector platforms [164]. In November 2016, the HVTN 702 trial, the first efficacy study in seven years, was started in South Africa with the goal to confirm and extend the partial protection of the RV144 trial by employing altered antigens, doses and vaccination schedules. Furthermore, much attention of vaccine research is at present centered on the development of therapeutic Tat vaccines, application of inactivated whole virus depleted of gp120 and the induction of bNAbs [164].

1.2 The viral envelope spike

The viral spike's crucial role in mediating viral infection and its exposed presence on the virion surface predetermine the viral envelope spike as the main target for vaccine development.

1.2.1 Biosynthesis

Mature and functional envelope spikes are trimers of non-covalently associated heterodimers of gp120 and gp41. The precursor pro-protein gp160 contains an N-terminal signal peptide, which targets the nascent peptide to the membrane of the endoplasmic reticulum (ER). Surprisingly, this signal peptide has a down-regulatory and inhibitory effect on Env folding as its co-translational cleavage is very slow and inefficient compared to other glycoproteins [168]. This is likely to be explained by the elevated number of charged amino acids present in the typically very hydrophobic signal peptide sequence [169]. Complete release of Env into the ER lumen as well as its membrane-anchored position are determined by the presence of a hydrophobic ribosomal stop-transfer sequence in gp41 [170,171]. Envelope is co-translationally modified by the addition of N-linked glycans within Asn-X-Ser/Thr sequons, with X being any amino acid except proline [172]. While the potential position of the N-linked glycan is determined by the protein sequence, the structure of the glycan is controlled by the host cell's glycosylation machinery and potential factors influencing the associated enzymes. The mammalian N-linked glycosylation (N-glycosylation) pathway in the ER and the Golgi apparatus is shown in Figure 1.3, beginning with the *en bloc* transfer of $Glc_3Man_9GlcNAc_2$ (Glc: glucose; Man: mannose; GlcNAc: *N*-acetylglucosamine) to amide groups of asparagines in potential N-glycosylation sites (PNGSs).

The ER-resident α-glucosidases I and II create monoglucosylated N-linked glycans, which interact with the folding chaperons and lectins, calnexin and calreticulin [173]. Once α-glucosidase II removes the final glucose, the glycoprotein is released from calnexin and calreticulin. Unless it is recognized as misfolded and re-glucosylated by the UDP-glucose glucosyltransferase, the protein can then leave the ER [174]. Re-glucosylated proteins undergo further chaperone-mediated folding cycles until they are either correctly folded, or disposed of via the ER-associated degradation

pathway. Folding of gp160 has been described as extremely slow, with gp160 residing in the ER longer than other glycoproteins [175]. Next to the above described effect of the signal peptide, ER maturation is prolonged by the correct formation and extensive isomerization of the intramolecular disulfide bonds of Env, which typically number around ten per protomer (of which nine are located in gp120) [175,176]. The α-glucosidase I and II inhibitor N-butyldeoxynojirimycin (NB-DNJ) has been investigated as a candidate anti-HIV-1 drug that targets this folding process [177]. Blocking entry of gp160 into the calnexin/calreticulin cycle leads to the formation of viral particles that are less infective, probably due to a conformational defect within the V1/V2 region that then inhibits membrane fusion [177-179]. An *in vitro* study into the use of NB-DNJ as an antiretroviral treatment yielded promising results, in that no resistance mutations were detected after 15-weeks cultivation of HIV-1 in the presence of NB-DNJ [177]. However, the off-target inhibition of gastrointestinal α-glucosidase has prevented clinical development for this indication [180].

Properly folded gp160 carrying $Man_9GlcNAc_2$ glycans moves through the ER-Golgi network, during which the N-linked glycans can be further trimmed by ER and Golgi α-mannosidases (Figure 1.3). As it will be highlighted later, the N-glycosylation trimming of multiple sites of Env stalls at the oligomannose series $Man_{5-9}GlcNAc_2$, leading to an N-linked glycosylation pattern dominated by minimally trimmed glycans that differs from that which is normally observed in human glycoproteins [176,181-184]. Complex-type glycosylation is initiated by the addition of a β1,2-linked *N*-acetylglucosamine to the 3-arm of $Man_5GlcNAc_2$. This is followed by further processing by Golgi-resident glycosidases and glycosyltransferases. The wide spectrum of hybrid- and complex-type glycans is cell type-/tissue-specific and can lead to a range of different glycoforms and microheterogeneity on individual glycan sites [185].

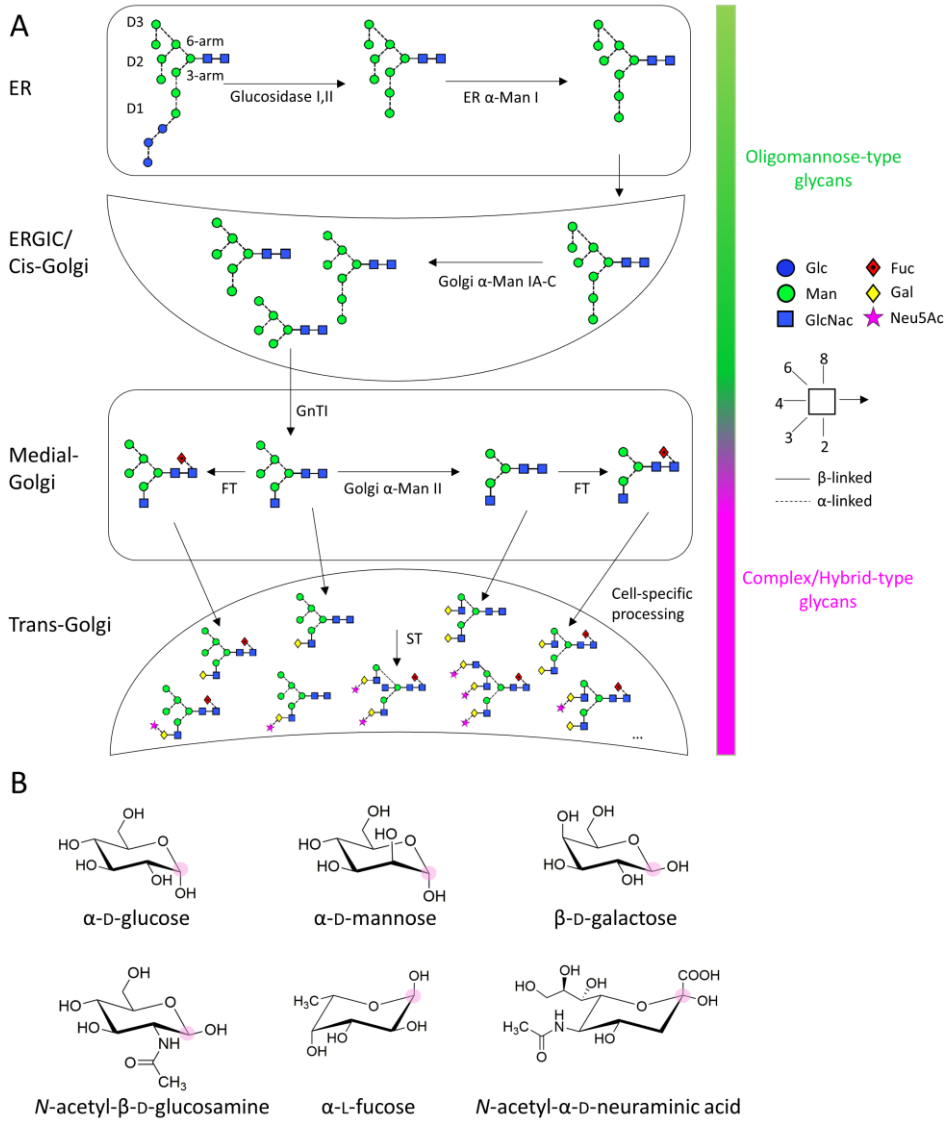

Figure 1.3: Mammalian N-glycosylation pathway
(A) In the ER, $Glc_3Man_9GlcNAc_2$ is transferred from a dolichol membrane anchor and asparagine-linked to the glycoprotein. The three terminal glucoses are removed by α-glucosidases I and II, followed by ER α-mannosidase I (ER α-Man I) removing the terminal mannose from the D2 arm. Golgi α-mannosidases IA-C (Golgi α-Man IA-C) are responsible for further mannose trimming leading to $Man_5GlcNAc_2$ in the ER-Golgi intermediate compartment (ERGIC) and *cis*-Golgi. $Man_5GlcNAc_2$ is then further processed by *N*-acetylglucosaminyltransferase I (GnTI) which initiates hybrid and complex glycan processing. $Man_5GlcNAc_2$ is also a substrate for Golgi-resident α1,6-fucosyltransferase (FT). Alternatively, further mannose trimming through the Golgi α-mannosidase II (Golgi α-Man II) can occur leading to $GlcNAcMan_3GlcNAc_2$. In the *trans*-Golgi, glycans are further processed by the action of cell-specific glycosyltransferases, sialyltransferases (ST) and fucosyltransferases. Glycan representation is shown according to the combined nomenclature of Harvey *et al*. and the Center for Functional Glycomics [186,187], see Appendix B. Numbering of indicated D1, D2 and D3 arms is adopted from the system of Vliegenhart *et al.*, [188]. (B) Structures in chair conformation of the most common monosaccharides of human N-glycans in their pyranose form. The anomeric centers are highlighted in pink.

Gp160 monomers trimerize in the ER, although the presence of non-functional dimers and tetramers has also been described [171,189,190]. The gp41 and gp120 subunits are generated when a protease, usually furin, cleaves the pro-protein gp160 glycoprotein [191-196]. Furin most probably cleaves gp160 in the *trans* Golgi network (TGN), but it is able to cycle between the TGN, the endosomal compartments and the cell surface and is also believed to be able to act in the early secretory pathway [192,197,198]. Furin cleaves at the C-terminus of the consensus sequence Arg-Glu-Lys-Arg [197]. Cleavage of gp160 is crucial for the structural and functional integration of the envelope spike, and thus for viral infectivity [184,199,200]. Noncovalently associated gp120 and gp41 trimers then assemble at the plasma membrane, where they are associated with Gag, and incorporated into new virions. The complete mechanism for the incorporation of Env is not yet fully understood. However, the for retroviruses unusually long cytoplasmic tail of gp41 and the Gag matrix protein are thought to play important roles in the process of incorporation [24,171].

Once assembled at the plasma membrane, Env is rapidly subjected to clathrin-mediated endocytosis [201]. This, as well as the shedding of gp120 caused by the rather weak gp41-gp120 interactions, leads to an exceptionally low number (about 14) of envelope spikes per virion [12]. Since a higher number of Env molecules has been reported to increase infectivity, as tested in a SIV model, HIV-1 must have other advantages explaining why it has evolved to carry a low number of spikes [202,203]. One explanation might be to avoid neutralization as the binding of bivalent immunoglobulin G (IgG) antibodies is disfavoured [204]. It has also been hypothesized that the particularly high mean epitope spacing of Env spikes slows down the development of bNAbs as the distance between two spikes is too high to overcome B cell tolerance mechanisms and hence impedes the development of self-reactive antibody intermediates [203].

1.2.2 Structure and function of Env

The type I fusion machine Env is metastable in its pre-fusion state and responsible for CD4 receptor recognition followed by fusion of the viral and host cell membranes. Figure 1.4 shows the overall schematic structure of Env. The gp120 subunit has a highly variable surface consisting of 5 variable

loops (V1-V5) that are interspersed by 5 constant regions. The sequence of the fusion-mediating gp41 subunit is more conserved consisting of an ectodomain, a membrane proximal external region (MPER), a transmembrane domain, and a cytoplasmic tail.

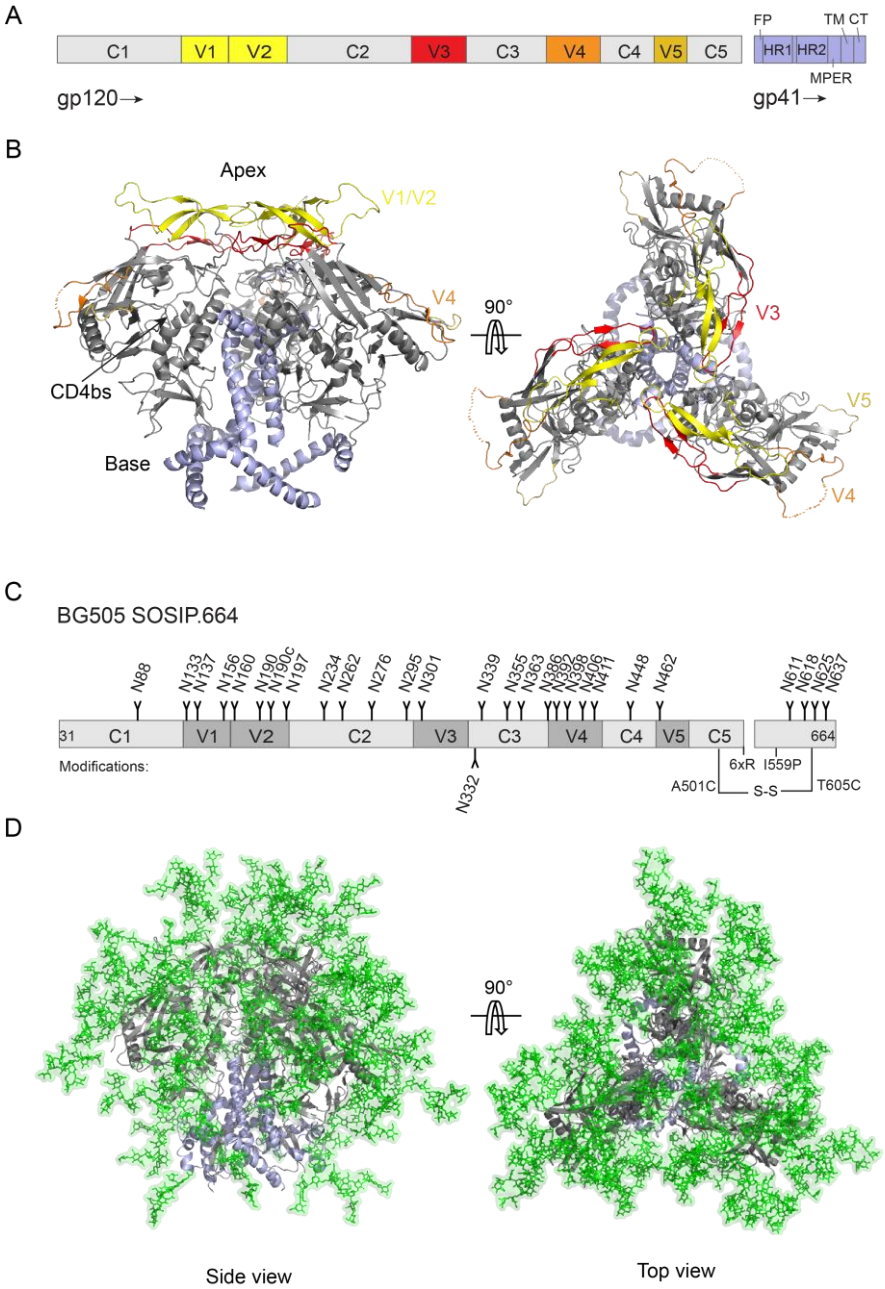

Figure 1.4: Structure of Env

(A) Primary structure of gp120 and gp41. Variable regions (V1-V5) of gp120 are colored, constant regions (C1-C5) are depicted in grey. Gp41 is shown in light purple. FP, fusion peptide; H1,H2, heptad repeat helices 1 and 2; MPER, membrane proximal external region; TM, transmembrane domain; CT, cytoplasmic tail. (B) Structure of a soluble BG505 SOSIP.664 Env trimer [205] in its closed, prefusion conformation. The variable regions and gp41 are colored as in A. Left: side view; Right: Top view. Images were made in Pymol using PDB ID 4NCO [206]. (C) Schematic representation of the BG505 SOSIP.664 construct including PNGSs and incorporated modifications. (D) Model of a fully glycosylated soluble BG505 SOSIP.664 trimer [13]. Glycans are shown in green. The model was made in Coot and Pymol on the basis of PDB ID 5ACO [207].

Structural studies of Env are relatively difficult because of the conformational dynamics of the molecule, the high degree of N-glycosylation, and the presence of variable loops. Despite these challenges, the publication of the first high resolution X-ray structure of a monomeric gp120 core in complex with CD4 near the end of the twentieth century by the laboratory of Peter Kwong, and a number of follow-up studies, have revealed fine structural details about the receptor-bound conformation of gp120 [208-213]. Furthermore, multiple groups have recently generated high resolution structures of intact, native-like trimers by X-ray crystallography and cryo-electron microscopy (cryo-EM), respectively [206,214-220]. The structures of monomeric gp120 all show a similar folding consisting of an N-terminal inner domain and a C-terminal outer domain, connected by the bridging sheet – a four-stranded antiparallel β-sheet [208-213].

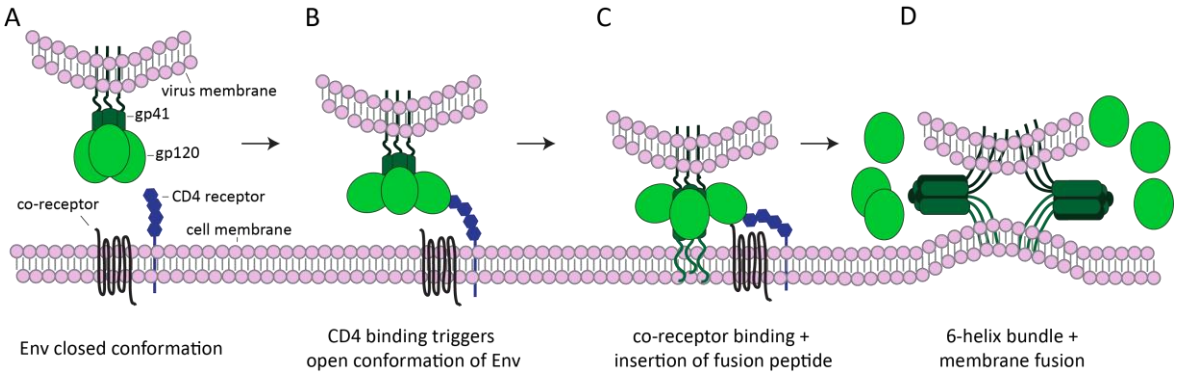

Figure 1.5: Model of Env-mediated HIV-1 membrane fusion
(A) HIV-1 trimer is anchored in the viral membrane and mediates fusion with the cell membrane of target cells. Env is a trimer of heterodimers of gp120 and gp41, which engage a closed conformation in their receptor-unbound state. (B) Upon interaction of gp120 with the first domain of the CD4 receptor, conformational changes lead to the formation and stabilization of the co-receptor binding site. (C) Env contacts a co-receptor (CCR5 or CXCR4). The trimer is pulled to the target cell membrane via bending of the CD4 receptor and co-receptor interaction. Co-receptor binding leads to the insertion of the fusion peptide of gp41 into the target cell membrane. (D) The gp41 subunits form a 6-helix bundle, composed of the two helices of each subunit, and membrane fusion occurs. The HIV-1 entry stoichiometry has been shown to vary for different HIV-1 strains [221].

Large structural rearrangements are induced in the viral spike upon CD4 binding, accompanied by large, unfavorable changes in entropy [222,223]. These changes include the formation and stabilization of the co-receptor binding site, consisting of the newly formed bridging sheet and the V3 loop. In this context, the V3 loop has been described as the primary determinant

of HIV-1 cell tropism [224]. Co-receptor binding then triggers the insertion of the N-terminal fusion peptide of gp41 into the target cell's lipid membrane, followed by the rearrangement the two heptad-repeat HR1 and HR2 α-helices forming a hairpin-like intermediate within each gp41 subunit and when folded together forming a 6-helix bundle that drives membrane fusion [225]. Figure 1.5 shows a structural model for the membrane-fusion process.

In order to improve trimer stability and to gain more detailed information, numerous different Env constructs such as trimers with a removed cleavage site, have been created and analyzed. However, it is now known that many constructs corresponding to uncleaved trimers do not represent the native conformation [214]. A rather recent breakthrough has been the development of the 'SOSIP' format containing several subtle modifications to generate a stable and soluble trimer mimic. These were generated by introducing an artificial disulfide bond between gp120 and the ectodomain of gp41 (SOS), which has been truncated at position 664 and thereby lacks the MPER and C-terminal domain of Env [205]. Stability was also increased by mutating an isoleucine residue to proline (IP) within the N-terminal heptad repeat region (HR1) of gp41 (combined: SOSIP.664 or simply SOSIP) [226,227]. Soluble trimers have clear advantages compared to membrane-bound versions regarding ease of production and protein handling. Furthermore, they led to substantial progress in the high resolution structural elucidation of Env.

Currently the most promising and most analyzed recombinant trimer mimic in vaccine development, BG505 SOSIP.664, is based on clade A transmitted/founder strain BG505 (Figure 1.4C). Compared to the original wild-type BG505 gp160, the sequence has been codon-optimized and epitopes of antibodies that depend on the N332 glycan have been introduced by a T332N point mutation [205]. It also contains a more susceptible furin cleavage site (Arg_6). This trimer displays native-like antigenic and structural properties [72,205,228]. The prefusion structure of BG505 SOSIP.664 was first resolved by X-ray crystallography and cryo-EM at 4.7 Å and 5.8 Å, respectively [206,217]. Further studies included higher resolution X-ray structures, that gave more complete information of gp41, and a cryo-EM structure of a fully glycosylated trimer at 4.36 Å [207,218,229].

All in all, structural studies on BG505 SOSIP.664 have provided the most complete and detailed picture of Env to date. The conserved gp41 fusion machinery resides at the trimer base, whereas the more variable gp120 head sits on top of gp41 (Figure 1.4B). The HR1 helices of gp41 reside in a three helix arrangement in the core of the 6-helix bundle and the HR2 helices form a membrane-proximal collar [218]. Both helices are shorter in the prefusion conformation compared to the postfusion conformation [214]. The trimer apex is comprised of the highly glycosylated, flexible and variable loops, V1, V2 and V3, which make stabilizing inter-protomer contacts and mask the underlying conserved regions [214]. The unglycosylated, conserved CD4 binding site (CD4bs) is located within a hydrophobic pocket between the inner and outer domain close to the protomer interface. CD4 and CD4bs-targeting antibodies need to approach Env from a particular angle in order to bind and successfully avoid surrounding glycans (in particular Asn276) and variable loops V1-V3 [214].

Env is covered by a dense shield of glycans (Figure 1.4D) that are a key element when considering structural and antigenic properties of Env. The very recently published cryo-EM structure of a membrane-bound, natively glycosylated Clade B JR-FL trimer (lacking its cytoplasmic tail) at 4.2 Å resolution [216], the X-ray structures of three soluble, fully glycosylated (although expressed in a GnTI-knockout cell line) Env trimers (including BG505 SOSIP.664) from clades A, B and G at 3.4-3.7 Å resolution [215] and the X-ray structure of natively glycosylated BG505 SOSIP.664 at 3.5 Å resolution have greatly enlarged our knowledge on the interlocking glycan network of Env [220]. However, cryo-EM and X-ray studies can only capture an averaged processing state on individual N-glycosylation sites and do not reflect the potential glycan microheterogeneity. The analysis of site-specific N-glycosylation can, however, be performed by mass spectrometry. Despite the very complicated target, multiple studies have been undertaken using different mass spectrometry techniques on a large variety of Env constructs (Section 1.2.4).

1.2.3 The glycan shield

Glycan structures on the surface of viruses usually function in disease transmission via interaction with host cell receptors. They also help pathogens to hide their variable protein surface from immune recognition. The HIV-1 viral spike is characterized by an unusually high abundance of glycosylation that leads to steric constraints within the glycan shield and hence a large presence of oligomannose-type glycans, which show lower structural variation compared to host cell glycoproteins.

The number of N-linked glycans in gp120 ranges from 18 to 33, with a median of 25 sites [230]. The extensive glycosylation of Env has previously been reported to shield the underlying protein surface from immune surveillance [60]. The glycan shield constantly evolves to provide steric hindrances to newly produced neutralizing antibodies. Such escape mutants show non-random shifts in position of their N-linked glycans [61]. Although the N-linked glycans derive from the host cell's glycosylation machinery (Figure 1.3), studies on recombinantly produced gp120 have revealed an unusually high and conserved population of oligomannose-type ($Man_{5-9}GlcNAc_2$) glycans [176,182,231,232]. The high density of glycans creates steric constraints that restrict the actions of ER and Golgi α-mannosidases responsible for trimming the N-linked glycan precursor $Man_9GlcNAc_2$ and thus leads to the presence of a cluster of oligomannose-type glycans, the 'intrinsic mannose patch' (IMP) [182,183]. The IMP is a characteristic feature of gp120 that is conserved across all HIV-1 clades [182,183,233] and longitudinally during infection [234]. The processing fate of individual glycans is determined by their position on Env. Analyses of recombinant soluble, native-like trimers [184], membrane-associated trimers [235] and virion-derived Env [182,183,236] all show that their oligomannose-type glycan contents are even higher than for gp120 monomers. This has led to the concept of an additional, 'trimer-associated mannose patch' (TAMP), thought to arise due to additional inter-protomer glycan-glycan and glycan-protein interactions [237]. However, the glycan sites forming any such TAMP have not previously been defined.

Compact folding seems to be a major driver behind the oligomannose-dominated profile of the glycan shield on native trimers. For example, uncleaved, non-native constructs that adopt a much more open and irregular conformation have a significantly reduced content of oligomannose-type glycans, because the now more accessible structures are efficiently processed [184,238]. N-glycosylation can thus serve as an indication for trimers with a native-like conformation [184]. Glycan analysis of the trimeric clade A Env mimic, BG505 SOSIP.664, showed an extensive population of oligomannose-type glycans on gp120 compared to a significantly higher abundance of processed, complex-type glycoforms on gp41 [184].

Sialic acids are terminal modifications on complex-type glycans (Figure 1.3) that show particular effects on the immune system. These effects seem to be linkage-specific with α2,6-linked sialic acids exerting an anti-inflammatory phenotype [239]. Evidence for this comes from the immunosuppressive activity of modified immunoglobulins, as well as the immune-modulatory role of CD22 present on the surface of B cells [239,240]. In HIV-1, the contribution of the sialic acid modification on the antiviral immune response has yet to be delineated. However, analysis of Env isolated from virus propagated in peripheral blood mononuclear cells (PBMC) showed that it was predominated by α2,6-linked sialic acids [241]. One established role of sialylation of N-linked glycans is the complement-mediated enhancement of HIV-1 infection due to the recruitment of the complement-regulatory factor H to gp41 [119,242]. Factor H recognizes sialic acids as 'self' and accelerates the decay of the C3 convertase C3bBb. It is also a cofactor for the serine protease factor I in the cleavage of C3b [243]. As a consequence, desialylation of Env promotes activation of the alternative complement pathway [244,245]. Besides modulating the activation of the humoral immune system, sialic acids are also proposed to modulate the cellular immune response. Specifically, α2,6-linked sialic acids are known to engage with inhibitory Siglecs on multiple immune cells [246]. In addition to these potential effects in natural HIV-1 biology, the presence of α2,6-linkages has consequences that need to be considered for recombinant models of the viral spike. Commonly used expression systems are usually dominated by α2,3-linked sialic acid moieties,

which may have implications for our understanding of bNAb epitopes involving complex-type glycans [241].

The role of O-linked glycosylation (O-glycosylation) in Env biology is uncertain. The strongest evidence that Env is indeed O-glycosylated comes from the observation that anti-Tn antibodies weakly neutralize HIV-1 [247]. The Tn epitope consists of a single *N*-acetylgalactosamine (GalNAc) linked to either a serine or a threonine. The abundance of any such O-linked epitope may be heavily influenced by the origin of the viral producer cell. O-glycosylation generally occurs on extended proline-rich regions, where tandem repeats of serine or threonine can become heavily O-glycosylated and thus form mucin-like domains. HIV-1, however, has no such regions. There have been reports of O-linked glycans (O-glycans) being identified on recombinant Env constructs at position T499 and T606 [232,235,248,249]. However, data regarding the presence of O-glycans on the native virus are conflicting; Stansell *et al.*, did not identify any O-linked glycans at T499, whereas Yang *et al.*, identified the core 1 structure Galβ1,3-GalNAc (termed T antigen) at this position [249,250].

1.2.4 Site-specific N-linked glycan analysis

In order to understand the fine structure of the glycan shield, a number of studies have performed site-specific analyses targeting HIV-1 Env N-glycosylation. These include work on various gp120 and gp140 constructs, membrane-bound material, and gp120 derived from virions, using a variety of different methods, most commonly mass spectrometry. The first study was conducted more than 25 years ago by Leonard *et al.*, who analyzed recombinant monomeric HIV-1_{IIIB} gp120 by a combination of enzymatic treatment and reversed-phase high-performance liquid chromatography (RP-HPLC). They found all 24 PNGSs to be fully occupied, with 11 sites containing oligomannose-/hybrid-type glycans [176]. Since then, improvements in mass spectrometry have led to successive studies providing a more detailed insight into the individual microheterogeneity and occupancy of each site [181,231,232,235,248,250-256]. Although clades, constructs, cell lines and purification methods varied between these different studies, they enabled the rough identification and

localization of complex- and oligomannose-type glycans on recombinant gp120. Broadly speaking, complex-type glycans are thought to be found in the C1, V1/V2 and V3 region of the glycoprotein, whereas under-processed, oligomannose-type glycans mainly reside within the C2 and C3 region i.e. the outer domain of Env. However, one of the main limitations of these studies is the lack of quantification when determining the microheterogeneity at individual N-glycosylation sites.

1.2.5 Glycans in immune escape

The HIV-1 glycan shield constantly evolves to escape the immune system [61]. N-glycosylation sites can be shifted or deleted as a result of mutations in the viral genome sequence. Nevertheless, the extent to which PNGSs are able to migrate is limited by structural features of the trimeric spike such as the non-glycosylated CD4 binding site and inter-protomer interfaces. In fact, the total number of PNGSs on Env has remained relatively constant, in spite of years of viral evolution [257].

Glycan shifts can be caused by just a single nucleotide change. In the Nx(S/T/N)x(S/T) motif, for example, exchanging the middle serine or threonine to asparagine moves the PNGS two positions along the protein sequence. As the codon triplets for S, N and half of the T codons are located next to each other on the codon table, this exchange can be achieved by simply changing the nucleotide triplet ACC (T) to AAC (N) [258]. One N-linked glycan site that has been reported to be vulnerable to this type of evolutionary migration is N332 [259]. A significant number of clade C founder viruses lack an N-linked glycan at position N332 and instead contain a glycan site at N334. During the course of infection, bNAbs can arise that target this particular glycan site. In one study, the virus has been shown to respond by first shifting N334 to N332, then after around two years of infection, the PNGS was shown to migrate back to N334 thereby thwarting the immune system once again [259]. Together, N332 and N334 are present in 93 % of all HIV-1 viruses and hence present a highly conserved feature of the glycan shield [78]. The glycan structure of these two sites has nearly exclusively been described as oligomannose [176,232,260]. Interestingly, bNAb PGT128 that targets the high mannose patch, in particular N332, is able to tolerate a shift to N334 in some viral isolates [259]. Similar observations have been reported for PGT121-7 [261]. The fact that the

immune system is able to overcome certain viral escape mutations within the glycan shield due to promiscuous glycan site recognition by bNAbs raises hopes that targeting the glycan shield could be a productive strategy in vaccine design.

1.3 A target for broadly neutralizing antibodies

The initial enthusiasm that followed the discovery of bNAbs in a small subset of HIV-1 infected patients was quickly damped as suspicions arose that many of these antibodies were actually self-reactive, therefore maybe largely eliminated from the B cell reservoir [262]. For example, the self-nature of the glycan shield underscored the potential difficulty in eliciting antibodies targeting Env. However, there have subsequently been waves of discovery of new potent and particularly broad bNAbs. Importantly, the majority of these bNAbs utilize N-glycosylation as a significant feature of their epitopes [263]. In parallel to these findings, it is now known that the formation of bNAbs within HIV-1 infected individuals is not as rare as originally thought, with up to around 30 % exhibiting notably active antibodies arising on average two years after infection, though in rare cases bNAb development as early as one year after infection has also been reported [264-266]. Unfortunately, patients that develop these bNAbs do not benefit from them themselves as the viral load and diversity is already too high by the time they evolve [267]. The observation that these antibodies do not arise very quickly, supports the notion that they operate at the edge of immune tolerance mechanisms and rely on rare mutations to achieve binding maturation. These features, which are described in detail below, clearly pose barriers for vaccine strategies designed to rapidly elicit bNAbs.

The time window and location for neutralization for any vaccine-induced antibody response is very narrow as it needs to prevent from the outset the establishment of a latent viral infection. However, numerous studies have shown that these bNAbs are able to provide passive protection from viral challenge with SHIV (chimeric simian/human immunodeficiency virus) in non-human primates which underlines and justifies efforts to elicit these antibodies through rationally

designed vaccine strategies [83-89]. In order to achieve this, it is likely that we require a more complete understanding of several fundamental areas such as the nature of the B cell maturation pathway and how germinal centers can be rendered more productive, how improved mimics of the envelope spike can be engineered, how bNAb epitopes can be rendered more immunogenic, and understanding how bNAb precursor germline B cells can be activated in prime and boost vaccination strategies.

1.3.1 Sites of vulnerability

The constantly increasing number of isolated bNAbs (about 100 at the beginning of 2017 according to a bNAb database [268]) targets defined, conserved regions of vulnerability on the HIV-1 Env glycoprotein (Figure 1.6). These regions include the mannose patch, the CD4 binding site, the MPER of gp41, glycan epitopes on the variable loops V1/V2 and V3, and the bridging region between the two subunits [269,270]. Many of these bNAbs recognize epitopes that are completely or partially composed of N-linked glycans [68-82]. Despite its potency in defending the virus against antibody-mediated neutralization, the dense HIV-1 glycan shield does contain vulnerabilities that can be exploited by the adaptive immune system.

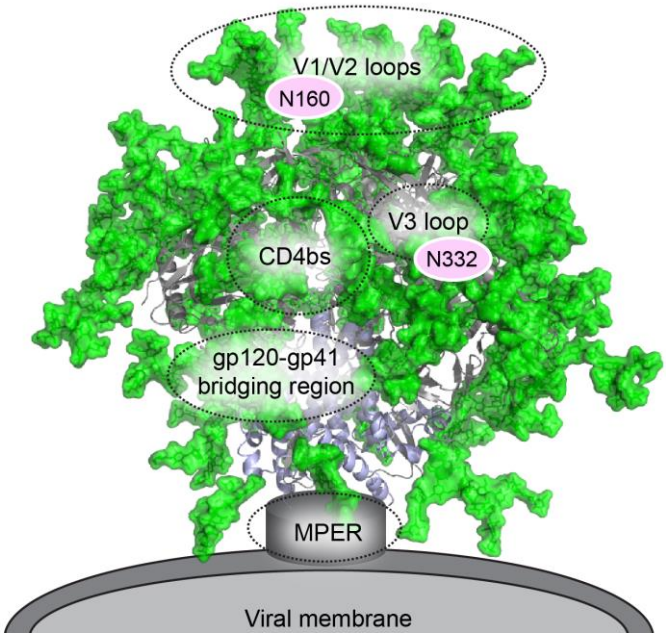

Figure 1.6: Sites of immune vulnerability on the HIV-1 envelope spike
HIV-1 bNAbs target five main regions on Env: The CD4bs (e.g. VRC01, ANC131, CH103); the MPER (e.g. 4E10, 2F5); the V1/V2 glycans – in particular N160 (e.g. PG9, PG16, CH01); the V3 loop and glycan N332 (e.g. PGT128, PGT125 and PGT138) and the gp120-gp41 bridging region including proximal glycans (e.g. 35022, PGT151). This figure is based on a model of fully glycosylated, trimeric Env (based on PDB ID 5ACO) [13].

Glycan-recognizing bNAbs target three main regions on Env: the N332 glycan (and the V3 loop), the N160 glycan (and the V1/V2 loops) and glycans at the gp120-gp41 interface [237]. The first bNAb identified to bind the HIV-1 glycan shield was 2G12 [74,271]. It has been shown to exclusively recognize conserved glycans on the gp120 outer domain, including N295, N332, N339 and N392 [272]. Binding of multiple N-linked glycans with high avidity is mediated through a unique domain-exchanged antibody structure that allows the formation of a multivalent surface [71]. The N332 glycan in the heart of the mannose patch on the outer domain of gp120 is also included in the epitopes of many other bNAbs, and hence has been dubbed the 'supersite of immune vulnerability' on the envelope spike [68,69,75,79]. Unlike 2G12, all other identified bNAbs targeting the glycan shield show non-domain-exchanged, Y-type antibody structures and contain both protein and glycan components as part of their epitopes [273]. They have also been shown to have much higher breadths and potencies compared to 2G12. For example, PGT128 is able to neutralize 72 % of circulating HIV-1 strains with a median IC_{50} of 0.02 µg/ml (compared to 2G12 – 32 % of

viruses with a median IC_{50} of 2.38 µg/ml) [68,69,79]. A common feature for N332-binding bNAbs (apart from 2G12) is the use of long third complementarity determining region of the antibody heavy chain (CDRH3) loops, which they employ to penetrate the glycan shield in order to interact with the V3/V4 loops, N332 and neighboring glycans [68,79,206]. Long CDRH3 loops are also observed among N160-recognizing antibodies. For example PG9 and PG16 form a large 'hammerhead' CDRH3 loop that contains tyrosine sulfation sites and is used to reach through the glycan shield and bind both the N160 and N156 glycans and the V1 loop [80,81,274]. PGT151 targets an epitope at the gp120-gp41 interface that relies on the presence of complex-type glycans on gp41 and protein epitopes on gp120 [73]. Moreover, it is noteworthy that autologous neutralizing antibodies have also been shown to specifically target defined holes in the glycan shield, which thus possibly present an additional site of vulnerability of the virus [275,276].

1.3.2 Unusual features of broadly neutralizing antibodies

BNAbs targeting HIV-1 have overcome tolerance mechanisms to self glycans, the usually weak nature of glycan-protein interactions and the protected protein surface of Env by the development of several unique characteristics.

- Long CDRH3
- Unusual post-translational modification (e.g. Tyrosine sulfation)
- Domain swapping (2G12)
- Auto- and polyreactivity
- Extensive somatic hypermutation

Many HIV-1 bNAbs, especially those targeting V1/V2 and V3, the bridging region, and MPER epitopes, contain long and charged CDRH3 sequences [277]. Whereas the typical length of a human B cell CDRH3 is between 8-16 residues, much longer sequences have been reported for bNAbs [278]. This generally permits the antibody to reach through the glycan shield in order to target more vulnerable protein regions. For example, PGT145, which binds the N160 glycan at the trimer apex, has a 33 residue long CDRH3, and the above mentioned 'hammerhead' CDRH3 of PG9 and

PG16 contains 30 residues that permit penetration of the glycan shield in order to reach the trimer apex [80,279-281]. Antibody 2F5, which targets the MPER, uses its long CDRH3 region (24 residues) to bind a linear epitope and extend a hydrophobic patch into the viral membrane, showing a different structural application for the same antibody maturation phenomenon [280,282]. Long CDRH3s are mainly attributed to original light chain recombination events selecting only a limited subset of germline genes, rather than to somatic hypermutation during antibody affinity maturation [277,283]. It was recently shown, that long CDRH3 sequences are in fact present in the naïve human B cell repertoire, supporting the idea to target bNAbs with this characteristic feature [284]. Furthermore, rather unusual post-translational modifications have been reported for bNAbs. For example, the CDRH3 of certain bNAbs carries a tyrosine sulfation, which has been reported to contribute to antibody binding and neutralization [279,285].

A property that is relatively common among HIV-1 bNAbs is poly- and autoreactivity [286,287]. It has been shown that bNAbs are generally more poly- and autoreactive than non-neutralizing antibodies [288]. This is striking as both characteristics are typically strongly deselected during B cell development; most naïve B cells are in fact poly- or autoreactive, but only 5 % of mature cells [289,290]. It has also been shown that B cells are capable of regaining poly- and autoreactivity during their maturation in germinal centers (Section 1.3.3) [291]. High polyreactivity is said to be strongly linked to the presence of long CDRH3s [292]. Polyreactivity allows bNAbs the bivalent heteroligation between one high- and one low-affinity epitope on HIV-1 and therefore increases the apparent binding affinity [287]. In this context it is also important to note that glycan-binding bNAb 2G12, which recognizes Manα1,2-Manα1,2-Man residues on the outer domain of Env, has been described to selectively bind to yeast mannans that display extended arrays of the same glycan epitope [71,74,293].

One explanation for the enhanced presence of autoreactive bNAbs could be the hypothesis that conserved, neutralizing HIV-1 epitopes mimic host proteins in order to avoid strong humoral responses [286]. Examples of autoreactive bNAbs are the four CD4bs specific antibodies VRC01,

VRC02, CH1063 and CH106, that all also recognize the human ubiquitin ligase E3A [288]. Avidity for the ligase correlates with neutralization breadth of the antibody [288]. MPER-recognizing antibodies 2F5 and 4E10 are self-reactive to human kynureninase and splicing factor 3b subunit 3, respectively [294]. Evidence that bNAbs to these epitopes might be impeded by the immune system comes from the hindered B cell development and activation in the corresponding knock-in mice through tolerance mechanisms [295-297]. Overall, the development of bNAbs carrying auto-and polyreactivity may be dependent on prolonged exposure to the antigen, as multiple B cell tolerance checkpoints need to be bypassed. Hence, their induction in healthy humans through vaccination might turn out to be very difficult [277,292,298].

Another common feature among bNAbs is the presence of extensive somatic hypermutation [69,299-301]. Normally, somatic hypermutation during antibody maturation are limited to the CDR regions, however, mutations in a HIV-1-targeting bNAb can also occur in the typically conserved framework regions (FWR) of the antibody [302]. These mutations have been shown to contribute to antibody binding [302]. There is also evidence of a positive correlation between the number of mutations and the development of breadth and potency of the antibody for the PGT121 family [303]. However, the presence of extensive mutations, including in the FWR, may be more of a hallmark of the length of time of bNAb development, rather than a trait of bNAb activity per se, as a partially germline-reverted form of bNAb VRC01 still shows considerable potency [304,305].

1.3.3 Development of broadly neutralizing antibodies

Naïve B cells circulate in the blood and lymphoid tissues and become activated by binding of antigens to their germline B cell receptors (BCR). These antigens can be either free or bound to antigen-presenting cells. B cell activation can be modulated and depends on a variety of additional factors such as T helper cells or PAMPs. Following a T cell-dependent activation, B cells migrate to draining lymph nodes and their development can take one of two turns. One option is that the B cells are recruited into extrafollicular responses, where they grow as low-affinity antibody-

producing plasmablasts [305]. These responses generally arise early during infection and are associated with hardly any somatic hypermutation [306]. The other option is the formation of a germinal center within the lymph nodes, where B cells proliferate and undergo class switching and affinity maturation through somatic hypermutation. The latter two are caused by the action of a B cell-specific, intrinsically expressed, activation-induced cytidine deaminase [307]. Follicular T helper cell (T_{FH}) and follicular dendritic cells (which secrete cytokines influencing B cell development) select affinity maturated B cells, which then leave the germinal center as memory cells or long-lived, circulating, antibody-secreting plasma cells. Memory B cells can re-enter the germinal center at a later stage when reactivated [305]. Plasmablasts and plasma cells are both sources of circulating antigen-specific antibodies in the blood serum. In terms of an HIV-1 infection, the primarily bone marrow-resident plasma cells are regarded to be the main source of HIV-1-specific antibodies [308]. A strong correlation between HIV-1 Env-specific plasma cells and HIV-1-specific circulating antibodies has recently been described, whereas a correlation between memory B cells and bNAbs remains elusive [308]. As most bNAbs are cloned from isolated HIV-1-specific memory B cells, these findings indicate that, although more difficult to assess, the bone marrow should be included as an important compartment for bNAb screening as well as evaluation of vaccine effects [305,308].

During an HIV-1 infection, the first humoral immune responses are IgG and IgM antibodies targeting gp41, which are developed within weeks after transmission. In contrast, anti-gp120 antibodies appear after an additional few weeks [129]. These initial IgG and IgM antibodies are capable of binding the virus, however they only have a low impact on acute-phase viremia [129]. Autologous neutralizing antibody responses have been shown to occur only several months after viral transmission [61,130,309,310]. Although these antibodies may show some cross-reactivity, a broad immune response that targets conserved epitopes on Env is usually only established after at least two years of infection in a subset of patients [264,311]. The development of antibody breadth is thought to be associated with the initial viral load and HIV-1 Env diversity, albeit not with disease

progression in general [312]. Case studies have revealed the maturation pathways in HIV-1 infected individuals that, over several years, drove the emergence of bNAbs against epitope clusters involving, the trimer apex, the CD4bs and the mannose patch [313-315]. In general, sequential rounds of virus evolution and the responding B cells create first narrow specificity NAbs and then virus escape mutants. This process of co-evolution and 'racing' against each other is repeated over many cycles until some antibodies mature sufficiently to be categorized as bNAbs. Interestingly, in cases where more than one bNAb has been isolated from the same HIV-1 patient, the antibodies often evolved from the same B cell lineage [316]. A recent study analyzed the longitudinal evolution of the VRC01 lineage of bNAbs in one individual over 15 years of infection [317]. Three diverse, multi-clade families of bNAbs could be isolated from this patient that all recognize the same CD4bs epitope. However, each family had developed a different structural solution to target the antigen. Remarkably, all three families likely originate from the same ancestor VRC01 B cell, indicating a high importance in early germline B cell selection for bNAb development. Additionally, it was shown that the VRC01 lineage developed with similar exceptionally high mutation rates as the virus during the course of infection [317]. Taken together, this study gives new insights into the evolutionary path of bNAbs while also demonstrating the complexity of their development.

1.3.4 Mechanisms of action

BNAbs are thought to act upon HIV-1 infection in a variety of different ways. As they directly bind to free virions in the plasma, they are able to neutralize the virus before host cell entry. This may happen by blocking viral attachment or fusion and the associated conformational changes within gp41 [318,319]. Direct, cell-free binding prevents further infection and also accelerates viral clearance in the plasma and maybe in tissues as well [320]. Next, some bNAbs can inhibit cell-to-cell transmission, both between lymphocytes and from lymphocytes to dendritic cells, by targeting viruses present at virological synapses [321-323]. Additionally, anti-gp120 antibodies (not anti-gp41 antibodies) were shown to efficiently block viral transfer from dendritic cells and macrophages to T cells [324,325].

Next to their neutralizing ability, Fc-mediated effector functions of bNAbs play an important role in inhibiting viral transmission and in passive immunotherapy in general [321]. These effector functions can be mediated through both cellular and soluble factors and include complement receptors as well as effector cells expressing Fc receptors [326]. The Fc domain can engage the complement system through classical and non-classical pathways resulting in lysis or phagocytosis of the antibody-bound infected cell or virus (CDC; cellular-dependent cytotoxicity) [326]. Antibodies opsonizing infected cells can further bind to Fc receptors on effector cells via their Fc domain and thus trigger cell lysis or phagocytosis. Binding to FcγRIIIa (most commonly expressed on natural killer cells) can lead to antibody-dependent cellular cytotoxicity (ADCC) and initiate apoptosis of the HIV-1 infected cell. Binding to FcγRIIa/b receptors (expressed on monocytes, macrophages and dendritic cells) can result in phagocytosis of the target cell (ADCP; antibody-dependent cellular phagocytosis) [326]. In addition, formation of immune complexes can enhance the antigen presentation by dendritic cells [320]. It is not yet fully understood which of the Fc-mediated activities plays the major role for the action of bNAbs, however, they are required for the antibody to exhibit its full potency both for clearing and preventing HIV-1 infections [320]. Moreover, bNAbs were shown to protect from mucosal transmission of HIV-1 in humanized mice and from rectal or vaginal viral challenge with SHIV in non-human primates [321]. It is not yet completely clear whether the reason for this is the inhibition of viral transcytosis or the intracellular neutralization of virions in epithelial cells [321]. Other impacting factors for passive protection of bNAbs could also be their ability to block viral cell-to-cell transmission or Fc-mediated effector functions [321].

1.3.5 Application in therapy

The application of bNAbs plays an important role in the treatment of HIV-1 infections. Passive immunotherapy not only has the capability to protect from viral challenge – as described earlier – but also significantly lowers the viral load in humanized mice, non-human primates and in the first human clinical trials [320]. Strikingly, application of a single bNAb was shown to be able to control

viremia to levels below detection in chronically infected non-human primates as long as antibody titers remained detectable [327,328]. The bNAb 3BNC117 has since been tested in a phase I clinical trial in humans; it lead to a significant reduction of viremia, providing a promising basis for further exploration of bNAb therapy in humans [329]. With regard to cure research, bNAbs are considered as part of a 'shock and kill' strategy with the goal to first activate viral replication in latent cells, followed by their immediate destruction [330]. While multiple classes of latency reversal agents (LRA) are being tested for driving the virus out of latency, T cells, natural killer cells and bNAbs are candidates for subsequent viral elimination strategies [326].

Multiple rational attempts to improve the efficacies of bNAbs have been investigated. These include engineering strategies to enhance breadth, potency, in vivo half-life or Fc-binding e.g. by altering the CDRH3 loop, construction of chimeric glycan-dependent bNAbs, or production of Fc non-fucosylated antibodies [81,331-333]. Additionally, bispecific antibody formats containing variable regions from different bNAbs have been explored [332]. For example, a bispecific IgG of VRC07 and PG9-16 (PG9-16 is a chimeric antibody based on PG9) displayed superior breadth and potency compared to its parent antibodies [334]. Antibody engineering and bispecific formats thus display very promising options for improving bNAbs in the use of prevention and treatment of HIV-1.

1.4 Strategies for vaccine design

1.4.1 Challenges

An effective HIV-1 vaccine will ideally stimulate the elicitation of bNAbs and also activate an effective $CD8^+$ cytotoxic T lymphocyte (CTL) response. As traditional and empirical vaccination approaches were either not applicable or did not result in effective immunization, current HIV-1 vaccine research focuses on rational immunogen design, though many challenges remain that must first be overcome. In order to prevent infection, it is crucial that a vaccine mediates sterilizing immunity and thus prevents the establishment of a latent viral reservoir. This is particularly challenging as the window of action for inhibiting HIV-1 infection is unusually short, whereas for most other vaccines protection against disease is usually sufficient. Moreover, a very broad immune response is required, that has the potential to tackle the enormous amount of genetically different, highly mutating HIV-1 strains. Sterilizing, broadly acting immunity will hopefully be provided through bNAbs, but immunogens eliciting an effective T cell response have the potential for a long-term control of viremia and therefore should not be neglected [335].

Many bNAbs target glycans on the surface of Env. However, the generation of antibodies to glycans has to overcome multiple hurdles as glycans can be rather poor immunogens [237]. Firstly, carbohydrate-protein interactions are generally weaker than protein-protein interactions requiring enhancement through avidity effects. Furthermore, the microheterogeneity, including varying, dynamic glycan conformations at single N-glycosylation sites, also weakens the immune response to individual glycans [237]. Additionally, as N-glycosylation is a common post-translational modification of many mammalian proteins, an intrinsic immune tolerance towards self N-linked glycans is to be expected, and thus there may be autoreactivity and negative selection towards these antibodies *in vivo* [336]. The exploitation of non-self features of the envelope glycan shield is nicely exemplified by bNAb 2G12 [74]. Mimicry of the 2G12 epitope has been exploited in various different immunogen design approaches (Section 1.4.3).

In the quest to elicit a bNAb response by vaccination, it remains to be determined which strategies, antigens, vectors and adjuvants will lead to the most promising effects. Several obstacles and questions remain to be answered and overcome, including concerns about the epitope dominance of non-neutralizing antibody epitopes or epitopes on variable, non-conserved regions of Env; concerns about the activation of BCRs if the germline antibody has low or no affinity to the antigen of its mature version; concerns about how to trigger the proper affinity maturation of bNAbs; as well as concerns about immune tolerance towards bNAbs containing unusual/unfavorable characteristics [316]. Immunogen design strategies aiming to induce either bNAbs or CTL responses as part of a complementary vaccination approach have recently been reviewed in great detail [335,337]. The foci of the next sections will be immunogen design and vaccination strategies to induce bNAbs.

1.4.2 Rational immunogen design to induce broadly neutralizing antibodies

HIV-1 vaccination research is dominated by a so-called 'reverse vaccine engineering' or 'antibody-guided' strategy, in which known bNAbs are used to rationally design immunogens aimed to induce similar broad and potent B cell responses [338,339]. Structural information about the bNAb epitopes gained by, for example, co-crystallization of a protective antibody with its antigen, are usually crucial for this strategy [339]. Thus far many different potential HIV-1 Env immunogens have been designed and evaluated (Figure 1.7).

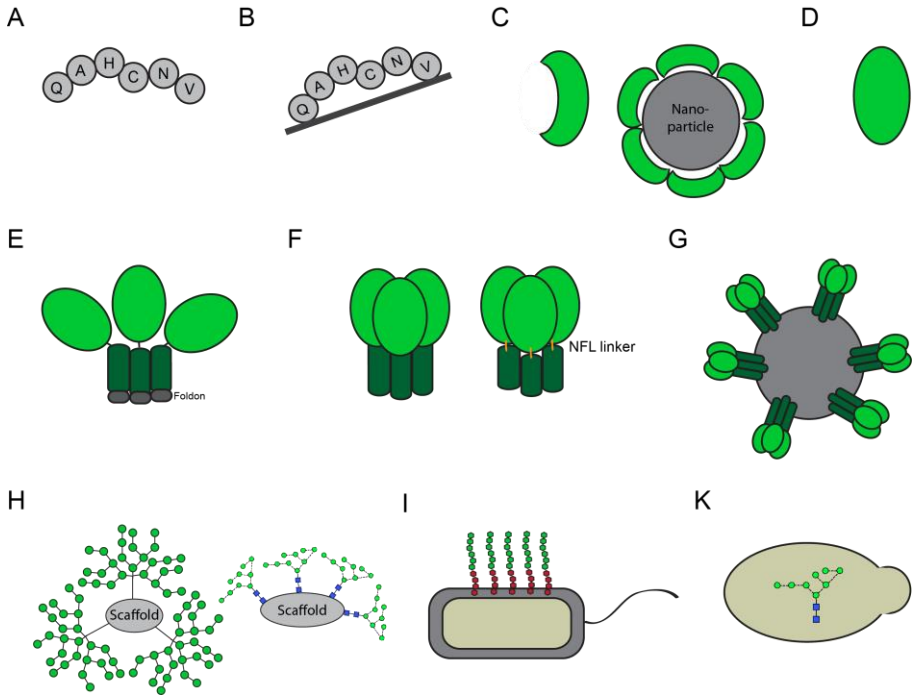

Figure 1.7: Overview of a selection of HIV-1 immunogens
(A) Peptide immunogens that contain linear epitopes [340-344]. (B) Peptide epitope scaffolds have been reported for the V3 region, the MPER and the CD4bs [345-349]. (C) Engineered outer domain (eOD) constructs. Monomeric (left) and modified, nanoparticle-multimerized eODs (right) have been investigated as potential immunogens [350-355]. (D) Gp120-based immunogens include monomeric gp120, hyperglycosylated gp120 and gp120 core constructs (deleted V1-V3 loops) [157,162,356-362]. (E) Uncleaved gp140 trimer usually stabilized by a foldon trimerization domain engage a non-native trimer structure [200,238,360,361,363-365]. (F) Native-like, stabilized and soluble trimers. Shown are a fully, cleaved trimer (left) and native, flexibly linked (NFL) trimer (right) [205,206,217,218,341,359,366]. (G) Particulate presented Env trimers can include presentation on nanoparticles, liposomes and virus-like particles [367-370]. (H) Synthetic carbohydrate antigens include for example oligosaccharides on small molecule scaffolds including $Man_9GlcNAc_2$ clusters (left) and Man_9 dendrimers (right) [371]. (I) Lipooligosaccharide expressed by gram-negative bacterium *Rhizobium radiobacter* is an analogue of the D1 arm (see Figure 1.3A) of oligomannose as present in the 2G12 epitope [372,373]. (K) Engineered yeast has been employed to produce modified oligomannose N-glycosylation structures to mimic the 2G12 epitope [374,375].

Peptide immunogens are among the earliest designed HIV-1 immunogens and are based on linear Env epitopes such as the V3 region and the MPER. Their employment in immunogenicity studies resulted at best in the elicitation of Tier 1 neutralizing antibodies (NAbs), and are thus most likely not sufficient to replace the complex conformational epitopes most bNAbs bind to [340-344]. Multiple other immunogen design strategies try to master the presentation of viral epitopes in a more native-like way in order to retain their antigenic character. Among these are studies on a variety of Env epitopes presented on protein scaffolds, which so far have not yet succeeded in

inducing a sufficiently effective neutralizing antibody response in animal experiments [345-349]. Many bNAbs bind to glycans as part of their epitopes, though mimicking the glycosylation state at a particular N-glycosylation site poses an additional challenge. Glycan-based immunogen design is a large research area on its own that will be outlined further below, however, larger immunogens that represent partial to almost complete envelope spikes, may impose similar steric hindrance phenomena to glycan processing enzymes and hence manage to mimic the emergence of the oligomannose patches. Engineered, germline-targeting outer domain (eOD) constructs, gp120 core proteins, and monomeric gp120 have been evaluated as vaccine candidates [156,162,341,353-355,358,376]. However, none of these strategies have yet shown a break-through in Tier 2 NAb induction. The limited immune response is thought to be attributed to less restricted access to epitopes on eOD and gp120 constructs that lead to antibody binding angles, particularly at the CD4bs, that are not compatible with the more restricted access to epitopes presented on a native trimer [341,360,377]. Furthermore, the interference of non-neutralizing epitopes on gp120, arising from the presence of the inner domain which is usually buried within the trimer, as well as the lack of trimer-specific bNAb epitopes (e.g. PG9/16 and PGT151), are likely explanations for the failure to induce Tier 2 neutralizing antibodies [70,72,341]. However, BG505 gp120 displays a noteworthy exception as this monomer managed to induce an autologous Tier 2 neutralizing antibody response in rabbits and is also known to be unusually immunogenic [359,378]. All in all, while these constructs may find utility in priming the immune response (Section 1.4.4), these results support the development of soluble trimeric mimics of Env trimer in order to properly present bNAb epitopes and avoid the possible immunodominance of non-neutralizing epitopes. Additionally, multiple neutralizing epitopes are presented allowing a polyclonal antibody response against different epitopes (thus providing barriers for emerging viral resistance mutants) [379].

Soluble gp140 trimers are generated by truncating gp41 leaving gp120 and a $gp41_{ECTO}$ domain that lacks the transmembrane region and the cytoplasmic tail, though these soluble trimers are very unstable, thus making it necessary to further stabilize the interaction between gp120 and

gp41. In one approach, uncleaved gp140 constructs are created by removing the furin cleavage site between gp120 and gp41 and sometimes by an additional introduction of a C-terminal trimerization motif (e.g. a foldon domain) [361,363-365]. However, multiple studies have shown that these trimers adopt a non-native conformation with the gp120 subunits dangling from the trimerized gp41 and exposing non-NAb epitopes [200,238,360]. Additionally, the formation of aberrant disulfides as well as an unusually high abundance of complex-type glycans was reported for uncleaved gp140 constructs, indicating protein misfolding and a non-native representation of the HIV-1 glycan shield [184,380]. Uncleaved gp140 immunogens were not able to induce NAbs against primary Tier 2 viruses [361,363,381].

A next generation of HIV-1 immunogens was initiated with the development of the soluble, native-like Env SOSIP.664 trimers (Section 1.2.2; Figure 1.4) with the leading example of BG505 SOSIP.664. BG505 SOSIP.664, as well as the clade B trimer, B41 SOSIP.664 successfully raised antibodies against the corresponding autologous Tier 2 virus [359]. The neutralizing epitope of BG505 SOSIP.664 was shown to be a breach in the glycan shield – a glycan hole composed of the lack of glycosylation at the conserved sites 241 and 289 [276]. Additionally, a study in mice revealed the immunodominance of a non-neutralizing epitope near the trimer base, indicating that further immunogen improvement to obscure these unwanted epitopes might be necessary [382]. One possible disadvantage of the SOSIP constructs is the requirement of furin cleavage for native-like trimer folding. In an alternative strategy, cleavage-independent trimers have been generated that contain a flexible peptide linker between the gp120 and gp41 subunits – termed native, flexibly linked (NFL) trimers [366]. These trimers also engage a native-like structure when analyzed using cryo-EM and first immunogenicity experiments in guinea pigs showed the elicitation of an autologous Tier 2 neutralizing antibody response [366,383].

Despite the advances in immunogen design brought by the soluble, native-like trimers, there is a large chance that vaccination with a recombinant protein will not be sufficiently immunogenic to induce a strong antibody response [384]. Virus-like particles (VLPs), liposomes and

inorganic or self-assembling protein-based nanoparticles are potential particulate delivery systems to display HIV-1 Env antigens [341,367]. Repetitive presentation of the antigen has several immunogenic advantages and will likely increase the longevity and potency of the antibody response [341]. Advantages include amongst others, an increased avidity of low-affinity bNAb epitopes, the potential to cross-link B cell receptors, and the binding of natural, circulating IgM to repetitively displayed antigens through high-avidity interactions leading to the activation of the complement system [341,384]. Furthermore, particulate presentation of Env also likely occludes the non-neutralizing epitopes at the trimer base [382]. Immunogenicity experiments using particulate trimer presentations so far yielded promising results and good neutralizing antibody responses. For example, rabbit studies using membrane-bound trimers on VLPs occasionally showed promising induction of a Tier 2 NAb antibody responses that displayed some cross-neutralizing activity against viruses lacking the N197 glycan [385]. The presentation of eOD constructs on nanoparticles enabled, in contrast to BG505 SOSIP.664, the activation of bNAb class VRC01 precursors in VRC01-heavy chain knock-in mice [353].

1.4.3 Carbohydrate-based Immunogens

Many efforts have been undertaken to design carbohydrate-based HIV-1 immunogens. Their development has been generally motivated by, and concentrates on, the mimicry of the bNAb 2G12 glycan epitope. 2G12 recognizes a cluster of α1,2-linked mannoses on the outer domain of Env via its unique domain-exchanged structure [74,386]. The rationale is that an immunogen containing a multivalent array of α1,2-linked mannoses might be capable of inducing 2G12-like antibodies to this specific epitope given it is presented in a sufficiently immunogenic context [336,387,388]. Chemically synthesized, multivalent oligomannose-glycan antigens have been created by clustering carbohydrates on rationally designed peptide [371,389-391], dendrimer [392,393], carbohydrate [394,395], DNA [396-399], steroid [400], gold nanoparticle [401] and biomacromolecular [402,403] scaffolds. Many of these constructs have been reported to bind to 2G12, however none of the antisera has so far been reported to show HIV-1 neutralization activity [371,399].

Another approach is the exploitation of naturally-derived carbohydrate antigens as mimics of the 2G12 epitope. For example, bacterial lipooligosaccharides have been investigated as potential immunogens [372,373]. Similar to the chemically designed immunogens, no neutralizing anti-HIV-1 activity was detected in raised antibody sera [372]. Further attempts to place key components of the epitope in a wider immunogenic context also include yeast strains genetically engineered to manipulate N-glycosylation. Knock-out mutants of glycan processing enzymes in *Saccharomyces cerevisiae* were used to generate mannans displaying extended arrays of α1,2-linked mannoses, as well as mannans that homogenously display the self-glycan $Man_8GlcNAc_2$ on its glycoproteins [374,375]. Antigenicity and immunogenicity studies using whole yeast cells of these mutants generally yielded antibody responses that were able to bind to oligomannose-type glycans but which often failed to bind gp120 [374,375,388]. Similarly, HIV-1 neutralization was reported to be either extremely weak or only detected for viruses that had been produced in the presence of kifunensine to force retention of $Man_9GlcNAc_2$ at all N-linked glycans [374,388]. A likely explanation is that these antibodies possibly recognize oligomannose structures that are not present on native virions and are localized outside the 2G12 epitope [388,404]. Similar results have been reported for glycoprotein immunogens that were produced in genetically engineered yeast [404,405].

Questions and uncertainties remain regarding whether or not there are any dangers of bypassing natural tolerance mechanisms to oligomannose glycans by immunogen development. However, as the innate immune system is highly sensitive to cell surface mannose residues, it is unlikely that mimicking this will have any untoward effects in the adaptive immune system. The sensitivity of the innate immune system to oligomannose is illustrated by its chronic activation and lupus-like pathology shown in mice deficient in Golgi α-mannosidase II [406]. Furthermore, passive transfer of bNAbs exhibiting specificity towards oligomannose-type glycans is well-tolerated. Several findings support the rationale of using glycan-targeting bNAbs as blueprints for HIV immunogen design. The elicitation of high titers of class-switched antibodies recognizing unusual,

disease-specific, self-glycan epitopes has been shown in cancer vaccine research [407,408]. Furthermore, autoimmune disorders caused by glycan-mimicking microbe infections exemplifies a way for the immune system to overcome glycosylation self-tolerance. In the case of the Guillain-Barré syndrome anti-glycolipid antibodies can be induced after intestinal infection with *Campylobacter jejuni*, manifested by ganglioside mimicry of the bacteria [409,410].

1.4.4 Vaccination strategies

The development of native-like trimer mimics as subunit vaccines will rely on the selection and usage of suitable adjuvants and delivery vectors that help to render a humoral and cellular immune response more effective. In terms of adjuvants, several new compounds including Toll-like receptor agonists are in clinical development to provide additional options alongside the most widely used aluminum hydroxide (Alum) and Freund's adjuvants [411]. The detailed discussion of vectors and adjuvants constitutes a whole separate area of vaccine design and is not within the scope of this thesis. However, BG505 SOSIP.664 trimers have successfully been shown to be stable when formulated in ISCOMATRIX adjuvant [359,412].

The rationally designed, native-like soluble trimers with occluded non-neutralizing epitopes that display multiple, correct bNAb epitopes have the potential to raise a broad, polyclonal antibody response. Ideally this will prevent the formation of viral escape mutants as well as act upon a panel of different HIV-1 subtypes. However, as the so far best characterized immunogen BG505 SOSIP.664 only managed to induce autologous NAbs, it is likely that a single Env trimer won't be sufficient for a broadly acting vaccine [341,359]. A simultaneous or sequential vaccination with recombinant trimers from different clades represents a promising alternative strategy to be explored [341].

Sequential immunization is also the basis of novel prime/boost strategies being developed to specifically target the naïve and intermediate mutation versions of germline bNAb ancestors [353,355,413]. Recombinant Env immunogens usually show little to no binding to the unmutated,

germline-reverted versions of bNAbs and their B cell receptors [212,299,414,415]. As described in Section 1.3.3, the virus and bNAbs co-evolve, thus rationalizing that it might be necessary to mimic this progress using specifically designed vaccination steps [298]. These would probably start with the activation of the relevant naïve B cell receptor, followed by immunogens that guide antibody development along the appropriate/desired path [341] (Figure 1.8). Env immunogen improvements to specifically engage germline precursors include trimers with specifically eliminated PNGSs, as well as germline-targeting outer domain constructs [354,355,414]. These strategies will need to be further evaluated in animal and human trials.

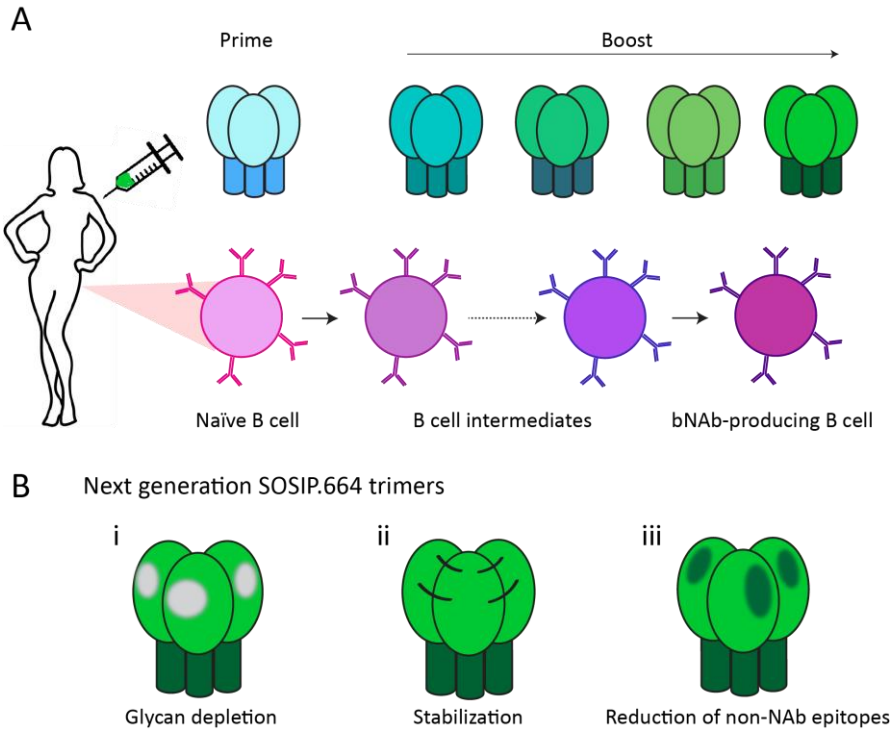

Figure 1.8: Towards a broadly neutralizing B cell response
(A) The idea for a sequential immunization approach is the initial engagement of a relevant naïve B cell receptor (priming) that is then guided into maturing towards a broad and potent bNAb-producing clone via sequential boosting with rationally designed immunogens. These immunogens are likely versions of native-like trimer mimics. (B) The SOSIP.664 design is the basis for a next generation of soluble trimers [416,417]. These include trimer mutants that are site-specifically glycan-depleted in order to engage naïve bNAb B cell receptors (i). SOSIP trimers are further stabilized by additional mutations or the introduction of chemical cross-linking [416,418] (ii). Additionally, mutations are introduced to limit the exposure of still remaining non-NAb epitopes such as e.g. the immunogenic V3 region [416] (iii).

Another approach to positively influence the evolution of bNAbs is the induction of more productive germinal centers together with an enhanced T_{FH} response [305]. As little is known about the factors that can drive T_{FH} responses during vaccination, a simpler option to positively influence bNAb development in germinal centers could be to deliver cytokines that mediate T_{FH}-like help, such as Interleukin-21 and/or Interleukin-12, as adjuvants [305,419,420]. Moreover, members of the tumor necrosis factor family B cell activating factor (BAFF) and proliferation-inducing ligand (APRIL) seem to be important for productive germinal centers and have shown promising results in vaccine development studies [305,421,422].

1.5 Fine structure of the HIV-1 glycan shield

The envelope spike of HIV-1 is extensively glycosylated. The high density of glycans imposes steric constraints on the host cell's glycan processing enzymes, thus leading to a large abundance of oligomannose-type glycans on Env. Most of the glycans are highly conserved and play crucial roles in the viral lifecycle. Although the glycan shield protects the highly mutative protein surface from the immune system and constantly evolves to escape antibody recognition, many very potent bNAbs have been shown to incorporate glycans into their epitopes. Elicitation of bNAbs by rational immunogen design is a main focus of structural-guided HIV-1 vaccine development. Thus, understanding the fine structure of the HIV-1 glycan shield on the virus and recombinant mimics of the trimeric viral spike, especially with regard to identifying the precise locations of unusual oligomannose-type glycans, is essential in guiding vaccination strategies.

Chapter 3 of this thesis focuses on the development and validation of a semi-quantitative mass spectrometry workflow to analyze the site-specific N-glycosylation of a recombinant Env trimer mimic.

Chapter 4 presents the site-specific composition of the HIV-1 glycan shield and identifies the location and microheterogeneity of oligomannose-type and complex-type N-glycosylation sites on the surface of Env. Furthermore, the effects of glycan site deletions on viral neutralization sensitivity and on the integrity of the glycan shield are explored.

Chapter 5 compares the site-specific N- and O-glycosylation profiles of monomeric, cleaved trimeric and uncleaved (termed pseudotrimeric [416]) Env glycoproteins and hence depicts how the formation of a natively glycosylated Env spike is controlled by its intrinsic structural features.

Finally, Chapter 6 and Chapter 7 probe the glycan shield by analyzing the N-glycosylation profiles of further vaccine candidates – a linker-stabilized, cleavage-independent trimer mimic and a glycan-depleted, bNAb germline-targeting recombinant trimer – and thus reveal interesting insights into Env folding and the robustness of the mannose patch.

2 Materials and Methods

2.1 Materials

Enzymes for glycan digests and cloning were purchased from New England Biolabs (Ipswich, MA, USA), unless stated otherwise. Proteases for mass spectrometry sample preparation were purchased from Promega (Fitchburg, USA), unless otherwise specified. Gibco tissue culture reagents were purchased from Thermo Fisher Scientific (Waltham, MA, USA). HPLC-grade and LC-grade solvents including water for HPLC and mass spectrometry were purchased from VWR International Ltd (Lutterworth, UK) and Fisher Scientific (Loughborough, UK). Other than that, water was Milli-Q grade. Chemicals were purchased from Sigma-Aldrich (St Louis, MO, USA), unless otherwise specified.

Primers were synthesized by Thermo Fisher Scientific (Waltham, MA, USA). AmpliTaq Gold PCR Master Mix was purchased from Applied Biosystems (Carlsbad, CA, USA). DNA purification kits (QIAprep Spin Miniprep Kit, Plasmid Maxi Kit, QIAquick Gel Extraction Kit were obtained from Qiagen (Crawley, UK). DNA Hyper Ladder 1 kb Plus and DNA loading buffer were from Bioline (London, UK). GelRed DNA gel stain was purchased from Biotium Inc (Hayworth, USA). DEPC-treated water was from Fisher Scientific (Loughborough, UK). XL-1 Blue competent cells were from Stratagene (La Jolla, USA). QuikChange Lightening DNA mutagenesis kits were purchased from Agilent Technologies (Santa Clara, USA). DNA sequencing was performed by Source Bioscience (Oxford, UK).

Pre-cast NuPAGE 4–12 % Bis-Tris polyacrylamide gels, Native-PAGE 3–12 % Bis-Tris polyacrylamide gels, NuPAGE loading buffer and reducing agent, Native-PAGE sample Prep Kit, 3-morpholinoethane-sulphonic acid (MES) buffer and Native-PAGE running buffer were purchased from Invitrogen, Thermo Fisher Scientific (Waltham, MA, USA). Precision Plus Kaleidoscope Standard was obtained from Biorad (Hemel Hempstead, UK). 1 ml Vivaspin 30- and 50-kDa cut-off concentrators, HiTrap Protein A HP 5 ml purification columns, Superdex 200 prep grade gel

filtrations columns and CNBr-activated Sepharose 4B were purchased from GE Healthcare (Waukeshua, WI, USA). Spe-ed Amide-2 cartridges were purchased from Applied Separations (Allentown, PA, USA). 96-well hydrophobic polyvinylidene fluoride (PVDF) membrane filtration plates 0.45 µm, Express Plus sterile filters 0.22 µm, Proteo Extract glycopeptide enrichment kit and C18 Ziptips were purchased from Merck Millipore (Darmstadt, Germany). Ammonium formate buffer (pH 4.4) and 2-AA labeled glucose homopolymer ladder were obtained from Ludger Ltd (Culham, UK).

2.2 Molecular biological methods

2.2.1 Plasmid constructs and cloning

The pPPI4 expression plasmid [226] carrying His-tagged BG505 SOSIP.664 was provided by Prof. Rogier Sanders (Cornell University, NY, USA) [205]. The pPPI4 expression vector was also used for the transient expression of non-His-tagged BG505 SOSIP.664, His-tagged BG505 gp120 and BG505 WT.SEKS. BG505 NFL2P.664 was expressed from pCDNA 3.1 vectors (Table 2.1). Cleaved envelope constructs were generated by co-transfection with plasmid pcDNA3.1-furin, which expresses recombinant furin [226]. 2G12 and PGT151 light chain and heavy chain antibody pIgG expression plasmids [423] were provided by Dr Katie Doores (King's College London) and Dr Torben Schiffner (The Scripps Research Institute, La Jolla, CA, USA), respectively.

Monomeric BG505 gp120 was inserted into the pPPI4 vector using *Bam*HI (3') and *Pst*I (5') restriction sites. Sequences were amplified by polymerase chain reaction (PCR) using primers containing the corresponding restriction sites (for sequences see Appendix A). PCR reactions were analyzed by electrophoresis with a 1 % agarose gel, and amplified PCR products were recovered. Insert and vector were digested with *Bam*HI and *Pst*I and then ligated using T4 DNA Ligase (4:1 ratio, v/v; 1 h at RT). This was followed by transformation into XL-1 Blue competent cells, according to manufacturer's instructions. Cultures were plated on to lysogeny broth (LB) agar plates containing 50 µg/ml carbenicillin and incubated at 37 °C over night.

2.2.2 Site-directed mutagenesis

Single and double mutants of a selection of N-linked glycan (N-glycan) sites in the pPPI4 plasmid carrying BG505 SOSIP.664, as well as in the BG505.T332 and BG505.T332N full-length Env proteins (Section 2.6; performed by Dr Katie Doores, King's College London), were made by changing asparagine (within the N-glycosylation sequence Asn-X-Ser/Thr, where X is any amino acid except proline) to alanine or (for the N160 site, only) lysine, using the QuikChange Lightening Mutagenesis system according to the manufacturer's instructions. Changes were verified by DNA sequencing. The primers used and the mutants created are listed in Appendix A.

2.3 Recombinant protein expression and purification

For this thesis different BG505 envelope glycoproteins were expressed, purified and analyzed. A number of them originate from collaborator laboratories. Table 2.1 summarizes the constructs, expression cell lines, purification methods and, if applicable, the laboratory they originate from. Usually, proteins were purified from culture supernatants using affinity chromatography followed by size-exclusion chromatography (SEC; gel filtration).

Table 2.1: Overview of analyzed BG505 envelope glycoproteins

Construct/Name	Cell line[a]	Purification[b]	Chapter	Additional information[c]
BG505 SOSIP.664	HEK 293T stable	2G12 + SEC	3 + 4	Provided by Dr Albert Cupo/Prof. John Moore (Weill Cornell Medical University)
BG505 SOSIP.664	HEK 293F transient	PGT151	4	His-tagged construct, used as the basis for a panel of glycan deletion mutants and a 334N migration mutant
Env-pseudoviruses BG505.T332 and BG505 T332N	HEK 293T		4	Produced by Dr Katie Doores (King's College London), used as the basis for a panel of glycan deletion mutants
BG505 SOSIP.664	HEK 293F transient	2G12 + SEC	4 + 5	Provided by Dr Albert Cupo/Prof. John Moore (Weill Cornell Medical University)
BG505 WT.SEKS	HEK 293F transient	2G12 + SEC	5	Provided by Dr Albert Cupo/Prof. John Moore (Weill Cornell Medical University)
BG505 gp120	HEK 293F transient	2G12 + SEC	5	His-tagged; cloned from BG505 SOSIP.664
BG505 NFL2P.664	CHO transient	Lectin + SEC + F105 negative selection + SEC [366]	6	His-tagged construct, provided by Dr Shailendra Kumar Sharma (The Scripps Research Institute)
BG505 NFL2P.664	HEK 293F transient	Lectin + SEC + F105 negative selection + SEC [366]	6	His-tagged construct, provided by Dr Shailendra Kumar Sharma (The Scripps Research Institute)
BG505 SOSIP.664	HEK 293F transient	Lectin + SEC + F105 negative selection + SEC [366]	6	His-tagged construct, provided by Dr Shailendra Kumar Sharma (The Scripps Research Institute)
BG505 SOSIP.664	CHO stable	2G12 + SEC	7	Provided by Dr Albert Cupo/Prof. John Moore (Weill Cornell Medical University)
BG505 SOSIP.v4.1-GT1	CHO stable	2G12 + SEC	7	Provided by Dr Albert Cupo/Prof. John Moore (Weill Cornell Medical University)

[a]HEK 293T, adherent human embryonic kidney cell line; HEK 293F, suspension human embryonic kidney cell line; CHO, Chinese hamster ovary cell line; stable, expression in a stable cell line; transient, transient expression.

[b]2G12, 2G12 affinity chromatography; SEC, size-exclusion chromatography; PGT151, PGT151-affinity chromatography; lectin, *Galanthus nivalis* lectin-affinity chromatography; F105 negative selection, negative selection by F105-affinity chromatography.

[c]Weill Cornell Medical University in NY, USA; King's College London in London, UK; The Scripps Research Institute in CA, USA.

2.3.1 Recombinant protein expression in HEK 293 and CHO cells

Recombinant BG505 envelope constructs as well as bNAbs were expressed transiently from human embryonic kidney (HEK) 293F suspension cell cultures in FreeStyle Expression Medium grown to a concentration of $1x10^6$ cells/ml. For transfection of a 200 ml culture, 200 µl FreeStyle Max transfection reagent and a total of 200 µg DNA were incubated in 10 ml serum-free OptiPro medium for 15 min. Trimeric BG505 SOSIP.664 constructs were transfected in a ratio of 4:1 of envelope DNA:furin DNA. Plasmids transcribing the light chain and the heavy chain of antibodies were transfected in a 3:1 ratio. The transfection mixture was then added to the 200 ml culture of HEK 293F cells and maintained shaking at 37 °C and 5 % CO_2. Cultures were incubated for 5–7 days, following which culture media were harvested, clarified by centrifugation (2000 *g* for 5 min) and sterile filtered through a 0.22 µm membrane. Recombinant protein-containing supernatants were then subjected to protein purification.

Stable HEK 293T and Chinese hamster ovary (CHO) Flp-In cell lines expressing both furin and envelope [424] were used for the production of BG505 SOSIP.664 and BG505 SOSIP.v4.1-GT1 (Table 2.1; performed by Dr Albert Cupo/Prof. John Moore, Weill Cornell Medical University).

2.3.2 Protein A chromatography

BNAbs used for neutralization experiments and in order to make 2G12- and PGT151-affinity columns were purified using a 5 ml HiTrap Protein A affinity column, according to the manufacturer's instructions. A 20 mM sodium phosphate buffer (pH 7.5), was used for equilibration and washing after sample loading. The antibody was eluted using a 0.1 M citric acid buffer (pH 3). The pH was immediately neutralized by the addition of an appropriate amount of 1 M Tris-HCl buffer (pH 9.0).

2.3.3 2G12- and PGT151-affinity purification

Recombinant envelope constructs were purified on either 2G12- or PGT151- affinity columns (Table 2.1). Affinity columns were made by coupling purified 2G12 or PGT151 antibodies, respectively, to

a cyanogen bromide (CNBr)-activated Sepharose 4B resin, according to the manufacturer's instructions and as previously described [205,238]. The filtered cell culture supernatant was passed through the column at a flow rate of 1 ml/min, the beads were washed with binding buffer (20 mM Tris-HCl, 500 mM NaCl, pH 8.0) and the Env proteins were eluted with 3 M $MgCl_2$ (pH 7.2). Eluted proteins were immediately buffer exchanged into 10 mM Tris-HCl, 75 mM NaCl (pH 8.0) and concentrated using 50 kDa cut-off Vivaspin columns.

2.3.4 Size-exclusion chromatography

Following affinity purification, monomeric gp120, trimeric envelope constructs and IgG antibodies were purified by SEC on an ÄKTA Start chromatography system running Unicorn 1.0 software (both GE Healthcare). A Superdex 200 prep grade column was used, pre-equilibrated with phosphate-buffered saline (PBS). The presence of protein was continuously monitored using absorbance at a wavelength of 280 nm. Fractions were collected and analyzed by Coomassie-stained sodium dodecyl sulfate-polyacrylamide gel electrophoresis (SDS-PAGE; monomers and antibodies) or Native-PAGE (trimers). Electrophoreses were carried out according to the manufacturer's instructions using respective buffers and standards. Fractions containing the target protein were pooled and concentrated. Protein concentrations were determined using a Nanodrop 1000 spectrophotometer.

2.4 Analysis of overall glycan profiles and compositions

2.4.1 In-gel release of N-linked glycans

N-linked glycans were enzymatically released from Env glycoproteins via in-gel digestion. Purified proteins were fractionated by reducing SDS-PAGE (addition of DL-Dithiothreitol; DTT) or by Native-PAGE and stained with Coomassie Blue. Following destaining, the bands corresponding to the trimeric protein (Native-PAGE) or $gp41_{ECTO}$ and gp120 (reducing SDS-PAGE) were excised and washed five times, alternating between acetonitrile and water. The proteins in the gel bands were

then digested *in situ* with Peptide-N-Glycosidase F (PNGase F), at 37 °C for 16 h, according to the manufacturer's instructions. The released glycans were extracted from the gel by washing with water, dried down in a SpeedVac concentrator and then either fluorescently labeled or subjected to ion mobility-electrospray mass spectrometry (IM-ESI MS).

2.4.2 Fluorescent labeling of N-linked glycans and HILIC-UPLC

Released glycans were fluorescently labeled with 2-aminobenzoic acid (2-AA). The labeling mixture comprises 30 mg/ml 2-AA and 45 mg/ml cyanoborohydride dissolved in a solution of 4 % w/v sodium acetate trihydrate, 2 % w/v boric acid in methanol. 80 µl of the labeling mixture was added to every glycan sample (dissolved in 30 µl water), vortexed and incubated at 80 °C for 1 h. Excess label was removed using Spe-ed Amide 2 cartridges, as described before [425]. The 2-AA labeled glycans were separated by hydrophilic interaction chromatography-ultra performance liquid chromatography (HILIC-UPLC) using a 2.1 mm x 10 mm Acquity BEH glycan column (1.7 µm particle size, Waters, Elstree, UK) in a Waters Acquity UPLC instrument. Glycans were separated by running the following gradient: time = 0 min (t = 0): 22 % A, 78 % B (flow rate 0.5 ml/min); t = 38.5: 44.1 % A, 55.9 % B (0.5 ml/min); t = 39.5: 100 % A, 0 % B (0.25 ml/min); t = 44.5: 100 % A, 0 % B; t = 46.5: 22 % A, 78 % B (0.25 ml/min), t = 46.6: 22 % A, 22 % B (0.5 ml/min), where solvent A was 50 mM ammonium formate (pH 4.4) and solvent B was acetonitrile. Fluorescence measuring occurred at an excitation wavelength of 250 nm and a detection wavelength of 428 nm. Empower 3 software was used for data processing.

2.4.3 Glycosidase digestion of released glycans

Digestion of released glycans with Endoglycosidase H (Endo H) was employed to measure the abundance of oligomannose-type (and hybrid-type) glycans. The 2-AA labeled glycans were resuspended in water and digested with Endo H for 16 h at 37 °C, according to the manufacturer's instructions, then extracted using a PVDF protein-binding membrane plate, again according to the manufacturer's instructions, and finally analyzed by HILIC-UPLC (Section 2.4.2). The relative

abundances of oligomannose-type glycans were determined by integrating the chromatograms with or without Endo H, following normalization.

Exoglycosidase digestions for glycan sequencing was performed in the same way using the following enzymes: Neuraminidase from *Clostridium perfringens*, β1,4-galactosidase from *Streptococcus pneumonia* (E-BG07; QA Bio, CA, USA), α-L-fucosidase from bovine kidney (F5884; Sigma-Aldrich), β-*N*-acetylglucosaminidase from *S. pneumonia* (E-GL01; QA Bio) and α-mannosidase from Jack bean (E-AM01; QA Bio).

2.4.4 Tandem ion mobility ESI MS analysis of released N-linked glycans

The total pool of released glycans from Env glycoproteins was analyzed using ion mobility MS. These results were the basis for the creation of a glycan library that was then used for the subsequent site-specific N-glycosylation analyses. Glycan samples were desalted with a Nafion membrane for 2 h, as described elsewhere [426]. They were then dissolved in a solution of methanol-water (1:1; vol/vol) containing 100 mM ammonium phosphate. Negative ion mass, collision-induced dissociation (CID) and ion mobility spectra were recorded with a Waters Synapt G2Si mass spectrometer (Waters Corp., MA, USA) fitted with a nano-electrospray ion source. Samples were infused through Waters thin-wall nanospray capillaries. The instrument was set up as follows: Electrospray capillary voltage: 1.2 kV; cone voltage: 150 V; ion source temperature: 80 °C; ion mobility gas (nitrogen) flow: 80 mL/min; T-wave velocity: 450 m/sec; T-wave peak height: 40 V; trap DC bias: 60 V. CID fragmentation was performed after mobility separation in the transfer cell with argon as the collision gas. The collision cell voltage (60-130 V) was adjusted according to the parent ion mass to give an even distribution of fragment ions across the mass range. The instrument was externally mass-calibrated with glucose oligomers (Glc_{2-13}) from dextran (*Leuconostoc mesenteroides*). Samples were digested with α-neuraminidase from *C. perfringens* if needed. Data acquisition and processing were carried out using the Waters Driftscope (version 2.8) software and MassLynx™ (version 4.1). Spectra were interpreted as described previously [427-430].

2.5 Site-specific glycosylation analysis

2.5.1 Proteolytic digestion of BG505 SOSIP.664 and glycopeptide enrichment

A 100-300 µg sample of Env glycoprotein in 50 mM Tris/HCl, 6 M Urea, pH 8.0 was used for proteolytic digestions. A final concentration of 5 mM of DTT was added during a 1 h incubation at 50 °C, followed by addition of 20 mM iodacetamide (IAA), for a further 1 h at RT in the dark. Any residual IAA was neutralized by adding 20 mM DTT for 1 h at RT. The protein was then buffer exchanged into 50 mM Tris/HCl (pH 8.0) using Vivaspin filters and digested with either trypsin, chymotrypsin or GluC (Mass Spectrometry Grade, Promega) or Pronase (Roche, Basel, Switzerland) at a ratio of 1:30 (w/w), according to the manufacturer's instructions. Combinations of proteases and sequential digests were also employed (specified in the relevant sections). Protease-digested samples were enriched for glycopeptides by using the ProteoExtract Glycopeptide Enrichment Kit, according to the manufacturer's instructions and dried down in a SpeedVac concentrator. Glycopeptides were then either directly analyzed by liquid chromatography-electrospray mass spectrometry (LC-ESI MS) or fractionated by RP-HPLC and subjected to Matrix-assisted laser desorption/ionization-time of flight mass spectrometry (MALDI-TOF MS).

Additionally, deglycosylated Env samples were prepared by digestion of tryptic and chymotryptic (non-glycopeptide enriched) peptides with Endo H (4 h, 37 °C), followed by digestion with PNGase F (4 h, 37 °C), according to the manufacturer's instructions. The processing state of the glycan site was then classified according to its susceptibility to Endo H and PNGase F. The basis of this assignment method is that Endo H cleaves oligomannose- and hybrid-type glycans but leaves a single GlcNAc moiety that is not removed by the subsequent PNGase F digestion (leads to deamidation at sites with complex-type glycans). Unoccupied PNGSs remain as unmodified asparagines. Deamidation of asparagines can also occur spontaneously as a non-enzymatic reaction in proteins and peptides [431], making this method unsuitable for exact quantifications. The information gained by this type of analysis is, however, sufficient for glycan classification into broad processing states.

2.5.2 RP-HPLC fractionation of tryptic glycopeptides

Glycopeptides were resuspended in PBS buffer and fractionated by RP-HPLC using a Jupiter C18 5 µm 250 x 4.5 mm column (300 Å, Phenomenex, CA, USA) and a Dionex U3000 LC system. The following gradient was run at a flow rate of 1 ml/min: time = 0 min (*t* = 0): 95 % A, 5 % B; *t* = 5: 95 % A, 5 % B; *t* = 90: 10 % A, 90 % B; *t* = 95: 10 % A, 90 % B; *t* = 97: 95 % A, 5 % B, where solvent A was 10 mM ammonium formate, pH 4.4 and solvent B was 10 mM ammonium formate in 80 % acetonitrile. Fractions were collected every minute for 90 min, dried down using a SpeedVac concentrator and resuspended in 20 mM $NaHCO_3$ buffer.

2.5.3 MALDI-TOF MS analysis of glycopeptides

Glycopeptide fractions were divided into two equal fractions. One half was directly analyzed by MALDI-TOF MS, whereas the other was deglycosylated using PNGase F, according to the manufacturer's instructions. Samples were desalted employing C18 Ziptips according to the manufacturer's instructions and then spotted onto a ground steel target plate in 2,5-dihydrobenzoic acid (DHB, 10 mg/ml in 50 % acetonitrile) matrix. MALDI-TOF MS was performed using an Autoflex™ Speed MALDI-TOF(/TOF) instrument (Bruker, Coventry, USA), operated in positive ion mode. Tandem MS (MS/MS) was performed on both glycopeptides and peptides to confirm peptide identity. In cases where the same peptide eluted in more than one fraction, the relevant fractions were pooled and re-analyzed. Acquired data were processed using DataAnalysis 3 software (Bruker). After baseline subtraction, a signal-to-noise ratio cut-off of 3 was applied. Peptides were manually identified by a combination of two approaches. MALDI-TOF MS/MS data were examined for the presence of characteristic glycopeptide fragment ions such as, for example, the $^{0,2}X$ ion $[M_{peptide}+83+H]^+$ or the Y1-ion $[M_{peptide}+203+H]^+$, which then enabled the mass of the peptide portion to be calculated [432]. In addition, MS and MS/MS data of the corresponding deglycosylated peptide-containing fractions were included in the peptide identification process. The following peptide modifications were considered: Carbamidomethylation of cysteine, oxidation of methionine, N-terminal Pyro-Glu conversion and deamidation of asparagine, as well

as sodium and potassium adducts. As a next step, the glycopeptide spectra were screened for plausible glycopeptide compositions based on the mass of the peptide portion and the generated glycan library. The relative abundance of different glycoforms on each peptide was determined by integrating the intensity of all isotopic peaks, and relating this value to the sum of the intensities of all identified glycoforms.

2.5.4 LC-ESI MS and MS/MS analysis of glycopeptides

Enriched glycopeptides were analyzed on a Q Exactive Orbitrap mass spectrometer (Thermo Fisher Scientific) and glycopeptides were desalted using a Dionex UltiMate 300 RS pump with Acclaim PepMap C18 300 µm ID x 5 mm trap at room temperature (RT). A flow rate of 12 µL/min was used for 4 min using 0.05 % trifluoroacetic acid (TFA) in water as the desalting buffer. Desalted peptides were separated using a Dionex UltiMate3000 RSLCnano pump with a 75 µm ID x 500 mm analytical column at 50 °C. A flow rate of 250 nl/min was used and peptides were eluted using a 2 h linear gradient of 4 % to 40 % buffer B over 120 min. Buffer A was 0.1 % formic acid in water and buffer B was 0.1 % formic acid in acetonitrile. MS data were acquired with XCalibur 3.0.63 (Thermo Fisher Scientific). A Top10 data dependent acquisition method was used. This method allows the selection, fragmentation and detection of ten precursors in a duty cycle time of 1.42 s. Higher energy collisional dissociation (HCD) fragmentation of glycopeptides was performed and led to the generation of low-molecular-weight oxonium ions, peptide fragmentation ions (predominantly y- and b-ions) and B- and Y-type fragmentation of glycosidic linkages ([433]; Appendix B). Data analysis and glycopeptide identification were performed using Byonic™ (Version 2.7) and Byologic™ software (Version 2.3; Protein Metrics Inc., CA, USA). First, acquired tandem MS spectra were analyzed with Byonic, considering the same peptide modifications as for MALDI-TOF MS analysis, a precursor mass tolerance of 4 ppm, a fragment mass tolerance of 10 ppm and two missed cleavages. For tryptic-digested samples, semi-tryptic cleavages were allowed. Chymotrypsin digestions were specified by C-terminal cleavage of Tyr, Phe, Trp, Leu and Met and GluC digestions by C-terminal cleavage of Asp and Glu. Unspecific searches were carried out in the case of pronase

digestions. The personalized glycan library was used in order to identify the compositions of glycosylated peptides. Byologic was then used for further data processing including relative quantification. Fragmentation spectra of identified glycopeptides were manually verified. The abundance of individual glycoforms was determined by adding up the intensities of the extracted-ion chromatograms (XICs) over all charge states. Relative abundance = [Intensity of one glycoform] / [Intensities of all glycoforms identified on the same peptide].

2.5.5 Site-specific O-glycosylation analysis

The presence and abundance of O-glycosylation was assessed by using Byonic™ and Byologic™ software to analyze LC-ESI MS spectra derived from tryptic-digested (not glycopeptide-enriched), deglycosylated Env, searching for the most common human O-glycans. Any exact mass matches of O-glycosylated peptides were manually confirmed by seeking the characteristic oxonium ions, as well as peptide fragmentation ions, among the HCD fragmentation data. The relative abundances of individual O-glycoforms and the corresponding unmodified peptide were determined by summing the intensities of the XICs over all charge states. Relative abundance = [Intensity of one glycoform] / [Intensities of all glycoforms identified on the same peptide].

2.6 Env-pseudovirus production and neutralization assays

Env-pseudoviruses and corresponding neutralization assays were performed by Dr Katie Doores (King's College London). To produce single round replication Env-pseudoviruses capable of single-cycle replication, HEK 293T cells were co-transfected (PEI, 1 mg/mL, 1:3 PEI:total DNA, Polysciences) with plasmids encoding Env and an Env-deficient genomic backbone (pSG3ΔEnv, 1:2 ratio). Glycosylation site deletions in the full-length envelope were made by site-directed mutagenesis (Section 2.2.2). Supernatants containing Env-pseudoviruses were harvested 72 h post transfection for use in neutralization assays based on TZM-bl target cells [434,435]. Briefly, a serial diluted antibody was pre-incubated with virus for 1 h at 37 °C in a 96-well, flat bottom plate. TZM-bl cells (20,000 cells/well) were added to the virus/antibody mixture and incubated for 72 h. When

the cells were lysed and luminescence was quantified via addition of Bright-Glo Luciferase substrate (Promega). To determine IC_{50} values, dose-response curves were fitted using nonlinear regression (GraphPad Prism).

3 Quantitative site-specific N-glycosylation analysis

The trimeric HIV-1 envelope glycoprotein is the sole target for bNAbs produced by the immune system during infection and is therefore a focus of vaccine design. In numerous studies, bNAbs provide passive protection from viral challenge to non-human primates [83-89]. Many of these bNAbs recognize epitopes that are wholly or partially composed of glycan structures [68-82]. HIV-1 Env is among the most heavily glycosylated proteins known, with glycans making up ~50 % of its total mass [11]. These abundant glycans have long been considered to shield the trimer from immune surveillance by occluding relatively conserved protein surfaces [61]; while this concept remains valid, it is also now evident that the glycan shield itself can be a target for bNAbs.

Defining the composition and microheterogeneity of individual glycan sites will crucially increase our knowledge of bNAb epitopes and is very important in guiding rational Env immunogen design. However, the site-specific N-glycosylation analysis of the HIV-1 glycan shield is particularly challenging due to the large number of glycans (median of 25 per monomer [230]) on Env. Multiple studies have so far been performed on recombinant monomeric Env [176,181,231,232,436], uncleaved gp140 [235,248,251-255], membrane-associated Env [235], fully cleaved, trimeric Env [256] and virion-derived gp120 [236,250]. These approaches are usually based on glycopeptide analysis by mass spectrometry and typically include protease digestion of the target glycoprotein followed by tandem liquid chromatography-electrospray ionization mass spectrometry (LC-ESI MS) using varying mass analyzers and fragmentation modes.

Glycoproteomics can be challenging due to glycan microheterogeneity and the low proportion of glycopeptides compared to peptides in protease-digested samples accompanied by ion suppression effects [437]. Hence, multiple strategies to enrich complex samples for glycopeptides have been developed. Among them are enrichment by lectin affinity chromatography, hydrazide-capture, boronic acid-based chemistry, graphitized carbon, size-exclusion chromatography and HILIC separation [432,437]. While some of these strategies like

lectin affinity bind to specific glycan structures, methods based on general chemical and physical properties of glycopeptides are more valuable for unbiased enrichments. An example for a powerful, unbiased stationary phase for glycopeptide enrichment zwitterionic-HILIC (ZIC-HILIC), which leads to the separation of compounds based on weak electrostatic interactions between the hydrophilic glycopeptides and the zwitterionic phase [437,438].

The glycan moiety and the peptide backbone of glycopeptides differ in their chemical properties and thus fragment under different conditions in tandem mass spectrometry. The two main fragmentation types to consider in tandem MS experiments are collision-induced dissociation (CID) and electron-transfer dissociation (ETD). CID predominantly leads to glycosidic bond cleavages of the B- and Y-type (nomenclature by Domon and Costello [439]; Appendix B) and also creates characteristic 'reporter' low-molecular-weight oxonium ions (fragment ions originating from the glycan moiety) that can serve as diagnostic ions for glycopeptides (Table B.2). Peptide backbone fragments such as b- and y-type ions are typically of lower abundance but can be increased by the usage of higher collision energies ([433]; Figure B.2). Higher-energy collision dissociation (HCD) fragmentation is a Thermo Orbitrap-specific version of CID, where fragmentation occurs external to the ion trap in an HCD cell, but leads to very similar fragmentation ions.

ETD, on the other hand, selectively creates peptide bond fragments through the transfer of gas-phase electrons from singly charged anions to multiply charged protonated peptides [432]. Peptide backbone fragments are predominantly c' ions and z· radical ions resulting from cleavage of the N-Cα bond and thus allow the determination of the peptide backbone as well as the site of glycosylation (Figure B.2). Therefore, tandem MS experiments using both CID and ETD can accurately assign the glycan moiety and the peptide backbone of a glycopeptide.

MALDI-TOF/TOF MS is also a powerful technique for the analysis of glycopeptides. Unlike electrospray ionization, MALDI solely creates singly charged ions and thus makes spectra interpretation and relative quantitation easier. Fragmentation of N-glycopeptides by MALDI-

TOF/TOF MS leads to a set of cleavages at or near the innermost GlcNAc with all resulting fragment ions retaining the peptide backbone [432]. Among the typically observed fragment ions are a $[M_{peptide}+H-17]^+$, $[M_{peptide}+H]^+$, the $^{0,2}X$ ion $[M_{peptide}+83+H]^+$ and the Y1-ion $[M_{peptide}+203+H]^+$, which enable the determination of the mass of the peptide portion due to very characteristic peak patterns ([432]; Figure B.3).

When determining the microheterogeneity of N-glycosylation sites, it is not only important to identify the individual glycoforms but also to gain information on their relative abundance. In a label-free quantification approach, the abundance of individual glycoforms is assessed by the relative abundance of signal intensities in the mass spectrum compared to other glycoforms attached to the same N-glycosylation site on the same proteolytic peptide. This is rationalized by the fact that ionization (protonation) of glycopeptides occurs on the peptide backbone and not on the glycan moiety. Hence, ionization efficiency of glycopeptides depends on the peptide sequence and mostly not on the type of glycans [440]. A multi-institutional study by the HUPO Human Disease Glycomics/Proteome Initiative generally assessed label-free quantification as reliable, especially for neutral glycans [441].

Although a number of the conducted site-specific glycosylation studies on HIV-1 Env managed to achieve almost full coverage [232,235,236,248,252,253,255], thorough assessment of the abundances of individual glycan structures is generally lacking. In this chapter, the development of a workflow for the semi-quantitative, site-specific glycosylation analysis of recombinant Env is described with the aim to decipher the complexity of the HIV-1 glycan shield. The generation of a protein-specific glycan library by ion mobility mass spectrometry provides the basis for subsequent glycopeptide analysis. Furthermore, glycopeptides are enriched using ZIC-HILIC resin. An orthogonal approach of MALDI-TOF MS and LC-ESI MS serves as an internal validation for the semi-quantification of Env glycopeptides by ion intensities.

3.1 Overview of methodology for site-specific glycosylation analysis

In order to characterize the microheterogeneity of individual N-glycosylation sites of Env glycoproteins, site-specific analysis using a combination of different methods was performed. Figure 3.1 schematically shows the strategy for analysis described in this chapter and employed throughout this thesis.

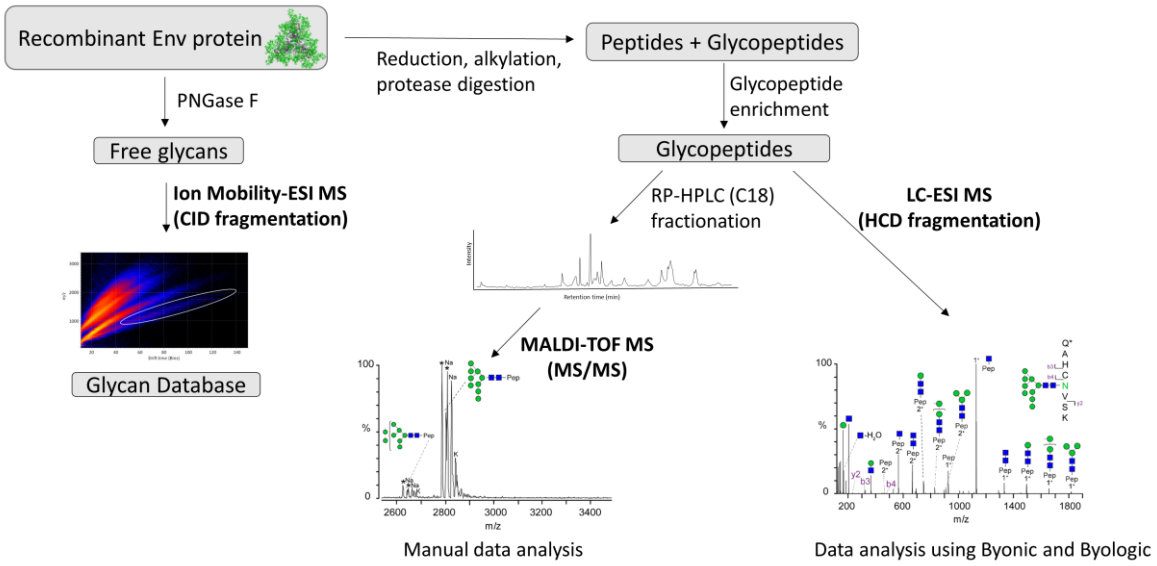

Figure 3.1: Schematic workflow for the validation of site-specific N-glycosylation analysis

In brief, characterization of Env glycoproteins starts by the creation of a protein-specific library of the total glycan pool by ion mobility mass spectrometry. Secondly, the protein is reduced, alkylated and digested with a panel of proteases, enriched for glycopeptides by ZIC-HILIC enrichment and then typically analyzed by LC-ESI MS. The relative abundance of different glycoforms on individual sites was determined using the glycopeptide ion intensities. In order to internally validate this workflow as well as the associated relative quantification of glycopeptides, in this Chapter, glycopeptides were also fractionated by reversed-phase (C18) HPLC and then subjected to MALDI-TOF MS analysis. Interpretation and data analysis of the MALDI-TOF MS spectra was performed manually, whereas Byonic and Byologic software (Proteinmetrics) was employed for data gained by LC-ESI MS. The glycan library was the basis for both approaches and helped to

lower the false discovery rate by only searching for the glycoforms that are actually present. Sections 3.2 and 3.3 will describe these steps individually.

The results presented in this chapter originate from the analysis of the native-like trimer BG505 SOSIP.664 (Figure 1.4C; amino acid sequence in Appendix A), recombinantly produced in HEK 293T (Table 2.1). The biological interpretation of the site-specific analysis of BG505 SOSIP.664 as well as the relation of the results to glycan deletion mutants and BG505 pseudovirus neutralization studies will be the focus of Chapter 4.

3.2 A glycan library generated by ion mobility mass spectrometry

To probe the glycan shield of HIV-1 in great detail, enzymatically released glycans from recombinant Env proteins were analyzed using ion mobility mass spectrometry with the help of Prof. David Harvey (University of Oxford) (Section 2.4.4). IM-ESI MS can be a valuable tool for the separation of glycan isomers as well as for cleaning up MS profiles from possible contaminants, thus being suitable for the analysis of low abundant samples [442,443]. Fragmentation of negative ions, which creates predominantly C-type glycosidic cleavages, A-type cross ring cleavages and D-ions (likely formed by C_{R-1}/Z cleavages), was used to assign structures and linkages of identified glycans (nomenclature by Domon and Costello [439] with an extension by Harvey [427,428,444]; Appendix B). Figure 3.2 shows negative ion electrospray spectra of unlabeled N-glycans released from the gp120 and gp41 subunits of BG505 SOSIP.664. Trimers were produced from a stable HEK 293T cell line and purified by 2G12-affinity chromatography, followed by SEC (Section 2.3) and provided by Prof. John Moore (Weill Cornell Medical University). In total, 52 and 59 structures (plus some isobaric glycans) were identified on gp120 and gp41, respectively (Appendix D). The compositions of the glycans were translated into a software-specific database (Byonic, Proteinmetrics) and thus provided the basis for LC-ESI MS analysis of corresponding glycopeptide spectra (Section 2.5.4).

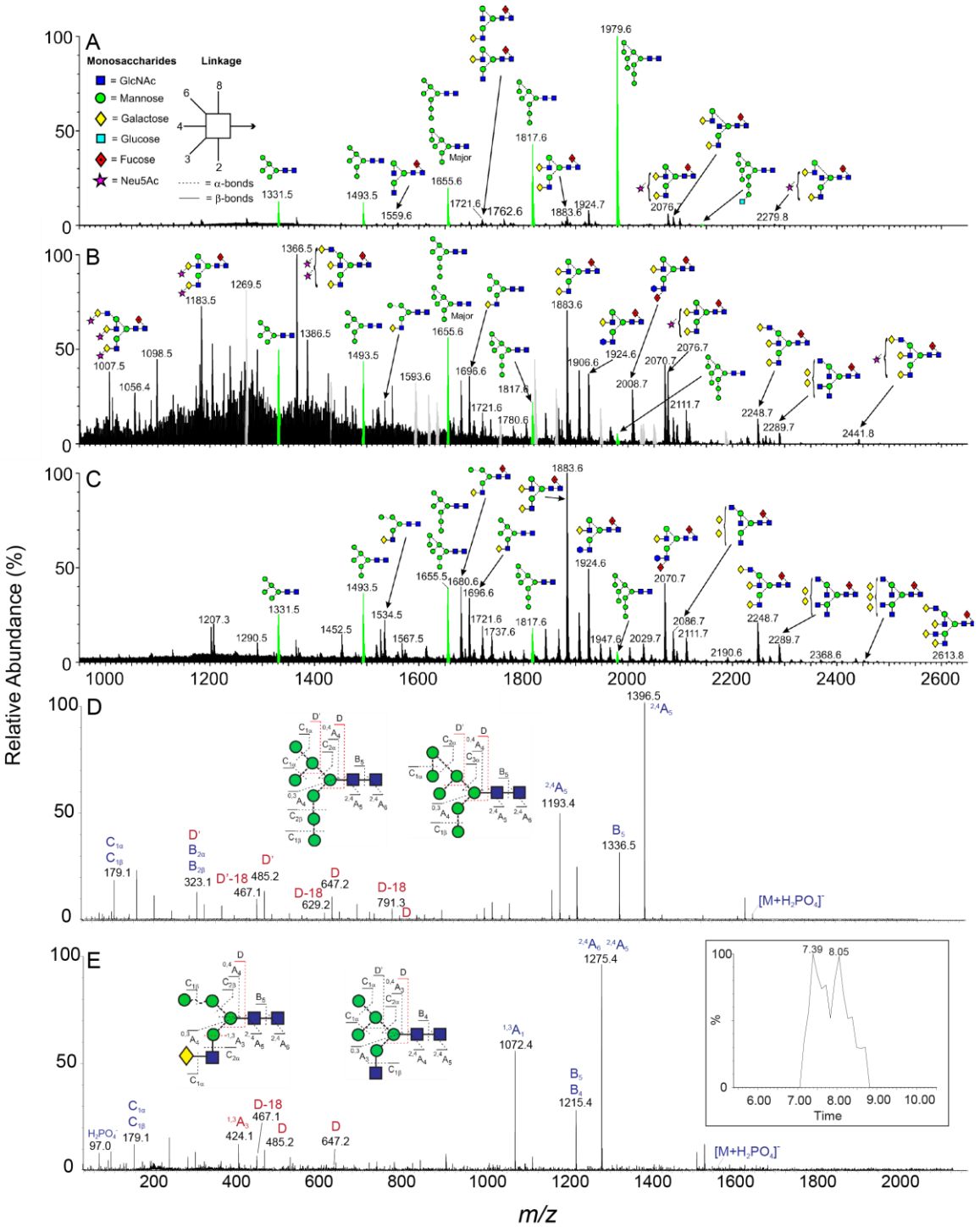

Figure 3.2: Negative ion electrospray spectra of N-glycans released from BG505 SOSIP.664 trimers
BG505 SOSIP.664 trimers (stable HEK 293T cell line). Negative ion MS spectra of gp120 glycans (A), $gp41_{ECTO}$ glycans (B) and mobility-extracted singly charged negative ions from desialylated $gp41_{ECTO}$ glycans (C). (D and E) Collision-induced dissociation spectra for two isobaric glycans derived from the transfer region of the Synapt G2Si instrument. The insets show the corresponding glycans as well as the numbering of the fragments. The numbering scheme follows that proposed elsewhere [439,444]. Fragments used to differentiate the two underlying structures are labeled in red. The inset in panel E shows the chromatographic separation of the two structures after ion mobility-extraction. Symbols are as explained in (A). The complete glycan library can be found in Appendix D.

3.3 Semi-quantification of glycopeptides by MALDI-TOF MS and LC-ESI MS

To assess the glycan microheterogeneity of recombinant Env glycoproteins in a site-specific way, sample preparation involves reduction, alkylation of cysteines with iodacetamide and in-solution digestion with one or more proteases into peptides and glycopeptides (Section 2.5.1). For reasons explained in the beginning of this chapter, the sample was then enriched for glycopeptides by ZIC-HILIC enrichment (Glycopeptide Enrichment Kit, Millipore). To test the efficiency of the glycopeptide enrichment and also whether there is a possible bias towards certain glycoforms, a trypsin-digested Env BG505 SOSIP.664 sample was analyzed before and after the enrichment. First, the samples were analyzed on an AmaZon Speed instrument (Bruker) in collaboration with Ludger Ltd. The base peak chromatogram of the post-enrichment sample shows the disappearance of peaks compared to the non-enriched sample (Figure 3.3A) indicating selective binding of glycopeptides to the ZIC-HILIC resin. The signal intensity, however, is significantly lower for the post-enrichment sample. Thus, it appears that a certain amount of glycopeptides was lost during the enrichment process. In Figure 3.3B, the comparison of the total 2-AA labeled glycan profiles (Section 2.4.2) of both samples shows almost no visible difference between the spectra. To summarize, although the glycopeptide enrichment of BG505 SOSIP.664 leads to a certain amount of sample loss, is does not show any obvious bias towards distinct glycoforms.

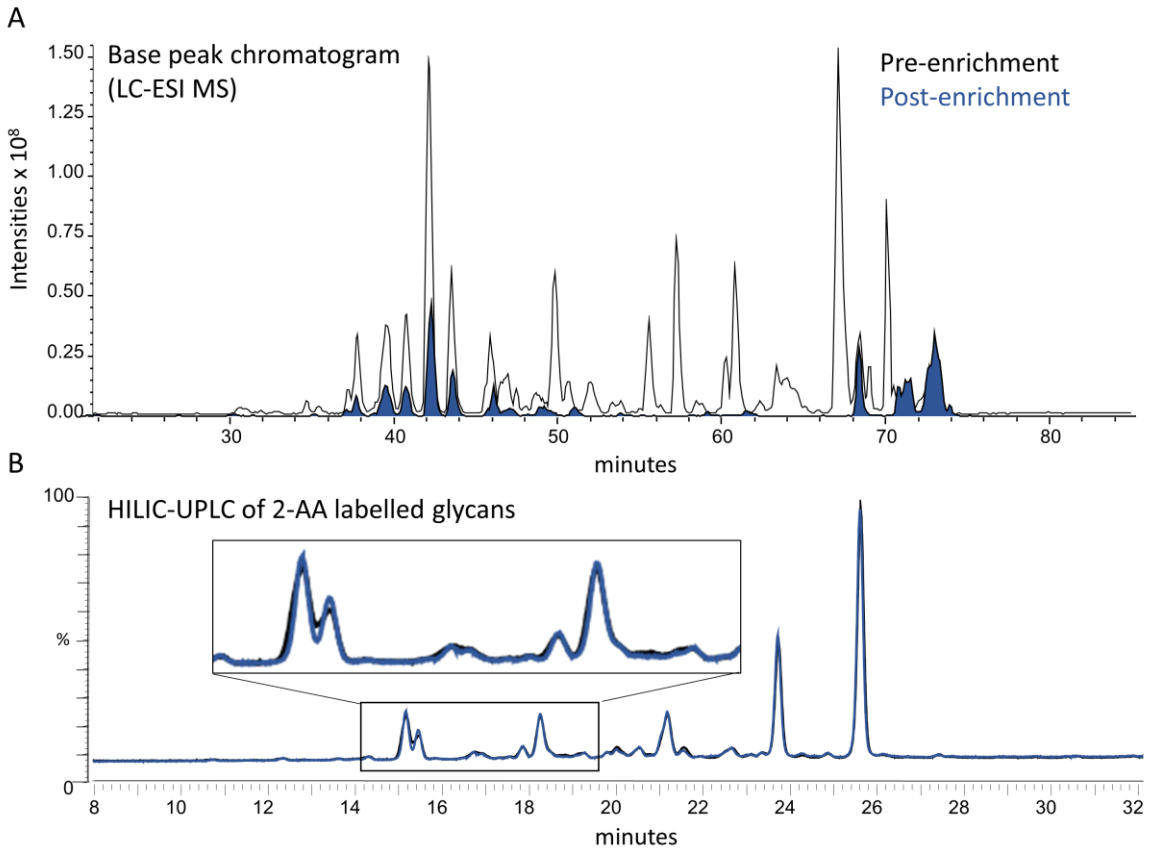

Figure 3.3: Assessment of glycopeptide enrichment
Reduced, alkylated and trypsin-digested BG505 SOSIP.664, produced in stable HEK 293T cells and purified by 2G12-affinity chromatography and SEC, was analyzed before (black) and after (blue) glycopeptide enrichment. (A) Base peak chromatograms of samples loaded onto a Thermo PepMap RSLC C18 column acquired using an AmaZon Speed instrument (in collaboration with Ludger Ltd., Abington, UK). Gradient from 2 % to 55 % acetonitrile over 90 min at a flow rate of 350 µl/min, with formic acid as the aqueous solvent. (B) HILIC-UPLC profiles of PNGase F-released and fluorescently labeled glycans from the same samples. Insets shows magnification of indicated area of chromatogram.

To quantify and specify the locations of glycoforms, a parallel mass spectrometric-approach exploiting two different ionization modes was used. In one strategy, glycopeptides from BG505 SOSIP.664 trimers generated by trypsin and chymotrypsin digestion, were first fractionated by RP-HPLC and then analyzed by MALDI-TOF MS (Section 2.5.3). A small portion of the RP-HPLC fractions was deglycosylated and analyzed by MALDI-TOF MS as well, thus facilitating the assignment of the peptide portion. Figure 3.4 shows an exemplary MALDI-TOF MS and fragmentation spectrum of the N276-containing tryptic peptide. For the quantification of relative glycoform abundances, protonated, as well as sodium and potassium adducts were included.

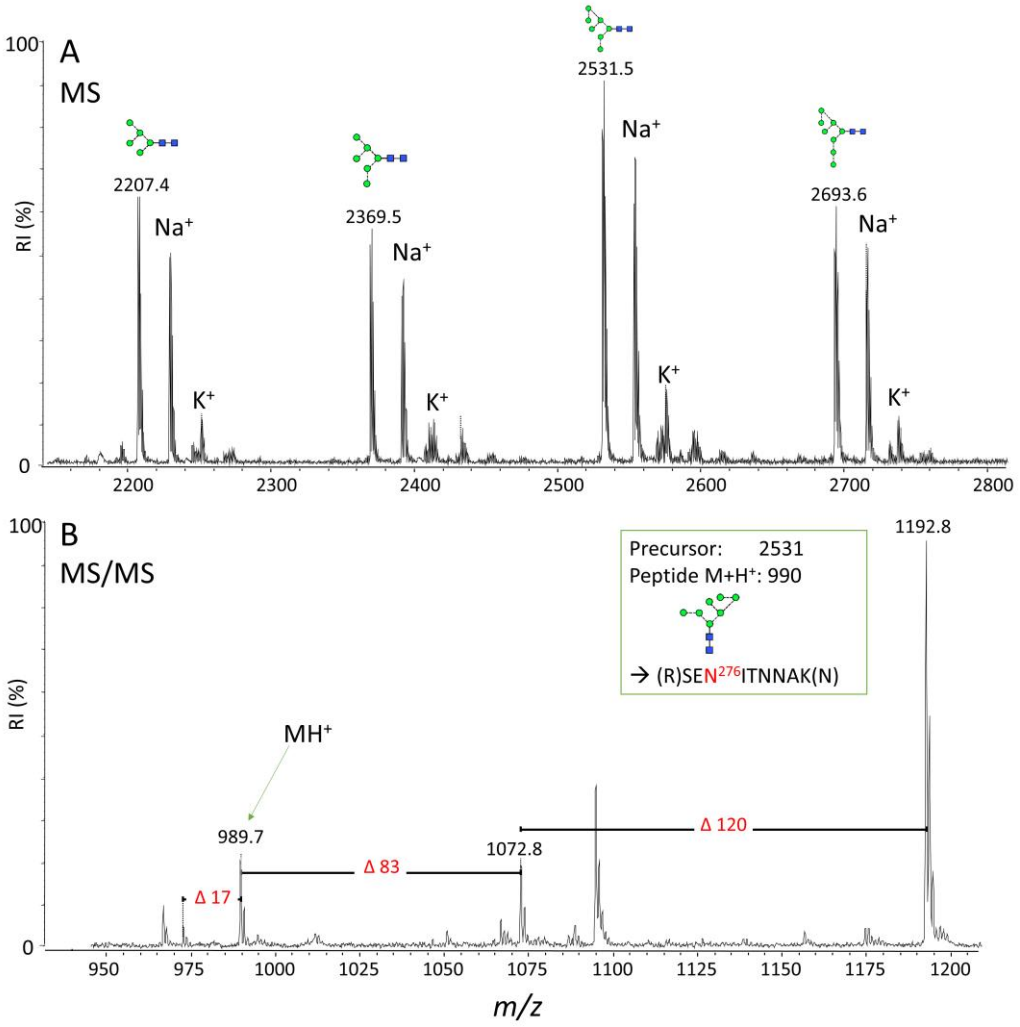

Figure 3.4: MALDI-TOF MS and MS/MS spectra of Asn276-glycan site of BG505 SOSIP.664
Trypsin-digested BG505 SOSIP.664 was fractionated by RP-HPLC and subjected to MALDI-TOF analysis using a Bruker Autoflex instrument in positive mode. (A) MALDI-TOF MS fraction 6 showing the oligomannose-type glycans of the N276-containing peptide SENITNNAK (HXB2 numbering, see Appendix A). Glycan structures corresponding to the observed glycopeptide masses are indicated and sodium (Na^+) and potassium (K^+) adducts are labeled. (B) MALDI-TOF MS/MS fragmentation spectrum of the *m/z* 2531 precursor glycopeptide. The characteristic glycan mass differences observed in MALDI-TOF glycopeptide fragmentations are indicated. RI, relative intensity.

In total, 11 of 28 glycan sites (for protein sequence of BG505 SOSIP.664, see Appendix A) could be isolated and quantified by assessment of the ion abundance by MALDI-TOF mass spectrometry; Figure 3.5 summarizes the identified glycan profiles (for peak lists, see Appendix E). Glycans are grouped as described in Appendix C. Briefly, the grouping is based on the number of residues within the oligomannose series (M) or the number of antennae (A) with and without core fucose (F) in a complex-type glycan.

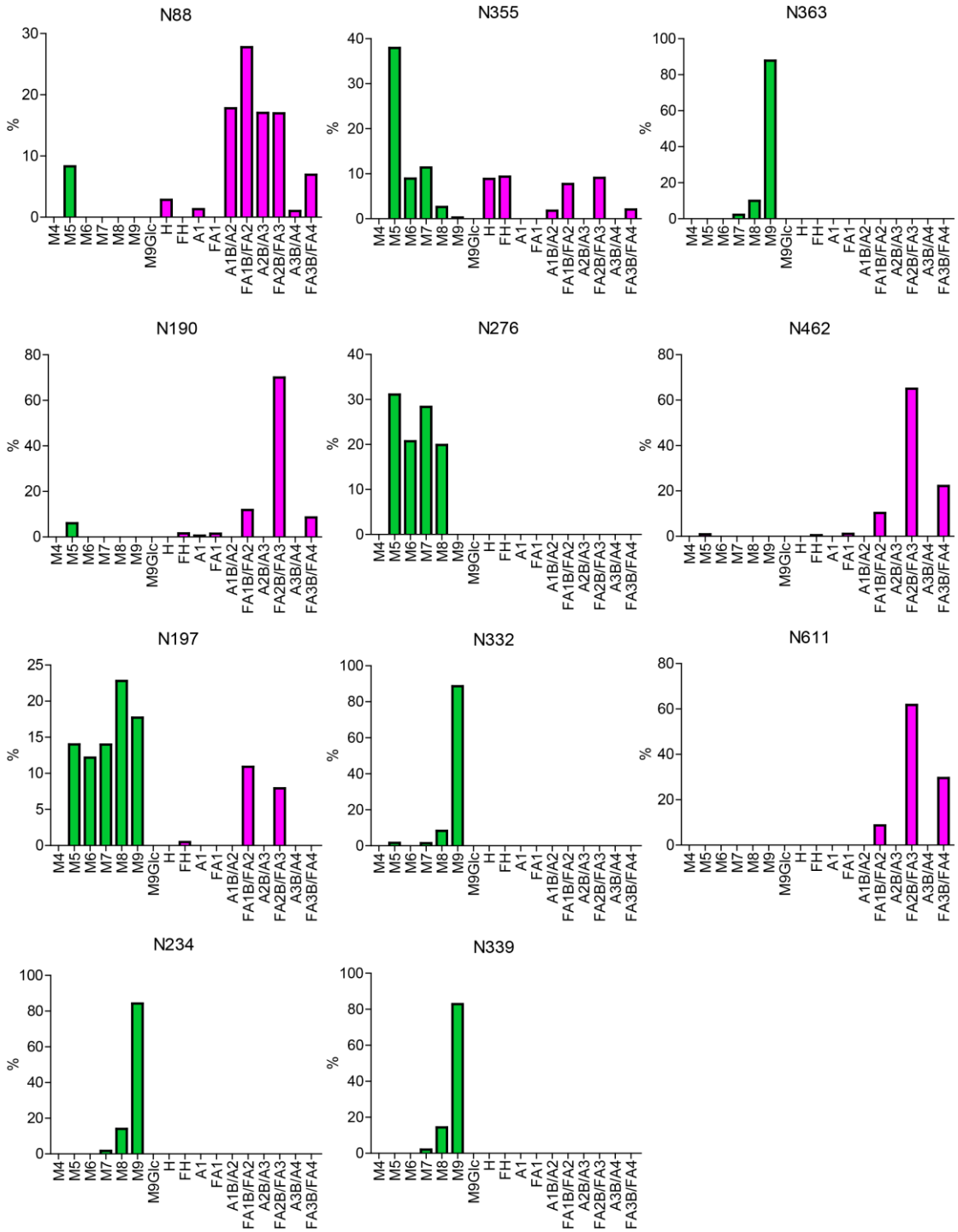

Figure 3.5: Relative quantification of N-glycosylation sites on BG505 SOSIP.664 trimers identified by MALDI-TOF MS

BG505 SOSIP.664 trimers were reduced, alkylated, digested with trypsin and then fractionated by RP-HPLC. Fractions were analyzed by MALDI-TOF MS and MS/MS in positive mode. In cases where glycopeptides eluted over more than one fraction, the relevant fractions were pooled and reanalyzed. The microheterogeneity at individual N-glycosylation sites was quantified in the following way: [Sum of areas of isotopic peaks of one glycoform] / [sum of areas of isotopic peaks of all glycoforms] x 100. The abundances of individual hybrid- and complex-type glycan species have been combined according to Appendix C. Green: oligomannose-type glycans; pink: hybrid- and complex-type glycans. Information on the peak lists corresponding to these data including intensities can be found in Appendix E.

In an alternative approach, the total pool of trypsin- and chymotrypsin-digested glycopeptides was analyzed by in-line LC-ESI MS using a Q Exactive Orbitrap mass spectrometer with HCD fragmentation (Section 2.5.4). Here again, the relative abundance of each specific glycan structure was determined by summing the ion-intensity of the corresponding glycopeptide over all identified charge states. Figure 3.6 shows the MALDI-TOF and LC-ESI MS/MS spectra of a tryptic peptide containing the N332 site. The quantifications displayed in Figure 3.6B and D give very similar results, both identifying $Man_9GlcNAc_2$ as the most prominent structure with more than 80 % abundance.

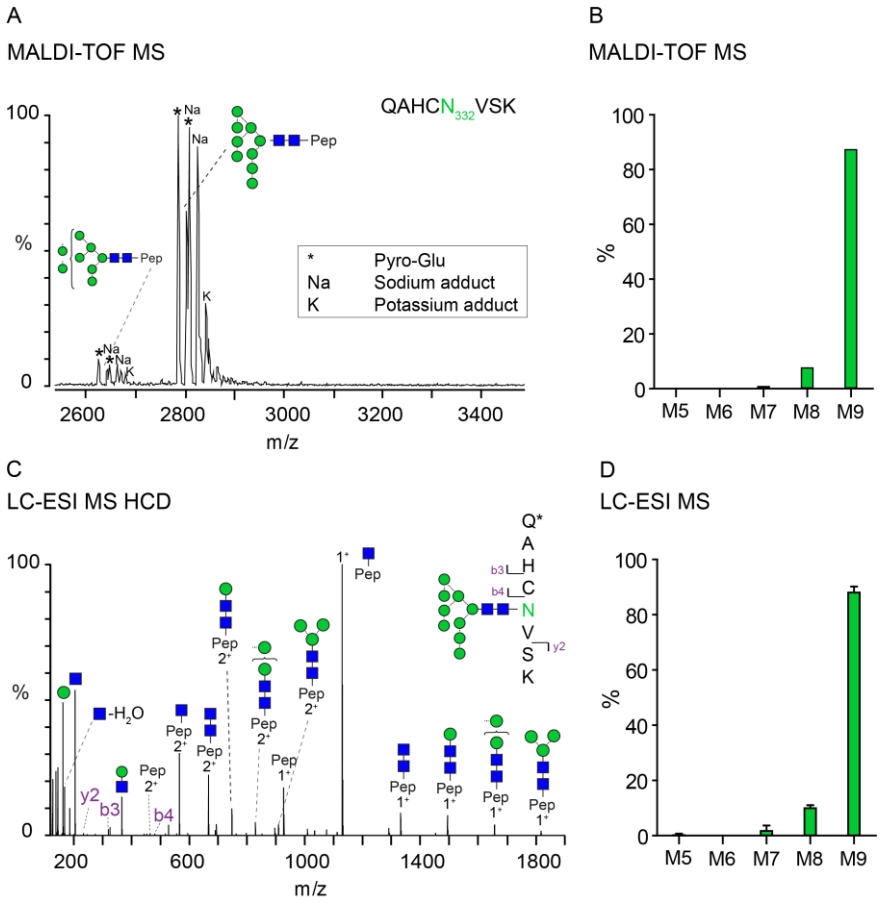

Figure 3.6: MALDI-TOF and LC-ESI MS HCD data and quantification for the N332 site
(A) MALDI-TOF MS spectrum of a tryptic glycopeptide containing N332. Observed modifications are indicated in the box and highlighted in the spectrum. (B) Quantification of peak areas observed in the MALDI-TOF spectrum. (C) LC-ESI MS HCD fragmentation of the same tryptic peptide containing N332. (D) Quantification of ion intensities for glycoforms identified for N332 and analyzed by LC-ESI MS. The error bars represent the standard error of the mean of four analytical replicates.

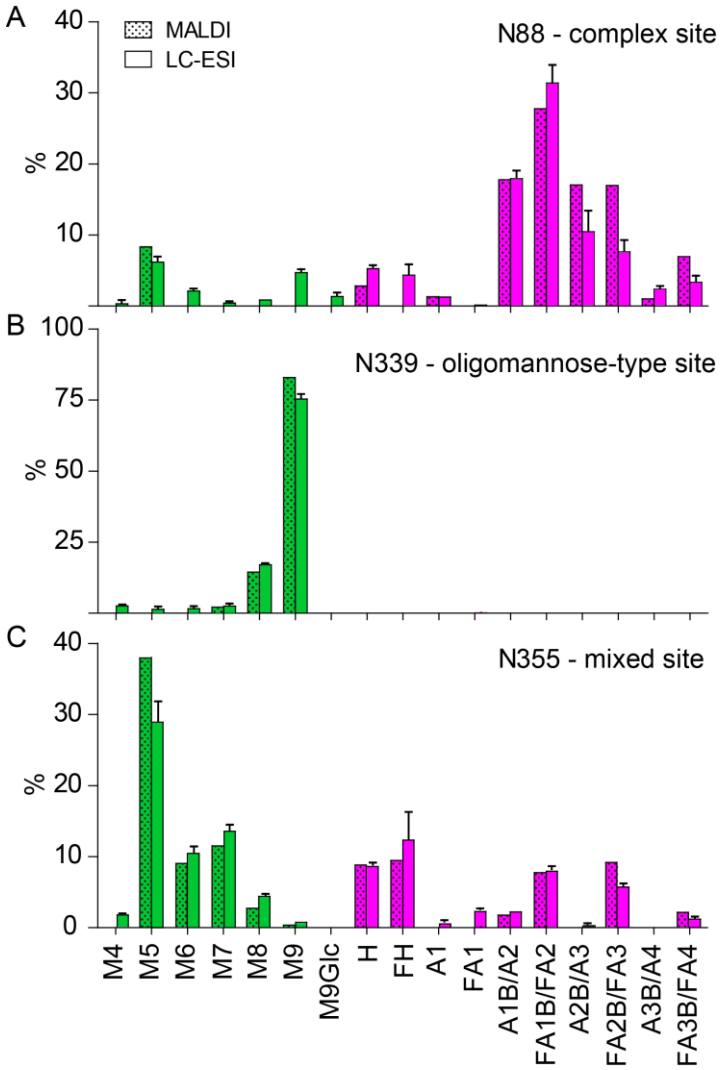

Figure 3.7: Comparison of glycan abundances determined by MALDI-TOF MS and LC-ESI MS. (A-C) Side-by-side bar graph representation of the relative glycan abundances determined by MALDI-TOF MS and LC-ESI MS for three representative sites identified by trypsin digests. Shown are examples of N-glycosylation sites dominated by complex-type glycans (pink; N88), oligomannose glycans (green; N339) or a mixture of structures (N355). Repeats (n=2) of the LC-MS ESI analysis were performed and the standard error of the mean is indicated on the bar graphs. Glycans were grouped as shown in Appendix C and quantified by summing up ion intensities. For information on peak lists, see Appendix E.

Relative quantification of glycopeptides has been validated previously, albeit using simpler targets [440]. Nevertheless, the complementary analytical approaches enabled an additional validation of the relative quantification. The glycan compositions derived by the two methods are compared in Figure 3.7, which shows three representative N-glycosylation sites corresponding to those dominated by oligomannose-structures, complex-type structures, or a mixed population of both glycan classes. The two datasets are highly concordant, indicating that each method reliably

captures the processing state of an isolated glycosylation site. Using the glycan database generated by the ion mobility MS of released glycans (Figure 3.2), analysis of the LC-ESI MS data allowed 20 of 28 occupied N-linked glycosylation sites on BG505 SOSIP.664 to be characterized in detail. The remaining 8 sites could not be quantified; they were present either on a peptide containing more than one N-glycan (e.g. N133 and N137) or on a glycopeptide that could not be identified with sufficient confidence (e.g. N398 and N625). The latter scenario is likely to be attributable to either incomplete occupancy of the N-glycosylation site, a low ionization efficiency of the peptide, or because the peptide is insufficient retained in the trapping column. The detailed presentation of the quantification results as well as their biological interpretation will be part of Chapter 4.

3.4 Steps towards complete N-glycosylation site coverage

Although analysis of BG505 SOSIP.664 by LC-ESI MS greatly increased the site coverage compared to MALDI-TOF MS (11/28 *vs* 20/28 quantified sites), complete coverage is very desirable. The workflow described here relies on glycopeptides that carry a single N-glycosylation site. Some of the sites on the heavily glycosylated Env cannot be separated by trypsin or chymotrypsin digest. Thus, digestions with GluC (and successive digestion of GluC and trypsin) and pronase were performed. Pronase, in particular, is mixture of nonspecific proteases that was conducive to increase the number of quantified N-glycosylation sites to 25 out of 28. The remaining sites could not successfully be separated by protease digests. In order to at least get an idea about their processing state and to be able to classify them into broad processing states, a successive digestion of non-glycopeptide enriched digests with Endo H followed by PNGase F (as described in Section 2.5.1) was performed. Endo H selectively cleaves oligomannose- and hybrid-type glycans and leaves a single GlcNAc residue attached to the asparagine (with the potential for a fucose substituent in the case of hydrolyzed hybrid-type glycans). The remaining complex-type glycans are removed by PNGase F, which converts asparagine into aspartate upon digestion. This approach does not allow exact quantification of the peptide abundances as deamidation (conversion of N to D) can also

occur spontaneously. It does, however, allow the broad classification into the most abundant processing state, even when present on doubly occupied peptides. Figure 3.8 shows an example of a doubly occupied peptide carrying the N133 (here oligomannose-type) and N137 (here complex-type) glycan sites (for amino acid sequence, see Appendix A) on BG505 SOSIP.664. HCD fragmentation allows the determination of the location of the previously oligomannose-type and complex-type glycan sites, if a sufficient amount of y- and b- peptide backbone fragments is visible.

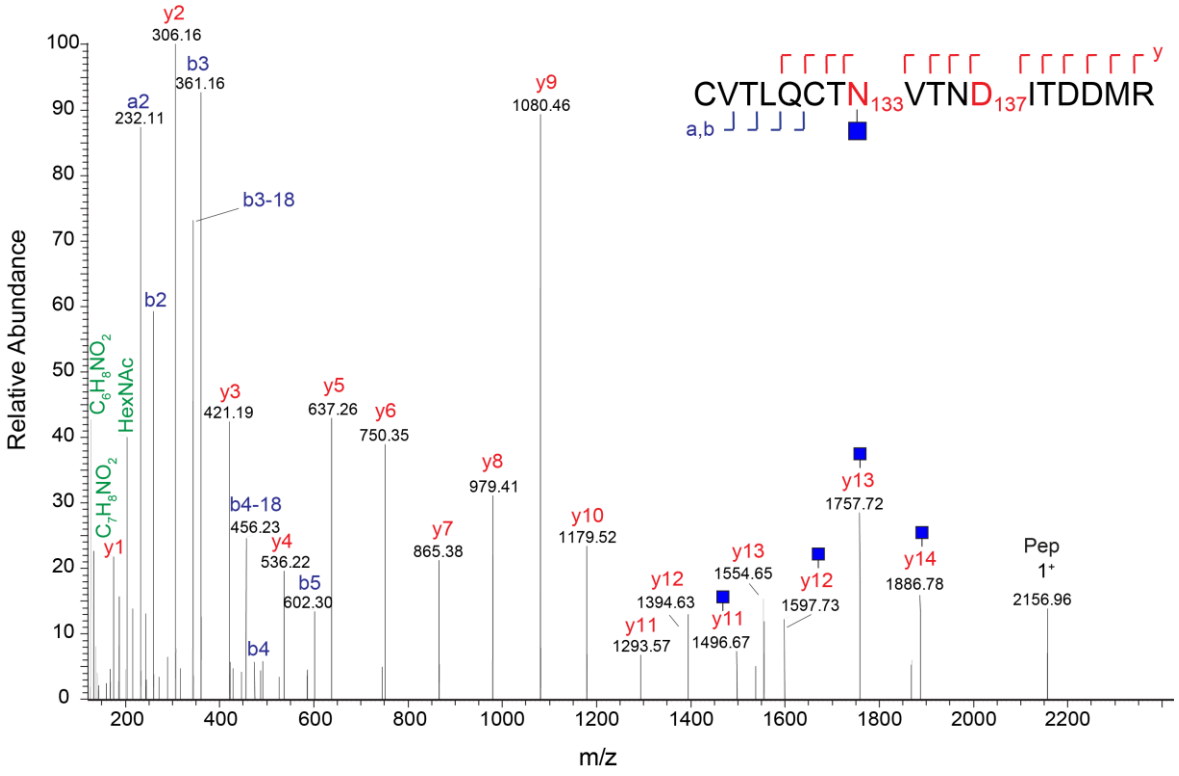

Figure 3.8: HCD-fragmentation MS/MS spectrum of a doubly occupied deglycosylated peptide
LC-ESI MS HCD fragmentation spectrum of the Endo H- and successively PNGase F-digested glycopeptide carrying the N133 and N137 N-glycosylation sites of BG505 SOSIP.664. In this example, N133 is occupied by an oligomannose-type (or hybrid-type) glycan and is thus susceptible to Endo H digestion. N137 is occupied by a complex-type glycan, hence resistant to Endo H and digested by PNGase F (converts asparagine into aspartate). Oxonium ions are labeled in green, b-/a-type ions in blue and y-type ions in red (Appendix B).

3.5 Conclusions

The strategy for the site-specific analysis of N-glycosylation outlined in this chapter represents a powerful method for the assessment of the microheterogeneity of recombinant HIV-1 Env (exemplified on the native-like trimer mimic BG505 SOSIP.664). The relative quantification performed here is based on ion intensities and rationalized by the fact that ionization is mostly independent of the glycan structure. Negatively charged glycans (here mainly *N*-acetylneuraminic acid; i.e. sialic acid), however, could lead to a certain amount of inaccuracy in the quantification. Loss of sialic acids caused by their rather weak glycosidic linkage can occur during sample preparation and has also been described to happen during MALDI-TOF MS [441,445]. While the loss of sialic acids is minimal during ESI MS, they can have an impact on the ionization efficiency [441]. One way to avoid a potential bias caused by sialic acids would be to analyze desialylated samples. This has been tried on a few test RP-HPLC-generated fractions analyzed by MALDI-TOF MS. The signal intensity, however, of neuraminidase-treated samples was significantly lower, probably due to the presence of an additional enzyme in the sample, and the relative quantification did not show any difference. In addition, the BG505 SOSIP.664 glycoprotein shows only a very low abundancy of sialic acids of about 5 % (Figure 4.2) making minimal quantitative bias from charged residues. Overall, the potential impact on sialic acids on the semi-quantitative workflow described here should be considered, however, the orthogonal approach of method development limits major influences on the data presented here.

Quantification of glycopeptides by MALDI-TOF MS and LC-ESI MS gave very similar results. LC-ESI MS was preferred, due to the increased N-glycosylation site coverage and as the data interpretation was supported by tailored software, subsequent site-specific analyses were performed by LC-ESI MS. As described in the beginning, a combination of ETD and CID (or HCD) would give the most complete, complementary information on both the glycan as well as the peptide portion of a glycopeptide. This is a methodology that can potentially be employed in future improvement of this workflow. One main advantage should be the possibility to identify doubly

occupied glycopeptides without aforementioned endoglycosidase strategies, because ETD can provide information on the site of glycosylation. However, access to ETD-capable instruments is not always feasible and the method developed here can confidently assign complex glycoprotein samples through complementary techniques. HCD fragmentation, supplemented with glycan structural libraries (IM-ESI MS) is sufficient due to high resolution spectra, the presence of characteristic oxonium ions, glycopeptide ions containing neutral losses of the terminal monosaccharides as well as the presence of a significant amount of y-type and b-type ions.

An important aspect when analyzing the microheterogeneity of glycoproteins, especially also with regard to immunogen design is the level of occupancy on the individual PNGSs. The workflow presented here does not provide any information on occupancy because of the undertaken glycopeptide enrichment step. It is always difficult to reconcile different aspects into one analytical strategy and determination of the occupancy of recombinant Env constructs thus relies on alternative methodologies. Recently, intact mass spectrometry of metabolically engineered gp120 was used to assess its global occupancy [446]. This study showed a very high occupancy level of recombinant gp120 N-glycosylation sites, however, the effect of metabolic engineering on protein occupancy during biosynthesis is unknown. A methodology to assess occupancy on a site-specific level has been developed by Prof. James Paulson's laboratory. Here, protease-generated (glyco)peptides are first treated with Endo H and then digested with PNGase F in O^{18}-water. This workflow is similar to the one described in this chapter in Section 3.4, but takes spontaneous deamidation of asparagines into account [447]. Conversion of Asn to Asp by PNGase F leads to a mass difference of +3 Da due to the incorporation of O^{18}; spontaneous deamidation shows a mass difference of +1 Da and unoccupied sites show now mass shift. Furthermore, it is important to consider that the degree of occupancy is likely influenced by the producer cell line and also whether or not a protein is codon-optimized [448].

4 Composition and antigenic effects of individual Env glycans

The Env spike is a trimer of heterodimers composed of the two subunits gp120 and gp41 and plays a crucial role in mediating host cell infection. The heavily glycosylated surface of Env has been referred to as the 'silent face' with the glycans acting to shield the underlying viral protein surface from immune surveillance [60-62]. The glycan shield constantly evolves to protect the virus from newly produced neutralizing antibodies. However, compared to the highly diverse protein component of Env, many of the potential N-glycosylation sites are well conserved; their total number has also remained relatively constant despite years of viral evolution [257,449]. Although derived from the host cell's glycosylation machinery, the high density of glycans leads to a large abundance of under-processed, oligomannose-type glycans ($Man_{5-9}GlcNAc_2$) [182,183,236,241,260]. The glycan shield is, therefore, surprisingly homogenous given the extent of glycosylation. These oligomannose-type glycans are mainly localized to a highly conserved area of the gp120 outer domain, the so-called 'intrinsic mannose patch', that presents numerous bNAb epitopes [69-71,74,79,273,436,450]. Because these studies were performed using recombinant gp120 monomers, it was uncertain at the time to what extent their glycan content mimicked the native, trimeric structure on HIV-1 virions [200,238,364,451]. Virion-derived trimers are hard to obtain in sufficient quantities for detailed characterizations, but oligomannose-rich regions are known to be present on both envelope glycoproteins extracted from HIV-1 virions [182,183,241] and membrane-associated recombinant Env [235]. Nonetheless, major knowledge gaps remain to be filled.

The soluble, recombinant BG505 SOSIP.664 trimer (Figure 1.4C) is the prototype of a class of native-like, Env-mimetic immunogens that is now being pursued in various vaccine-development programs [205,359]. On the BG505 SOSIP.664 trimers, the total glycosylation profile of the gp120 subunits is dominated by large, oligomannose-type structures of the $Man_{8-9}GlcNAc_2$ type, while more complex-type structures are found on gp41 [184]. Defining the detailed composition of the

glycan shield will be crucial to increase our understanding of bNAb epitopes and will help to guide rational antibody-based immunogen design strategies.

In this chapter, a quantitative site-specific N-glycosylation analysis (based on the workflow presented in Chapter 3) shows the fine structure of the glycan shield of the BG505 SOSIP.664 trimer. The results confirm the remarkable dominance of oligomannose-type glycans and reveal a mosaic of glycan microclusters bearing under-processed glycans, especially in areas covering the gp120 outer domain and at the trimer interfaces. At the trimer apex, there is a microcluster of glycans of mixed processing state, with both under-processed and complex structures present. In contrast, highly variable, but also highly processed, complex-type glycans occupy the sites present on gp41 and on the most proximal gp120 regions at the trimer base. Deleting specific PNGSs does not markedly affect the overall glycosylation profile of the BG505 SOSIP.664 trimer, but can directly or indirectly influence the neutralization sensitivity of HIV-1 BG505 Env-pseudotyped viruses.

4.1 Fine structure of the glycan shield of an Env trimer mimic

The design and structure of the native-like BG505 SOSIP.664 trimer have been described in Section 1.2.2 and elsewhere [205,206,217,226-228,451]. BG505 SOSIP.664 trimers were produced from HEK 293 cells and purified by 2G12-affinity chromatography followed by size-exclusion chromatography (Section 2.3). The enzymatically released and fluorescently labeled N-glycans were analyzed by HILIC-UPLC to determine the trimer's overall glycan profile (Figure 4.1). Endo H cleavage of the released glycan pool established that 63 % of the total glycans found on the trimer were of the oligomannose-type. The majority of these are located on the gp120 subunit (70 % oligomannose), whereas gp41 shows a higher abundance of complex-type glycans (22 % oligomannose).

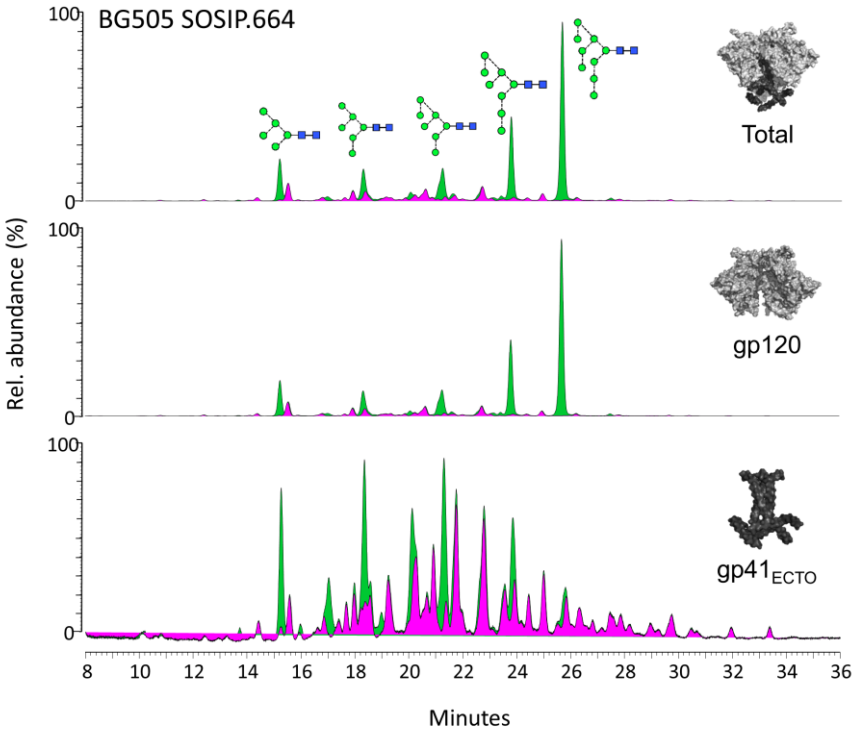

Figure 4.1: Glycosylation pattern of BG505 SOSIP.664 trimers
HILIC-UPLC profiles of enzymatically released and 2-AA-labeled N-linked glycans from BG505 SOSIP.664 trimers stably produced in HEK 293T cells and purified by 2G12-affinity chromatography/SEC. Top profile: gp140 glycans; middle profile: gp120 glycans and bottom profile: gp41 glycans. Oligomannose- and hybrid-type glycans (green) were identified by their sensitivity to Endo H digestion (chromatograms before and after Endo H digestion are overlaid). Pink indicates complex-type glycans. Rel., relative. The oligomannose series is indicated with the appropriate structures representing the most abundant isomer.

To probe the glycan structures in greater detail and to facilitate the processing of subsequent site analysis data, a database of the N-glycans present was generated (compare workflow described in Chapter 3). For this purpose, labeled glycans released from the gp120 and gp41 subunits were analyzed separately by IM-ESI MS (Figure 3.2). Consistent with the HILIC-UPLC data, a significant oligomannose population was present on gp120. Additionally, fine structural details of the highly processed gp41 glycans were obtained, which were dominated by asialylated galactose-terminating bi- and triantennary structures (Figure 3.2B and C). The abundance of sialic acid-containing glycans on the BG505 SOSIP.664 trimer was generally low (less than 5 % of the total glycan pool), as determined by neuraminidase digestion of the 2-AA-labeled glycan pool released from BG505 SOSIP.664 (Figure 4.2)

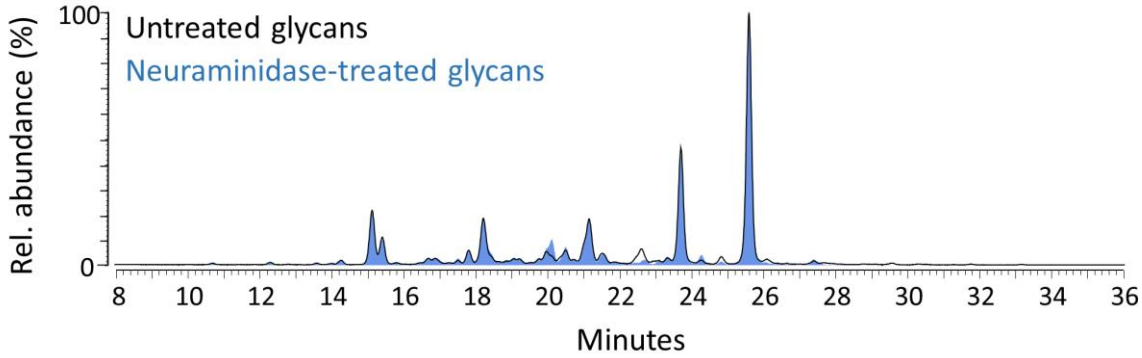

Figure 4.2: Neuraminidase digestion of glycans released from BG505 SOSIP.664
2-AA labeled glycans were digested with neuraminidase from *Clostridium perfringens* and analyzed by HILIC-UPLC. Rel., relative. The chromatograms of untreated glycans and neuraminidase-treated glycans are overlaid.

Overall, the HILIC-UPLC and IM-ESI MS data confirm that the glycosylation sites on the gp120 subunits are largely dominated by oligomannose-type structures, whereas more highly processed glycans dominate on gp41. However, there are exceptions to these generalizations on both subunits, which will be explored later. The site-specific variation in glycan structures arises from the intersection between the folding of Env into its quaternary structure and how the producer cell's processing enzymes then see the folded trimer. To quantify the distribution of under-processed oligomannose-type glycans and specify the locations of the highly processed complex-type glycans, the mass spectrometry approach described and assessed in Chapter 3 was employed. Figure 4.3 shows the site-specific N-glycosylation profiles for BG505 SOSIP.664 trimers and a map of the distribution of the different processing states across the trimer surface, based on a model on its cryo-EM structure at 4.36 Å resolution [207].

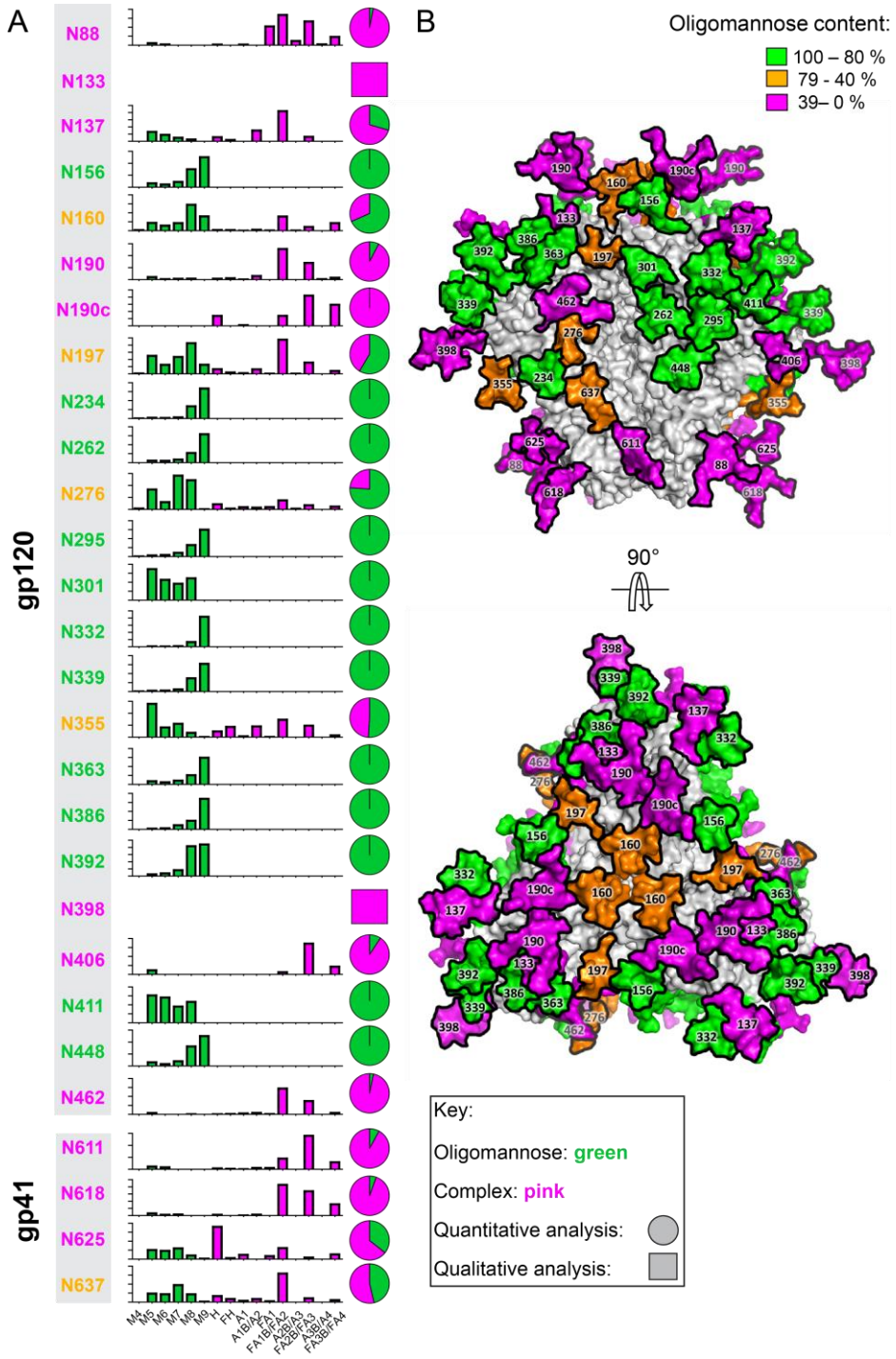

Figure 4.3: Quantitative site-specific N-glycosylation profiles of BG505 SOSIP.664 trimers
(A) Glycosylation profiles of all 28 N-glycosylation sites of BG505 SOSIP.664, transiently produced in HEK 293F cells. The trimers were digested with trypsin, chymotrypsin, pronase, GluC, or GluC plus trypsin and then analyzed by LC-ESI MS. Glycans were grouped as shown in Appendix C. The bar graphs represent the means of two analytical replicates; the pie charts summarize the quantification of oligomannose-type (green) and complex-/hybrid-type glycans (pink) on individual sites. For information on peak lists, corresponding percentages and glycan library, see Appendix D and Appendix E. (B) Model of a fully glycosylated BG505 SOSIP.664 trimer. The model was constructed using PDB ID 5ACO [207] with the following glycans modelled in according to the processing state: Oligomannose-type ($Man_9GlcNAc_2$; [452]), processed (galactosylated biantennary glycan (from PDB ID 1L6X) and mixed sites ($Man_5GlcNAc_2$; [452]).

The model reveals a mosaic of sites carrying oligomannose-type glycans, complex-type glycans or a mixture of both. However, the distribution is not random, and a network of underprocessed, oligomannose-type glycans is evident across the trimer surface. The heterogeneity of the glycan processing states indicates that there must be hotspots of accessibility to the producer cell's glycan-processing enzymes. The trimer apex is covered by a ring of six glycans created by two individual sites (N156 and N160) from the V1/V2 regions of each of the three protomers. All six glycans in this ring are minimally processed, which can likely be attributed to inter-glycan interactions among these topologically proximal structures that shield each of them from the processing enzymes. $Man_9GlcNAc_2$ moieties dominate at the N156 position, whereas the N160 glycan is slightly more processed although still predominantly of the oligomannose-type (Figure 4.3). Glycans N234 and N276 near CD4bs also behave as a linked, minimally processed pair on each individual gp120 protomer, and it can be noted that they are separated at the Asn Cα positions by only 10.6 Å (PDB ID 5ACO [207]). This degree of proximity may again be sufficient for bidirectional protection from enzymatic processing, albeit with one partner again being slightly more shielded than the other. Thus, here, N276 is partially oligomannose-trimmed towards $Man_5GlcNAc_2$ with some hybrid-type and small complex-type structures also present, whereas N234 is even less processed.

A further example of how the dense clustering of glycans may sterically impede the access of glycan processing enzymes to their substrates involves the mannose patch on the gp120 outer domain. Two densely packed microclusters are centered on residues N295 and N392 that, together, form a large patch of predominantly $Man_9GlcNAc_2$ glycans (Figure 4.3). Here, the N295 glycan is intimately embraced by its counterparts at positions N262, N448, N332 and N301. The N392, N363 and N386 glycans form a closely packed microcluster, with their Cα-atoms as close together as 7.1 Å (N363 to N392), 8.8 Å (N363 to N386) and 11.5 Å (N386 to N392) (PDB ID 5ACO [207]). This roughly triangular array of glycans is further surrounded by those on N137, N197, N133 and N339. The N332 glycan, a key component of the so-called 'supersite of immune vulnerability'

[68,69,75,79], resides at the heart of this site. Its location between the two component microclusters links them into a single large oligomannose patch that stretches around the entire gp120 outer domain. The N332 glycan itself is in close contact with, or proximity to, N295, N301 and N137. Overall, the mannose patch is stabilized by the now revealed glycan-glycan interactions within and/or between the two individual microclusters.

Complex-type glycans dominate the N- and C-termini of the BG505 SOSIP.664 trimer, which are located very close to one another at the structure's base (Figure 4.3). In particular, the highly processed gp120 N88 glycan is located immediately proximal to the gp41 subunit. Of the four glycan sites on gp41, N611 and N618 display a broad range of complex-type glycans, whereas N625 and N637 are less extensively processed; a significant proportion of these structures are in oligomannose-type form. An explanation for the mixed-processing status of the N637 glycan could be trimer-induced steric hindrance caused by its proximity to gp120 glycans N234 and N276.

4.2 N332 – Impact of migration and deletion on the mannose patch

The N332 glycan in the heart of the mannose patch is clearly dominated by $Man_9GlcNAc_2$ moieties on BG505 SOSIP.664, as shown both by MALDI-TOF MS and LC-ESI MS (Figure 3.6; Figure 4.3A). Glycan migration from N332 and N334 is a common viral escape mechanism and together both of these sites are more than 90 % conserved. On that note, the transmitted/founder virus isolated from the BG505 infant 6-weeks after birth does not contain an N-glycosylation site at position N332 [205,453]. The SOSIP.664 trimer is based on a clone from the week-6 isolate, but with the N332 glycan specifically introduced to create epitopes for the multiple bNAbs that recognize it [68,69,74,79,261]. To assess the impact of deletion and migration of the introduced N332 glycan, BG505 SOSIP.664 (i.e., N332 present) trimers, BG505 SOSIP.664 334N (i.e. N332 shifted to position 334) and its N332A mutant were cloned, expressed in HEK 293F cells and analyzed by examination of the overall glycan profiles (Section 2.2.2; for primers see Appendix A).

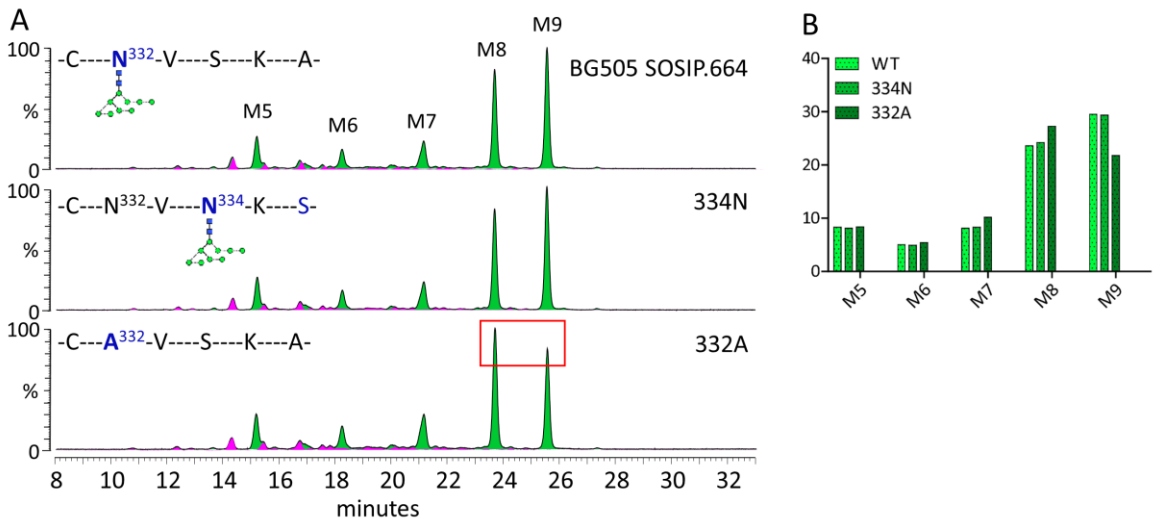

Figure 4.4: Glycosylation analysis of N332 deletion and migration to N334 in BG505 SOSIP.664
(A) HILIC-UPLC profiles of 2-AA-labeled glycans released from BG505 SOSIP.664 (WT; upper panel), 334N (middle panel) and 332A (bottom panel) mutant trimers. Protein were transiently expressed in HEK 293F cells and purified by PGT151-affinity chromatography. Glycans were released by in-gel digestion of the trimer band resolved on a native gel. Changes made in amino acid sequence of the mutants (blue) are shown in the top left corner of each profile. Green: oligomannose- and hybrid-type glycans; pink: complex-type glycans. The red box highlights the shift in Man8:Man9 ratio in the 332A mutant. (B) Comparison of the abundancies of oligomannose-type glycans of the three trimers. Bar graphs show means of analytical replicates (n=3) + standard deviations; error bars are too small to be visible.

Glycan migration from N332 to 334 shows almost no impact on the abundance of oligomannose-type glycans on BG505 SOSIP.664 (Figure 4.4). This suggests that the intrinsic mannose patch can tolerate this kind of glycan migration possibly explaining why this is a commonly observed escape route of HIV-1. Comparing the two HILIC-UPLC profiles of BG505 SOSIP.664 (i.e. N332 present) and the N332 glycan deletion mutant shows, however, that the knocked-out N332 glycan reshapes the overall glycan profile. Or, in other words, that the introduction of N332 into the BG505 SOSIP.664 sequence has a significant influence on the glycan shield. Thus, compared to the standard trimer, the glycans released from the N332A mutant contain fewer $Man_9GlcNAc_2$ moieties but more $Man_8GlcNAc_2$, such that the latter was now the most prominent N-glycan structure (Figure 4.4). An interpretation of this observation could be that the presence of the N332 glycan influences the composition of the multiple, closely proximal glycans within the mannose patch. A likely mechanism for this effect is steric obstruction of α-mannosidase enzymes [260].

4.3 Effect of glycan site deletions on neutralization sensitivity and structure integrity

To determine the impact of glycan deletions on bNAb sensitivity, various PNGSs from the BG505.T332 (i.e., wild-type BG505) and the BG505.T332N Env-pseudotyped viruses (note that the BG505.T332N virus has the same glycosylation sites as BG505 SOSIP.664 trimers [205,359]) were removed. The neutralization profiles for a range of bNAbs to multiple epitopes were determined: CD4bs (PGV04), mannose-patch binding (PGT121, PGT128, PGT130 and PGT135), V1/V2 loop (PG9 and PGT145) and gp120/gp41-interface (PGT151) (Figure 1.6; Section 2.6). As expected, when glycans known to be key components of epitopes were absent, bNAb sensitivity was substantially reduced or lost entirely (Figure 4.5). For example, removing the N156 or N160 glycans from either of the BG505 test viruses reduced the neutralization activities of PG9 and PGT145; and likewise for glycans N295 or N301 with PGT128 and PGT130. However, some unexpected outcomes could also be observed. Thus, eliminating the N197 glycan substantially reduced (BG505.T332) or entirely ablated (BG505.T332N) the neutralization activity of the V1/V2-binding bNAb PGT145 (Figure 4.5). This finding is consistent with a report that PGT145 fails to neutralize the viral strain JR-FL that naturally lacks the N197 glycan [454]. Similarly, deleting the N197 glycan from the BG505.T332 virus also reduced its sensitivity to PG9. N197 carries a mixture of oligomannose-type and complex-type glycans (Figure 4.3A) and is located at the trimer apex near the protomer interface. Its removal could indirectly affect the binding of various mannose-dependent bNAbs by perturbing the glycans at the trimer apex.

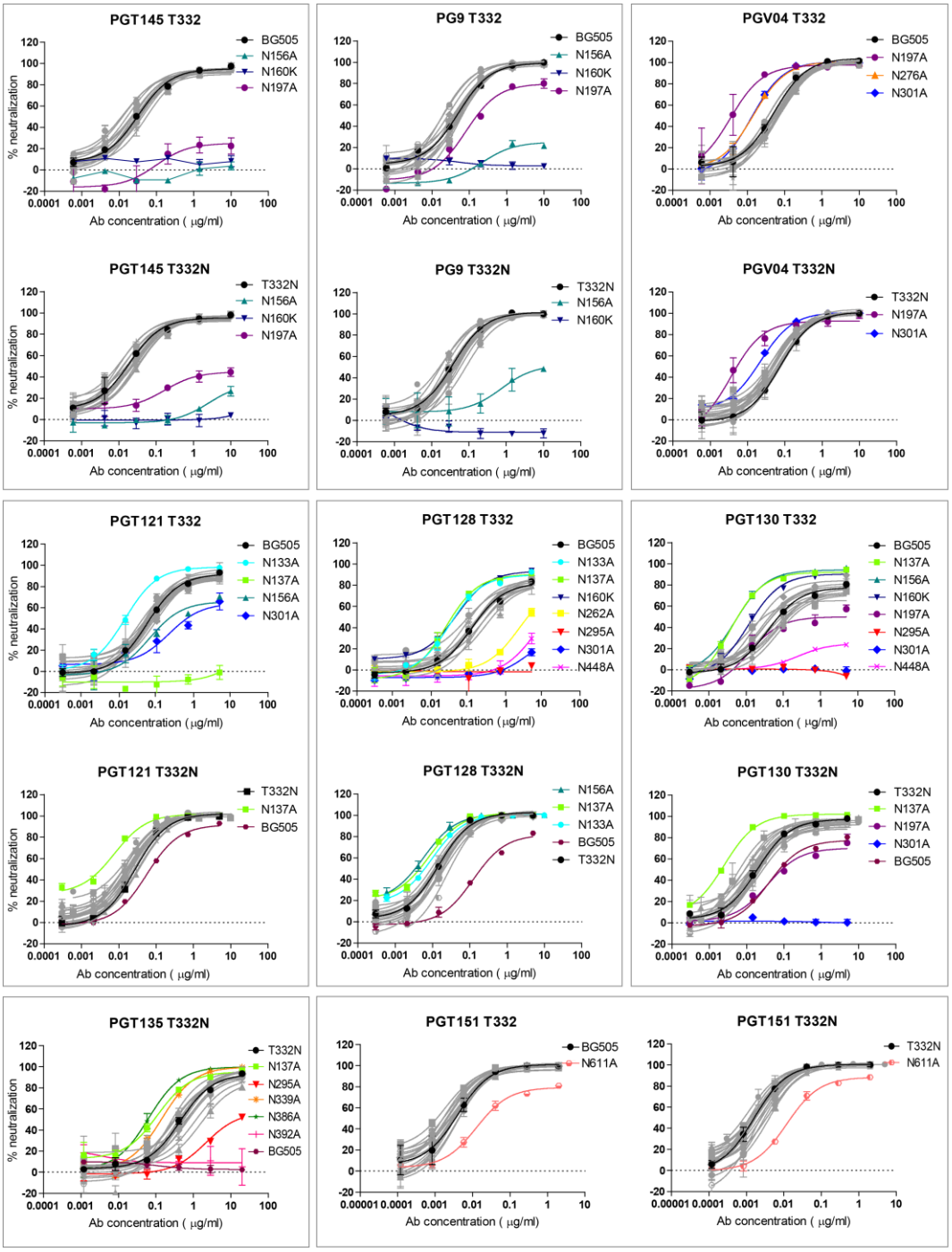

Figure 4.5: Glycan site modulation of viral neutralization by glycan-dependent bNAbs
Neutralization of wild-type BG505 (termed BG505.T332 in the main text) and BG505.T332N Env-pseudoviruses, and a panel of glycan-deletion mutant Env-pseudoviruses, by bNAbs PGT145, PG9, PGV04, PGT121, PGT128, PGT130, PGT135 and PGT151. The presence or absence of the N332-glycan is indicated above each panel (i.e., T332 or T332N). The plots show data from one experiment that is representative of at least two measurements. Error bars are mean values derived from two duplicate wells, +/- SEM. The glycan-deletion mutants based on the BG505.T332 virus were not analyzed for their sensitivity to PGT135, as this antibody is highly N332-dependent and the parental virus already lacks this glycan [79]. Mutant Env-pseudoviruses with markedly increased or decreased neutralization sensitivity compared to the remaining panel are highlighted using the colors shown in the legends. The full list of PNGS deletions is listed in Appendix A. Neutralization assays were performed by Dr Katie Doores/Stefanie Krumm (King's College London).

To further explore some of these phenomena, several double PNGS deletion mutant trimers on the BG505 SOSIP.664 N332A background were created, together with the corresponding single mutants. The trimers were produced as described above and their glycan profiles were analyzed by HILIC-UPLC. The relative impact of single site deletions on the abundance of oligomannose-type glycans was generally significantly less than when two sites were deleted (Figure 4.6).

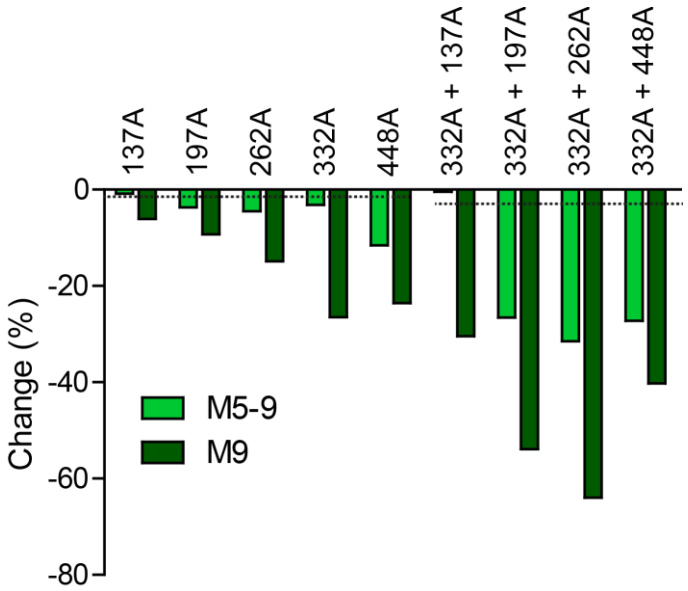

Figure 4.6: Impact of individual glycans on total trimer glycosylation
The figure shows the effects of a panel of single and double glycan site deletions on the overall abundance of oligomannose-type glycans (M5-9; green), as well as on the individual abundance of $Man_9GlcNAc_2$ (M9; dark green). His-tagged BG505 SOSIP.664 trimers were transiently expressed in HEK 293F cells and purified by PGT151 affinity chromatography. Bands corresponding to the trimeric protein were excised from native gels and subjected to glycan analysis. The abundance of oligomannose-type glycans were determined by integration of corresponding HILIC-UPLC peaks with or without Endo H treatment. The y-axis represents the change in percentage of oligomannose-type glycans of a mutant relative to the non-mutated BG505 SOSIP.664 trimer control and is calculated as follows: Percentage change = [(% oligomannose in control - % oligomannose in mutant) / (% oligomannose in control)] x 100. The two dashed lines represent the decrease in oligomannose abundance predicted to arise solely by the deletion of one or two N-glycosylation sites that are exclusively occupied by oligomannose-type glycans when present on the control trimer. For corresponding UPLC profiles, see Appendix F.

However, it is notable that the overall reduction in oligomannose content transcends what would be predicted solely from the engineered loss of the individual glycans. As noted above, the N332 site has a significant influence on the wider composition of the glycan shield on BG505

SOSIP.664 trimers. This observation is reinforced by studies using mannose-patch binding bNAbs and mutant viruses (Figure 4.5). Specifically, the BG505.T332 virus (which lacks the N332 glycan) is more affected by the deletion of additional glycans, compared to BG505.T332N (which contains it). Thus, unexpectedly, the glycan epitopes for PGT128 and PGT130 are particularly strongly impaired when the N448 glycan is deleted from the BG505.T332 virus, more so than seen with BG505.T332N. Of note is that, in the SOSIP.664 trimer context, the double deletion of N332 and N448 has a relatively strong impact on the overall abundance of oligomannose, as does the dual elimination of N332 and N262 (Figure 4.6). In addition, deleting the N262 glycan likewise reduces the sensitivity of the BG505.T332 virus to neutralization by PGT128. However, the impact of removing the N262 glycan may be explained by its critical role in gp120 folding [455,456] and in influencing the conformation of the N301 glycan [457].

Conversely, and unexpectedly, certain bNAbs to the mannose-patch epitopes more potently neutralize BG505 virus mutants that lack some outer domain glycans. Deleting the N137 glycan renders both BG505 test viruses more sensitive to PGT128 and PGT130, and makes BG505.T332N more vulnerable to PGT121 and PGT135, but the corresponding change has no meaningful effect on oligomannose content in the SOSIP.664 trimer context (Figure 4.6). The likely explanation is that the loss of the N137 glycan increases the overall accessibility of the mannose-patch epitopes but without affecting the average composition of the glycan shield [413,450].

The CD4bs antibody PGV04 more strongly neutralized the N197 and N301 single deletion mutants of the BG505.T332 and BG505.T332N viruses. This outcome is consistent with, and extends, a recent report that deleting the N197 glycan from a diverse panel of HIV-1 isolates generally increases their sensitivity to CD4bs bNAbs, presumably via increased epitope accessibility [458].

4.4 Conclusions

The site-specific N-glycosylation analysis of a recombinant Env mimic reveals the extremes of glycan processing and protection that are displayed across the surface of the densely glycosylated Env trimer. The interlocking network of glycans likely promotes the presence of particular carbohydrate structures despite the underlying and much greater diversity at the amino acid sequence level.

It is important to note that the BG505 SOSIP.664 trimer used for these glycan site analyses is a soluble protein. It lacks not only the transmembrane region of gp41, but also the membrane-proximal external region (MPER) [228,451]. The highly processed N611 and N618 glycans are each likely to be located very close to where the MPER would be located (Figure 4.3B). Thus, in the context of full-length Env, additional shielding effects created by the MPER and the virion or cell membrane may provide additional constraints on processing of the nearby N611 and N618 sites. Even though the overall glycosylation profile of a soluble SOSIP.664 trimer and a sequence-matched, membrane-associated Env ΔCT trimer are broadly similar [184], there may be structurally explicable differences in how specific sites are processed in the different contexts.

The fine structure of the BG505 SOSIP.664 glycan shield allows inferences with regard to known bNAb epitopes. For example, the PG9 epitope is critically dependent on the trimer apex glycans N156 and N160 [70,274,459]. On the BG505 SOSIP.664 trimer, the N156 site is exclusively occupied by oligomannose-type glycans, mainly $Man_9GlcNAc_2$ (Figure 4.3A). This observation is in marked contrast with a report that sialylated, complex-type structures play a critical role in how PG9 recognizes the N156 glycan [459], and also with the proposal that sialylated hybrid-type glycans are targeted by the related PG16 antibody [81]. These studies used isolated fragments of the trimer and while antibodies may be able to bind such fragments their glycans may not be close mimics of the native setting. A related observation is that, in the trimer context, N160 can now be seen to be occupied by a mixed array of glycans in which $Man_8GlcNAc_2$ predominates. This new information supersedes the suggestion, based on simpler structures, that processed, $Man_5GlcNAc_2$ moieties play a critical role in how PG9 recognizes the N160 glycan [459]. It is unclear how the

presence of kifunensine-induced $Man_9GlcNAc_2$ moieties impedes viral neutralization by PG9 and PG16 [460]. One explanation is that PG9 and PG16 may simply not bind $Man_9GlcNAc_2$ structures very well. However, an alternative hypothesis is that driving all three N160 glycans to the larger structure (i.e., by the use of kifunensine) distorts the packing of the trimer apex, with implications for the presentation of the PG9 epitope. Overall, here it is shown that the PG9 epitope, in the trimer context, is substantially more oligomannose-tolerant/dependent than has been thought. These findings are concordant with the observation that PG9 binds comparably to BG505 SOSIP.664 trimers irrespective of whether they are produced in HEK 293T cells (which permit glycan processing) or GnTI-deficient HEK 293S cells (which restrict glycans to oligomannose forms) [274].

5 Architecture of the cleavage-dependent mannose patch

The two subunits of the Env spike, gp120 and gp41, are generated when a protease, usually furin, cleaves the pro-protein gp160 glycoprotein [191-196]. Furin most probably cleaves gp160 in the TGN, but it is able to cycle between the TGN, the endosomal compartments and the cell surface and is also believed to be able to act in the early secretory pathway [192,197,198]. Furin is an important factor in Env immunogen production as it is now commonly co-expressed to generate fully cleaved, recombinant, soluble trimers that structurally mimic native Env [205,461]. In contrast, structural and antigenic analyses of many uncleaved Env constructs show that they adopt non-native conformations, with gp120 subunits dangling from a gp41 core, unless additional modifications are made to overcome the defect [200,238,360,462]. Cleavage is, therefore, important for the structural integrity of the trimer, which in turn greatly influences how the trimer is glycosylated [184,238].

Several studies on monomeric gp120 proteins have demonstrated the presence of an 'intrinsic mannose patch' (IMP) at the outer domain of gp120, which arises because the glycan shield creates steric constraints that restrict the actions of ER and Golgi α-mannosidases [176,182,183,231,232,260]. Analyses of recombinant soluble, native-like trimers [13,184], membrane-associated trimers [235] and virion-derived Env [182,183,236] all show that their oligomannose-type glycan contents are even higher than for gp120 monomers, implying that a 'trimer-associated mannose patch' (TAMP) exists [237]. However, the glycan sites forming any such TAMP have not previously been defined.

Compact folding seems to be major driver behind the oligomannose-dominated N-glycosylation profile of the glycan shield on native trimers. For example, uncleaved, non-native constructs that adopt a much more open and irregular conformation have a significantly reduced content of oligomannose-type glycans, because the now more accessible structures are efficiently processed [184,238]. Here, these uncleaved, non-native glycoproteins are referred to as

pseudotrimers [416], to reflect their lack of the three-fold symmetry that is a characteristic feature of the structures of natively folded trimers [206,217].

In this chapter, the detailed effect of cleavage-induced, native-like trimerization on N-glycan processing is revealed. Quantitative, site-specific analysis of a set of comparably expressed and purified monomeric (i.e., gp120), uncleaved pseudotrimeric and fully cleaved trimeric envelope glycoproteins of the same genotype (i.e., BG505) identifies the location of the cleavage-dependent TAMP. Thus, the glycans that form the TAMP are found in regions near the trimer apex and the protomer interface. It is shown that, compared to pseudotrimers, these regions are even more highly processed on monomeric gp120, implying that the oligomerization events impose additional regional restrictions on glycan processing. This finding is echoed across the panel of glycoproteins in the analysis of O-linked glycosylation at T499 near the trimer base, which is present at almost unmeasurable levels on native-like trimers. These findings emphasize how the glycan shield is influenced by the quaternary structure of the Env spike, and highlight the relevance of native-like structures to Env vaccine development.

5.1 Glycosylation processing on monomeric, uncleaved and cleaved Env proteins

To thoroughly investigate the influence of trimerization- and cleavage-induced structural integrity on Env glycosylation, comparable conditions were used to express and purify monomeric gp120, native-like SOSIP.664 trimers and uncleaved, non-native WT.SEKS gp140 pseudotrimers, all based on the BG505 genotype (Table 2.1; BG505 SOSIP.664 and WT.SEKS gp140 were provided by Prof. John Moore/Dr Al Cupo, Weill Cornell Medical University). The design and characteristics of these proteins have been described previously [205,206,226-228,359,451]. The WT.SEKS construct differs from SOSIP.664 in that it lacks the stabilizing SOSIP mutations and contains an inactivated furin cleavage site (RRRRRR mutated to SEKS); the resulting uncleaved pseudotrimers have a non-native conformation [200]. The monomeric gp120 protein is isogenic with the gp120 subunit of the SOSIP.664 trimer. The designs of all three constructs are summarized in Figure 5.1A. The three proteins were all produced in transiently transfected HEK 293F cells and purified using 2G12 affinity chromatography, followed by size exclusion chromatography (Section 2.3).

N-linked glycans were enzymatically released from all three constructs, fluorescently labeled and analyzed by HILIC-UPLC (Figure 5.1B). Using Endo H to digest the oligomannose-type glycans and by integration of the resulting chromatograms, oligomannose-type glycans were shown to account for ∼36 % (gp120 monomers), ∼35 % (WT.SEKS gp140) and ∼68 % (SOSIP.664 trimers) of the total glycan populations. This outcome is consistent with a previous report that complex-type glycans are significantly more abundant on uncleaved pseudotrimers than on native-like trimers [184]. Although the analyses of the WT.SEKS and SOSIP.664 glycoproteins include contributions from the four glycans on gp41, the overall outcome is dominated by the 24 glycan sites on gp120. In summary, the total content of oligomannose-type glycans in both the monomeric gp120 and uncleaved gp140 forms of BG505 Env are quite similar, with each exhibiting approximately half the oligomannose content of the native-like SOSIP.664 trimers.

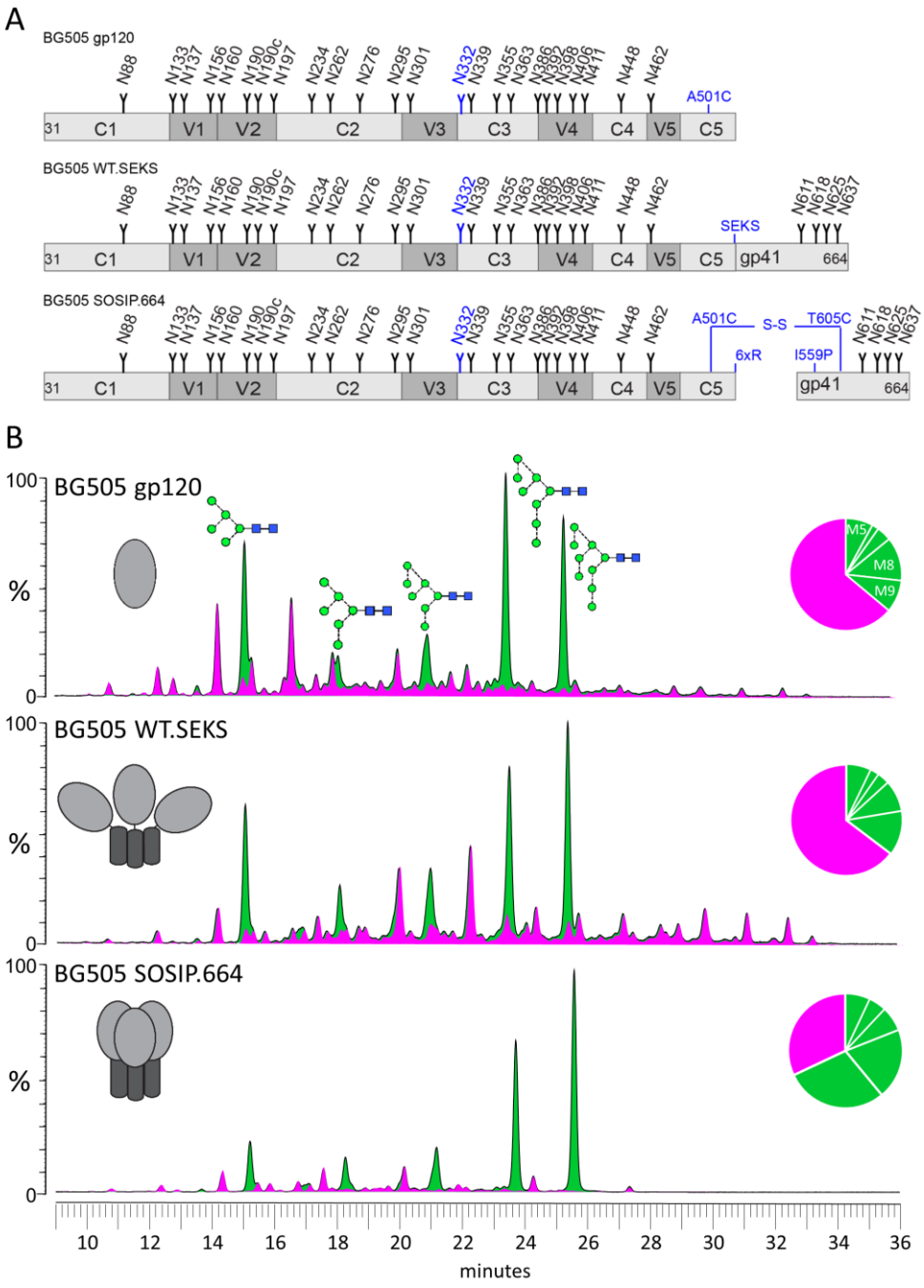

Figure 5.1: Design and glycosylation pattern of BG505 gp120, WT.SEKS and SOSIP.664
(A) Schematic representation of the BG505 gp120, WT.SEKS and SOSIP.664 constructs. Changes to the wild type BG505 sequence are highlighted in blue. (B) HILIC-UPLC profiles of the enzymatically released N-linked glycans of the three constructs, transiently produced in HEK 293F cells and purified by 2G12 affinity chromatography, followed by SEC. Oligomannose- and hybrid-type glycans (green) were identified by their sensitivity to Endo H digestion. Peaks corresponding to complex-type glycans are shown in pink. The peaks were integrated and the pie charts summarize the quantification of the peak areas. Glycan symbols as shown in Figure 5.2 representing the most abundant isomer.

To facilitate the subsequent site-specific N-glycosylation analysis of the gp120, WT.SEKS and SOSIP.664 glycoproteins, and to probe their glycan structures in greater detail (workflow described in Chapter 3), libraries of enzymatically released, unlabeled glycans using IM-ESI MS. The mobility-extracted singly charged glycans from the three glycoproteins are shown in Figure 5.2. A significant population of oligomannose-type $Man_{5-9}GlcNAc_2$ glycans is present on all three glycoproteins and is most evident in the BG505 SOSIP.664 spectrum. This observation is consistent with the HILIC-UPLC data presented in Figure 5.1. Ion mobility mass spectrometry using negative fragmentation mode allows the detailed assignment of isomeric glycan structures [463]. The number and type of glycan structures identified for the gp120, WT.SEKS and SOSIP.664 proteins are with about 90 identified structures highly similar, although the abundances vary (for information of location of glycan libraries, see Appendix D). Fine structural details of the diversity of complex-type glycans present on all three constructs were revealed. The extremes of glycan processing, including the presence of terminal fucoses, sulfates, GlcNAcs and GalNAcs, are directed by the producer cell's glycosylation machinery. In contrast, the oligomannose-type glycans represent an intrinsic structural feature of Env [184].

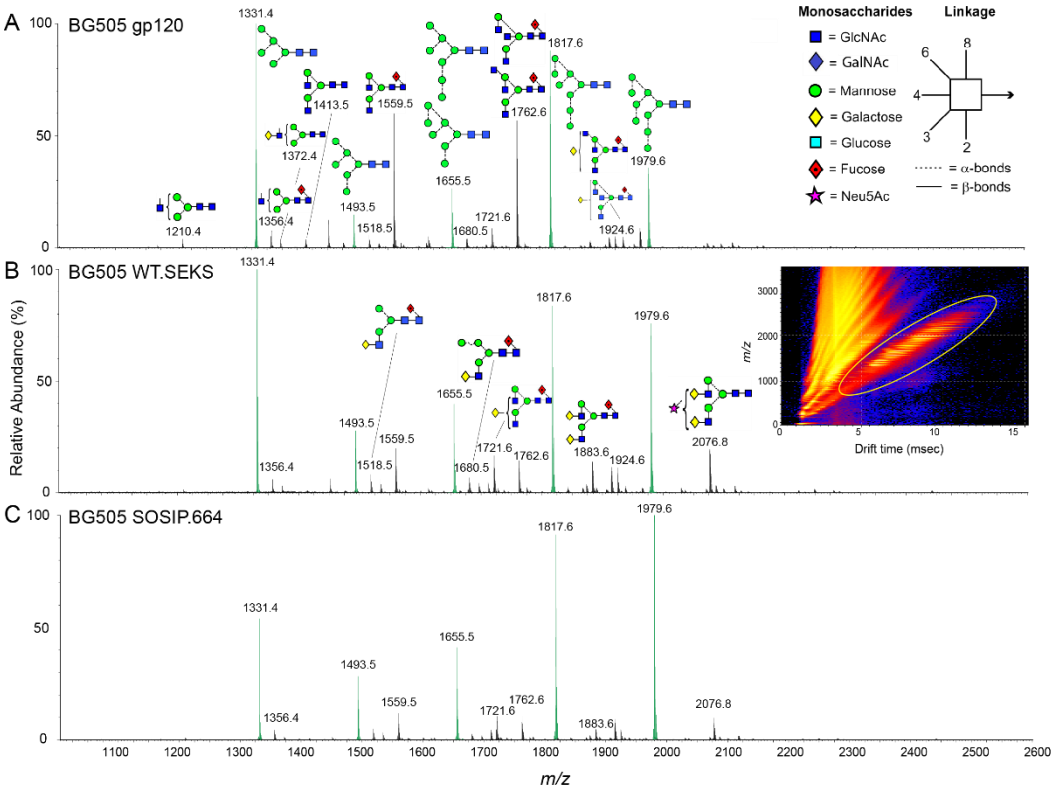

Figure 5.2: Ion mobility mass spectrometry analysis of BG505 Env glycosylation
Mobility-extracted singly charged negative ion electrospray spectra of N-linked glycans found on BG505 Env proteins: (A) gp120 monomers, (B) WT.SEKS pseudotrimers, (C) SOSIP.664 trimers. Symbols are as explained in a key in Panel A. The inset in Panel B shows an example of a DriftScope image derived from gp120 monomers, with singly charged ions encircled with a yellow oval. Plotted is the ion drift time *vs m/z* with ion abundance being translated into a heat map. The peaks of the oligomannose series $Man_{5\text{-}9}GlcNAc_2$ are highlighted in green. Location of a list of identified glycans is in Appendix D.

5.2 Quantitative site-specific N-glycosylation analysis

Quantitative, site-specific N-glycosylation analysis using in-line LC-ESI MS (Section 2.5.4) was performed, to thoroughly investigate how the formation of native-like, cleavage-induced trimers influences the glycan shield. A panel of different proteases was used to create peptides and glycopeptides from the gp120, WT.SEKS and SOSIP.664 proteins, enriched glycopeptide populations and then quantified the relative abundances of individual glycans by assessing the ion intensities over all charge states. The quantified and summarized data for the three Env constructs shows that the processing of distinct N-glycosylation sites in the glycan shield of gp120 monomers and pseudotrimers is very similar, but also quite different from the native-like SOSIP.664 trimers (Figure 5.3).

Quantitative site-specific glycan profiles of comparably expressed and purified BG505 gp120 and WT.SEKS gp140 proteins were not derived previously. Their availability now allows a comparison with SOSIP.664 trimers that reveals key aspects of how Env is glycosylated. Where quantitative site-specific data could not be obtained, the processing states of these sites could be broadly classified according to their susceptibility to sequential Endo H and PNGase F digestions (Sections 2.5.1 and 3.4; Appendix E). To display the site-specific glycosylation analysis and facilitate structural interpretation, the distribution of the different glycan processing states was mapped across the BG505 gp120 monomer (Figure 5.4A) and SOSIP.664 trimer (Figure 5.4B), using a model of a fully glycosylated trimer derived from a cryo-electron microscopy structure (Figure 4.3, [207]). All the glycosylation sites are displayed, with the sites classified as mainly oligomannose, mainly complex or mixed.

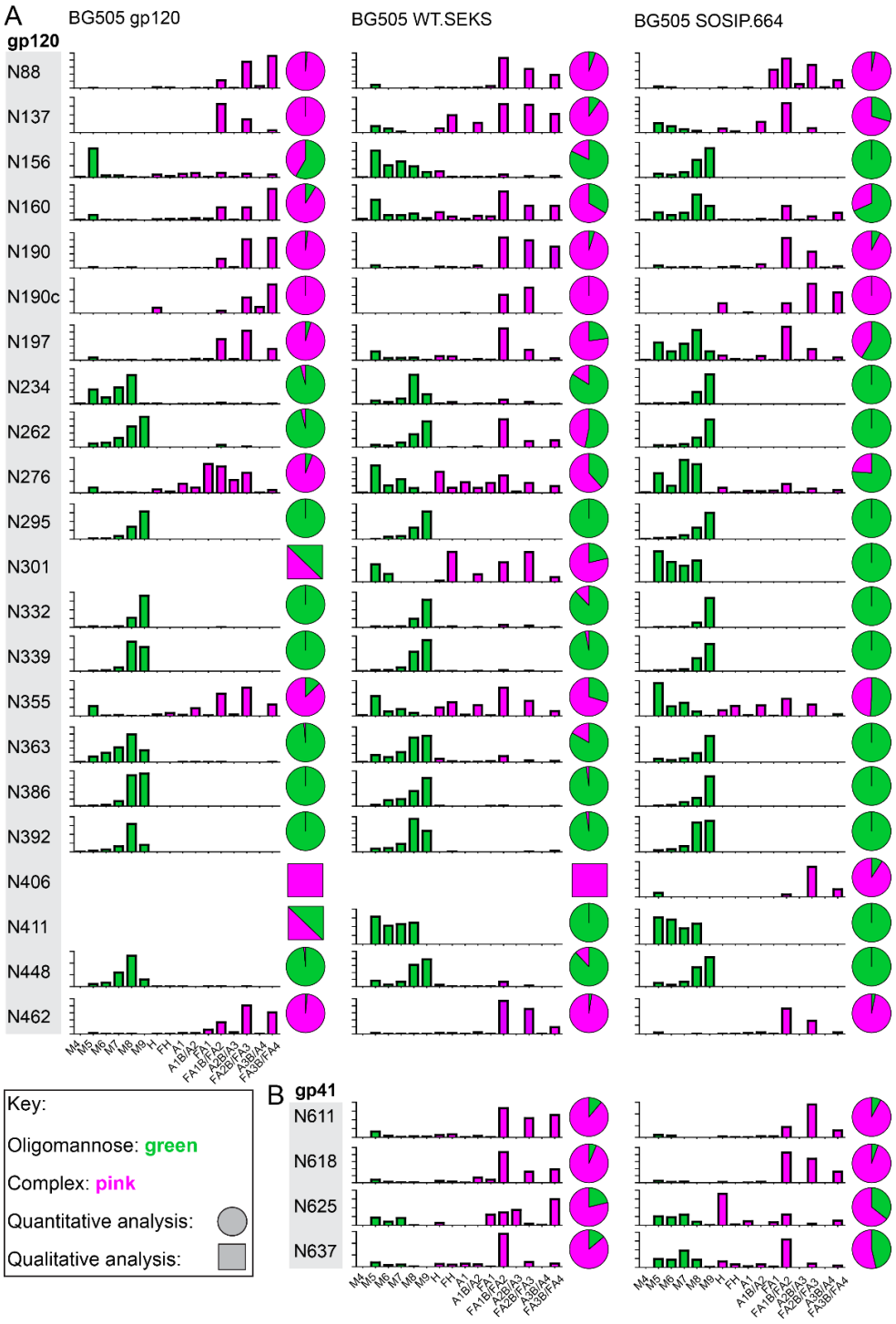

Figure 5.3: Quantitative site-specific N-glycosylation of BG505 Env glycoproteins
Relative quantification of the N-glycosylation sites on the gp120 subunit (A) and the gp41 subunit (B) of gp120 monomers (no gp41 present), WT.SEKS pseudotrimers and SOSIP.664 trimers. Quantifications are based on the peak lists in Appendix E. Glycans are categorized as shown in Appendix C. The bar graphs represent the means of two analytical replicates, and the quantification of oligomannose-type (green) and complex-/hybrid-type glycans (pink) on individual sites is summarized in the pie charts. The processing state of sites where no quantitative analysis could be performed have been classified by qualitative analysis of Endo H and PNGase F-treated glycopeptides, summarized as colored squares. Qualitative data for N133 and N398 is incorporated into Figure 5.4.

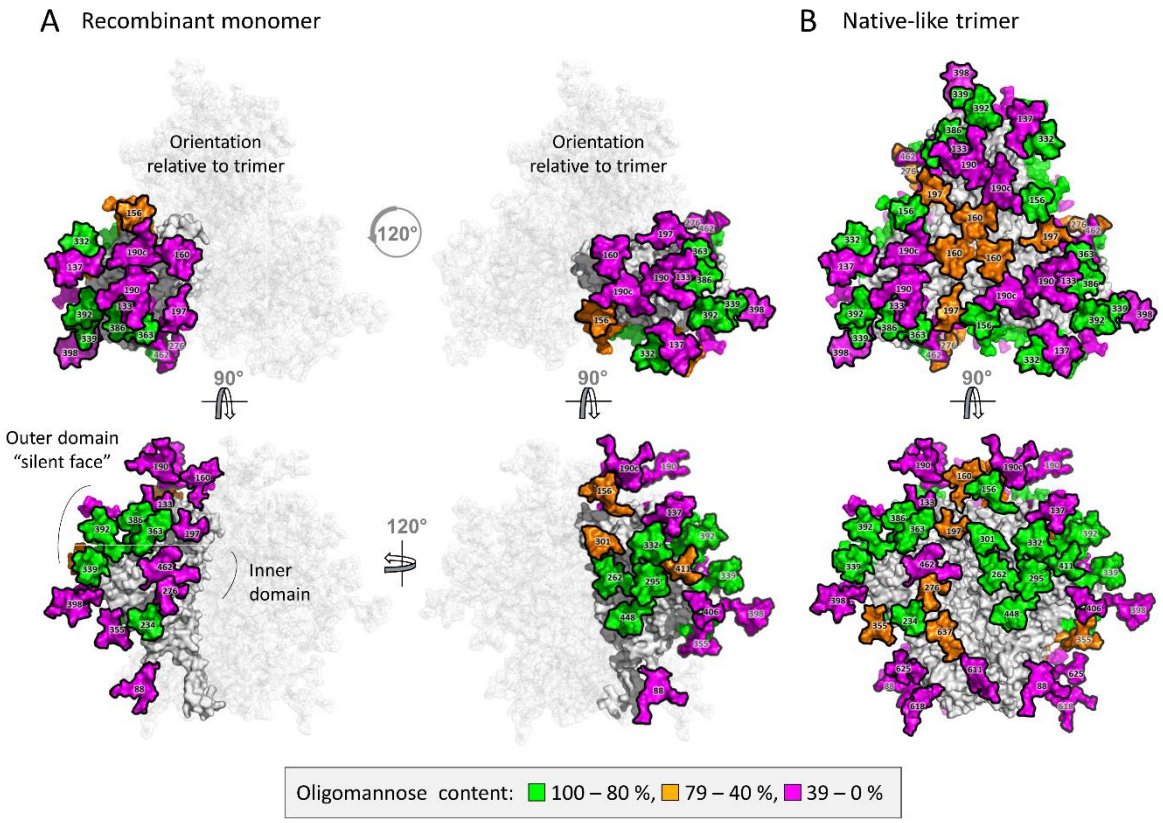

Figure 5.4: Models of a fully glycosylated BG505 gp120 monomer and a SOSIP.664 trimer
Models of the (A) glycosylated gp120 monomer and (B) glycosylated SOSIP.664 trimer are derived from the one described in Chapter 4 [13]. The monomer is oriented as it would appear if *in situ* as a subunit of the SOSIP.664 trimer. The glycans on the models are colored according to their oligomannose-content. N-glycosylation sites of which quantitative results of sufficient quality could not be obtained were classified by qualitative analysis according to their susceptibility to Endo H and PNGase F digestion.

The site-specific analysis of BG505 gp120 reveals numerous positions where exclusively or almost exclusively oligomannose-type glycans are present. These sites define the gp120 IMP [182]. Of note is that the glycan repertoire is highly similar for the corresponding locations in the gp120 subunits of the uncleaved WT.SEKS pseudotrimer and the SOSIP.664 trimer (Figure 5.3A). However, whereas $Man_9GlcNAc_2$ moieties dominate the sites forming the IMP on SOSIP.664 trimers (e.g., N234, N295, N363, N339 and N392), there is additional, but modest, trimming of these sites toward smaller oligomannose glycans on the gp120 monomer and the pseudotrimer. Other sites on the gp120 monomer that contain a significant population of complex-type glycans are less processed on the native-like trimer (e.g., N137, N156, N160, N197, N276 and N355). The overall dominance

of oligomannose-type glycosylation, however, is conserved among the three Env proteins, which supports the definition of the IMP as an intrinsic feature of the gp120 protein, whatever its quaternary context [182]. The IMP is formed by an interlocked network of two main oligomannose microclusters that center around the N295, N332, N392 glycans (Figure 5.5). Many of these oligomannose-dominated glycan sites are among the most conserved glycans on Env (Figure 5.5B) [78].

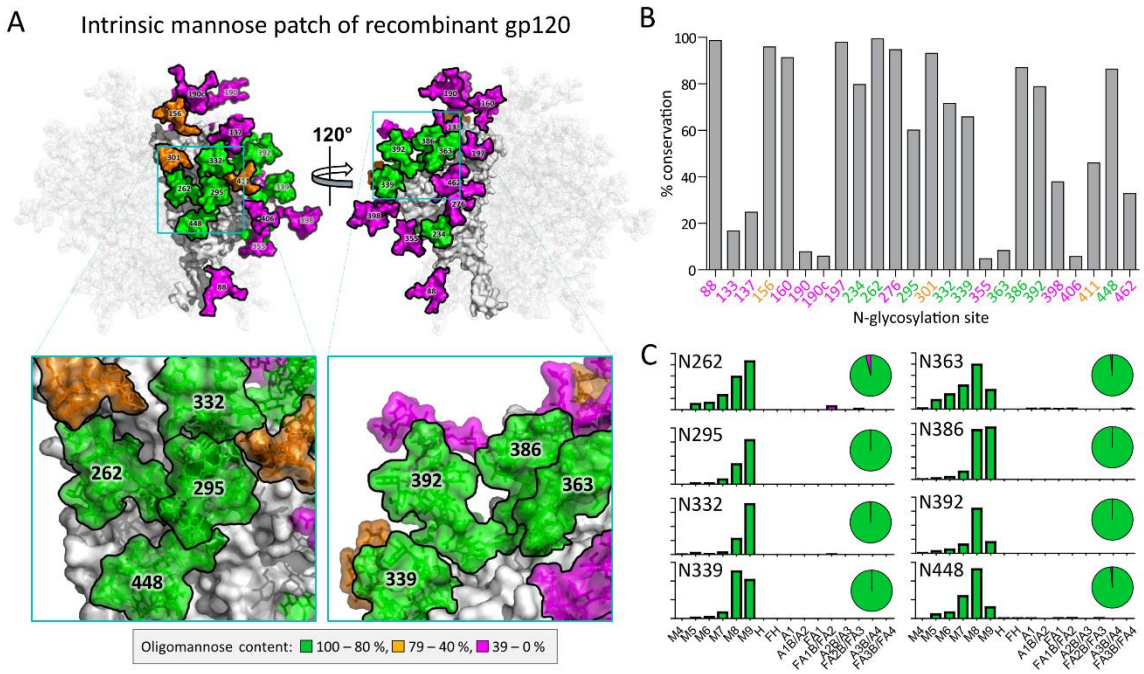

Figure 5.5: Fine structure of the IMP of gp120
(A) Glycan crowding in the outer domain of recombinant monomeric BG505 gp120 leads to an intrinsic mannose patch consisting of two main oligomannose-microclusters, centered around N295 and N392 (see magnifications). (B) Bar graphs of the percentage of conservation of the 24 N-glycosylation sites on BG505 gp120 [78]. (C) Site-specific glycosylation profiles of IMP gp120 glycans (Figure 5.3). Green, oligomannose; pink, complex/hybrid.

The N295 site seems to be comparably protected from glycan processing enzymes on all three constructs; it is the only site where the quaternary context and cleavage status does not increase glycan processing (Figure 5.3). The highly conserved 'supersite of immune vulnerability' [79] N332 on the uncleaved WT.SEKS glycoprotein carries a small population of complex-type glycans whereas this site is entirely oligomannose on both the cleaved SOSIP.664 trimer and the

gp120 monomer. A likely explanation is that the conformationally heterogeneous pseudotrimers include a sub-population on which processing enzymes can access and modify this antigenically important site at the heart of the IMP. The site-specific glycosylation of the gp41 subunits of the BG505 WT.SEKS pseudotrimer and the BG505.664 trimer (Figure 5.3B) are largely similar in that complex-type glycosylation dominates. However, the native-like trimer has elevated population of oligomannose glycans at N625 and N637 indicating steric inaccessibly in those regions.

5.3 Native-like trimers impose interprotomer control of glycan processing

Based on the BG505 SOSIP.664 glycosylation map, two heat maps displaying the site-specific increase in oligomannose glycans on the structure of the cleaved trimer relative to the gp120 monomer (Figure 5.6A) and pseudotrimer (Figure 5.6B) were created. The cleavage-dependent formation of native-like trimers has a significant effect on the processing state of several glycans, including those at the trimer apex and the protomer interface. The increase in oligomannose glycans on the native trimer relative to the monomer or pseudotrimer can be viewed as a decrease in enzymatic processing consistent with the structural constraints that limit processing. For example, the glycan at N276 on SOSIP.664, near the CD4bs, has a ~75 % oligomannose content whereas the corresponding value at the same site on the gp120 monomer is ~5 %; N276 is the gp120 glycan that differs the most in this regard (Figure 5.6A). Other glycans similarly but less profoundly affected are N156 (~60 % oligomannose on monomer *vs* 100 % on trimer, hence a 40 percentage point increase in Figure 5.6) N160 (~60 percentage point increase) and N197 (~50 percentage point increase); each of these sites is located at the trimer apex or protomer interface and so is in a different quaternary context on the SOSIP.664 trimer compared to the gp120 monomer. Similarly, the outer domain N355 glycan is highly processed on monomeric gp120 but is a mixed glycan site (~40 percentage point increase in oligomannose) on the SOSIP.664 trimer. Here, the model suggests that the presence (trimer) or absence (monomer) of proximal gp41 glycans may be the key influence (Figure 5.4).

The formation of native-like trimers also has subtle influences on glycan trimming within the IMP. Thus, several IMP glycans are slightly less trimmed on the trimers, leading to an elevation in the abundance of $Man_9GlcNAc_2$ and an associated reduction in $Man_{5\text{-}8}GlcNAc_2$ (N234, N339, N363, N386, N392 and N448) and/or a slight decrease in complex-type glycans (N234, N262 and N363) (Figure 5.3).

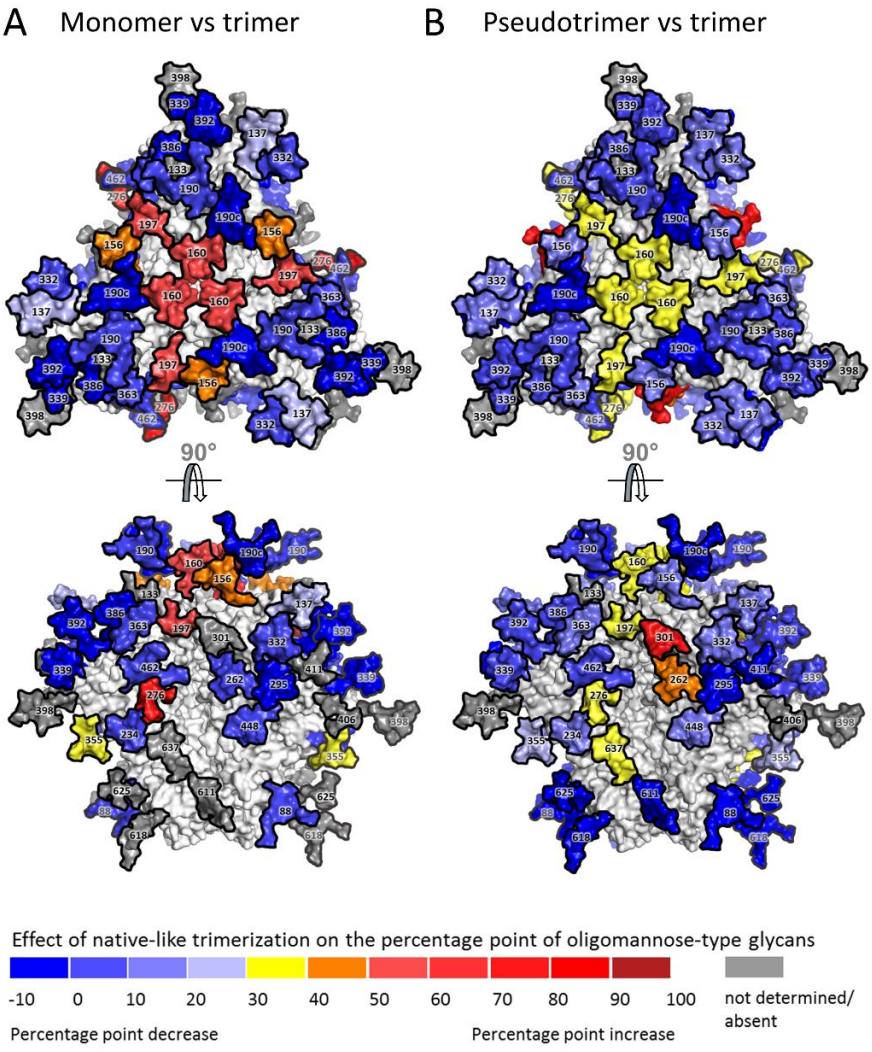

Figure 5.6: Heat map on the surface of the trimer showing the increase in oligomannose glycans of BG505 SOSIP.664 trimers compared to monomers and pseudotrimers
The increase in oligomannose content was calculated for sites where quantitative data were available. To derive the heat map, a percentage point is calculated at each glycosylation site corresponding to the arithmetic difference of two percentages; the percentage of oligomannose-type glycan for each of these sites on gp120 monomers (A) or WT.SEKS pseudotrimers (B) was subtracted from the corresponding percentage for SOSIP.664 trimers.

Broadly similar differences in glycan processing were also found when SOSIP.664 trimers were compared with the uncleaved, non-native pseudotrimers (Figure 5.6B). The differences were quantitatively smaller than for the gp120 monomer *vs* SOSIP.664 trimer comparison, as is apparent from the color gradient of the heat map, but were qualitatively similar. Thus, there was a ∼35 percentage point increase in oligomannose for the N160 and N197 glycans at the apex of the native trimer compared to the pseudotrimer, whereas the corresponding increase for the N156 glycan was 20 percentage points. The biggest difference between the two proteins was seen for the N301 site near the protomer interface; that glycan almost completely switches from highly processed on the pseudotrimer to oligomannose-dominated on the SOSIP.664 trimer. It was not possible to gain quantitative site-specific data for the N301 site on gp120 monomers, but the qualitative deglycosylation experiments did indicate that it had a mixed processing state (Appendix E).

Of note is the N262 glycan, which is known to play a critical role in gp120 folding [456,464]. While this site is exclusively dominated by oligomannose-type glycans on SOSIP.664, it has a mixed composition (∼50 % complex-type glycans) on the pseudotrimer, although $Man_9GlcNAc_2$ still remained the most prominent oligomannose-type structure. One explanation may be that more than one folding state exists within the total population of pseudotrimers, for example a sub-population in which aberrant disulfide bonds have formed [465]. The gp41 glycan that differs most between SOSIP.664 trimers and the pseudotrimers is N637, which resides near the protomer interface, very close to N276. Thus, there is an increase of more than 30 percentage points in oligomannose at the N637 site on the native trimer compared to the pseudotrimer (Figure 5.3). The remaining gp120 glycans near the IMP, and the other gp41 glycans, differ only subtly between the SOSIP.664 trimer and the pseudotrimer, similar to what was seen for the gp120 monomer comparison described above.

Overall, a glycan patch with increased mannose content is uniquely present on the fully cleaved, native-like SOSIP.664 trimer. This trimer-associated mannose patch (TAMP) wraps around

the trimer apex and the protomer interface and includes, at minimum, the N156, N160, N197, N262, N276, N301 and N637 glycans.

5.4 Trimer formation constrains processing at a fractionally occupied O-glycosylation site

Recombinant Env glycoproteins have been reported to contain O-linked glycans at gp120 position T499 [232,235,248,249]. LC-ESI MS spectra from the deglycosylated tryptic digests of the three Env constructs were searched for exact mass matches of O-glycosylated peptides. They were confirmed by the presence of the characteristic oxonium ions as well as by using HCD fragmentation data (Section 2.5.4). Thus, it was possible to identify a microheterogeneity of commonly known O-glycans on T499 of each BG505 Env protein, mainly of the mono- and di-sialyl core 1 type, but with highly different fractional occupancies (Figure 5.7 and Appendix E). The relative abundance of individual O-glycan structures were quantified the same way as for the N-linked glycans by adding up the ion intensities over all charge states for the individual glycopeptides. By including the non-glycosylated peptide, which contains an unmodified threonine, in this quantification the fractional occupancy of the T499 site could be determined.

O-glycan occupancy of the T499 site was highest for monomeric gp120 at ~7 %, compared to ~1 % and ~0.2 % for the pseudotrimers and SOSIP.664 trimers, respectively (i.e., 7- to 35-fold reductions compared to gp120). Therefore it can be concluded, that while T499 is indeed a potential site for O-glycosylation on gp120, it is only rarely occupied, and even less so on the pseudotrimer and SOSIP.664 trimer. The T499 site is located close to the C-terminus of gp120, so the nearby presence of gp41 may impose steric constraints on the glycosyltransferases. Furthermore, the structures of the native-like BG505 SOSIP.664 soluble trimer and the JR-FL membrane-associated trimer show that the T499 site is not surface exposed when gp41 is present [206,216,217]. Indeed, in the native trimer context, the bulk of an O-glycan would not be accommodated within the gp120-gp41 interface, where T499 is located.

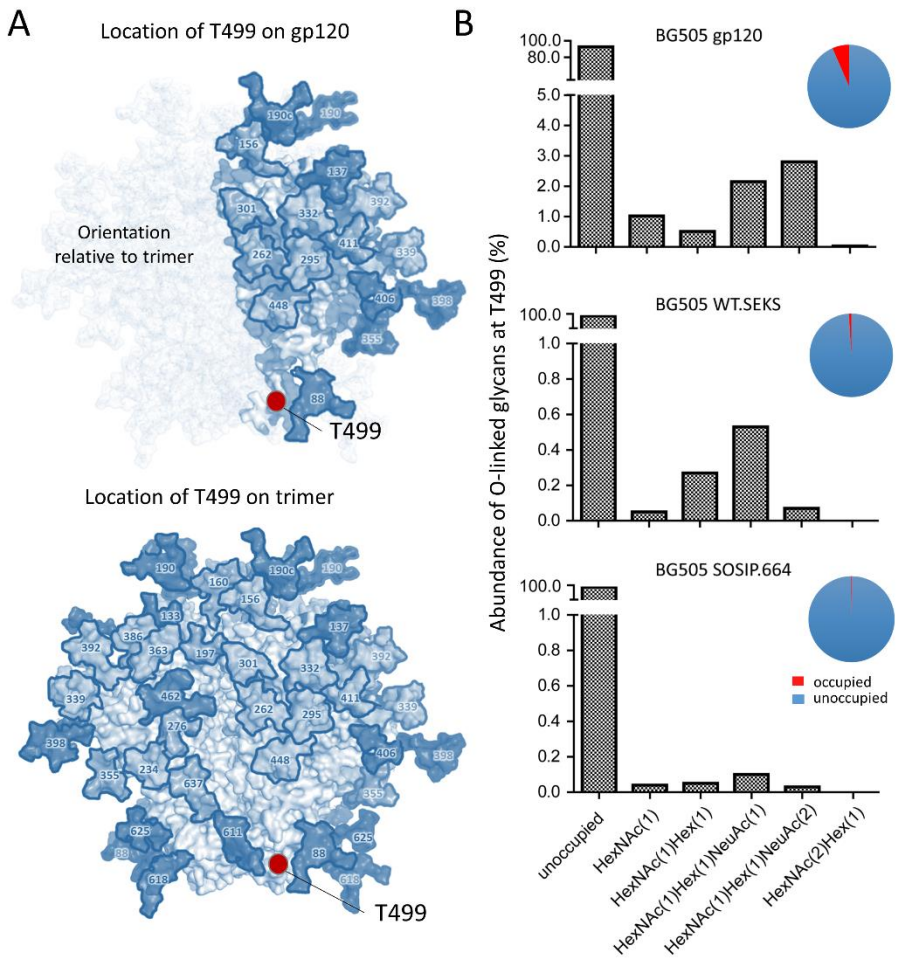

Figure 5.7: O-glycosylation of recombinant Env glycoproteins
(A) The location of the T499 O-glycosylation site is highlighted in red on the BG505 SOSIP.664 trimer model. (B) Quantification of the O-glycans identified on the gp120, WT.SEKS and SOSIP.664 Env proteins.

5.5 Conclusions

In this chapter, quantitative site-specific N-glycosylation analysis on isogenic monomeric, cleaved and uncleaved soluble Env glycoproteins was used to show that the formation of native-like trimers markedly affects the integrity of the glycan shield by providing additional protection from α-mannosidase processing. The 'trimer-induced mannose patch' was a previously postulated concept for how the glycan shield is remodeled upon oligomerization [237]. Its existence can now be confirmed and its location can be mapped on the trimer surface (Figure 5.8).

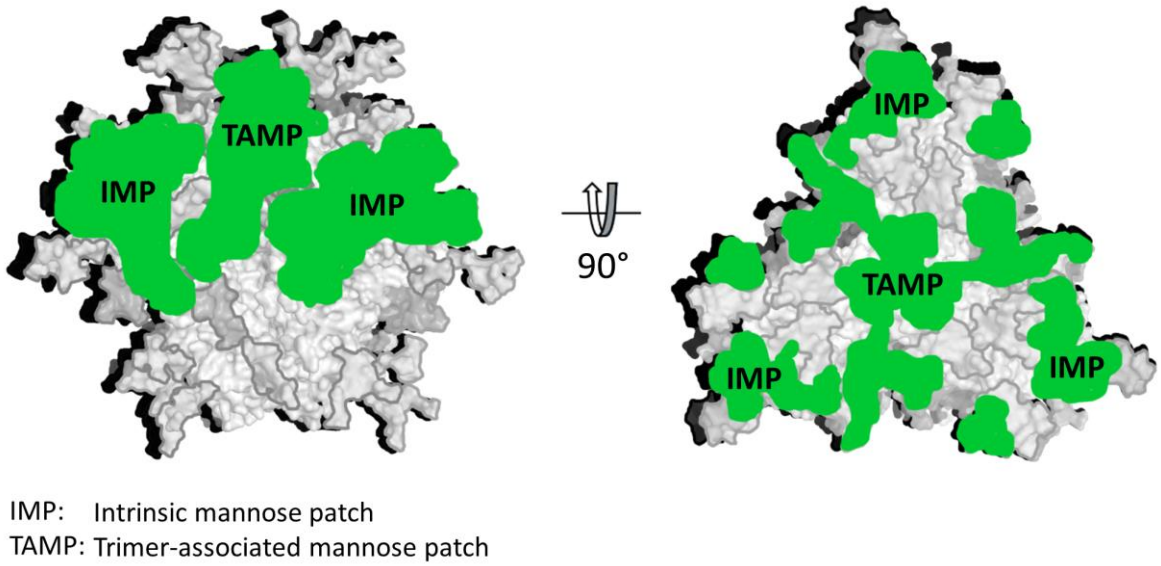

Figure 5.8: The trimer-associated mannose patch
Schematic depicting the localization of the intrinsic and the trimer-associated mannose patches (green) on the surface of the recombinant SOSIP trimer mimic. See text for details.

Furthermore, it is shown that the adoption of this characteristic glycosylation signature requires the formation of a compact, native-like trimer, and not simply the presence of multiple gp120 subunits within the same Env protein. In other words, like the gp120 monomers, the pseudotrimers lack a TAMP (Figure 5.9). The influence of furin cleavage on Env glycosylation processing points towards two possible models of Env maturation. Furin cleavage of the proprotein, gp160, could generate compactly folded trimers, which are then protected against subsequent post-furin α-mannosidase activity [184,466]. Alternatively, it could be hypothesized that the

protease selectively cleaves particular glycoforms of Env. Given the observation that furin overexpression leads to complete gp160 cleavage and that uncleaved gp160 can be partially processed by *in vitro* incubation with recombinant furin [194,461], it is here suggested that post-furin α-mannosidase activity is important in Env maturation. One aspect to be resolved is how to reconcile these observations with the proposed distribution of the enzymes and the substrate along the secretory pathway.

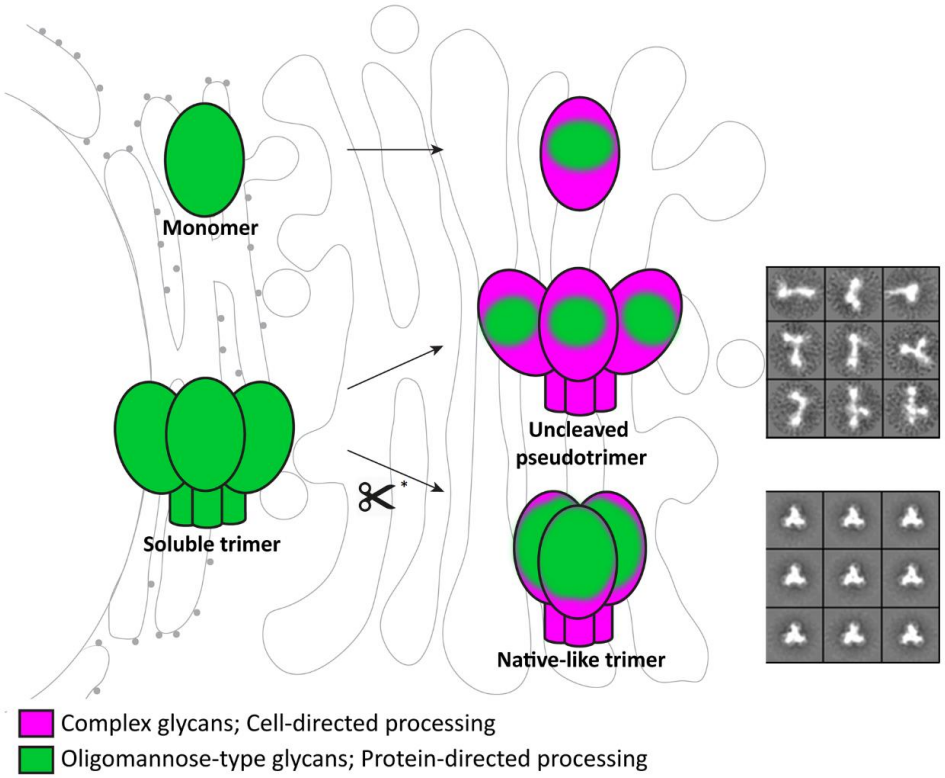

Figure 5.9: Envelope cleavage induces a TAMP
Trafficking through the secretory pathway exposes the glycoprotein to α-mannosidases and other glycan processing enzymes, which generally lead to the conversion of oligomannose-type glycans (green) to complex-type glycans (pink). However, intrinsic structural features of Env determine to which degree glycans can be accessed and processed by these enzymes. The outer domain of monomeric gp120 is characterized by a dense cluster of glycans that limits accessibility of ER and Golgi α-mannosidases and thus leads to the emergence of an intrinsic mannose patch, which is present on all presented Env constructs. Cleaved Env engages a compact quaternary structure that further constraints glycan processing and induces the formation of an additional trimer-associated mannose population. Uncleaved, non-native Env pseudotrimers, however, have an open and irregular structure (inset cryo-EM image) that allows easier access to processing glycans and hence leads to an elevation in complex-type glycans. (*) See Chapter 6 for an example of a cleavage-independent native-like trimer mimic.

The BG505 WT.SEKS pseudotrimers carry sub-populations of complex-type glycans on N-glycosylation sites (N234, N262, N332 and N363) where under-processed, oligomannose-type $Man_{8-9}GlcNAc_2$ structures predominate on the native-like SOSIP.664 trimers. The presence of molecules with processing at these sites within the pseudotrimer preparation is consistent with non-native folding and the impact of any aberrantly formed disulfide bonds. The heat maps in Figure 5.6 show how the structural constraints that apply to the native trimer lead to an increase in oligomannose content. A converse perspective is that the loss of those constraints increases the processing of multiple glycans on the gp120 monomers and pseudotrimers. The outcome is generally an increase in the trimming of oligomannose-type glycans towards smaller forms, and in the population of complex-type glycans (e.g. N355).

The detailed site-specific N-glycosylation profiles help us to understand how the different Env immunogen designs drive differences in the processing of key glycans. For example, the gp120 monomers and WT.SEKS pseudotrimers bind the trimer-reactive, apex-recognizing bNAbs PG16 and PGT145 poorly or not at all [200,205]. The inability of the non-native Env proteins to present these conformationally-sensitive epitopes is also reflected in their aberrant profiles of the glycan-sites near the trimer apex. For example, the N160 site on the native-like trimer is dominated by oligomannose-type glycans whereas bi-, tri- and tetra-antennary complex-type glycans predominate on the pseudotrimer. It can also be noted that the oligomannose content of the N276 glycan on SOSIP.664 trimers is ∼70 percentage points greater compared to the same site on the gp120 monomer. Indeed, N276 was the gp120 glycan that differed the most between the trimer and the monomer in this regard. The N276 site was also more processed on the pseudotrimer than on the native-like trimer (35 percentage points lower oligomannose content). The N276 glycan is located near the CD4bs, where it plays a role in shielding key epitopes for bNAbs of the VRC01 class [467]. An oligomannose-type glycan at this position forms part of the epitope of the CAP257-RH1 antibody isolated from a donor infected with a clade C HIV-1 strain [468]. The high oligomannose status of the N276 glycan on native-like SOSIP.664 trimers may therefore reflect the composition

of the same glycan on virion-associated Env (i.e., in the CAP257-RH1 donor). Inducing VRC01-class bNAbs is the goal of several Env vaccine programs based on targeting specific precursors of these antibodies in the human germline repertoire, followed by a boosting regimen intend to drive the maturation of any initially induced precursors. These programs use a variety of Env proteins including those based on gp120 outer domains, gp120 monomers or non-native gp140s [469-471]. The glycoform compositions of these immunogens will need to be determined experimentally but some sites (including, when present, N276) may be more highly processed than on native trimers, based on what can observed with the BG505 gp120 monomers and pseudotrimers. The implications for the design of germline-targeting priming and boosting immunogens would need to be considered.

6 Cleavage-independent Env exhibits native-like constraints on glycan processing

The replication of the native glycan shield of HIV-1 Env is an important aspect in B cell-based immunogen design. Well-ordered, cleaved trimers of the SOSIP design are currently considered the most superior candidate immunogens. They display a very homogenous, oligomannose-dominated glycosylation profile, which is regarded as typical for native-like viral glycosylation and generally correlates to a native-like structure of Env [184]. The recombinant production of fully cleaved SOSIP trimers, however, requires the overexpression of furin, which can possibly be regarded as a disadvantage. Uncleaved gp140 trimers have been shown to adopt an irregular, non-native conformation and, as explored in Chapter 5, contain a reduced abundancy of oligomannose-type glycans [184,200]. Nevertheless, recently a different strategy to create soluble, cleavage-independent trimers was developed based on the introduction of a flexible linker between the gp120 and gp41 subunits (Figure 6.1) that does not require furin co-expression. These constructs are termed 'NFL' (native, flexibly linked) trimers and were shown to contain antigenic, biophysical and structural properties consistent with native-like Env [366]. The flexible peptide linker consists of glycine and serine (2 x G_4S) and was used to replace the furin cleavage site. The thus provided conformational mobility of Env allows a native-like orientation, albeit gp120 and gp41 remaining covalently linked [366].

In this chapter, a detailed N-glycosylation analysis of a clade A BG505 NFL2P.664 trimer (here NFL trimer) is presented and compared to BG505 SOSIP.664 (SOSIP trimer). The cleavage-independent trimer exhibits an oligomannose-dominated, native-like glycosylation profile. The data suggest the possibility of a furin-independent maturation for natively folded and glycosylated Env in the secretory pathway.

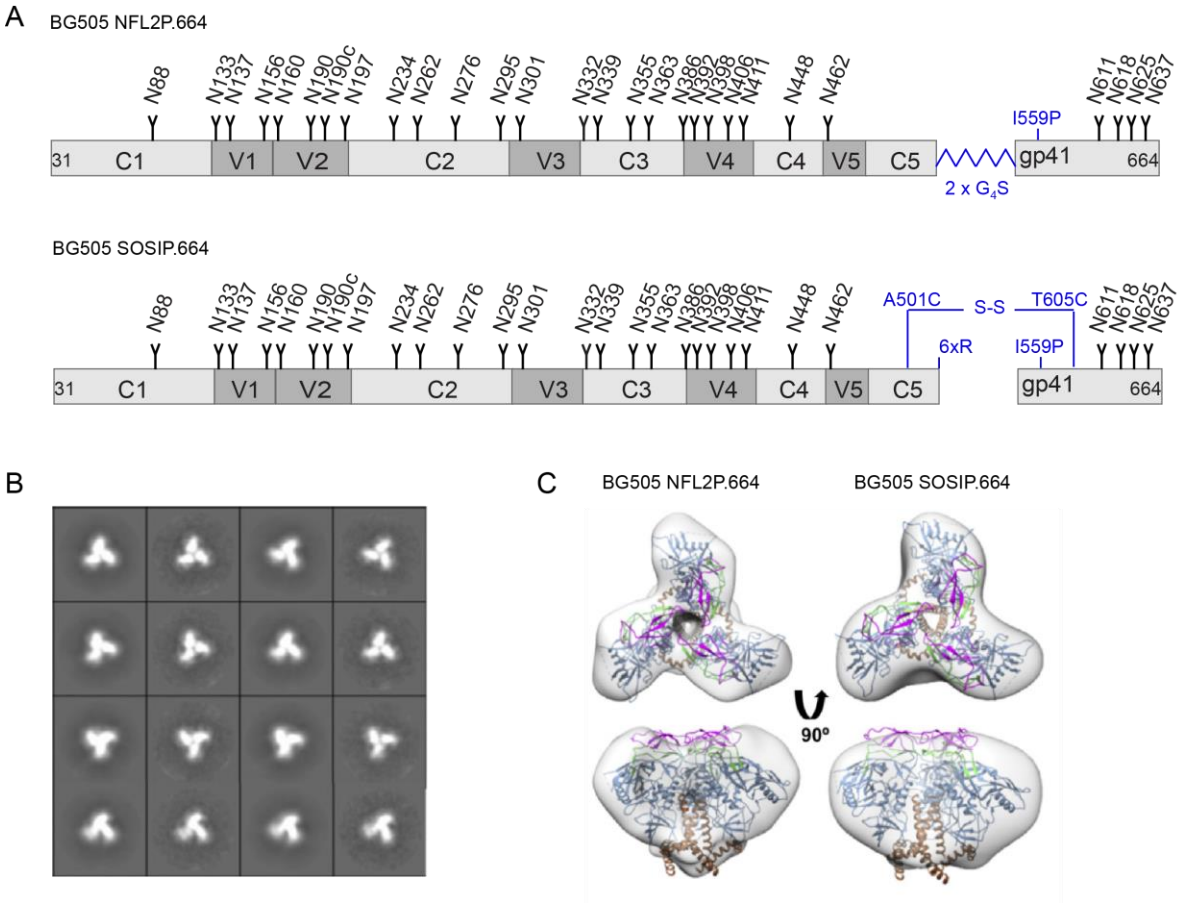

Figure 6.1: Schematic representation and structure of BG505 NFL2P.664 compared to SOSIP.664
(A) Schematic representation of the BG505 NFL2P.664 and SOSIP.664 constructs. Changes are highlighted in blue. (B) Negative stain EM analysis of BG505 NFL2P.664, adapted from [366]. (C) EM 3D reconstructions of unliganded BG505 NFL2P.664 and BG505 SOSIP.664 in gray with BG505 SOSIP.664 crystal structure (PDB 3J5M) fitted within (blue, gp140; V1V2, magenta; V3, green; gp41, brown). Figure adapted from [366].

6.1 N-glycosylation profile of native, flexibly linked Env trimers

The design of BG505 NFL2P.664 has been described previously [366] and is summarized in Figure 6.1. CHO- and HEK 293F cell-produced BG505 NFL2P.664 trimers as well as HEK 293F cell-produced BG505 SOSIP.664 comparators (Table 2.1) were provided by Dr Shailendra Kumar Sharma (The Scripps Research Institute). The trimers were transiently expressed and purified via a combination lectin-affinity chromatography, followed by SEC and negative selection using a F105 mAB affinity column (F105 is a non-NAb). Well-ordered trimers did not bind to the F105 column and could be found in the flow through, which was subjected to another round of SEC purification [366].

For overall N-glycosylation profiling, glycans were enzymatically released, fluorescently labeled and analyzed by HILIC-UPLC (Section 2.4.2). The glycosylation profiles of the cleavage-independent NFL2P.664 trimers are highly similar to that of fully cleaved SOSIP.664 (Figure 6.2).

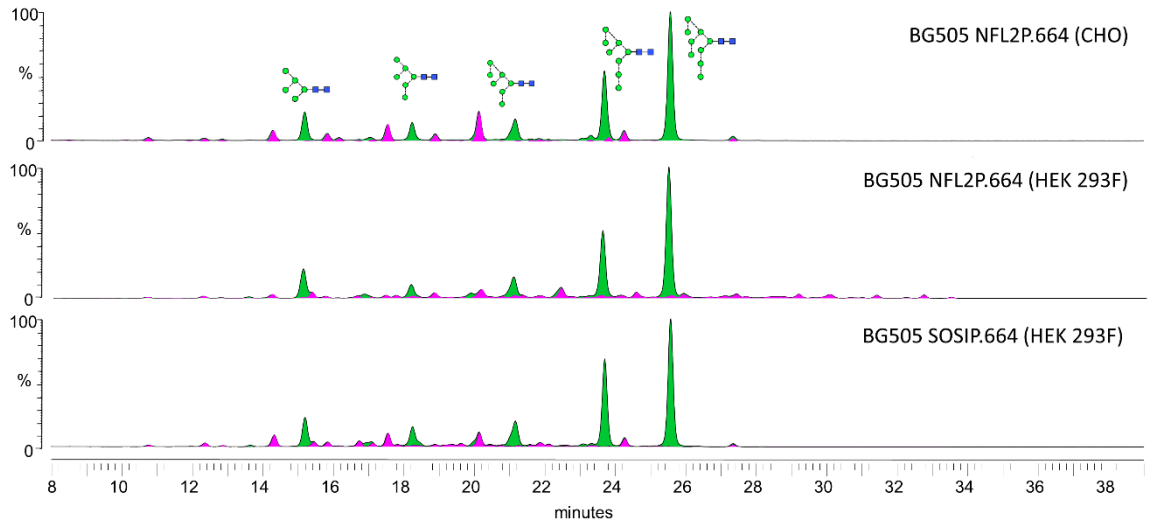

Figure 6.2: Overall glycan profiles of BG505 NFL2P.664 and SOSIP.664 trimers
HILIC-UPLC profiles of fluorescently labeled glycans from CHO cell- (upper panel) HEK 293F cell- (middle panel) produced BG505 NFL2P.664 and HEK 293F cell-produced BG505 SOSIP.664. All trimer were purified in the same way as described in [366]. Peaks corresponding to oligomannose- and hybrid-type glycans in green whereas those corresponding to complex-type glycans are in pink. The oligomannose series is indicated with the appropriate structures representing the most abundant isomer.

In order to investigate whether or not the locations of oligomannose-type and complex-type glycans coincide in the NFL trimer and the SOSIP trimer, site-specific N-glycosylation analysis (as described in Chapter 3), was performed. Information on the protein-specific IM-ESI MS-generated glycan libraries for CHO cell- and HEK 293F cell-produced BG505 NFL2P.664 can be found in Appendix D. As it is also evident from Figure 6.2, the dominance of oligomannose-type glycans is independent from the producer cell line. The glycan libraries reveal only small differences in the types and abundance of hybrid and complex-type glycans on NFL trimers originating from both cell lines.

When compared to the previously presented site-specific data from BG505 SOSIP.664, the location of microclusters on the NFL trimers is highly similar (although purified differently; Figure 6.3). While there are a few sites that display differences in the ratio of oligomannose- *vs* complex-type glycans, both compared to BG505 SOSIP.664 and between the two different producer cell lines, the mannose patch wrapping around the outer domains of the trimer is preserved. As described before (Section 4.1), it centers around the N295, N332, N392 glycans and also includes N234, N262, N339, N363, N386 and N448 – all carrying $Man_9GlcNAc_2$ as the most prominent structure. The complex-type glycans are again located mainly near the N- and C-terminus of the single chain trimers (Figure 6.3). One main difference, however, is the N-glycosylation site at N160. While it was found to contain a mixture of oligomannose- and complex-type glycans on SOSIP, here it is exclusively oligomannose. As described in Chapter 5, N160 is part of TAMP and influenced by the quaternary structure of Env. The observation that the N160 glycan is more under-processed on the NFL trimers compared to SOSIP may possibly reflect small structural differences around the trimer apex. Similarly, N197 – also part of the TAMP and also residing in proximity to the trimer apex – shows a higher abundance of oligomannose-type glycans (Figure 6.3). Figure 6.4 shows a direct comparison of the processing the states near the trimer apex of NFL and SOSIP trimers, including the locations of N160 and N197.

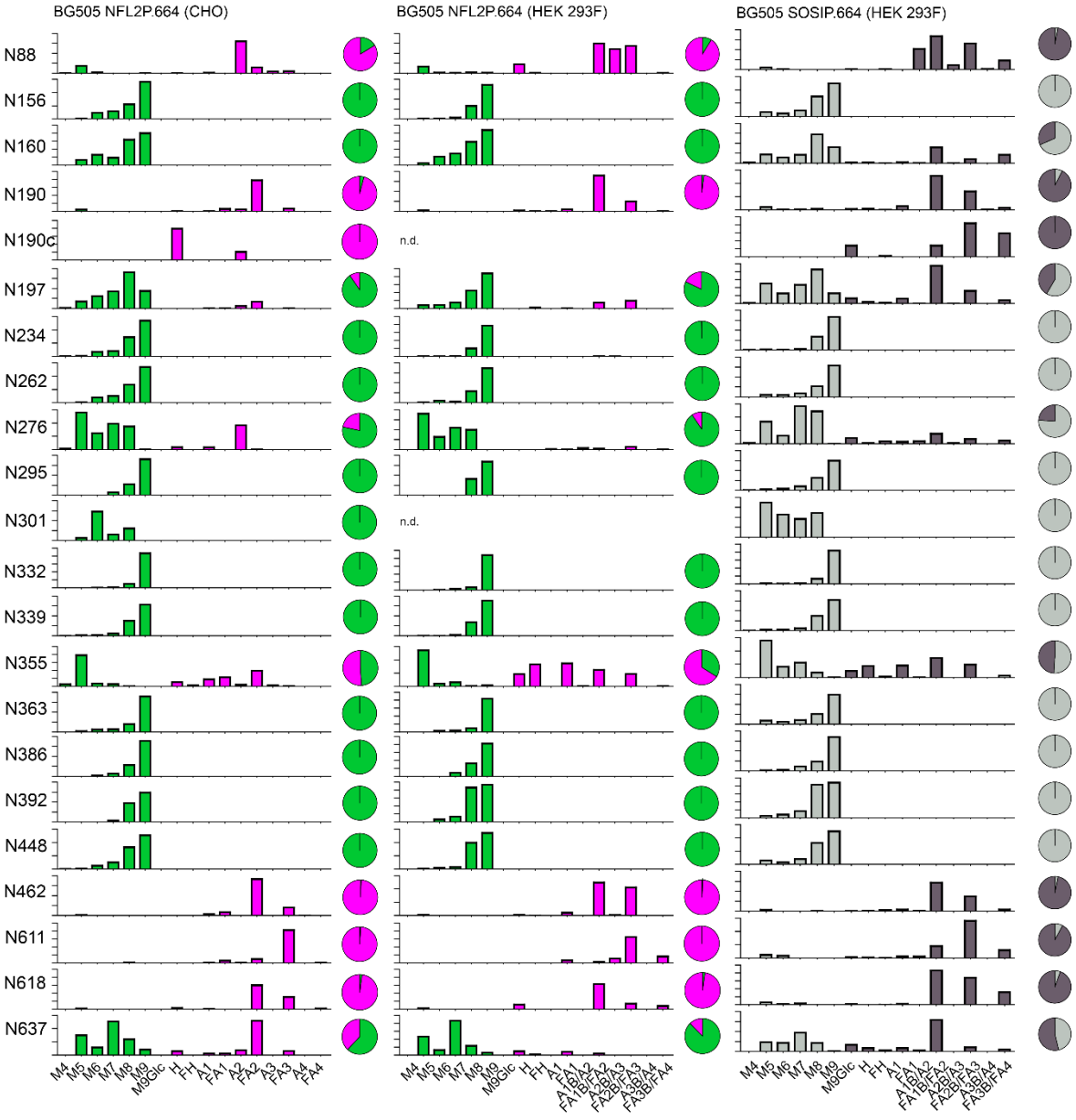

Figure 6.3: Quantitative site-specific N-glycosylation of single chain NFL trimers
Relative quantification of the N-glycosylation sites identified on BG505 NFL2P.664 trimers produced in CHO cells (left panel) and HEK 293F cells (middle panel), purified by negative selection [366]. For information on the location of peak lists of identified tryptic and chymotryptic glycopeptides, see Appendix E. The bar graphs represent the means of two analytical replicates, and the quantification of oligomannose-type (green) and complex-/hybrid-type glycans (pink) on individual sites is summarized in the pie charts. For site-specific comparison, the right panel in grey displays data from HEK 293F cell-produced BG505 SOSIP.664, purified by 2G12-affinity chromatography and SEC (data presented as part of Chapters 4 and 5 and reproduced here to aid comparison). Light grey, oligomannose-type glycans; dark grey, complex-type glycans.

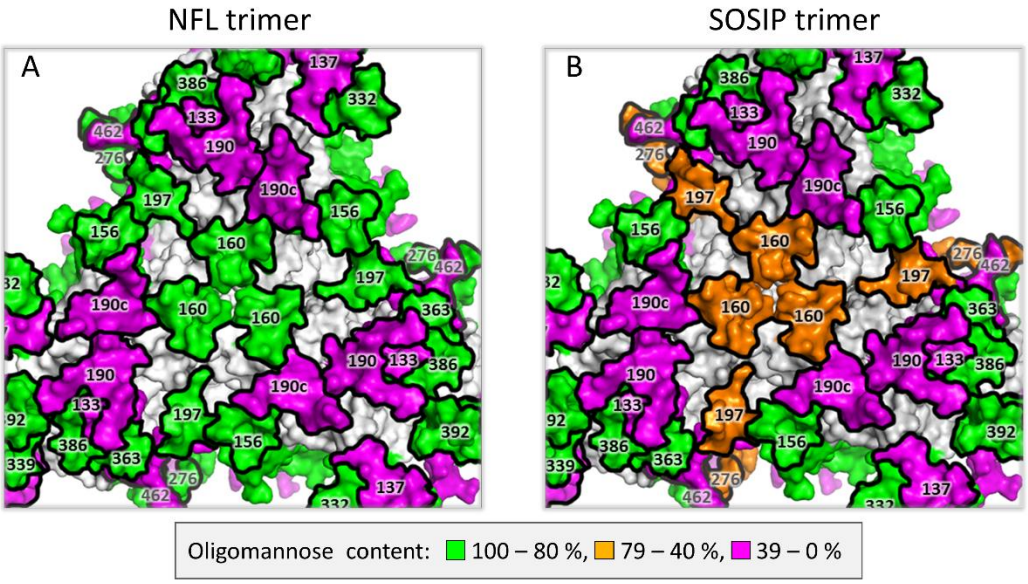

Figure 6.4: Processing of glycans near the trimer apex
The model was constructed using PDB ID 5ACO [207] as previously described in Chapter 4. The glycans are color-coded according to their processing state (see key on the Figure). (A) Glycan processing of HEK 293 F cell-produced BG505 NFL2P.664, purified by lectin chromatography, SEC and negative selection. For data, see Figure 6.3. (B) Glycan processing of HEK 293 F cell-produced BG505 SOSIP.664, purified by 2G12-affinity chromatography and SEC. For data, see Figure 6.3.

While it is possible that a slight difference in glycan processing around the trimer apex can be attributed to structural differences in that region, the NFL and SOSIP trimers in Figure 6.4 were not expressed and purified under the same conditions and should thus only be conditionally compared. A crystal structure of BG505 NFL2P.664 could provide additional information on the potential for conformational variations within that region.

6.2 Conclusions

In this chapter, the glycosylation of a cleavage-independent, flexibly-linked, soluble clade A BG505 trimer was found to be highly similar to that of the corresponding fully cleaved BG505 SOSIP.664. Native-like properties of the NFL trimers were previously reported [366], and are supported by the glycosylation data presented here. The large abundance and location of oligomannose-type glycans reveal that steric protection from glycan processing is maintained. As highlighted in Chapter 5, Env glycosylation is dictated by its quaternary structure and not solely by glycan density effects. The presence of a linker in the single chain gp120-gp41 constructs allows the adoption of a native-like fold. Thus, they differ from previous reported uncleaved, irregular folded Env constructs in that they do not show the in Chapter 5 reported elevated glycan processing. While a furin-independent way of producing native-like, soluble trimers has advantages for vaccine design, it also provides interesting insights into Env maturation. The data indicate the option of a furin-independent pathway in the secretory system. As discussed in Chapter 5, the main hypothesis is that furin acts early in the secretory pathway and allows the formation of a quaternary structure that provides protection from oligomannose-trimming enzymes. The NFL construct design could allow a similar early engagement of native-like protein folding due to spatial flexibility between the gp120 and gp41 subunits leading to steric protection from processing enzymes. The Env maturation model in Figure 5.9 is thus likely just one simplified version of (a) much more complex pathway(s). Overall, the data presented in this chapter show that a native Env carbohydrate mimicry can be achieved by an appropriate cleavage-independent trimer design, hence offering new opportunities for HIV-1 immunogen development.

7 Integrity of glycosylation processing of a glycan-depleted trimeric HIV-1 Env immunogen targeting B cell lineages

Various soluble, native-like Env trimers rooted in the prototypic BG505 SOSIP.664 design are now platforms for the creation of Env immunogens aimed at inducing a broad and potent B cell response [205,359]. They have also facilitated an ever-increasing understanding of the structure and function of the Env trimer and the multiple bNAb epitopes displayed on its surface [206,215,217,413,472]. Some SOSIP.664 trimers can induce strong NAb responses against the autologous neutralization-resistant (Tier 2) primary viruses, which had been generally difficult to achieve using earlier designs of Env proteins [359]. The SOSIP.664 design can be improved by introducing additional stabilizing changes to make SOSIP.v4.1 variants. These modified trimers are less immunogenic for antibodies to the immunodominant gp120 V3-region that neutralize sensitive Tier 1 viruses but not their more relevant Tier 2 counterparts [473].

A central goal of various Env vaccine development programs is to improve the breadth of the elicited antibody response, a step in the path towards true bNAbs. Viral diversification under immune selection pressure can gradually drive substantial increases in the breadth and potency of an initially narrow and often weak initial NAb response [474]. This knowledge of a natural process guides vaccination strategies based on priming with an Env immunogen that is specifically designed to activate B cell receptors on naïve cells in the germline (gl) so that they produce bNAb precursors (gl-bNAbs). These initial responses can then be boosted with one or more engineered immunogen(s) that sequentially guide the B cells to mature and produce antibodies with a bNAb-like phenotype [298,301,475-477].

A version of the BG505 SOSIP.v4.1 trimer, termed SOSIP.v4.1-GT1 (germline-targeting trimer version 1; GT1 trimer for short) was specifically modified to confer the ability to bind multiple different gl-bNAbs, specifically ones directed against the trimer apex and the CD4bs [417]. Compared to the BG505 SOSIP.664 and SOSIP.v4.1 trimers, the GT1 variant contains 15 amino-acid

substitutions and a 7-residue deletion that facilitate gl-bNAb binding. Four of these changes involve the elimination of potential N-glycosylation sites near the CD4bs to remove impediments to the binding of gl-bNAbs [318,350,354,414,417]. Several other changes in V2 enhance the binding of gl-bNAbs to trimer-apex epitopes; here, deletion of 7 residues from V2 removes a PNGS near the apex. Overall, the glycan shield of the GT1 trimer lacks 15 N-glycosylation sites (5 per protomer), three of which (N197, N276 and N386) are highly conserved, with a prevalence of more than ~85 % across multiple HIV-1 strains [449]. Figure 7.1 summarizes the design of the GT1 trimers.

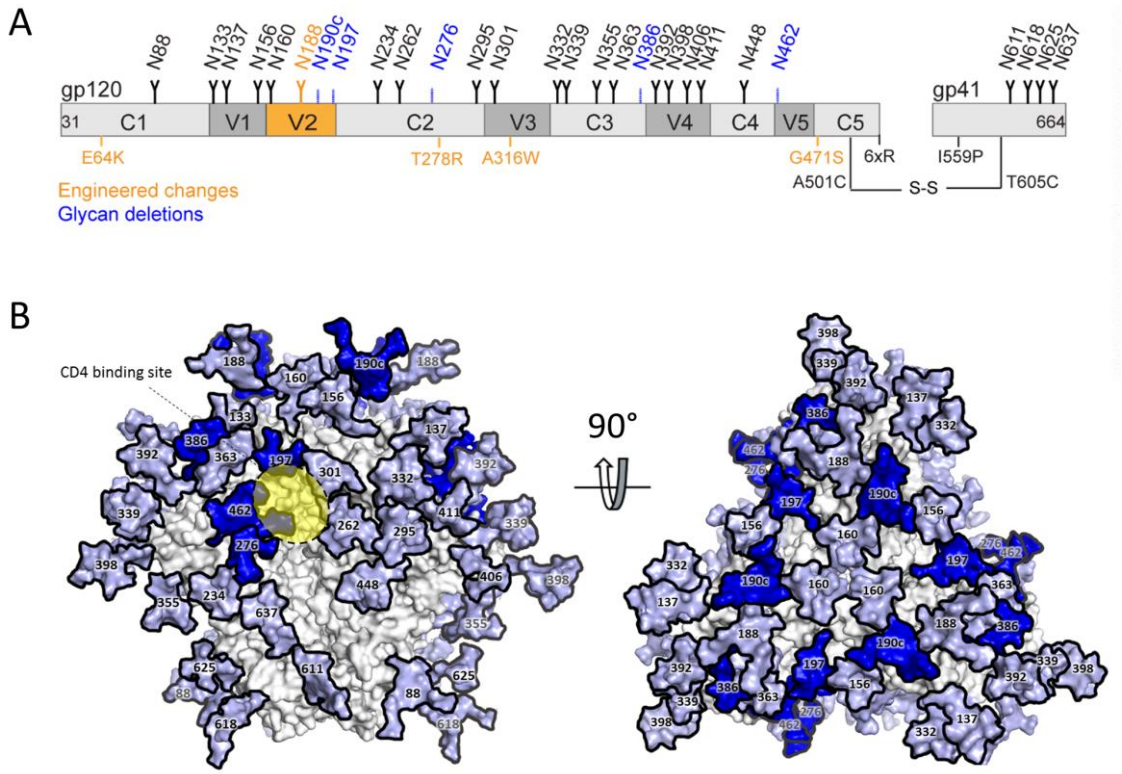

Figure 7.1: Design of BG505 SOSIP.v4.1-GT1 trimers
(A) Schematic representation of the BG505 SOSIP.v4.1-GT1 construct. The constant (C1-C5) and variable (V1-V5) regions of gp120 are highlighted in light and dark grey, respectively. The stabilizing substitutions present in the SOSIP.664 construct are shown in black, modifications that create the SOSIP.v4.1-GT1 construct are labeled in orange. Additional changes to the latter construct, including a deletion in V2, are described in detail elsewhere [417]. The SOSIP.664 glycans are shown as black icons, with the ones deleted from the GT1 construct colored blue. (B) The glycans deleted from the GT1 trimer are highlighted in light blue on a model of the fully glycosylated BG505 SOSIP.664 trimer (the remaining glycans are in dark blue). The approximate location of the CD4bs is highlighted in yellow. The model was constructed using PDB ID 5ACO [207] as previously described in Chapter 4.

Despite these modifications, the BG505 SOSIP.v4.1-GT1 trimer retains a native-like structure and has biophysical and biochemical properties similar to the SOSIP.664 and SOSIP.v4.1 versions from which it was derived [417]. However, unlike these precursor trimers, GT1 binds multiple gl-bNAbs and activates B cells expressing these in vitro. Furthermore, when tested as an immunogen in various knock-in mouse models, GT1 triggers the production of CD4bs-targeting (gl-VRC01 and gl-CH103) and N332/V3-directed (gl-PGT121) germline antibodies [417].

This chapter presents a quantitative, site-specific N-glycosylation analysis of BG505 SOSIP.v4.1-GT1 trimers purified from a stable CHO cell line for comparison with a similar analysis of the SOSIP.664 precursor trimer that was produced and purified in the same way. Hence, the impact of removing 15 PNGSs on the overall composition of the Env glycan shield can be assessed. While GT1 trimer glycans in close proximity to deleted sites were slightly more processed than on the SOSIP.664 comparator, the overall processing state of the N-glycans was remarkably stable. The targeted removal of individual glycan sites does not perturb the overall architecture of the glycan shield, a finding that should support the further use of this Env immunogen design strategy.

7.1 Glycan-depleted GT1 trimers retain an oligomannose glycan signature

The design and structure of BG505 SOSIP.v4.1-GT1 trimers has been described elsewhere and is summarized in Figure 7.1 [417]. Trimers were produced in a stable CHO cell line, using the same method as previously described for BG505 SOSIP.664 [424] and purified by 2G12-affinity chromatography followed by SEC. Both GT1 trimers as well as the comparably produced and purified SOSIP.664 comparator were provided by Prof. John Moore/Dr Al Cupo (Weill Cornell Medical University). The overall glycan profiles of the BG505 GT1 and SOSIP.664 trimers were compared. The N-glycans were enzymatically released, fluorescently labeled and analyzed by HILIC-UPLC (Section 2.4.2). The abundance of oligomannose-type glycans ($Man_{5\text{-}9}GlcNAc_2$) was determined by cleavage of the labelled glycan pool with Endo H (Figure 7.2). Both trimers yielded very similar, oligomannose-dominated glycosylation profiles, as previously reported for BG505 SOSIP.664 (Chapter 4; [184]).

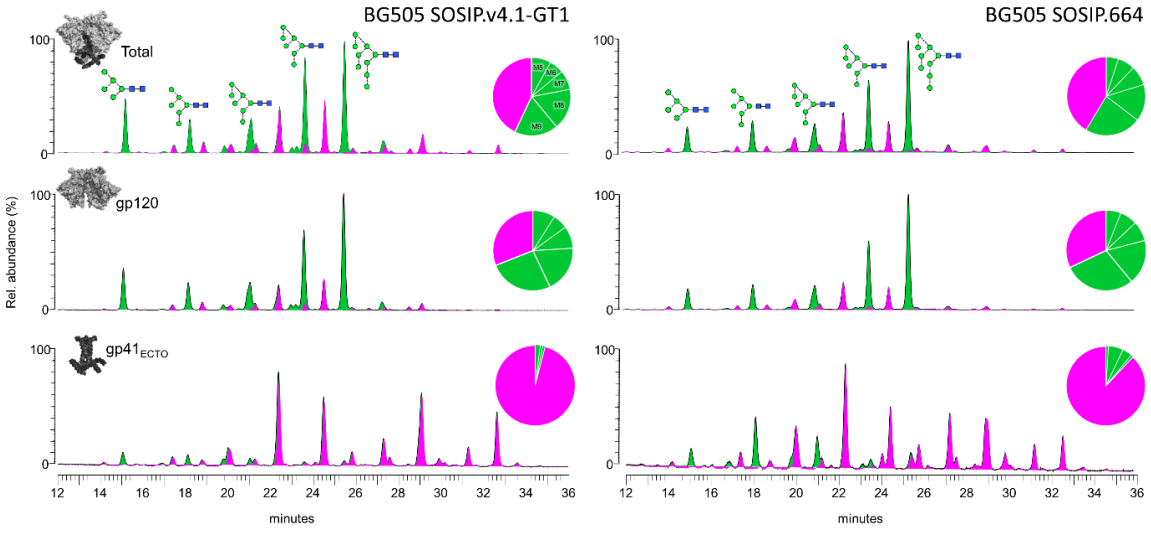

Figure 7.2: Glycosylation profiles of BG505 SOSIP.v4.1-GT1 and SOSIP.664 trimers from CHO cells
HILIC-UPLC profiles of fluorescently-labelled N-linked glycans from BG505 SOSIP.v4.1-GT1 (left) and SOSIP.664 (right) trimers produced in CHO cells and purified by 2G12-affinity chromatography followed by SEC. Trimers were provided by Prof. John Moore/Al Cupo (Weill Cornell Medical University). Oligomannose- and hybrid-type glycans (green) were identified by their sensitivities to Endo H digestion. Peaks corresponding to complex-type glycans are depicted in pink. The pie charts summarize the quantification of the glycan processing states, as determined by integration of the chromatogram. Glycan sequencing data derived by exoglycosidase digestion of the GT1 trimer are shown in Figure 7.3.

Figure 7.3 shows the glycan sequencing and corresponding structural assignment of the CHO cell-produced GT1 glycan profile by exoglycosidase digestion.

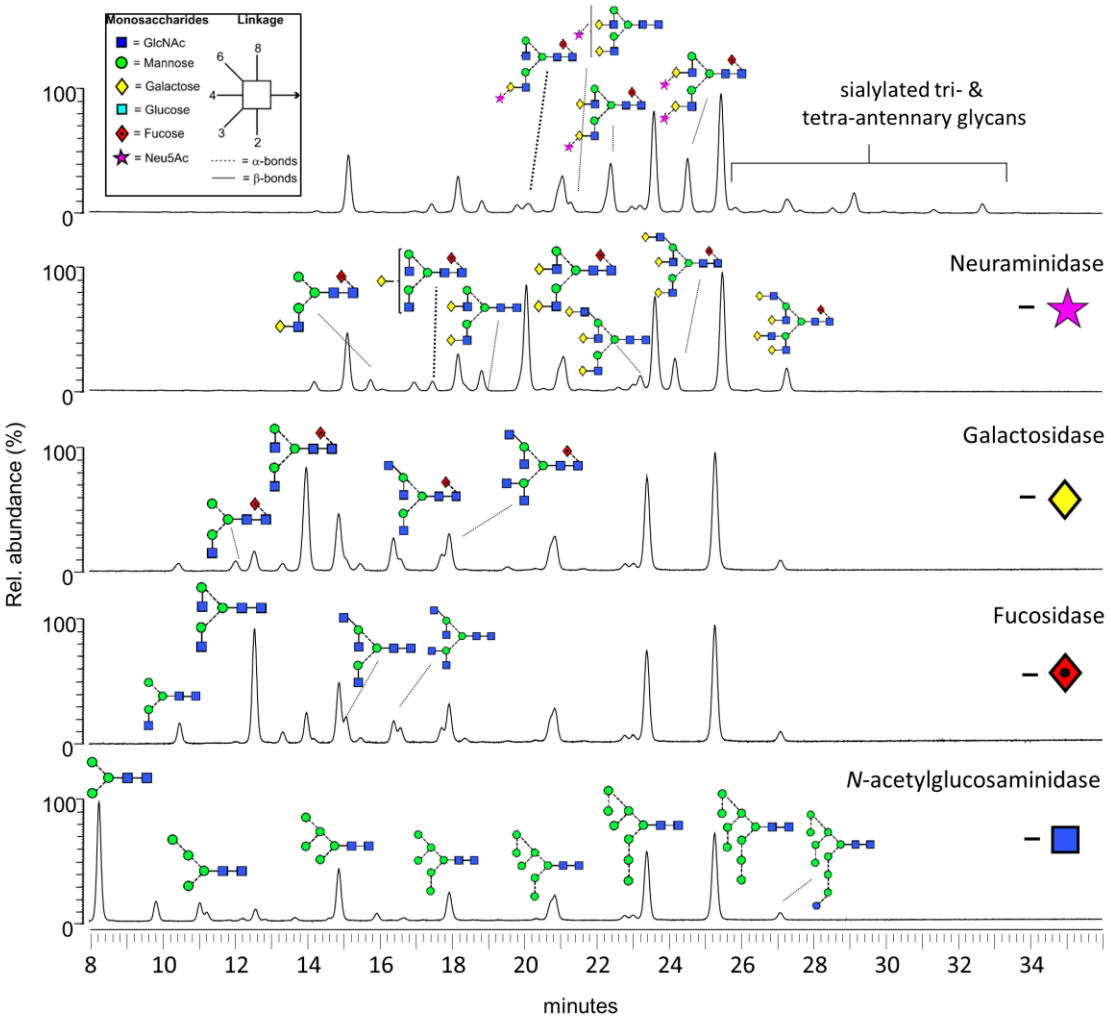

Figure 7.3: Glycan sequencing of BG505 SOSIP.v4.1-GT1 trimers by exoglycosidase digestion
Peaks were assigned by a sequential enzymatic digestion of 2-AA labeled glycans with a panel of exoglycosidases, followed by HILIC-UPLC analysis. The top panel shows the undigested glycan profile of BG505 SOSIP.v4.1-GT1 trimers produced in CHO cells. The profiles below represent digestions with the following exoglycosidases: Neuraminidase from *Clostridium perfringens*, β1,4-galactosidase from *Streptococcus pneumonia*, α-L-fucosidase from bovine kidney and β-*N*-acetylglucosaminidase from *S. pneumonia*. Rel., relative.

The overall oligomannose contents of the GT1 and SOSIP.664 trimers were almost identical (57 % and 59 %, respectively). It can, however, be noted that the abundance of $Man_8GlcNAc_2$ in relation to $Man_9GlcNAc_2$ was elevated for GT1 (Figure 7.2). The slight, producer-cell independent increase in overall α-mannosidase processing for GT1 presumably reflects the elimination of five

glycans that are present on the SOSIP.664 trimer and the consequent exposure of some nearby sites (see below). The glycan profile of the GT1 trimer gp41 subunit is almost exclusively dominated by complex-type glycans, whereas oligomannose type glycans are somewhat more abundant on gp41 from SOSIP.664 (4 % on GT1 *vs* 12 % on SOSIP trimers) (Figure 7.2). This shift may reflect subtle changes in the local environment of individual glycans neighboring the gp120 glycans

To probe the influence of glycan depletion on the glycan shield in greater detail a database of all identified glycan structures IM-ESI MS was generated, both to characterize the range of different N-linked glycans and then to facilitate a subsequent site-specific N-glycosylation analysis (Figure 7.4, Appendix D). Negative ion fragmentation was used to accurately assign the structure and major isomers of the glycans [463]. The IM-ESI MS spectrum shows that the gp120 subunit of the GT1 trimer has a significant population of oligomannose-type glycans (Figure 7.4A), which is consistent with the HILIC-UPLC glycan analysis (Figure 7.2).

Compared to BG505 SOSIP.664 trimers produced in stable HEK 293T cells (Figure 4.1) and transient HEK 293F cells (Figure 5.1), a less diverse range of complex-type glycans on the same trimers produced in CHO cells was found. This kind of variation reflects the different glycan-processing activities in the two cell types. For example, CHO cells do not express a functional *N*-acetylglucosaminyltransferase III [478], which generates bisecting glycans. No glycans with terminal sulfates, GalNAcs, or terminal α2,6-sialic acids were identified on the CHO cell-produced trimers. A higher degree of sialylation on CHO cell-derived proteins, compared to HEK 293, has been reported previously [479]. Consistent with that report, here, a high abundance of sialylated glycans on both of the CHO cell-produced SOSIP.664 and GT1 trimers was found, as determined by a neuraminidase digest of the glycan pool (Figure 7.3). The sialic acid moieties on these trimers are entirely α2,3-linked, as indicated by the absence of the characteristic *m/z* 306 ion from the tandem ion mobility fragmentation spectrum (Figure 3E) [480]. The dominance of under-processed, oligomannose-type $Man_{5\text{-}9}GlcNAc_2$ glycans is, nevertheless, well conserved between the two different producer cells.

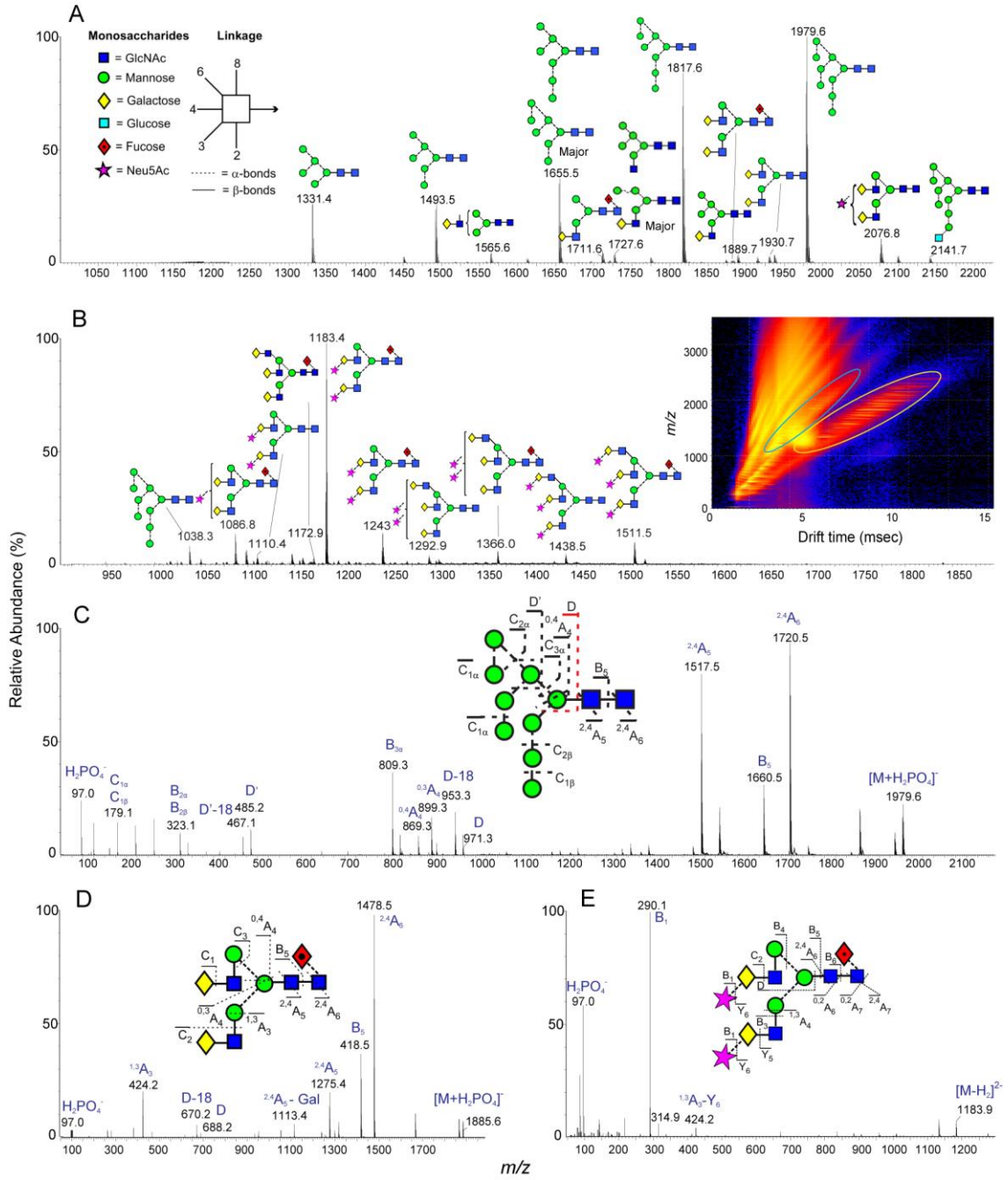

Figure 7.4: Ion mobility mass spectrometric analysis of BG505 SOSIP.v4.1-GT1 glycans
Negative ion electrospray spectra of N-glycans enzymatically released from the gp120 subunit of CHO cell-produced BG505 SOSIP.v4.1-GT1 trimers. (A) Mobility-extracted singly charged negative ions found on gp120. The corresponding singly charged ions are encircled with the yellow oval in the DriftScope image (*m/z* against drift time) in Panel B. (B) Mobility extracted doubly charged negative ions found on gp120. The ions are encircled with a blue oval in the DriftScope image. (C-E) Collision-induced dissociation spectra for three distinct glycans derived from the transfer region of the Synapt G2Si instrument. The insets to panels C, D and E show the corresponding glycans as well as the numbering of the fragments. Panel E shows only the low mass region to emphasize the missing *m/z* 306 ion, the absence of which is diagnostic of α2,3-linked sialic acids. The numbering scheme follows that proposed elsewhere [439]. The glycan symbols are shown on panel A. For glycan libraries of the SOSIP.664 and GT1 trimers, see Appendix D.

Overall, the glycome analyses of CHO cell-derived BG505 SOSIP.664 and GT1 trimers and HEK 293T cell-derived BG505 SOSIP.664 trimers described here and elsewhere concur: protein-directed glycosylation events yield the predominant oligomannose glycoforms, and cell type-dependent events create sub-populations of complex-type glycans [184]. The conserved oligomannose patches include the epitopes for multiple bNAbs and are one of the key properties of Env immunogens that need to be preserved when trimers are further engineered.

7.2 Site-specific N-glycosylation analysis reveals a robust oligomannose-patch

To better understand the effect of eliminating selected sites on the overall glycan shield of the GT1 trimer, a quantitative, site-specific N-glycosylation analysis on protease-digested glycopeptides by LC-ESI MS was performed (see workflow in Chapter 3). The site-analysis data show that the overall ratio between oligomannose- and complex-type glycans is highly similar for CHO cell-produced SOSIP.664 and GT1 trimers (Figure 7.5; inset pie charts), and also when compared with the corresponding data for the SOSIP.664 trimers produced in HEK 293F cells (Figure 4.3).

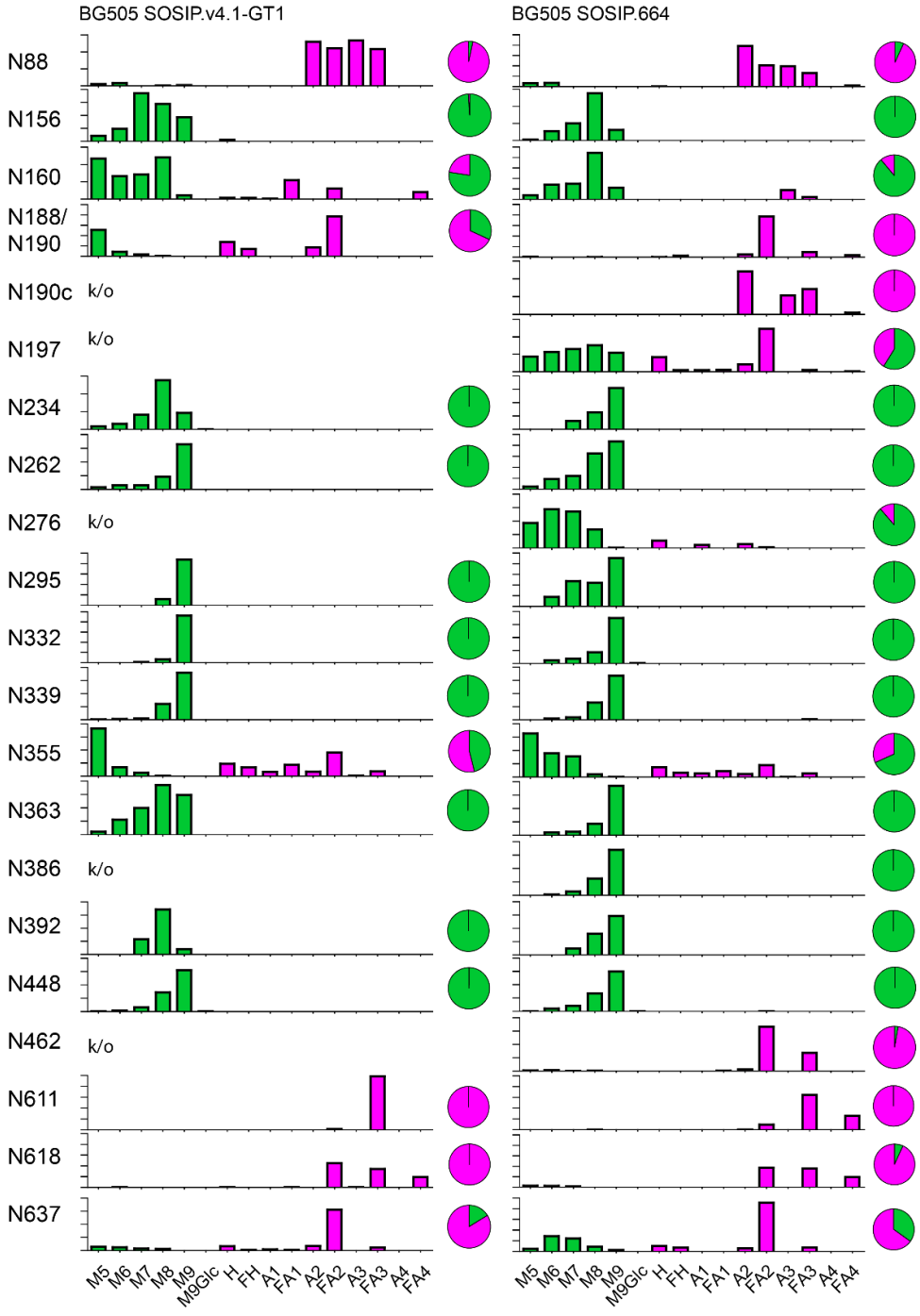

Figure 7.5: Quantitative site-specific N-glycosylation analysis
Relative quantification of N-glycosylation sites on the BG505 SOSIP.v4.1-GT1 and SOSIP.664 trimers. Quantitative data could be obtained for 16 and 21 glycan sites for the SOSIP.v4.1-GT1 and SOSIP.664 trimers, respectively. The trimers were digested with trypsin or chymotrypsin, enriched for glycopeptides and analyzed by LC-ESI MS. For SOSIP.v4.1-GT1, the bar graphs represent the means of two analytical replicates, for SOSIP.664 one analysis was performed. The pie charts summarize the quantification of oligomannose-type (green) and complex-/hybrid-type glycans (pink) on individual sites. The analysis was based on a glycan library generated by ion mobility ESI mass spectrometry (Appendix D). The abundances of individual species in different categories have been combined according Appendix C. k/o, knock-out (N-glycosylation site deletion).

However, a detailed inspection of the underlying profiles reveals several examples of elevated trimming within the oligomannose glycan series on the GT1 trimer compared to SOSIP.664, exemplified by a drop in $Man_9GlcNAc_2$ and a higher abundance of $Man_{5-8}GlcNAc_2$. This phenomenon is particularly evident at the N234, N363 and N392 sites where the $Man_9GlcNAc_2$ to $Man_8GlcNAc_2$ ratio inverts (i.e., $Man_9GlcNAc_2$ is predominant at these sites on SOSIP.664, but $Man_8GlcNAc_2$ on GT1). The implication is that α-mannosidase processing occurs to a greater extent at these sites on the GT1 trimer, which is understandable as these three sites are very close to positions from which PNGSs were deleted (Figure 7.6). For example, it is likely that mannose trimming at N392 is impeded by the presence of the nearby N386 glycan on the SOSIP.664 trimer, but can occur more readily on GT1, which lacks N386. Of note is that, despite the deletion of three surrounding glycan sites (N386, N462 and N197), the N363 glycan on the GT1 trimer was slightly more trimmed compared to SOSIP.664 but still remained oligomannose-type. The implication is that there are still significant impediments to the further processing of this glycan, such as the N392 glycan and/or ones located in V2 (Figure 7.1). Hence, there may be significant redundancy among the various steric factors that impede α-mannosidase trimming at sites within the intrinsic and trimer-associated mannose patches where oligomannose glycans are particularly densely clustered.

Elevated processing toward smaller oligomannose-type glycans was also seen at the N156 and N160 sites in the V1-V2 region of the GT1 trimer, which may again reflect the reduction in the local glycan density caused by the removal of the nearby N190c and N197 glycans. The 7 amino-acid deletion that shortens V2 could also be contributory. The model of the glycosylated trimer, presented in Figure 7.6, implies that the steric restriction to the processing of the N160 glycan may be driven by the inter-protomer clustering of the three N160 glycans where they converge at the trimer apex. Evidence for clustering is provided by cryo-EM and X-ray crystallography structures of BG505 SOSIP.664 trimers [206,217] and has been shown to limit α-mannosidase processing by

comparison of the native-like BG505 SOSIP.664 N160 glycans to those of monomeric and uncleaved gp160 pseudotrimers (Chapter 5).

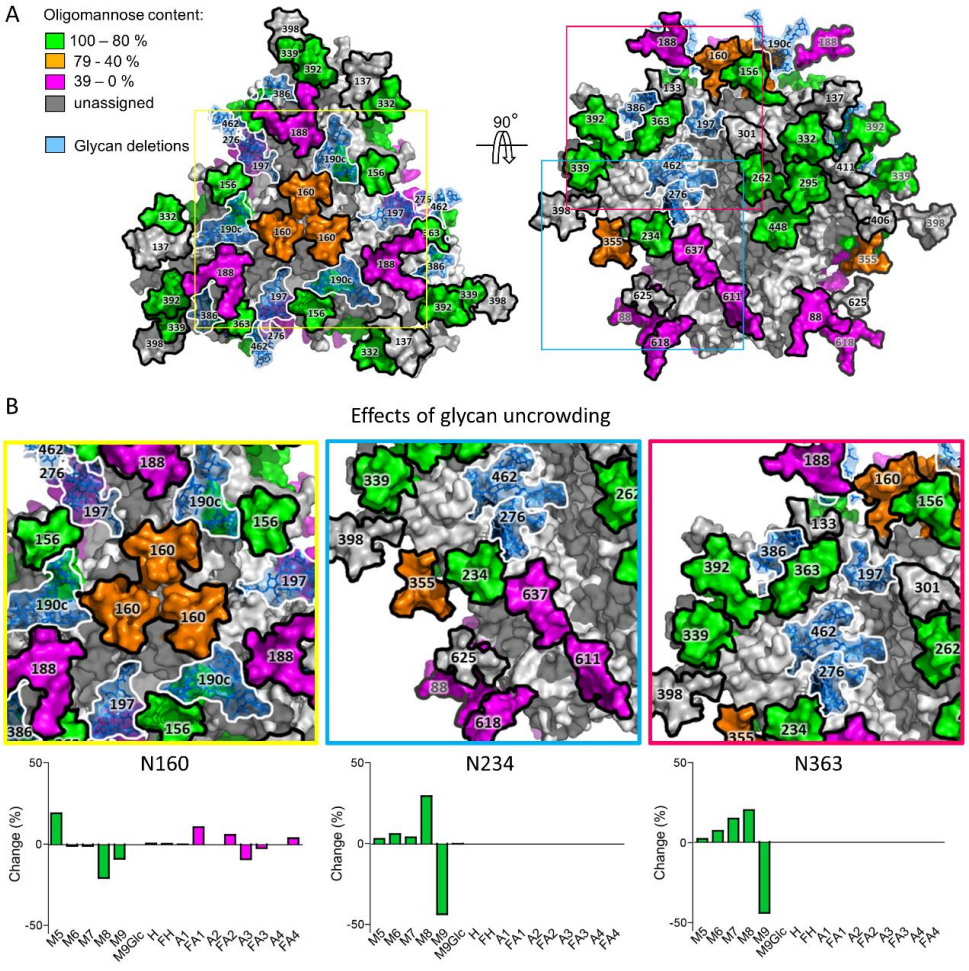

Figure 7.6: Processing of glycans on the glycan-depleted GT1 trimer
(A) The model is based on the one presented in Figure 7.1, but with the glycans deleted from the GT1 trimer now shown in 'ghost' form (i.e., light blue with a white border). The remaining glycans are color-coded according to their processing state (see key in Figure Panel A). (B) Magnification of three sites (N160, N234 and N363) to highlight the effects of the reduction in local glycan density on the GT1 trimer. Underneath these images are difference plots of the % change in glycan abundances for GT1 compared to SOSIP.664.

The design of the GT1 trimer involved eliminating three glycans proximal to the CD4bs (N197, N276 and N462). While these changes have a moderate impact on the nearby N363 glycan, the processing of the other CD4bs-proximal glycans (N262 and N448) is little changed. This finding is consistent with there being multiple locally stabilizing factors that influence the accessibility of glycans to processing enzymes. Thus, the N262 glycan is known to form extensive interactions with

the polypeptide chain [206,481]; and the N448 glycan is presumably protected by its immediate neighbors (N295 and N262). Glycan N301 is also very close to the CD4bs, but it was not possible to obtain quantitative data on this site. Overall, the data confirm and extend how local glycan clustering can be sufficient to protect a glycan from processing [260].

7.3 Conclusions

The preservation of site-specific processing of the SOSIP.v4.1-GT1 trimer glycans has substantive implications for our understanding of the glycan shield and for Env immunogen design. That glycan processing is substantially unchanged despite the elimination of 15 PNGSs from the trimer reveals the considerable redundancy in how the local environment of each glycan acts to limit the processing activity of α-mannosidases. In other words, the loss of one glycan from a local cluster does not usually eliminate the steric constraints on the processing of its neighbors. These observations are consistent with the preservation of the mannose patch across clades despite variation in its precise composition [182]. They also support the hypothesis that local glycan processing is largely preserved when the glycan shield evolves over time in infected people, as part of the immune evasion process [234]. An additional implication is that the presence of oligomannose-type glycans remains a fundamental feature of virion-associated Env proteins despite the extensive variation in their amino-acid sequence. By extension, variation in the location of individual glycans seems unlikely to compromise other properties oligomannose-type glycans confer on HIV-1, such as lectin-mediated virion trafficking [99] and complement activation through the mannose-binding lectin.

The robustness of the mannose patch on glycan-depleted trimers has implications for immunogen design. Thus, localized engineering around the predicted epitopes of gl-bNAb expressing B cells does not adversely influence glycan processing in any global way. Hence, many glycan-dependent epitopes will be present or almost fully assembled at the earliest stages of immunization.

8 Discussion

8.1 Principles controlling HIV-1 Env glycosylation

In this thesis, quantitative site-specific N-glycosylation analysis of a recombinant trimeric Env mimic has revealed new insights into the HIV-1 glycan shield. While the remarkable abundance of oligomannose-type glycans has been reported previously [176,182-184,215,236], a systematic, quantitative site-specific study on the microheterogeneity at individual sites has so far been missing. Here, the simplicity and diversity of glycan processing are mapped on the surface of the Env mimic BG505 SOSIP.664 (Figure 4.3). The glycan shield contains a mosaic of dense clusters of oligomannose-type glycans, especially in areas covering the gp120 outer domain and at the trimer interfaces. The trimer apex shows both under-processed and complex-type glycans, whereas most of the gp120 glycans at the trimer base and the gp41 glycans are highly processed.

This study has been performed on truncated, soluble trimers, which lack the MPER and the C-terminal domain. In the context of virions, however, the envelope spike is membrane-bound which triggers the question of possible additional constraints on processing as a result of the proximity of certain Env glycans to the membrane. This is not a simple question as membrane localization brings the glycoprotein in closer proximity to the enzymes and membrane association is known to enhance the processing of complex-type glycans [482]. However, a study on the comparison of recombinant, membrane-bound and uncleaved, soluble Env indicates a higher abundance of oligomannose, in particular in the gp41 region [235]. In addition, analysis of virion-derived gp120 suggests the membrane proximal glycan N88 to be occupied by oligomannose-type glycans [236], whereas only a very minor population of such glycans were observed on recombinant Env constructs. The site-specific effect of membrane proximity on virion-derived gp41 is unknown, although the bNAb PGT151 is known to interact with gp41 glycans and preferentially binds complex-type glycans [72,73]. This is consistent with glycan profiling of the virally-derived gp41,

which revealed highly processed complex-type glycans with a sub-population of oligomannose- and hybrid-type glycans [241].

Here, the comparison of site-specific data gained from clade A BG505 SOSIP.664 trimer mimics with related alternative Env immunogens (monomers, uncleaved pseudotrimers, uncleaved NF-linked trimers and glycan-depleted trimers) – all based on the same genetic background – has given detailed insights into the structural principles controlling Env glycosylation and into the properties of the HIV-1 glycan shield. Overall, there are multiple structural and cellular factors that shape the glycosylation of the envelope spike. Firstly, the high density of glycans on the outer domain of gp120 gives rise to the presence of the intrinsic mannose patch through steric restriction of the processing enzymes that require extensive glycan recognition interfaces (Figure 5.5). Secondly, a cleavage-induced, trimeric quaternary structure imposes additional steric constraints at the protomer interface leading to the emergence of a trimer-associated mannose patch (Chapter 5). It was also shown that a TAMP is not necessarily limited to trimers of the fully cleaved SOSIP-design, but can arise in the context of flexibly linked, native-like constructs (Chapter 6). Thirdly, there may be an elevated amount of oligomannose-type glycans in membrane proximal regions (see above). Finally, the producer cell can shape the portfolio of complex-type glycans (i.e. the types of complex glycans differ when proteins are expressed in HEK 293 *vs* CHO cells). With the analysis of the germline-targeting Env trimer in Chapter 7, the remarkable stability of the oligomannose patches despite the removal of ~20 % glycans is revealed. This suggests a multi-factored integrity of the glycan shield that can compensate for glycan deletions while still imposing steric restrictions on glycan processing enzymes and thus preserving its under-processed, oligomannose features. Figure 8.1 exemplifies the steric protection of the N332-site from oligomannose trimming by multiple surrounding glycans and thus provides an explanation for how the removal of almost a fifth of all glycans can have such small impact on the overall glycosylation processing.

8.2 Resolving the mannose paradox

There is an apparent contradiction in that glycans are directed to be in an oligomannose-type state by steric restriction and yet those same glycans are accessible for antibody and lectin recognition [483]. With the advent of recent structural data, this apparent conflict can now be resolved [260,484]. Overlaying the crystal structure of the enzyme-substrate complex of the catalytic domain of the ER α1,2-mannosidase I [484] with the model of the fully glycosylated Env trimer shows how the mannosidase enzyme wraps around target glycans. In contrast, bNAbs are able to recognize glycans while also penetrating the glycan shield [68,207]. This principle is illustrated by the comparison of the attempted digestion of the N332 glycan by ER α1,2-mannosidase I with the recognition mode of bNAb PGT128 (Figure 8.1). Enzymatic processing is limited by multiple surrounding glycans that clash with the enzyme and thus prevent mannose trimming (Figure 8.1A), highlighting the persistence of the mannose patch despite an evolving glycan shield [234,260]. Broad and potent neutralizing antibodies, such as PGT128, however, manage to adjust to the high density of glycosylation by reaching in between glycans and incorporating them into their epitopes [68,207] (Figure 8.1B).

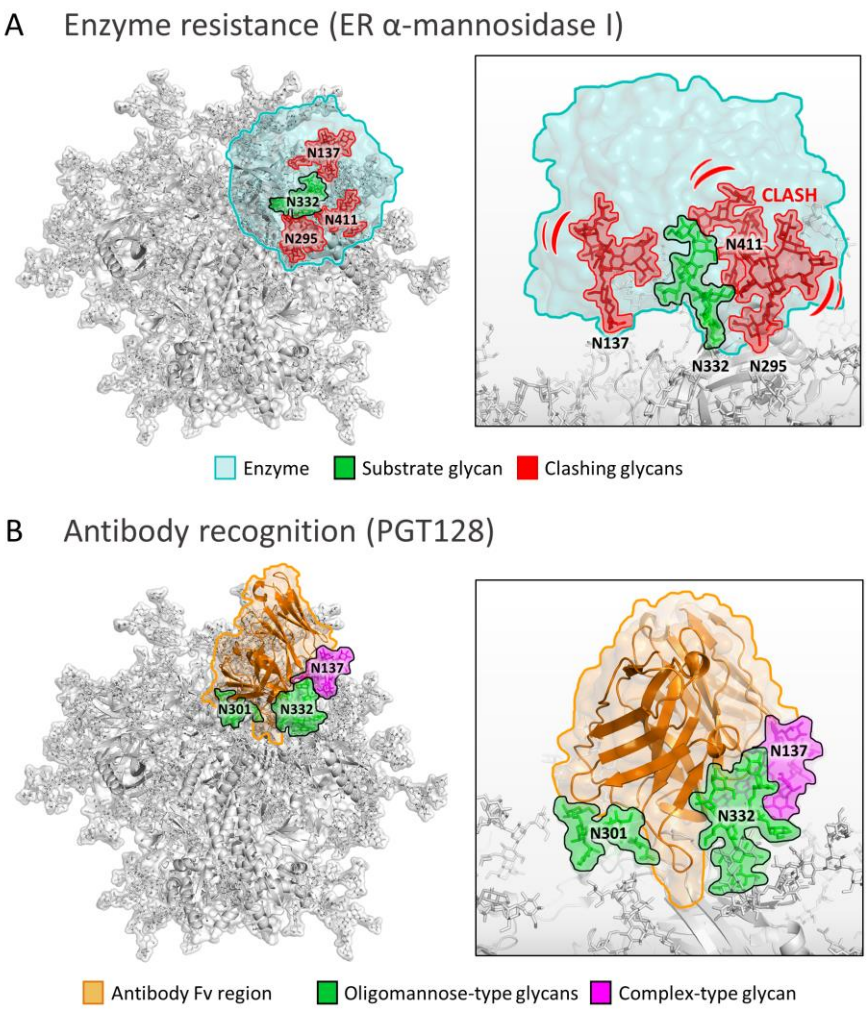

Figure 8.1: Enzyme resistance and antibody recognition of the HIV-1 glycan shield
(A) ER α1,2-mannosidase I (PDB ID 5KIJ) [484] (cyan) was modelled to bind the $Man_9GlcNAc_2$ N332 glycan (green) on a fully glycosylated model of a previously described model of BG505 SOSIP.664 [13]. The surrounding glycans that sterically clash with enzyme recognition of N332 are highlighted in red. (B) The Fab variable region of bNAb PGT128 (PDB ID 5ACO) (orange) targets the N301 glycan and also interacts and depends on additional nearby glycans [207]. Green: oligomannose-type glycans; pink: complex-type glycans. Removal of the N137 glycan has been shown to increase virus neutralizing by PGT128 in a BG505 virus also lacking the N332 glycan [261].

8.3 Strategies to elicit anti-mannose immune responses

In order to elicit potent and broad neutralizing antibodies against glycan epitopes, immunological tolerance to 'self' glycan structures must be overcome. In addition, bNAbs need to demonstrate a substantial amount of plasticity in their recognition and tolerate viral diversity and glycan escape mutants. In terms of HIV-1 vaccine design, the exploitation of non-self features of the envelope glycan shield is nicely exemplified by bNAb 2G12, a uniquely domain-exchanged antibody, which

exclusively recognizes an oligomannose glycan epitope on the outer domain of gp120 [74]. Mimicry of the 2G12 epitope has been exploited in various different immunogen design approaches, including glycan clustering on rationally designed peptide, dendrimer, carbohydrate, DNA, steroid, gold nanoparticle and biomacromolecular scaffolds (Section 1.4.3). To date, none of these synthetic approaches have yielded neutralizing antibodies. Encouragingly, however, yeast-based immunogens engineered to mimic the terminal motifs of human oligomannose-type glycans did elicit a weak antibody response mirroring 2G12 specificity [374]. The elicitation of high titers of class-switched antibodies recognizing unusual, disease-specific, self-glycan epitopes has been shown in cancer vaccine research [407,408]. Furthermore, mimicry of the natural immune response to glycans in infection and in the development of anti-glycolipid autoimmune conditions has been proposed to be a fertile ground for developments in HIV-1 immunogen design [293,336]. Together these findings point towards an immunogen design strategy that preserves conserved, key features of the HIV-1 glycan shield, such as the glycan clustering, whilst potentially adding a sufficiently high amount of non-self signals that drive the arising antibody response [336,387].

8.4 The glycan shield as a target for vaccine design

The development of a vaccine against HIV-1 providing sterilizing immunity presents a formidable challenge. The antigenic diversity of the virus has rendered all previously developed vaccine strategies ineffective. However, there have been several areas of advancement which give grounds for optimism. Central among these has been the discovery of bNAbs that are potent at titers achievable by typical vaccination regimens.

Rational vaccine design has led to the development and evaluation of many different potential Env immunogens (Figure 1.7). An increasingly widespread opinion is that a native-like representation of Env where multiple bNAb epitopes are presented but non-neutralizing antibody epitopes occluded [416,473]. As many bNAb epitopes include glycans, the integrity of the glycan shield is a key factor that needs to be considered in Env immunogen design. However, the target

of a potential vaccine are early transmitted/founder viruses. Detailed N-glycosylation analyses of these is currently lacking, although a dominance of oligomannose-type glycans has been reported [252]. Compared to Env in chronic infections, transmitted/founder viruses were shown to have shorter V1/V2 loops and to (on average) possess a lower number of PNGSs [485-487]. A compact apex region has been associated with enhanced viral fusion [488], which could provide an advantage during acute infection events. In the further course of infection, priorities shift and the HIV-1 glycan shield evolves to evade the emerging immune response. A quantitative site-specific analysis of early transmitted/founder viruses would be of particular interest for rational immunogen design.

One focus of vaccine design is the development of multistage vaccination regimes that guide the affinity maturation of Env-targeting antibodies towards fully matured bNAbs. Native-like SOSIP trimers were shown to successfully induce autologous Tier 2 neutralizing antibodies responses in rabbits and macaques [359,473]. The challenge is now to broaden this narrow immune response into the development of bNAbs. During infection, the virus and the immune system can co-evolve, thus leading to viral escape mutants but also to antibody affinity maturation [313,314]. Rationally designed immunogens, such as the one described in Chapter 7, were developed to specifically prime B cell lineages with the potential to evolve into bNAb-producing clones. Boosting with one or more additional Env immunogens may then guide antibody maturation into breadth and potency [298,476,477]. In this context, it is very reassuring that the glycan-depleted GT1 remains natively glycosylated and thus possesses preserved glycan-dependent bNAb epitopes.

HIV-1 is a highly genetically diverse retrovirus that makes vaccine development particularly difficult. The glycan shield, however, presents a considerably more homogenous target for vaccine design compared to the underlying heterogeneous protein surface. Site-specific glycan-composition data such as those described in this thesis should be valuable guides to the design and use of Env immunogens intended to induce bNAbs against virion-associated epitopes that either contain, or are influenced by, glycans of defined compositions.

List of Abbreviations

2-AA	2-aminobenzoic acid
A	Adenine; antennae
ADCC	Antibody-dependent cellular cytotoxicity
ADCP	Antibody-dependent cellular phagocytosis
AIDS	Acquired immune deficiency syndrome
α-Man	α-mannosidase
Arg	Arginin
Asn	Asparagine
BCR	B cell receptor
bNAb	Broadly neutralizing antibody
C	Cytosine; mass spectrometry fragmentation ion
C1-C5	Constant regions 1 to 5
cART	Combined antiretroviral therapy
CCR5	C-C chemokine receptor 5
CD4bs	CD4 binding site
CDC	Cellular-dependent cytotoxicity; Center for Disease Control and Prevention
CFG	Center for Functional Glycomics
CHO	Chinese hamster ovary
CID	Collision-induced dissociation
CLR	C-type lectin receptor
cryo-EM	Cryo-electron microscopy
CT	Cytoplasmic tail
CTL	Cytotoxic T lymphocyte
CXCR4	CXC-chemokine receptor 4
DC-SIGN	Dendritic cell-specific ICAM3-grabbing non-integrin
Da	Dalton
DEPC	Diethyl pyrocarbonate
DHB	2,5-dihydrobenzoic acid
DNA	Deoxyribonunleic acid
DTT	Dithiothreitol
Endo H	Endoglycosidase H
Env	Envelope glycoprotein of HIV-1
eOD	Engineered outer domain
ER	Endoplasmic reticulum
ERGIC	ER-Golgi intermediate compartment
ESI	Electrospray
ETD	Electron-transfer dissociation
FDA	US Food and Drug Administration
FP	Fusion peptide
Fuc	Fucose
FWR	Framework regions

G	Guanine
Gal	Galactose
GalNAc	*N*-acetylgalactosamine
GL/gl	Germline
Glc	Glucose
GlcNAc	*N*-acetylglucosamine
GnTI	*N*-acetylglucosaminyltransferase I
Gp	Glycoprotein
HAART	Highly active antiretroviral therapy
HCD	Higher energy collisional dissociation
HEK	Human embryonic kidney
Hex	Hexose
HILIC	Hydrophilic interaction chromatography
HIV-1	Human immunodeficiency virus type 1
HPLC	High-performance liquid chromatography
HR1/2	Heptad repeat helices 1/2
GALT	Gut-associated lymphoid tissue
IAA	Iodacetamide
Ig	Immunoglobulin
IM	Ion mobility
IMP	Intrinsic mannose patch
LC	Liquid chromatography
LRA	Latency reversal agents
kDa	kilo Dalton
k/o	knock-out
LB	Lysogeny broth
LRA	Latency reversal agents
Man	Mannose
MALDI	Matrix-assisted laser desorption/ionization
MBL	Mannose-binding lectin
MPER	Membrane-proximal external region
MS	Mass spectrometry
MS/MS	Tandem mass spectrometry
N	Asparagine
NAbs	Neutralizing antibodies
NB-DNJ	*N*-butyldeoxynojirimycin
Neu5Ac	Sialic acid
NF-κB	Nuclear factor kappa B
NFL	Native, flexibly linked
N-glycan	N-linked glycans
N-glycosylation	N-linked glycosylation
O-glycan	O-linked glycan
O-glycosylation	O-linked glycosylation
ORF	Open reading frames
PAGE	Polyacrylamide gel electrophoresis

PAMP	Pathogen-associated molecular pattern
PBMC	Peripheral blood mononuclear cell
PBS	Phosphate-buffered saline
PCR	Polymerase chain reaction
PEI	Polyethylenimine
PNGase F	Peptide-N-Glycosidase F
PNGS	Potential N-glycosylation site
PRR	Pattern recognition receptor
PVDF	Polyvinylidene fluoride
RI	Relative intensity
RP-HPLC	Reversed-phase-HPLC (see above)
RNA	Ribonucleic acid
RT	Reverse transcriptase; room temperature
S	Serine
SEC	Size-exclusion chromatography
SEM	Standard error of the mean
Siglec-1	Sialic acid-recognizing Ig superfamily lectins-1
SDS-PAGE	Sodium dodecyl sulfate-polyacrylamide gel electrophoresis
SHIV	Chimeric simian/human immunodeficiency virus
SOS	see SOSIP
SOSIP	Gp140 trimer with an addition disulfide bond (SOS) and an isoleucine to proline mutation (IP)
SP	Signal peptide
T	Threonine; thymine
TAMP	Trimer-associated mannose patch
T_{FH}	Follicular T helper cell
TFA	Trifluoroacetic acid
TGN	*Trans* Golgi network
TOF	Time of flight
TM	Transmembrane domain
UPLC	Ultra performance liquid chromatography
V1-V5	Variable loops 1 to 5
VLP	Virus-like particle
WT	Wild-type
XIC	extracted-ion chromatogram
ZIC-HILIC	Zwitterionic hydrophilic interaction chromatography

Appendix A Primers and Env sequences

Table A.1: Primers for cloning, mutagenesis and sequencing

Name	Sequence (5'–to–3')	Purpose
BG505gp120PstI_pPPI4_f	TATGCTGCAGATGGACGCTATGAAAAGGGGGCTGTG	Cloning
BG505gp120BamHI_pPPI4_r	TATCGGATCCTCGTCCGACCACTCGCCTTTTGCATCG	Cloning
BG505 SOSIP.664 137A	GTACAAACGTGACTAACGCTATCACCGACGATATGCG	Mutagenesis
BG505 SOSIP.664 197A	CAGGCTGATCAATTGCGCCACCAGTGCCATTACAC	Mutagenesis
BG505 SOSIP.664 262A	CAGCTGCTGCTGGCTGGATCTCTGGCC	Mutagenesis
BG505 SOSIP.664 332A	CAGGCACACTGTGCTGTGAGCAAGGCTAC	Mutagenesis
BG505 SOSIP.664 448A	GTGATTCGATGTGTCAGCGCTATCACAGGCCTGATTC	Mutagenesis
BG505_SOSIP_334N_f	GCAGGCACACTGTAATGTGAACAAGTCTACATGGAACGAG	Mutagenesis
BG505_SOSIP_334N_r	CTCGTTCCATGTAGACTTGTTCACATTACAGTGTGCCTGC	Mutagenesis
full-length Env N133A	CTCTACAGTGTACCGCTGTCACCAATAATATC	Mutagenesis
full-length Env N137A	CCAATGTCACCAATGCTATCACTGATGACATG	Mutagenesis
full-length Env N156A	GAGGGGAGAATTAAAAGCCTGCTCTTTC	Mutagenesis
full-length Env N160K	AACTGCTCTTTCAAGATGACCACAGAGCTAAGG	Mutagenesis
full-length Env N190A	ACGAGAATCAAGGTGCTAGGAGTAATAATAGTA	Mutagenesis
full-length Env N190cA	CGAGAATCAAGGTGCTAGGAGTAATAATAGTAAC	Mutagenesis
full-length Env N197A	GATTAATAAATTGTGCTACCTCAGCCATTAC	Mutagenesis
full-length Env N262A	CTCAACTGCTGTTAGCTGGCAGTCTAGCAG	Mutagenesis
full-length Env N276A	ATGATTAGATCTGAAGCTATCACAAACAATGC	Mutagenesis
full-length Env N295A	ACGCCTGTGCAAATTGCTTGTACCAGACCTAAC	Mutagenesis
full-length Env N301A	GTACCAGACCTAACGCCAATACAAGGAAAAG	Mutagenesis
full-length Env T332N	GACAAGCACATTGTAATGTCAGTAAAGCAA	Mutagenesis
full-length Env N339A	GTCAGTAAAGCAACATGGGCTGAAACTTTGGG	Mutagenesis
full-length Env N386A	GAATTTTTCTATTGTGCCACATCAGGCCTGTTC	Mutagenesis
full-length Env N392A	CATCAGGCCTGTTCGCTAGCACTTGGATTAG	Mutagenesis
full-length Env N448A	AATAAGATGTGTATCAGCCATTACAGGGCTAATA	Mutagenesis
full-length Env N611A	TAATGTGCCCTGGGCCTCTAGTTGGAGTAATA	Mutagenesis
full-length Env N618A	TTGGAGTAATAGAGCCCTGAGTGAGATATGGG	Mutagenesis
full-length Env N625A	AGTGAGATATGGGACGCTATGACCTGGCTGC	Mutagenesis
full-length Env N637A	GGGATAAAGAAATTAGCGCCTACACACAGATAA	Mutagenesis
pPPI4_Seq_f	CTGCCGCGCGCGCCACCAGAC	Sequencing
pPPI4_Seq_r	CAACTAGAAGGCACAGTCGAGGC	Sequencing

Dataset A.1: Env glycoprotein sequences

N-glycosylation sites are colored in red and numbered according to the HXB2 reference numbering scheme. Changes in the sequence are indicated in green. BG505 SOSIP.664 glycoproteins were analyzed with and without a His-tag (as indicated in the appropriate places).

BG505 SOSIP.664

AENLWVTVYYGVPVWKDAETTLFCASDAKAYETEKHNVWATHACVPTDPNPQEIHLEN^{88}VTEEFNM
WKNNMVEQMHTDIISLWDQSLKPCVKLTPLCVTLQCTN^{133}VTNN^{137}ITDDMRGELKN^{156}CSFN^{160}M
TTELRDKKQKVYSLFYRLDVVQINENQGN^{190}RSN^{190c}NSNKEYRLINCN^{197}TSAITQACPKVSFEPI
PIHYCAPAGFAILKCKDKKFN^{234}GTGPCPSVSTVQCTHGIKPVVSTQLLLN^{262}GSLAEEEVMIRSE
N^{276}ITNNAKNILVQFNTPVQIN^{295}CTRPNN^{301}NTRKSIRIGPGQAFYATGDIIGDIRQAHCN^{332}VS
KATWN^{339}ETLGKVVKQLRKHFGN^{355}NTIIRFAN^{363}SSGGDLEVTTHSFNCGGEFFYCN^{386}TSGLFN^{3}
^{92}STWISN^{398}TSVQGSN^{406}STGSN^{411}DSITLPCRIKQIINMWQRIGQAMYAPPIQGVIRCVSN^{448}IT
GLILTRDGGSTN^{462}STTETFRPGGGDMRDNWRSELYKYKVVKIEPLGVAPTRC^{501}KRRVVGRRRRR
RAVGIGAVFLGFLGAAGSTMGAASMTLTVQARNLLSGIVQQQSNLLRAP^{559}EAQQHLLKLTVWGIK
QLQARVLAVERYLRDQQLLGIWGCSGKLICC^{605}TNVPWN^{611}SSWSNRN^{618}LSEIWDN^{625}MTWLQWD
KEISN^{637}YTQIIYGLLEESQNQQEKNEQDLLALD

BG505 gp120

AENLWVTVYYGVPVWKDAETTLFCASDAKAYETEKHNVWATHACVPTDPNPQEIHLEN^{88}VTEEFNM
WKNNMVEQMHTDIISLWDQSLKPCVKLTPLCVTLQCTN^{133}VTNN^{137}ITDDMRGELKN^{156}CSFN^{160}M
TTELRDKKQKVYSLFYRLDVVQINENQGN^{190}RSN^{190c}NSNKEYRLINCN^{197}TSAITQACPKVSFEPI
PIHYCAPAGFAILKCKDKKFN^{234}GTGPCPSVSTVQCTHGIKPVVSTQLLLN^{262}GSLAEEEVMIRSE
N^{276}ITNNAKNILVQFNTPVQIN^{295}CTRPNN^{301}NTRKSIRIGPGQAFYATGDIIGDIRQAHCN^{332}VS
KATWN^{339}ETLGKVVKQLRKHFGN^{355}NTIIRFAN^{363}SSGGDLEVTTHSFNCGGEFFYCN^{386}TSGLFN^{3}
^{92}STWISN^{398}TSVQGSN^{406}STGSN^{411}DSITLPCRIKQIINMWQRIGQAMYAPPIQGVIRCVSN^{448}IT
GLILTRDGGSTN^{462}STTETFRPGGGDMRDNWRSELYKYKVVKIEPLGVAPTRC^{501}KRRVVGRGSGS
GGSGHHHHHHHH

BG505 WT.SEKS

AENLWVTVYYGVPVWKDAETTLFCASDAKAYETEKHNVWATHACVPTDPNPQEIHLEN^{88}VTEEFNM
WKNNMVEQMHTDIISLWDQSLKPCVKLTPLCVTLQCTN^{133}VTNN^{137}ITDDMRGELKN^{156}CSFN^{160}M
TTELRDKKQKVYSLFYRLDVVQINENQGN^{190}RSN^{190c}NSNKEYRLINCN^{197}TSAITQACPKVSFEPI
PIHYCAPAGFAILKCKDKKFN^{234}GTGPCPSVSTVQCTHGIKPVVSTQLLLN^{262}GSLAEEEVMIRSE
N^{276}ITNNAKNILVQFNTPVQIN^{295}CTRPNN^{301}NTRKSIRIGPGQAFYATGDIIGDIRQAHCN^{332}VS
KATWN^{339}ETLGKVVKQLRKHFGN^{355}NTIIRFAN^{363}SSGGDLEVTTHSFNCGGEFFYCN^{386}TSGLFN^{3}
^{92}STWISN^{398}TSVQGSN^{406}STGSN^{411}DSITLPCRIKQIINMWQRIGQAMYAPPIQGVIRCVSN^{448}IT
GLILTRDGGSTN^{462}STTETFRPGGGDMRDNWRSELYKYKVVKIEPLGVAPTRAKRRVVGSEKSAVG
IGAVFLGFLGAAGSTMGAASMTLTVQARNLLSGIVQQQSNLLRAIEAQQHLLKLTVWGIKQLQARV
LAVERYLRDQQLLGIWGCSGKLICTTNVPWN^{611}SSWSNRN^{618}LSEIWDN^{625}MTWLQWDKEISN^{637}Y
TQIIYGLLEESQNQQEKNEQDLLALD

BG505.v4.1-GT1

AENLWVTVYYGVPVWKDAETTLFCASDAKAYETKKHNVWATHACVPTDPNPQEIHLEN^{88}VTEEFNM
WKNNMVEQMHTDIISLWDQSLKPCVKLTPLCVTLQCTN^{133}VTNN^{137}ITDDMRGELKN^{156}CSFN^{160}M
TTELRDKRQKVHALFYKLDIVPINENQN^{188}TSYRLINCNTAAITQACPKVSFEPIPIHYCAPAGFA
ILKCKDKKFN^{234}GTGPCPSVSTVQCTHGIKPVVSTQLLLN^{262}GSLAEEEVMIRSEDIRNNAKNILV
QFNTPVQIN^{295}CTRPNN^{301}NTRKSIRIGPGQWFYATGDIIGDIRQAHCN^{332}VSKATWN^{339}ETLGKV
VKQLRKHFGN^{355}NTIIRFAN^{363}SSGGDLEVTTHSFNCGGEFFYCDTSGLFN^{392}STWISN^{398}TSVQG
SN^{406}STGSN^{411}DSITLPCRIKQIINMWQRIGQAMYAPPIQGVIRCVSN^{448}ITGLILTRDGGSTDST
TETFRPSGGDMRDNWRSELYKYKVVKIEPLGVAPTRC^{501}KRRVVGRRRRRRAVGIGAVFLGFLGAA
GSTMGAASMTLTVQARNLLSGIVQQQSNLLRAP^{559}EAQQHLLKLTVWGIKQLQARVLAVERYLRDQ
QLLGIWGCSGKLICC^{605}TNVPWN^{611}SSWSNRN^{618}LSEIWDN^{625}MTWLQWDKEISN^{637}YTQIIYGLL
EESQNQQEKNEQDLLALD

BG505 NFL2P.664

AENLWVTVYYGVPVWKDAETTLFCASDAKAYETEKHNVWATHACVPTDPNPQEIHLEN^{88}VTEEFNM
WKNNMVEQMHTDIISLWDQSLKPCVKLTPLCVTLQCTN^{133}VTNN^{137}ITDDMRGELKN^{156}CSFN^{160}M
TTELRDKKQKVYSLFYRLDVVQINENQGN^{190}RSN^{190c}NSNKEYRLINCN^{197}TSAITQACPKVSFEPI
PIHYCAPAGFAILKCKDKKFN^{234}GTGPCPSVSTVQCTHGIKPVVSTQLLLN^{262}GSLAEEEVMIRSE
N^{276}ITNNAKNILVQFNTPVQIN^{295}CTRPNN^{301}NTRKSIRIGPGQAFYATGDIIGDIRQAHCN^{332}VS
KATWN^{339}ETLGKVVKQLRKHFGN^{355}NTIIRFAN^{363}SSGGDLEVTTHSFNCGGEFFYCN^{386}TSGLFN^{3}
^{92}STWISN^{398}TSVQGSN^{406}STGSN^{411}DSITLPCRIKQIINMWQRIGQAMYAPPIQGVIRCVSN^{448}IT
GLILTRDGGSTN^{462}STTETFRPGGGDMRDNWRSELYKYKVVKIEPLGVAPTRAKRRVVGGGGGSGG
GGSAVGIGAVFLGFLGAAGSTMGAASMTLTVQARNLLSGIVQQQSNLLRAP^{559}EAQQHLLKLTVWG
IKQLQARVLAVERYLRDQQLLGIWGCSGKLICTTNVPWN^{611}SSWSNRN^{618}LSEIWDN^{625}MTWLQWD
KEISN^{637}YTQIIYGLLEESQNQQEKNEQDLLALDGGGGSHHHHHHHH

Appendix B Glycan nomenclature and fragmentation

Throughout this thesis, the symbolic representation of glycans follows that of Harvey *et al.*, with residues in both the schematic diagrams and the molecular graphics following the color scheme of the Center for Functional Glycomics (CFG) [186,187]. Terminal α1,2-linked mannose residues of oligomannose-type glycans are termed D1, D2 and D3, according to the system introduced by Vliegenthart [188] (Figure B.1). Of note is that the D1-D3 oligomannose-arms differ from the glycan fragment D-ions (Figure B.2C). Glycan names are generated according to Table B.1.

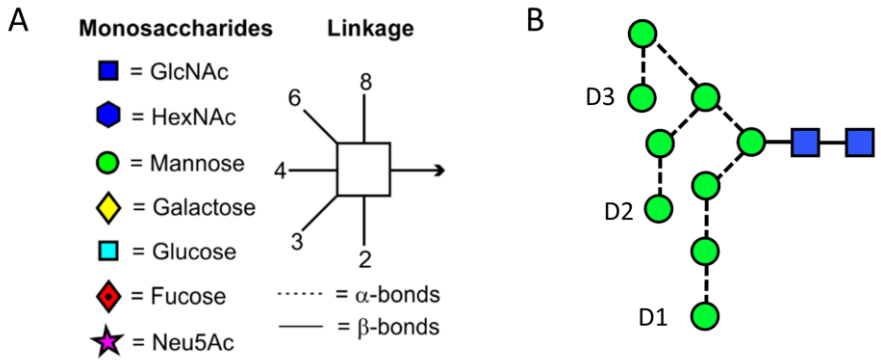

Figure B.1: Glycan nomenclature
See text for details.

Table B.1: Nomenclature for describing N-linked oligosaccharide structures

Term	Definition
A(1-4)	Number of antennae linked to trimannosyl core A1: monoantennary; A2: biantennary; A3: triantennary; A4: tetraantennary
B	Bisecting *N*-acetylglucosamine (GlcNAc)
F	Core fucose, α1,6-linked
G(1-4)	Number of (sub)terminal galactose residues
M	Mannose
Glc	Glucose
S(1-4)	Number of terminal sialic acid residues

Peptide fragmentation ions generated by tandem mass spectrometry are labeled according to the nomenclature by Roepstorff and Fohlman [489]. Fragments can be detected when they carry at least one charge. Carbohydrate fragmentation ions (Figure B.2) are labeled using the Domon and Costello nomenclature [439] with an extension by Harvey [427,428,444]. D-ions are likely formed by C_{R-1}/Z cleavages. Note that the use of subscripts in describing fragmentation ions differentiates this nomenclature from the above to describe particular monosaccharides within a glycan.

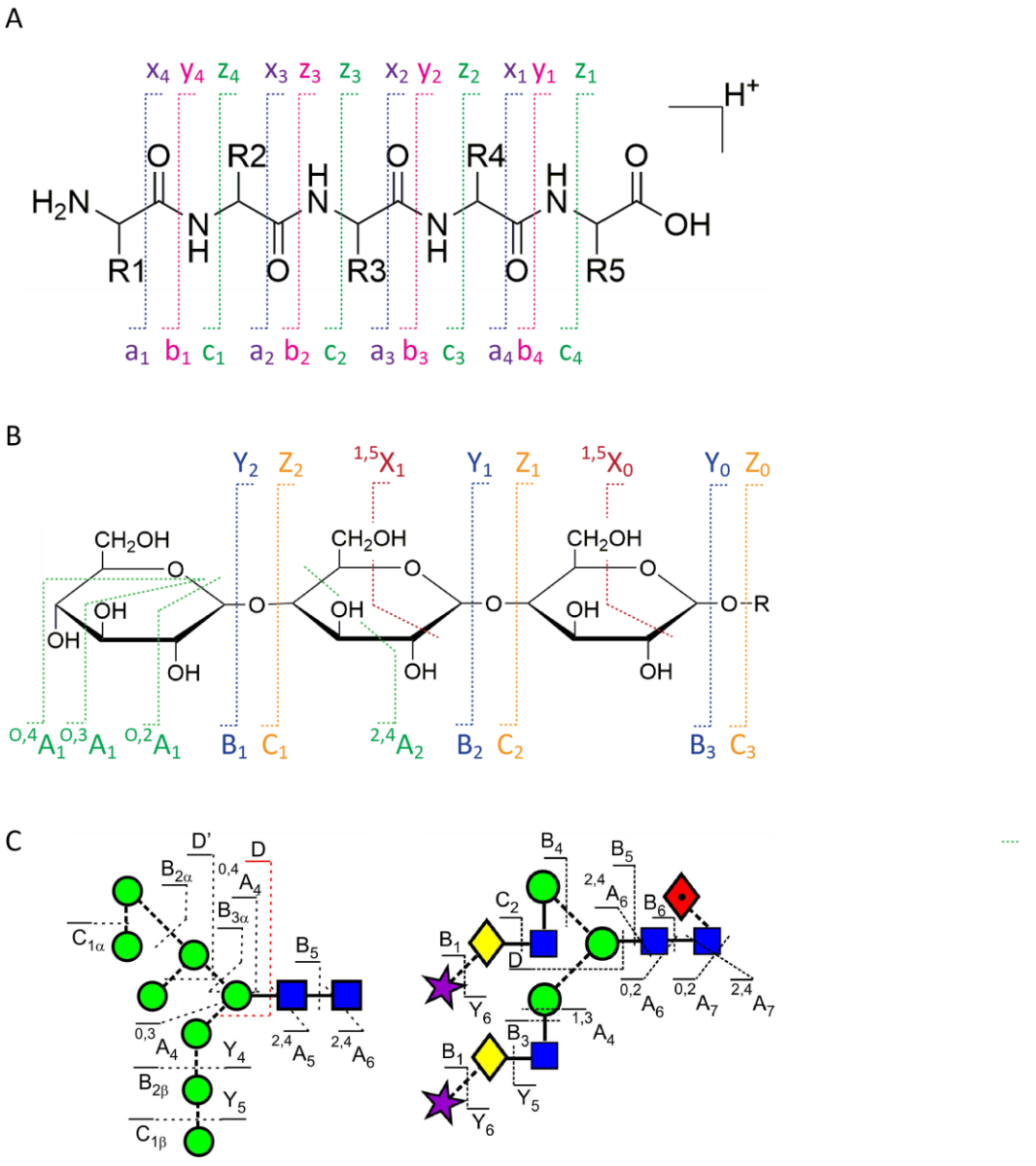

Figure B.2: Peptide and glycan fragmentation generated by tandem mass spectrometry
(A) Ions generated by the fragmentation of the peptide backbone [489]. (B) Ions generated by fragmentation of glycans [439]. (C) Characteristic ions generated by fragmentation of N-glycans illustrated on $Man_8GlcNAc_2$ (left) and FA2G2S2 (right), including labeling of D- and D'-ions (The D-ion is highlighted in red on the left structure) [443].

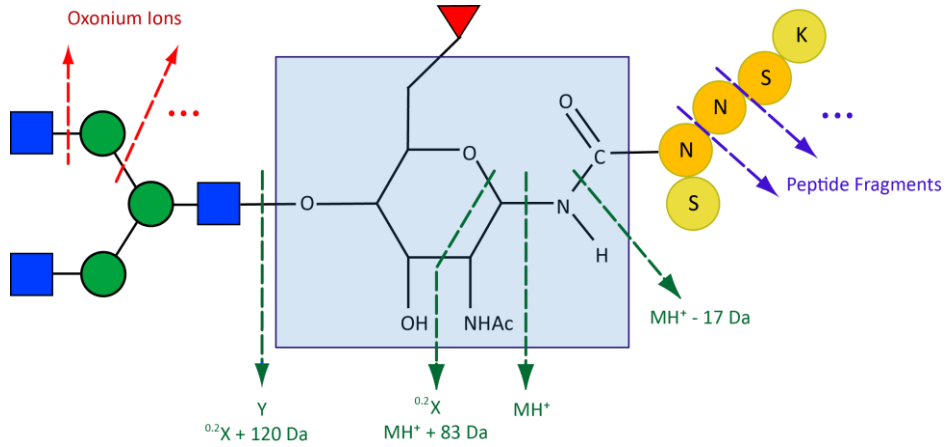

Figure B.3: Typically observed fragmentation pattern of N-glycopeptides by MALDI-TOF/TOF MS
Figure adapted from the Bruker brochure 'Explore and discover new possibilities with GlycoQuest'.

Table B.2 Characteristic oxonium ions originating from tandem MS of glycopeptides
Adapted from Mechref [490].

m/z	Description[a]
127.06	Hex - $2H_2O$
138.05	HexNAc - several functional groups
147.07	Fuc
163.06	Hex
168.09	HexNAc - $2H_2O$
186.09	HexNAc – H_2O
204.09	HexNAc
274.09	NeuAc – H_2O
292.08	NeuAc
366.14	HexHexNAc
528.19	HexHexNAcHex
657.23	NeuAcHexHexNAc

[a]Hex, Hexose (e.g. mannose or galactose); HexNAc, *N*-acetyhexosamine (e.g. *N*-acetylglucosamine or *N*-acetylgalactosamine); Fuc, fucose; NeuAc, *N*-acetylneuraminic acid (sialic acid); - H_2O, loss of water.

Appendix C Classification of glycans

Table C.1: Classification of identified N-linked glycan compositions
Glycan names are constructed as follows: Mn = number (n) of mannose residues; An = number (n) of antennae (e.g. A3 = triantennary); Gn = number (n) of galactose residues; F in the front of the name indicates the presence of a core fucose. See Table B.1.

Group Name	Members[a]
M4	M4
M5	M5
M6	M6
M7	M7
M8	M8
M9	M9
M9Glc	M9Glc
H/Hybrid	M4A1G1, M5A1G1, M6A1G1, M4A1G1S1, M5A1G1S1,
FH/Fucosylated-Hybrid	FM4A1G1, FM5A1G1, FM4A1G1S1, FM5A1G1S1
A1	A1, A1G1, A1G1S1
FA1	FA1, FA1G1, FA1G1S1
A1B/A2	A2, A2G1, A2G2, A2G1S1, A2G2S2
FA1B/FA2	FA2, FA2G1, FA2G2, FA2G1S1, FA2G2S1, FA2G2S2
A2B/A3	A2B, A2BG1, A2BG2, A3G3, A3G2S1, A3G3S1, A3G3S2, A3G3S3
FA2B/FA3	FA2B, FA2BG1, FA2BG2, FA3G3, FA3G3S1, FA3G3S2, FA3G3S3, FA2BG2S1
A3B/A4	A4, A4G1, A4G2, A4G3, A4G4, A4G4S1, A4G4S2, A4G4S3, A4G4S4
FA3B/FA4	FA3B, FA4G1, FA3BG1, FA3BG2, FA3BG3, FA4G4, FA4G4S1, FA4G4S2, FA4G4S3, FA4G4S4

[a]Isobaric glycans are not listed. Unusual glycan structures with terminal fucoses, sulfates or *N*-acetylgalactosamines are categorized according to the number of their antennae.

Appendix D Glycan libraries generated by ion mobility mass spectrometry

Information on where to access the glycan libraries generated in this thesis, can be found beneath Table D.1. Table D.1 shows the glycan library created as part of the development of the site-specific workflow for N-glycosylation analysis in Chapter 3 and is representative for additionally generated glycan libraries, which can be accessed online. Glycan symbols are shown both as explained in Appendix B and according to the CFG nomenclature.

Table D.1: Library of glycan structures identified on BG505 SOSIP.664, produced in HEK 293T cells

m/z		z	Ion[1]	Composition					Found in		Structure	
Found	Calc.			HexNAc	Hex	Fuc	Neu5Ac	SO_4	gp41	gp120	Oxford	CFG
1169.3	1169.3	1	a	2	4	0	0	0	-	+	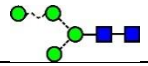	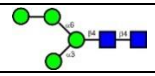
1331.4	1331.4	1	a	2	5	0	0	0	+	+	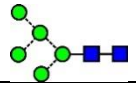	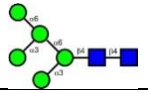
1493.5	1493.5	1	a	2	6	0	0	0	+	+	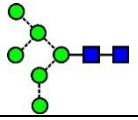	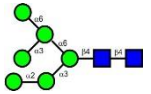
1655.5	1655.5	1	a	2	7	0	0	0	+	+	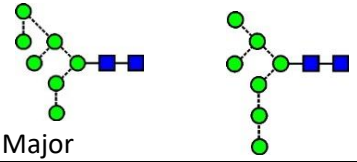 Major	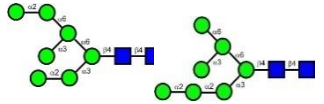
1817.6	1817.6	1	a	2	8	0	0	0	+	+	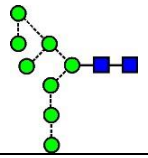	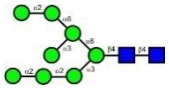

1979.6	1979.6	1	a	2	9	0	0	0	+	+	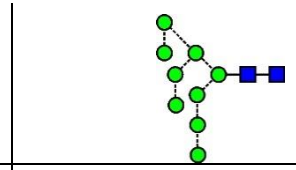	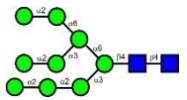
2141.6	2141.7	1	a	2	10	0	0	0	-	+	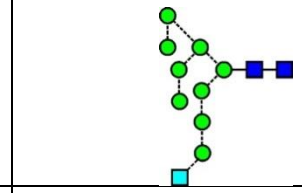	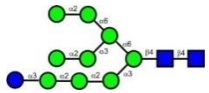
1210.4	1210.4	1	a	3	3	0	0	0	-	+	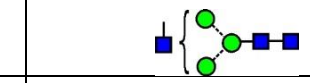	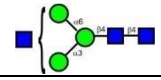
1356.4	1356.4	1	a	3	3	1	0	0	+	+	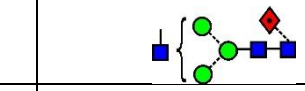	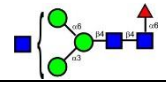
1372.4	1372.4	1	a	3	4	0	0	0	+	+	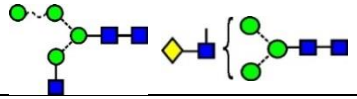	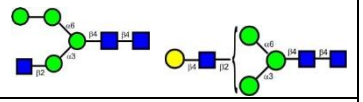
1565.5	1565.5	1	b	3	4	0	1	0	-	+	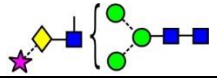	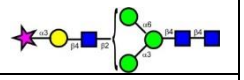
1518.5	1518.5	1	a	3	4	1	0	0	+	+	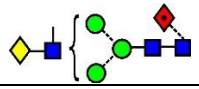	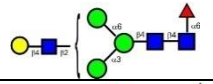
1711.6	1711.6	1	b	3	4	1	1	0	-	+	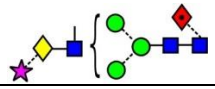	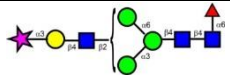
1534.5	1534.5	1	a	3	5	0	0	0	+	+	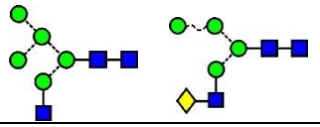	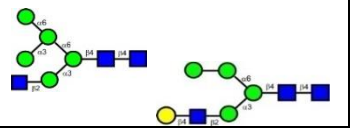

1727.6	1727.6	1	b	3	5	0	1	0	+	+	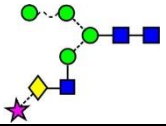	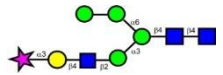
1680.5	1680.5	1	a	3	5	1	0	0	+	+	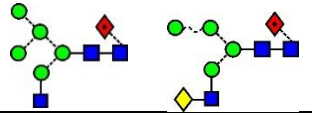	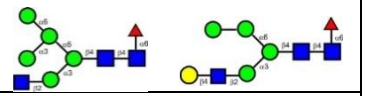
1873.7	1873.7	1	b	3	5	1	1	0	+	+	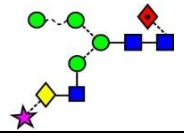	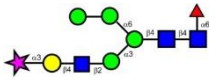
1696.5	1696.5	1	a	3	6	0	0	0	+	+	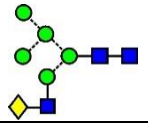	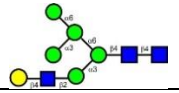
1889.7	1889.7	1	b	3	6	0	1	0	+	+	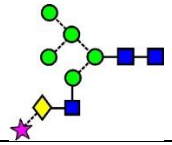	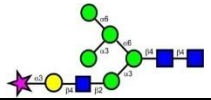
1842.6	1842.6	1	a	3	6	1	0	0	+	+	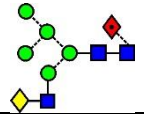	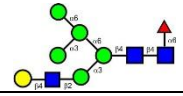
2035.7	2035.7	1	b	3	6	1	1	0	+	+	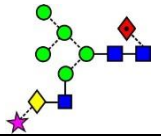	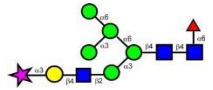
1413.5	1413.5	1	b	4	3	0	0	0	-	+	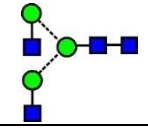	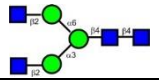

1559.5	1559.5	1	a	4	3	1	0	0	-	+	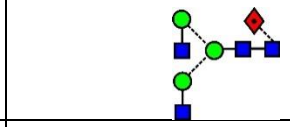	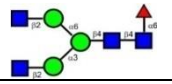
1575.5	1575.5	1	a	4	4	0	0	0	+	+	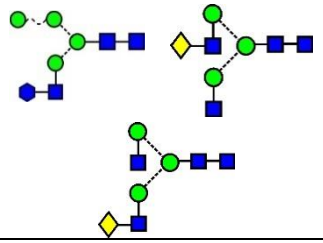	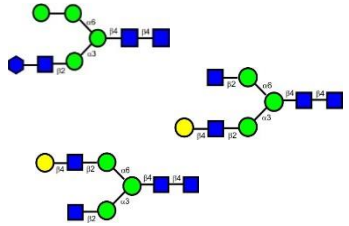
1768.6	1768.6	1	b	4	4	0	1	0	+	+	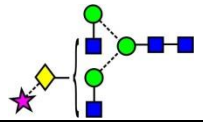	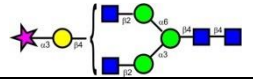
1721.6	1721.6	1	a	4	4	1	0	0	+	+	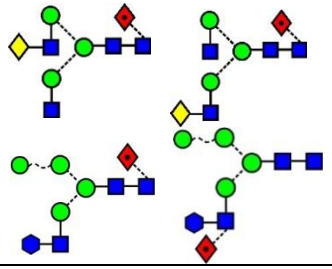	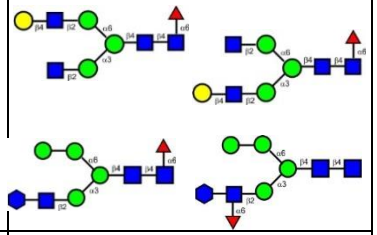
1914.7	1914.7	1	b	4	4	1	1	0	+	+	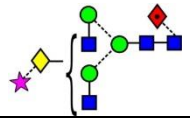	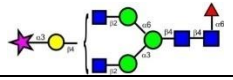
1867.6	1867.6	1	a	4	4	2	0	0	+	-	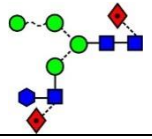	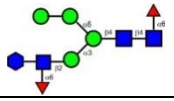

1737.6	1737.6	1	a	4	5	0	0	0	+	+	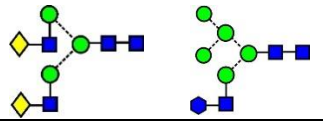	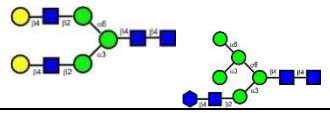
1930.7	1930.7	1	b	4	5	q	1	0	+	+	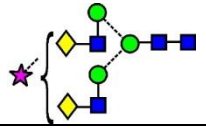	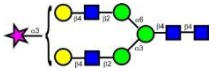
1883.6	1883.6	1	a	4	5	1	0	0	+	+	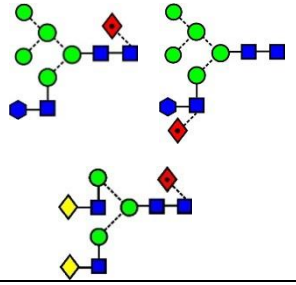	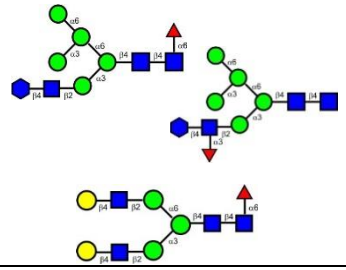
2076.7	2076.7	1	b	4	5	1	1	0	+	+	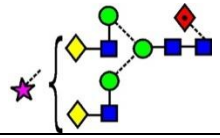	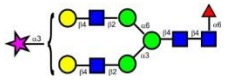
1183.5	1183.4	2	d	4	5	1	2	0	-	+	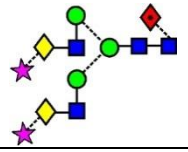	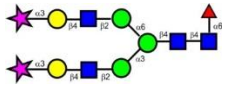
2029.7	2029.7	1	a	4	5	2	0	0	+	-	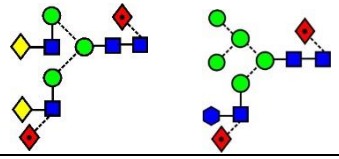	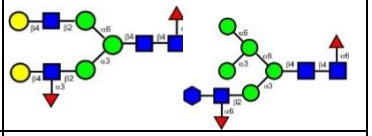
	1616.5	1	a	5	3	0	0	0	-	?	Not fragmented	Not fragmented

1762.6	1762.6	1	a	5	3	1	0	0	+	+	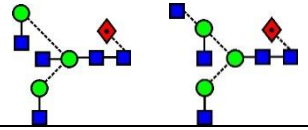	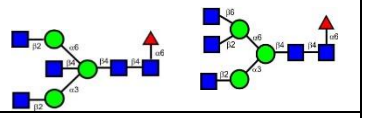
1778.6	1778.6	1	a	5	4	0	0	0	-	+	Not fragmented	Not fragmented
1924.6	1924.6	1	a	5	4	1	0	0	+	+	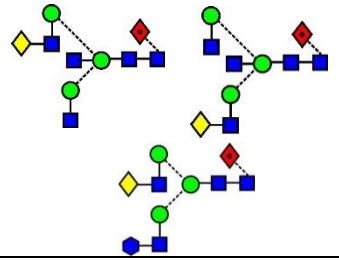	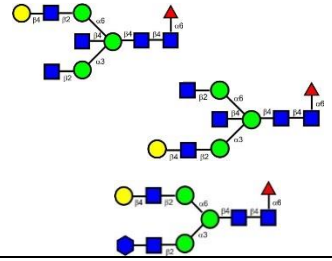
2117.8	2117.8	1	b	5	4	1	1	0	+	+	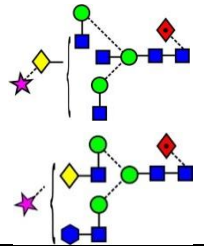	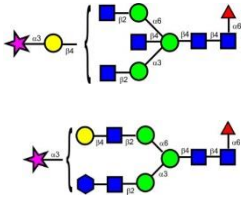
1906.6	1906.6	1	b	5	4	1	0	1	+	-	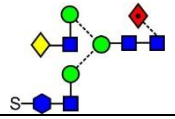	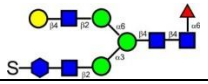
2070.7	2070.7	1	a	5	4	2	0	0	+	+	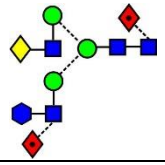	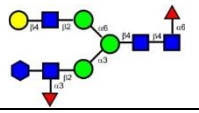

2263.8	2263.8	1	b	5	4	2	1	0	+	-	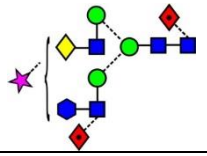	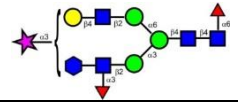
2133.8	2133.8	1	b	5	5	0	1	0	+	+	Not fragmented	Not fragmented
2086.7	2086.7	1	a	5	5	1	0	0	+	+	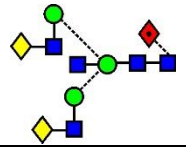	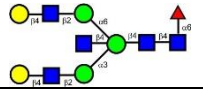
2279.8	2279.8	1	b	5	5	1	1	0	+	+	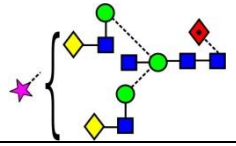	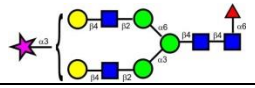
2295.8	2295.8	1	b	5	6	0	1	0	-	+	Not fragmented	Not fragmented
2248.7	2248.8	1	a	5	6	1	0	0	+	+	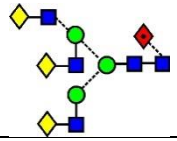	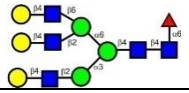
2441.8	2441.9	1	b	5	6	1	1	0	+	+	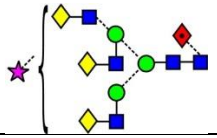	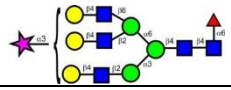
1366	1366	2	d	5	6	1	2	0	+	+	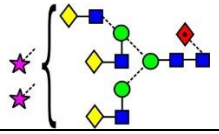	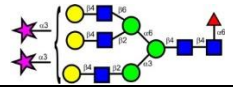

1007.5	1007.3	3	c	5	6	1	3	0	+	-	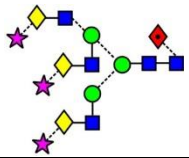	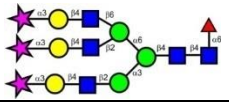
1965.7	1965.7	1	a	6	3	1	0	0	+	-	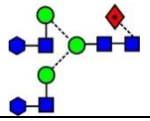	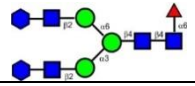
2158.7	2158.8	1	b	6	3	1	1	0	+	-	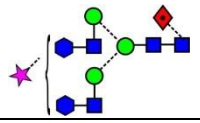	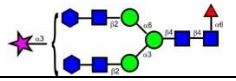
1947.7	1947.7	1	b	6	3	1	0	1	+	-	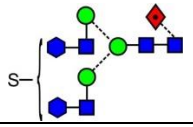	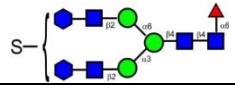
2111.7	2111.7	1	a	6	3	2	0	0	+	-	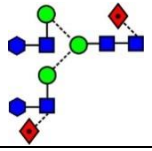	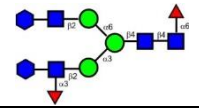
2093.7	2093.7	1	b	6	3	2	0	1	+	-	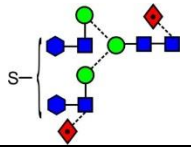	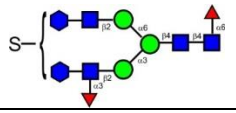
2257.8	2257.8	1	a	6	3	3	0	0	+	-	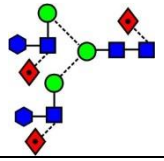	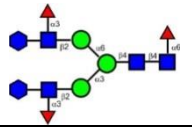
1899.6	1899.6	1	a	6	4	0	0	0	-	+	Not fragmented	Not fragmented
2127.7	2127.7	1	a	6	4	1	0	0	+	+	Not fragmented	Not fragmented

2289.7	2289.8	1	a	6	5	1	0	0	+	+	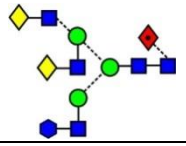	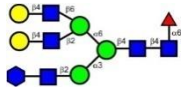
2482.8	2482.9	1	b	6	5	1	1	0	+	-	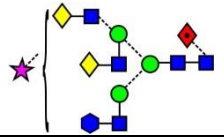	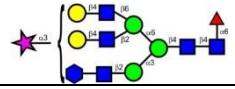
1386.5	1386.5	2	d	6	5	1	2	0	+	-	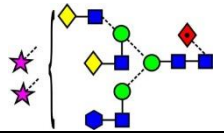	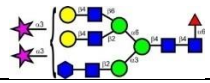
1021.1	1021	3	c	6	5	1	3	0	+	-	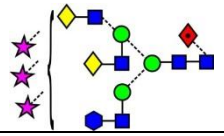	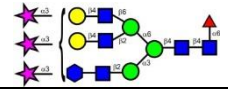
2271.8	2271.8	1	b	6	5	1	0	1	+	-	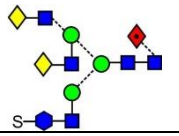	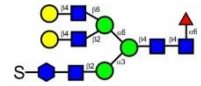
2435.8	2435.8	1	a	6	5	2	0	0	+	-	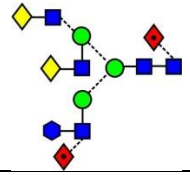	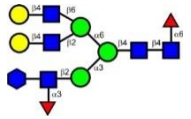
2628.9	2629	1	b				1	0	+	-	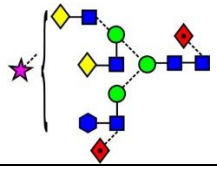	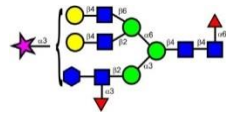

2451.8	2451.8	1	a	6	6	1	0	0	+	-	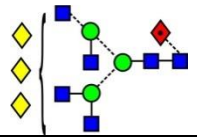	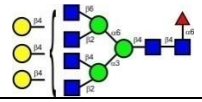
2644.9	2644.9	2	d	6	6	1	1	0	-	+	Not fragmented	Not fragmented
1467.5	1467.5	2	d	6	6	1	2	0	-	+	Not fragmented	Not fragmented
2613.9	2613.9	1	a	6	7	1	0	0	+	+	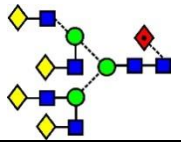	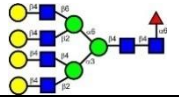
1548.5	1548.5	2	d	6	7	1	2	0	+	+	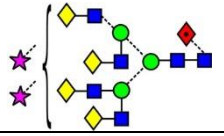	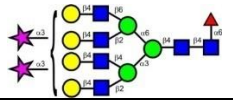
1694.1	1694.1	2	d	6	7	1	3	0	+	+	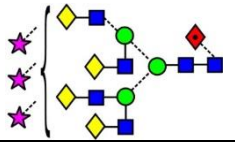	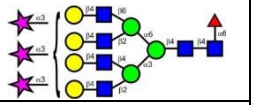
2331.1	2330.8	1	a	7	4	1	0	0	+	-	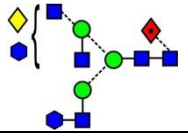	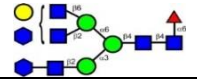
2523.9	2523.9	1	b	7	4	1	0	1	+	-	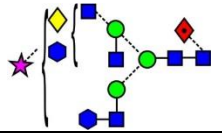	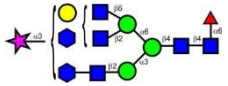

1) Ions:

a = $[M+H_2PO_4]^-$

b = $[M-H]^-$

c = $[M-H_3]^{3-}$

d = $[M-H_2]^{2-}$

The following glycan libraries are deposited online:

Datatset D.1: Online location of deposited glycan libraries

- BG505 SOSIP.664 produced from stable HEK 293T cells (Chapters 3 and 4), as part of Behrens *et al.*, 2016 [13]. URL: http://dx.doi.org/10.1016/j.celrep.2016.02.058 (Table S1)

- BG505 SOSIP.664, BG505 gp120 and BG505 WT.SEKS produced from transient HEK 293F cells (Chapters 4 and 5), as part of Behrens *et al.*, 2017 [491].
  URL: http://jvi.asm.org/content/early/2016/10/27/JVI.01894-16/suppl/DCSupplemental
  (Table S1)

- BG505 NFL2P.664, produced from transient CHO and transient HEK 293F cells (Chapter 6)
  URL: https://ora.ox.ac.uk/objects/uuid:104383d4-36e4-437e-85e2-b1da780c20e8
  (DOI: 10.5287/bodleian:6rZgV5P11, Table S1)

- BG505 SOSIP.v4.1-GT1 and BG505 SOSIP.664, produced from stable CHO cells (Chapter 7)
  URL: https://ora.ox.ac.uk/objects/uuid:104383d4-36e4-437e-85e2-b1da780c20e8
  (DOI: 10.5287/bodleian:6rZgV5P11, Table S2)

Appendix E Location of mass spectrometry peak lists

Dataset E.1: Online location of lists of glycopeptides identified by MALDI-TOF MS

- Identified glycopeptides resulting from trypsin- and chymotrypsin-digested BG505 SOSIP.664 (stable HEK 293T cells) by MALDI-TOF MS (Chapter 3) are deposited online as part of Behrens *et al*., 2016 [13].
  URL: http://dx.doi.org/10.1016/j.celrep.2016.02.058 (Table S3)

Dataset E.2: Online location of lists of peptides and glycopeptides identified by LC-ESI MS

- Identified glycopeptides of trypsin- and chymotrypsin-digested BG505 SOSIP.664 (stable HEK 293 T cells) by LC-ESI MS (Chapter 3) are deposited online as part of Behrens *et al*., 2016 [13]. URL: http://dx.doi.org/10.1016/j.celrep.2016.02.058 (Tables S4 and S5)

- Identified peptides and glycopeptides of trypsin-, chymotrypsin-, GluC plus trypsin-and pronase-digested, as well as deglycosylated BG505 SOSIP.664, BG505 gp120 and BG505 WT.SEKS (stable HEK 293 T cells) by LC-ESI MS (Chapters 4 and 5) are deposited online as part of Behrens *et al.*, 2017 [491].
  URL: http://jvi.asm.org/content/early/2016/10/27/JVI.01894-16/suppl/DCSupplemental (Tables S2-S7)

- Identified glycopeptides of trypsin- and chymotrypsin-digested BG505 NFL2P.664 (transient CHO and HEK 293F cells) by LC-ESI MS (Chapter 6) are deposited online.
  URL: https://ora.ox.ac.uk/objects/uuid:104383d4-36e4-437e-85e2-b1da780c20e8
  (DOI: 10.5287/bodleian:6rZgV5P11, Table S3)

- Identified glycopeptides of trypsin- and chymotrypsin-digested BG505 SOSIP.v4.1-GT1 and BG505 SOSIP.664 (stable CHO cells) by LC-ESI MS (Chapter 7) are deposited online.
  URL: https://ora.ox.ac.uk/objects/uuid:104383d4-36e4-437e-85e2-b1da780c20e8
  (DOI: 10.5287/bodleian:6rZgV5P11, Table S4)

Appendix F HILIC-UPLC profiles of deletion mutants

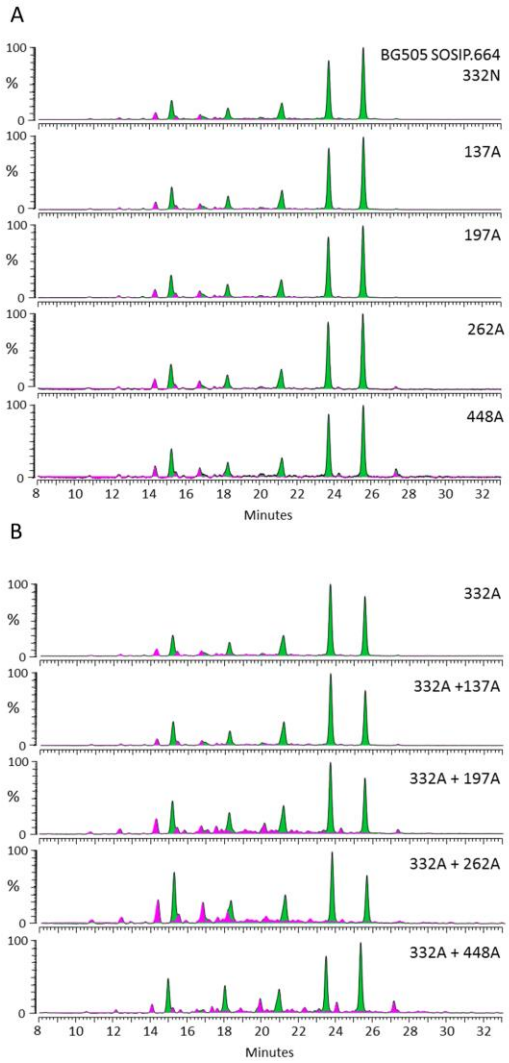

C

	Man5	Man6	Man7	Man8	Man9	sum
BG505 SOSIP.664	8	5	9	24	30	75
137A	9	5	9	24	28	75
332A	8	5	10	27	22	73
197A	9	5	8	23	27	73
262A	10	6	8	23	25	72
332A	8	5	10	27	22	73
448A	10	6	8	20	23	67
332A+137A	9	6	12	27	21	75
332A+197A	9	6	9	18	14	55
332A+262A	12	5	8	16	11	52
332A+448A	9	7	8	14	18	55

Figure F.1: HILIC-UPLC profiles of a panel of PNGS-deletion mutants of BG505 SOSIP.664 trimers

A selection of single and double N-glycosylation site knockout mutants of the His-tagged BG505 SOSIP.664 trimer, together with the unmodified control trimer, were expressed by transient transfection of HEK 293F cells and purified by PGT151 affinity chromatography. The eluted Env proteins were resolved by BN-PAGE and the bands corresponding to trimers were excised. N-glycans were released from the gel bands using PNGase F and fluorescently labelled. Glycan profiles with and without Endo H digestion were analyzed by HILIC-UPLC. Peaks corresponding to oligomannose-type and hybrid-type glycans are depicted in green, complex-type glycans in pink. (A) The panel of single PNGS knockout mutants. (B) The corresponding panel of N332A double PNGS knockout mutants. (C) Abundances (as percentages of total glycans) of oligomannose-type glycans $Man_{5-9}GlcNAc_2$ (Man5-Man9). The changes seen in the various mutants, relative to the BG505 SOSIP.664 control trimers, are presented in Figure 4.6.

Appendix G Publications and attended conferences

Publications*

- Behrens A-J, Crispin M. Structural principles controlling HIV envelope glycosylation. *Curr. Opin. Struct. Biol.* 2017, 44:125-133.
- Behrens A-J, Seabright GE, Crispin M. Targeting glycans of HIV envelope glycoproteins for vaccine design. Book Chapter in Chemical Biology of Glycoproteins. Royal Society of Chemistry. (Editor: Wang, L.-X.). 2017, Chaper 11.
- Behrens A-J, Harvey DJ, Milne E, Cupo A, (…), Moore JP, Crispin M. Molecular architecture of the cleavage-dependent mannose patch on a soluble HIV-1 envelope glycoprotein trimer. *J. Virol.* 2017, 91:e01894-16.
- Behrens A-J, Vasiljevic S, Pritchard LK, Harvey DJ, Andev RS, Krumm SA, (...), Crispin M. Composition and antigenic effects of individual glycan sites of a trimeric HIV-1 envelope glycoprotein. *Cell Rep.* 2016, 14:2695-2706.
- Calow J*, Behrens A-J[#], Mader S, Bockau U, (…), Hartmann MWW, Crispin M. Antibody production using a ciliate generates unusual antibody glycoforms displaying enhanced cell-killing activity. *mAbs* 2016, 8, 1498-1511.

  [#]shared first co-authorship
- Medina-Ramirez M, Garces F, Escolano A, Skog P, de Taeye SW, Moral-Sanchez I, (...), Yasmee A, Behrens A-J, (…), Sanders RW. Design and crystal structure of a native-like HIV-1 envelope trimer that engages multiple broadly neutralizing antibody precursors in vivo. *J. Exp. Med.* 2017, in press.
- Struwe WB, Stuckmann A, Behrens A-J, Pagel K, Crispin M. Global N-glycan site occupancy of HIV-1 gp120 by metabolic engineering and high-resolution intact mass spectrometry. *ACS Chem. Biol.* 2017, 12:357-361.
- Halldorsson S, Behrens A-J, Harlos K, Huiskonen JT, Elliott RM, Crispin M, Brennan B, and Bowden TA. Structure of a phleboviral envelope glycoprotein reveals a consolidated model of membrane fusion. *Proc. Natl. Acad. Sci. USA* 2016, 113, 7154-7159.
- Stewart-Jones GBE, Soto C, Lemmin T, Chuang G-Y, Druz A, Kong R, Thomas V, Wagh K, Zhou T, Behrens A-J, (…), Mascola JR, Kwong PD. Trimeric HIV-1-Env structures define glycan shields from clades A, B, and G. *Cell* 2016, 165, 1-14.
- Pritchard LK, Spencer DI, Royle L, Bonomelli C, Seabright GE, Behrens A-J, […], Doores KJ, Crispin M. Glycan clustering stabilizes the mannose patch of HIV-1 and preserves vulnerability to broadly neutralizing antibodies. *Nat. Commun.* 2015, *6*, 7479.

*: List contains publications accepted for publishing by the time of printing this thesis

Attended conferences and seminars

07/2017	Eurocarb, Barcelona, Spain, poster presentation
03/2017	HIV Vaccines C9 Keystone symposia, Steamboat Springs, CO, USA, poster presentation
02/2017	GlycoBioTec conference, Berlin, Germany, oral presentation: 'Fine structure of the HIV-1 glycan shield'
10/2016	EMBO Workshop: Glycosylation in the Golgi complex, Vico Equense, Italy, poster presentation
10/2016	HIV Research for Prevention (HIVR4P), Chicago, IL, USA, oral presentation: 'Composition and antigenic effects of individual glycan sites of the HIV-1 glycan shield'
09/2016	British Mass Spectrometry Society Meeting, Eastbourne, UK, oral presentation: 'Site-specific N-glycan analysis of an HIV1 Env trimer mimic'
05/2016	Biopharma Analysis Seminar organized by Sciex, Cambridge, UK, oral presentation: 'Site-specific N-glycan analysis of an HIV1 Env trimer mimic'
04/2016	Chemical Immunology Conference from the British Society for Immunology, Oxford, UK
04/2016	EAVI2020 Research Call, teleconference, oral presentation: 'Quantitative site-specific analysis of a SOSIP trimer'
03/2016	CHAVI-ID Research Focus meeting, teleconference, oral presentation: 'Site-specific N-glycosylation of an Env mimic'
01/2016	Scripps CHAVI-ID Retreat, La Jolla, CA, USA
07/2015	Summer School Mass Spectrometry in Biotechnology & Medicine, Dubrovnik, Croatia, oral and poster presentation: 'Targeting the glycan shield of the trimeric HIV-1 envelope spike'

References

1. AIDS info on Web page URL: http://aidsinfo.unaids.org/. accessed on 10/01/2017.

2. Burton DR, Ahmed R, Barouch DH, Butera ST, Crotty S, Godzik A, (...), Wyatt R. A Blueprint for HIV Vaccine Discovery. *Cell Host Microbe* 2012, 12:396-407.

3. Fee E, Brown TM. Michael S. Gottlieb and the Identification of AIDS. *Am. J. Public Health* 2006, 96:982-983.

4. Gottlieb MS, Schlanker HM, Fan PT, Saxon A, Weismann JD. Pneumocystis Pneumonia - Los Angeles. *MMWR (CDC)* 1981, 30:1-3.

5. Barré-Sinoussi F, Ross AL, Delfraissy J-F. Past, present and future: 30 years of HIV research. *Nat. Rev. Microbiol.* 2013, 11:877-883.

6. Dilley KA, Ni N, Nikolaitchik OA, Chen J, Galli A, Hu W-S. Determining the frequency and mechanisms of HIV-1 and HIV-2 RNA copackaging by single-virion analysis. *J. Virol.* 2011, 85:10499-10508.

7. Marlink R, Kanki P, Thior I, Travers K, Eisen G, Siby T, (...), Gueye EH. Reduced rate of disease development after HIV-2 infection as compared to HIV-1. *Science* 1994, 265:1587-1590.

8. Buonaguro L, Tornesello ML, Buonaguro FM. Human immunodeficiency virus type 1 subtype distribution in the worldwide epidemic: pathogenetic and therapeutic implications. *J. Virol.* 2007, 81:10209-10219.

9. Plantier J-C, Leoz M, Dickerson JE, De Oliveira F, Cordonnier F, Lemée V, (...), Simon F. A new human immunodeficiency virus derived from gorillas. *Nat. Med.* 2009, 15:871-872.

10. Campbell S, Rein A. In vitro assembly properties of human immunodeficiency virus type 1 Gag protein lacking the p6 domain. *J. Virol.* 1999, 73:2270-2279.

11. Lasky LA, Groopman JE, Fennie CW, Benz PM, Capon DJ, Dowbenko DJ, (...), Berman PW. Neutralization of the AIDS retrovirus by antibodies to a recombinant envelope glycoprotein. *Science* 1986, 233:209-212.

12. Zhu P, Liu J, Bess J, Jr., Chertova E, Lifson JD, Grise H, (...), Roux KH. Distribution and three-dimensional structure of AIDS virus envelope spikes. *Nature* 2006, 441:847-852.

13. Behrens A-J, Vasiljevic S, Pritchard LK, Harvey DJ, Andev RS, Krumm SA, (...), Crispin M. Composition and antigenic effects of individual glycan sites of a trimeric HIV-1 envelope glycoprotein. *Cell Rep.* 2016, 14:2695-2706.

14. HIV database on Web page URL: http://www.hiv.lanl.gov/. accessed on 15/03/2016.

15. Dalgleish AG, Beverley PC, Clapham PR, Crawford DH, Greaves MF, Weiss RA. The CD4 (T4) antigen is an essential component of the receptor for the AIDS retrovirus. *Nature* 1984, 312:763-767.

16. Klatzmann D, Champagne E, Chamaret S, Gruest J, Guetard D, Hercend T, (...), Montagnier L. T-lymphocyte T4 molecule behaves as the receptor for human retrovirus LAV. *Nature* 1984, 312:767-768.

17. Deng H, Liu R, Ellmeier W, Choe S, Unutmaz D, Burkhart M, (...), Landau NR. Identification of a major co-receptor for primary isolates of HIV-1. *Nature* 1996, 381:661-666.

18. Dragic T, Litwin V, Allaway GP, Martin SR, Huang Y, Nagashima KA, (...), Paxton WA. HIV-1 entry into CD4+ cells is mediated by the chemokine receptor CC-CKR-5. *Nature* 1996, 381:667-673.

19. Zhu T, Mo H, Wang N, Nam DS, Cao Y, Koup RA, Ho DD. Genotypic and phenotypic characterization of HIV-1 patients with primary infection. *Science* 1993, 261:1179-1181.

20. van't Wout AB, Kootstra NA, Mulder-Kampinga GA, Albrecht-van Lent N, Scherpbier HJ, Veenstra J, (...), Schuitemaker H. Macrophage-tropic variants initiate human immunodeficiency virus type 1 infection after sexual, parenteral, and vertical transmission. *J. Clin. Invest.* 1994, 94:2060-2067.

21. Davies JF, 2nd, Hostomska Z, Hostomsky Z, Jordan SR, Matthews DA. Crystal structure of the ribonuclease H domain of HIV-1 reverse transcriptase. *Science* 1991, 252:88-95.

22. Arhel N. Revisiting HIV-1 uncoating. *Retrovirology* 2010, 7:96.

23. Neil SJ, Zang T, Bieniasz PD. Tetherin inhibits retrovirus release and is antagonized by HIV-1 Vpu. *Nature* 2008, 451:425-430.

24. Freed EO. HIV-1 assembly, release and maturation. *Nat. Rev. Microbiol.* 2015, 13:484-496.

25. Finzi D, Hermankova M, Pierson T, Carruth LM, Buck C, Chaisson RE, (...), Siliciano RF. Identification of a reservoir for HIV-1 in patients on highly active antiretroviral therapy. *Science* 1997, 278:1295-1300.

26. Chun TW, Stuyver L, Mizell SB, Ehler LA, Mican JA, Baseler M, (...), Fauci AS. Presence of an inducible HIV-1 latent reservoir during highly active antiretroviral therapy. *Proc. Natl. Acad. Sci. USA* 1997, 94:13193-13197.

27. Siliciano RF, Greene WC. HIV latency. *Cold Spring Harb. Perspect. Med.* 2011, 1:a007096.

28. Cohn LB, Silva IT, Oliveira TY, Rosales RA, Parrish EH, Learn GH, (...), Nussenzweig MC. HIV-1 integration landscape during latent and active infection. *Cell* 2015, 160:420-432.

29. Hladik F, McElrath MJ. Setting the stage: host invasion by HIV. *Nat. Rev. Immunol.* 2008, 8:447-457.

30. Ganor Y, Bomsel M. HIV-1 transmission in the male genital tract. *Am. J. Reprod. Immunol.* 2011, 65:284-291.

31. Sodora DL, Gettie A, Miller CJ, Marx PA. Vaginal transmission of SIV: assessing infectivity and hormonal influences in macaques inoculated with cell-free and cell-associated viral stocks. *AIDS Res. Hum. Retroviruses* 1998, 14:119-123.

32. Keele BF, Giorgi EE, Salazar-Gonzalez JF, Decker JM, Pham KT, Salazar MG, (...), Shaw GM. Identification and characterization of transmitted and early founder virus envelopes in primary HIV-1 infection. *Proc. Natl. Acad. Sci. USA* 2008, 105:7552-7557.

33. Joseph SB, Swanstrom R, Kashuba AD, Cohen MS. Bottlenecks in HIV-1 transmission: insights from the study of founder viruses. *Nat. Rev. Microbiol.* 2015, 13:414-425.

34. Salazar-Gonzalez JF, Salazar MG, Keele BF, Learn GH, Giorgi EE, Li H, (...), Shaw GM. Genetic identity, biological phenotype, and evolutionary pathways of transmitted/founder viruses in acute and early HIV-1 infection. *J. Exp. Med.* 2009, 206:1273-1289.

35. Mehandru S, Poles MA, Tenner-Racz K, Horowitz A, Hurley A, Hogan C, (...), Markowitz M. Primary HIV-1 infection is associated with preferential depletion of CD4+ T lymphocytes from effector sites in the gastrointestinal tract. *J. Exp. Med.* 2004, 200:761-770.

36. Wang X, Rasmussen T, Pahar B, Poonia B, Alvarez X, Lackner AA, Veazey RS. Massive infection and loss of CD4+ T cells occurs in the intestinal tract of neonatal rhesus macaques in acute SIV infection. *Blood* 2007, 109:1174-1181.

37. Brenchley JM, Price DA, Douek DC. HIV disease: fallout from a mucosal catastrophe? *Nat. Immunol.* 2006, 7:235-239.

38. Brenchley JM, Schacker TW, Ruff LE, Price DA, Taylor JH, Beilman GJ, (...), Douek DC. CD4+ T cell depletion during all stages of HIV disease occurs predominantly in the gastrointestinal tract. *J. Exp. Med.* 2004, 200:749-759.

39. Arthos J, Cicala C, Martinelli E, Macleod K, Van Ryk D, Wei D, (...), Fauci AS. HIV-1 envelope protein binds to and signals through integrin alpha4beta7, the gut mucosal homing receptor for peripheral T cells. *Nat. Immunol.* 2008, 9:301-309.

40. Gorny MK, Pan R, Williams C, Wang XH, Volsky B, O'Neal T, (...), Zolla-Pazner S. Functional and immunochemical cross-reactivity of V2-specific monoclonal antibodies from HIV-1-infected individuals. *Virology* 2012, 427:198-207.

41. Byrareddy SN, Arthos J, Cicala C, Villinger F, Ortiz KT, Little D, (...), Ansari AA. Sustained virologic control in SIV+ macaques after antiretroviral and alpha4beta7 antibody therapy. *Science* 2016, 354:197-202.

42. Ochsenbauer C, Edmonds TG, Ding H, Keele BF, Decker J, Salazar MG, (...), Kappes JC. Generation of transmitted/founder HIV-1 infectious molecular clones and characterization of their replication capacity in CD4 T lymphocytes and monocyte-derived macrophages. *J. Virol.* 2012, 86:2715-2728.

43. King DF, Siddiqui AA, Buffa V, Fischetti L, Gao Y, Stieh D, (...), Shattock RJ. Mucosal tissue tropism and dissemination of HIV-1 subtype B acute envelope-expressing chimeric virus. *J. Virol.* 2013, 87:890-899.

44. Sattentau QJ, Stevenson M. Macrophages and HIV-1: An Unhealthy Constellation. *Cell Host Microbe* 2016, 19:304-310.

45. Baxter AE, Russell RA, Duncan CJ, Moore MD, Willberg CB, Pablos JL, (...), Sattentau QJ. Macrophage infection via selective capture of HIV-1-infected CD4+ T cells. *Cell Host Microbe* 2014, 16:711-721.

46. Simon V, Ho DD. HIV-1 dynamics in vivo: implications for therapy. *Nat. Rev. Microbiol.* 2003, 1:181-190.

47. McMichael AJ, Borrow P, Tomaras GD, Goonetilleke N, Haynes BF. The immune response during acute HIV-1 infection: clues for vaccine development. *Nat. Rev. Immunol.* 2010, 10:11-23.

48. Rodriguez B, Sethi AK, Cheruvu VK, Mackay W, Bosch RJ, Kitahata M, (...), Lederman MM. Predictive value of plasma HIV RNA level on rate of CD4 T-cell decline in untreated HIV infection. *Jama* 2006, 296:1498-1506.

49. Schacker TW, Hughes JP, Shea T, Coombs RW, Corey L. Biological and virologic characteristics of primary HIV infection. *Ann. Int. Med.* 1998, 128:613-620.

50. Borrow P, Lewicki H, Hahn BH, Shaw GM, Oldstone MB. Virus-specific CD8+ cytotoxic T-lymphocyte activity associated with control of viremia in primary human immunodeficiency virus type 1 infection. *J. Virol.* 1994, 68:6103-6110.

51. Koup RA, Safrit JT, Cao Y, Andrews CA, McLeod G, Borkowsky W, (...), Ho DD. Temporal association of cellular immune responses with the initial control of viremia in primary human immunodeficiency virus type 1 syndrome. *J. Virol.* 1994, 68:4650-4655.

52. Veazey RS, DeMaria M, Chalifoux LV, Shvetz DE, Pauley DR, Knight HL, (...), Lackner AA. Gastrointestinal tract as a major site of CD4+ T cell depletion and viral replication in SIV infection. *Science* 1998, 280:427-431.

53. Mattapallil JJ, Douek DC, Hill B, Nishimura Y, Martin M, Roederer M. Massive infection and loss of memory CD4+ T cells in multiple tissues during acute SIV infection. *Nature* 2005, 434:1093-1097.

54. Doitsh G, Galloway NL, Geng X, Yang Z, Monroe KM, Zepeda O, (...), Greene WC. Cell death by pyroptosis drives CD4 T-cell depletion in HIV-1 infection. *Nature* 2014, 505:509-514.

55. Berger EA, Murphy PM, Farber JM. Chemokine receptors as HIV-1 coreceptors: roles in viral entry, tropism, and disease. *Annu. Rev. Immunol.* 1999, 17:657-700.

56. Regoes RR, Bonhoeffer S. The HIV coreceptor switch: a population dynamical perspective. *Trends Microbiol.* 2005, 13:269-277.

57. Nguyen DH, Hildreth JE. Evidence for budding of human immunodeficiency virus type 1 selectively from glycolipid-enriched membrane lipid rafts. *J. Virol.* 2000, 74:3264-3272.

58. Chan R, Uchil PD, Jin J, Shui G, Ott DE, Mothes W, Wenk MR. Retroviruses human immunodeficiency virus and murine leukemia virus are enriched in phosphoinositides. *J. Virol.* 2008, 82:11228-11238.

59. Brugger B, Glass B, Haberkant P, Leibrecht I, Wieland FT, Krausslich HG. The HIV lipidome: a raft with an unusual composition. *Proc. Natl. Acad. Sci. USA* 2006, 103:2641-2646.

60. Wyatt R, Kwong PD, Desjardins E, Sweet RW, Robinson J, Hendrickson WA, Sodroski JG. The antigenic structure of the HIV gp120 envelope glycoprotein. *Nature* 1998, 393:705-711.

61. Wei X, Decker JM, Wang S, Hui H, Kappes JC, Wu X, (...), Shaw GM. Antibody neutralization and escape by HIV-1. *Nature* 2003, 422:307-312.

62. Moore JP, Sodroski J. Antibody cross-competition analysis of the human immunodeficiency virus type 1 gp120 exterior envelope glycoprotein. *J. Virol.* 1996, 70:1863-1872.

63. Pino M, Erkizia I, Benet S, Erikson E, Fernandez-Figueras MT, Guerrero D, (...), Izquierdo-Useros N. HIV-1 immune activation induces Siglec-1 expression and enhances viral trans-infection in blood and tissue myeloid cells. *Retrovirology* 2015, 12:37.

64. Izquierdo-Useros N, Lorizate M, McLaren PJ, Telenti A, Krausslich HG, Martinez-Picado J. HIV-1 capture and transmission by dendritic cells: the role of viral glycolipids and the cellular receptor Siglec-1. *PLoS Pathog.* 2014, 10:e1004146.

65. Motswaledi MS, Kasvosve I, Oguntibeju OO. The role of red blood cells in enhancing or preventing HIV infection and other diseases. *Biomed Res. Int.* 2013, 2013:758682.

66. Neil SJ, McKnight A, Gustafsson K, Weiss RA. HIV-1 incorporates ABO histo-blood group antigens that sensitize virions to complement-mediated inactivation. *Blood* 2005, 105:4693-4699.

67. Arendrup M, Hansen JE, Clausen H, Nielsen C, Mathiesen LR, Nielsen JO. Antibody to histo-blood group A antigen neutralizes HIV produced by lymphocytes from blood group A donors but not from blood group B or O donors. *AIDS* 1991, 5:441-444.

68. Pejchal R, Doores KJ, Walker LM, Khayat R, Huang P-S, Wang S-K, (...), Wilson IA. A potent and broad neutralizing antibody recognizes and penetrates the HIV glycan shield. *Science* 2011, 334:1097-1103.

69. Walker LM, Huber M, Doores KJ, Falkowska E, Pejchal R, Julien J-P, (...), Poignard P. Broad neutralization coverage of HIV by multiple highly potent antibodies. *Nature* 2011, 477:466-470.

70. Walker LM, Phogat SK, Chan-Hui P-Y, Wagner D, Phung P, Goss JL, (...), Burton DR. Broad and potent neutralizing antibodies from an African donor reveal a new HIV-1 vaccine target. *Science* 2009, 326:285-289.

71. Calarese DA, Scanlan CN, Zwick MB, Deechongkit S, Mimura Y, Kunert R, (...), Wilson IA. Antibody domain exchange is an immunological solution to carbohydrate cluster recognition. *Science* 2003, 300:2065-2071.

72. Blattner C, Lee JH, Sliepen K, Derking R, Falkowska E, de la Pena AT, (...), Ward AB. Structural delineation of a quaternary, cleavage-dependent epitope at the gp41-gp120 interface on intact HIV-1 Env trimers. *Immunity* 2014, 40:669-680.

73. Falkowska E, Le KM, Ramos A, Doores KJ, Lee JH, Blattner C, (...), Burton DR. Broadly neutralizing HIV antibodies define a glycan-dependent epitope on the prefusion conformation of gp41 on cleaved envelope trimers. *Immunity* 2014, 40:657-668.

74. Scanlan CN, Pantophlet R, Wormald MR, Ollmann Saphire E, Stanfield R, Wilson IA, (...), Burton DR. The broadly neutralizing anti-human immunodeficiency virus type 1 antibody 2G12 recognizes a cluster of alpha1-->2 mannose residues on the outer face of gp120. *J. Virol.* 2002, 76:7306-7321.

75. Mouquet H, Scharf L, Euler Z, Liu Y, Eden C, Scheid JF, (...), Bjorkman PJ. Complex-type N-glycan recognition by potent broadly neutralizing HIV antibodies. *Proc. Natl. Acad. Sci. USA* 2012, 109:3268-3277.

76. Scharf L, Scheid JF, Lee JH, West AP, Chen C, Gao H, (...), Bjorkman PJ. Antibody 8ANC195 reveals a site of broad vulnerability on the HIV-1 envelope spike. *Cell Rep.* 2014, 7:785-795.

77. Garces F, Sok D, Kong L, McBride R, Kim HJ, Saye-Francisco KF, (...), Wilson IA. Structural evolution of glycan recognition by a family of potent HIV antibodies. *Cell* 2014, 159:69-79.

78. Huang J, Kang BH, Pancera M, Lee JH, Tong T, Feng Y, (...), Connors M. Broad and potent HIV-1 neutralization by a human antibody that binds the gp41–gp120 interface. *Nature* 2014, 515:138-142.

79. Kong L, Lee JH, Doores KJ, Murin CD, Julien JP, McBride R, (...), Wilson IA. Supersite of immune vulnerability on the glycosylated face of HIV-1 envelope glycoprotein gp120. *Nat. Struct. Mol. Biol.* 2013, 20:796-803.

80. McLellan JS, Pancera M, Carrico C, Gorman J, Julien J-P, Khayat R, (...), Kwong PD. Structure of HIV-1 gp120 V1/V2 domain with broadly neutralizing antibody PG9. *Nature* 2011, 480:336-343.

81. Pancera M, Shahzad-Ul-Hussan S, Doria-Rose NA, McLellan JS, Bailer RT, Dai K, (...), Kwong PD. Structural basis for diverse N-glycan recognition by HIV-1-neutralizing V1-V2-directed antibody PG16. *Nat. Struct. Mol. Biol.* 2013, 20:804-813.

82. Freund NT, Horwitz JA, Nogueira L, Sievers SA, Scharf L, Scheid JF, (...), Nussenzweig MC. A new glycan-dependent CD4-binding site neutralizing antibody exerts pressure on HIV-1 In vivo. *PLoS Pathog.* 2015, 11:e1005238.

83. Hessell AJ, Poignard P, Hunter M, Hangartner L, Tehrani DM, Bleeker WK, (...), Burton DR. Effective, low-titer antibody protection against low-dose repeated mucosal SHIV challenge in macaques. *Nat. Med.* 2009, 15:951-954.

84. Hessell AJ, Rakasz EG, Poignard P, Hangartner L, Landucci G, Forthal DN, (...), Burton DR. Broadly neutralizing human anti-HIV antibody 2G12 is effective in protection against mucosal SHIV challenge even at low serum neutralizing titers. *PLoS Pathog.* 2009, 5:e1000433.

85. Hessell AJ, Rakasz EG, Tehrani DM, Huber M, Weisgrau KL, Landucci G, (...), Burton DR. Broadly neutralizing monoclonal antibodies 2F5 and 4E10 directed against the human immunodeficiency virus type 1 gp41 membrane-proximal external region protect against mucosal challenge by simian-human immunodeficiency virus SHIVBa-L. *J. Virol.* 2010, 84:1302-1313.

86. Mascola JR, Lewis MG, Stiegler G, Harris D, VanCott TC, Hayes D, (...), Birx DL. Protection of Macaques against pathogenic simian/human immunodeficiency virus 89.6PD by passive transfer of neutralizing antibodies. *J. Virol.* 1999, 73:4009-4018.

87. Mascola JR, Stiegler G, VanCott TC, Katinger H, Carpenter CB, Hanson CE, (...), Lewis MG. Protection of macaques against vaginal transmission of a pathogenic HIV-1/SIV chimeric virus by passive infusion of neutralizing antibodies. *Nat. Med.* 2000, 6:207-210.

88. Moldt B, Rakasz EG, Schultz N, Chan-Hui PY, Swiderek K, Weisgrau KL, (...), Burton DR. Highly potent HIV-specific antibody neutralization in vitro translates into effective protection against mucosal SHIV challenge in vivo. *Proc. Natl. Acad. Sci. USA* 2012, 109:18921-18925.

89. Gautam R, Nishimura Y, Pegu A, Nason MC, Klein F, Gazumyan A, (...), Martin MA. A single injection of anti-HIV-1 antibodies protects against repeated SHIV challenges. *Nature* 2016, 533:105-109.

90. Altfeld M, Gale M, Jr. Innate immunity against HIV-1 infection. *Nat. Immunol.* 2015, 16:554-562.

91. Sauter D, Kirchhoff F. HIV replication: a game of hide and sense. *Curr. Opin. HIV AIDS* 2016, 11:173-181.

92. Jakobsen MR, Olagnier D, Hiscott J. Innate immune sensing of HIV-1 infection. *Curr. Opin. HIV AIDS* 2015, 10:96-102.

93. Silvin A, Manel N. Innate immune sensing of HIV infection. *Curr. Opin. Immunol.* 2015, 32:54-60.

94. Drickamer K. C-type lectin-like domains. *Curr. Opin. Struct. Biol.* 1999, 9:585-590.

95. van Kooyk Y, Rabinovich GA. Protein-glycan interactions in the control of innate and adaptive immune responses. *Nat. Immunol.* 2008, 9:593-601.

96. Robinson MJ, Sancho D, Slack EC, LeibundGut-Landmann S, Reis e Sousa C. Myeloid C-type lectins in innate immunity. *Nat. Immunol.* 2006, 7:1258-1265.

97. de Witte L, Nabatov A, Pion M, Fluitsma D, de Jong MA, de Gruijl T, (...), Geijtenbeek TB. Langerin is a natural barrier to HIV-1 transmission by Langerhans cells. *Nat. Med.* 2007, 13:367-371.

98. Cassol E, Cassetta L, Rizzi C, Gabuzda D, Alfano M, Poli G. Dendritic cell-specific intercellular adhesion molecule-3 grabbing nonintegrin mediates HIV-1 infection of and transmission by M2a-polarized macrophages in vitro. *AIDS* 2013, 27:707-716.

99. Geijtenbeek TB, Kwon DS, Torensma R, van Vliet SJ, van Duijnhoven GC, Middel J, (...), van Kooyk Y. DC-SIGN, a dendritic cell-specific HIV-1-binding protein that enhances trans-infection of T cells. *Cell* 2000, 100:587-597.

100. van der Aar AMG, Gringhuis SI, Geijtenbeek TBH: Innate recognition of HIV-1 glycans: Implications for infection, transmission and immunity. In *HIV glycans in infection and immunity*. Edited by Pantophlet R; 2014. vol 1.

101. Dong C, Janas AM, Wang JH, Olson WJ, Wu L. Characterization of human immunodeficiency virus type 1 replication in immature and mature dendritic cells reveals dissociable cis- and trans-infection. *J. Virol.* 2007, 81:11352-11362.

102. Turville SG, Santos JJ, Frank I, Cameron PU, Wilkinson J, Miranda-Saksena M, (...), Cunningham AL. Immunodeficiency virus uptake, turnover, and 2-phase transfer in human dendritic cells. *Blood* 2004, 103:2170-2179.

103. Kwon DS, Gregorio G, Bitton N, Hendrickson WA, Littman DR. DC-SIGN-mediated internalization of HIV is required for trans-enhancement of T cell infection. *Immunity* 2002, 16:135-144.

104. Hijazi K, Wang Y, Scala C, Jeffs S, Longstaff C, Stieh D, (...), Kelly CG. DC-SIGN increases the affinity of HIV-1 envelope glycoprotein interaction with CD4. *PLoS One* 2011, 6:e28307.

105. Turville SG, Cameron PU, Handley A, Lin G, Pohlmann S, Doms RW, Cunningham AL. Diversity of receptors binding HIV on dendritic cell subsets. *Nat. Immunol.* 2002, 3:975-983.

106. Figdor CG, van Kooyk Y, Adema GJ. C-type lectin receptors on dendritic cells and Langerhans cells. *Nat. Rev. Immunol.* 2002, 2:77-84.

107. Stambach NS, Taylor ME. Characterization of carbohydrate recognition by langerin, a C-type lectin of Langerhans cells. *Glycobiology* 2003, 13:401-410.

108. Valladeau J, Ravel O, Dezutter-Dambuyant C, Moore K, Kleijmeer M, Liu Y, (...), Saeland S. Langerin, a novel C-type lectin specific to Langerhans cells, is an endocytic receptor that induces the formation of Birbeck granules. *Immunity* 2000, 12:71-81.

109. Hladik F, Sakchalathorn P, Ballweber L, Lentz G, Fialkow M, Eschenbach D, McElrath MJ. Initial events in establishing vaginal entry and infection by human immunodeficiency virus type-1. *Immunity* 2007, 26:257-270.

110. Yu Q, Yu R, Qin X. The good and evil of complement activation in HIV-1 infection. *Cell. Mol. Immunol.* 2010, 7:334-340.

111. Aasa-Chapman MM, Holuigue S, Aubin K, Wong M, Jones NA, Cornforth D, (...), McKnight A. Detection of antibody-dependent complement-mediated inactivation of both autologous and heterologous virus in primary human immunodeficiency virus type 1 infection. *J. Virol.* 2005, 79:2823-2830.

112. Sullivan BL, Knopoff EJ, Saifuddin M, Takefman DM, Saarloos MN, Sha BE, Spear GT. Susceptibility of HIV-1 plasma virus to complement-mediated lysis. Evidence for a role in clearance of virus in vivo. *J. Immunol.* 1996, 157:1791-1798.

113. Senaldi G, Peakman M, McManus T, Davies ET, Tee DE, Vergani D. Activation of the complement system in human immunodeficiency virus infection: relevance of the classical pathway to pathogenesis and disease severity. *J. Infect. Dis.* 1990, 162:1227-1232.

114. Ebenbichler CF, Thielens NM, Vornhagen R, Marschang P, Arlaud GJ, Dierich MP. Human immunodeficiency virus type 1 activates the classical pathway of complement by direct C1 binding through specific sites in the transmembrane glycoprotein gp41. *J. Exp. Med.* 1991, 174:1417-1424.

115. Haurum JS, Thiel S, Jones IM, Fischer PB, Laursen SB, Jensenius JC. Complement activation upon binding of mannan-binding protein to HIV envelope glycoproteins. *AIDS* 1993, 7:1307-1313.

116. Hart ML, Saifuddin M, Spear GT. Glycosylation inhibitors and neuraminidase enhance human immunodeficiency virus type 1 binding and neutralization by mannose-binding lectin. *J. Gen. Virol.* 2003, 84:353-360.

117. Spear GT, Zariffard MR, Xin J, Saifuddin M. Inhibition of DC-SIGN-mediated trans infection of T cells by mannose-binding lectin. *Immunology* 2003, 110:80-85.

118. Schmitz J, Zimmer JP, Kluxen B, Aries S, Bogel M, Gigli I, Schmitz H. Antibody-dependent complement-mediated cytotoxicity in sera from patients with HIV-1 infection is controlled by CD55 and CD59. *J. Clin. Invest.* 1995, 96:1520-1526.

119. Pinter C, Siccardi AG, Lopalco L, Longhi R, Clivio A. HIV glycoprotein 41 and complement factor H interact with each other and share functional as well as antigenic homology. *AIDS Res. Hum. Retroviruses* 1995, 11:971-980.

120. Bajtay Z, Speth C, Erdei A, Dierich MP. Cutting edge: productive HIV-1 infection of dendritic cells via complement receptor type 3 (CR3, CD11b/CD18). *J. Immunol.* 2004, 173:4775-4778.

121. Thieblemont N, Haeffner-Cavaillon N, Ledur A, L'Age-Stehr J, Ziegler-Heitbrock HW, Kazatchkine MD. CR1 (CD35) and CR3 (CD11b/CD18) mediate infection of human monocytes and monocytic cell lines with complement-opsonized HIV independently of CD4. *Clin. Exp. Immunol.* 1993, 92:106-113.

122. Coleman CM, Gelais CS, Wu L. Cellular and viral mechanisms of HIV-1 transmission mediated by dendritic cells. *Adv. Exp. Med. Biol.* 2013, 762:109-130.

123. Wu L, KewalRamani VN. Dendritic-cell interactions with HIV: infection and viral dissemination. *Nat. Rev. Immunol.* 2006, 6:859-868.

124. Turnbull EL, Wong M, Wang S, Wei X, Jones NA, Conrod KE, (...), Borrow P. Kinetics of expansion of epitope-specific T cell responses during primary HIV-1 infection. *J. Immunol.* 2009, 182:7131-7145.

125. Goonetilleke N, Liu MK, Salazar-Gonzalez JF, Ferrari G, Giorgi E, Ganusov VV, (...), McMichael AJ. The first T cell response to transmitted/founder virus contributes to the control of acute viremia in HIV-1 infection. *J. Exp. Med.* 2009, 206:1253-1272.

126. Kaufmann DE, Bailey PM, Sidney J, Wagner B, Norris PJ, Johnston MN, (...), Rosenberg ES. Comprehensive analysis of human immunodeficiency virus type 1-specific CD4 responses reveals marked immunodominance of gag and nef and the presence of broadly recognized peptides. *J. Virol.* 2004, 78:4463-4477.

127. Crooks ET, Moore PL, Franti M, Cayanan CS, Zhu P, Jiang P, (...), Binley JM. A comparative immunogenicity study of HIV-1 virus-like particles bearing various forms of envelope proteins, particles bearing no envelope and soluble monomeric gp120. *Virology* 2007, 366:245-262.

128. Moore PL, Crooks ET, Porter L, Zhu P, Cayanan CS, Grise H, (...), Binley JM. Nature of nonfunctional envelope proteins on the surface of human immunodeficiency virus type 1. *J. Virol.* 2006, 80:2515-2528.

129. Tomaras GD, Yates NL, Liu P, Qin L, Fouda GG, Chavez LL, (...), Haynes BF. Initial B-cell responses to transmitted human immunodeficiency virus type 1: virion-binding immunoglobulin M (IgM) and IgG antibodies followed by plasma anti-gp41 antibodies with ineffective control of initial viremia. *J. Virol.* 2008, 82:12449-12463.

130. Richman DD, Wrin T, Little SJ, Petropoulos CJ. Rapid evolution of the neutralizing antibody response to HIV type 1 infection. *Proc. Natl. Acad. Sci. USA* 2003, 100:4144-4149.

131. Stamatatos L, Morris L, Burton DR, Mascola JR. Neutralizing antibodies generated during natural HIV-1 infection: good news for an HIV-1 vaccine? *Nat. Med.* 2009, 15:866-870.

132. van Gils MJ, Euler Z, Schweighardt B, Wrin T, Schuitemaker H. Prevalence of cross-reactive HIV-1-neutralizing activity in HIV-1-infected patients with rapid or slow disease progression. *AIDS* 2009, 23:2405-2414.

133. Landais E, Huang X, Havenar-Daughton C, Murrell B, Price MA, Wickramasinghe L, (...), Poignard P. Broadly Neutralizing Antibody Responses in a Large Longitudinal Sub-Saharan HIV Primary Infection Cohort. *PLoS Pathog.* 2016, 12:e1005369.

134. Muro-Cacho CA, Pantaleo G, Fauci AS. Analysis of apoptosis in lymph nodes of HIV-infected persons. Intensity of apoptosis correlates with the general state of activation of the lymphoid tissue and not with stage of disease or viral burden. *J. Immunol.* 1995, 154:5555-5566.

135. Fischl MA, Richman DD, Grieco MH, Gottlieb MS, Volberding PA, Laskin OL, (...), et al. The efficacy of azidothymidine (AZT) in the treatment of patients with AIDS and AIDS-related complex. A double-blind, placebo-controlled trial. *New Engl. J. Med.* 1987, 317:185-191.

136. Clavel F, Hance AJ. HIV drug resistance. *New Engl. J. Med.* 2004, 350:1023-1035.

137. Cuevas JM, Geller R, Garijo R, Lopez-Aldeguer J, Sanjuan R. Extremely High Mutation Rate of HIV-1 In Vivo. *PLoS Biol.* 2015, 13:e1002251.

138. Coffin JM. HIV population dynamics in vivo: implications for genetic variation, pathogenesis, and therapy. *Science* 1995, 267:483-489.

139. Preston BD, Poiesz BJ, Loeb LA. Fidelity of HIV-1 reverse transcriptase. *Science* 1988, 242:1168-1171.

140. Roberts JD, Bebenek K, Kunkel TA. The accuracy of reverse transcriptase from HIV-1. *Science* 1988, 242:1171-1173.

141. Mansky LM, Temin HM. Lower in vivo mutation rate of human immunodeficiency virus type 1 than that predicted from the fidelity of purified reverse transcriptase. *J. Virol.* 1995, 69:5087-5094.

142. Holland JJ, De La Torre JC, Steinhauer DA. RNA virus populations as quasispecies. *Curr. Top. Microbiol. Immunol.* 1992, 176:1-20.

143. Arts EJ, Hazuda DJ. HIV-1 antiretroviral drug therapy. *Cold Spring Harb. Perspect. Med.* 2012, 2:a007161.

144. Ngemu EK, Khayeka-Wandabwa C, Kweka EJ, Choge JK, Anino E, Oyoo-Okoth E. Effectiveness of option B highly active antiretroviral therapy (HAART) prevention of mother-to-child transmission (PMTCT) in pregnant HIV women. *BMC research notes* 2014, 7:52.

145. Collier AC, Coombs RW, Schoenfeld DA, Bassett RL, Timpone J, Baruch A, (...), Corey L. Treatment of human immunodeficiency virus infection with saquinavir, zidovudine, and zalcitabine. AIDS Clinical Trials Group. *New Engl. J. Med.* 1996, 334:1011-1017.

146. Kelleher AD, Carr A, Zaunders J, Cooper DA. Alterations in the immune response of human immunodeficiency virus (HIV)-infected subjects treated with an HIV-specific protease inhibitor, ritonavir. *J. Infect. Dis.* 1996, 173:321-329.

147. Autran B, Carcelain G, Li TS, Blanc C, Mathez D, Tubiana R, (...), Leibowitch J. Positive effects of combined antiretroviral therapy on CD4+ T cell homeostasis and function in advanced HIV disease. *Science* 1997, 277:112-116.

148. Lederman MM, Connick E, Landay A, Kuritzkes DR, Spritzler J, St Clair M, (...), Kessler H. Immunologic responses associated with 12 weeks of combination antiretroviral therapy consisting of zidovudine, lamivudine, and ritonavir: results of AIDS Clinical Trials Group Protocol 315. *J. Infect. Dis.* 1998, 178:70-79.

149. Baeten JM, Donnell D, Ndase P, Mugo NR, Campbell JD, Wangisi J, (...), Partners Pr EPST. Antiretroviral prophylaxis for HIV prevention in heterosexual men and women. *New Engl. J. Med.* 2012, 367:399-410.

150. Mehta S, Moore RD, Graham NM. Potential factors affecting adherence with HIV therapy. *AIDS* 1997, 11:1665-1670.

151. Atkinson MJ, Petrozzino JJ. An evidence-based review of treatment-related determinants of patients' nonadherence to HIV medications. *AIDS Patient Care STDs* 2009, 23:903-914.

152. Morris BJ, Klausner JD. In developed countries male circumcision prevalence is inversely related to HIV prevalence. *Isr. J. Health Policy Res.* 2015, 4:40.

153. Abdool Karim SS, Baxter C. Microbicides for prevention of HIV infection: clinical efficacy trials. *Curr. Top. Microbiol. Immunol.* 2014, 383:97-115.

154. Chun TW, Engel D, Berrey MM, Shea T, Corey L, Fauci AS. Early establishment of a pool of latently infected, resting CD4(+) T cells during primary HIV-1 infection. *Proc. Natl. Acad. Sci. USA* 1998, 95:8869-8873.

155. Cohen YZ, Dolin R. Novel HIV vaccine strategies: overview and perspective. *Ther. Adv. Vaccines* 2013, 1:99-112.

156. Flynn NM, Forthal DN, Harro CD, Judson FN, Mayer KH, Para MF. Placebo-controlled phase 3 trial of a recombinant glycoprotein 120 vaccine to prevent HIV-1 infection. *J. Infect. Dis.* 2005, 191:654-665.

157. Pitisuttithum P, Gilbert P, Gurwith M, Heyward W, Martin M, van Griensven F, (...), Choopanya K. Randomized, double-blind, placebo-controlled efficacy trial of a bivalent recombinant glycoprotein 120 HIV-1 vaccine among injection drug users in Bangkok, Thailand. *J. Infect. Dis.* 2006, 194:1661-1671.

158. Gray G, Buchbinder S, Duerr A. Overview of STEP and Phambili trial results: two phase IIb test-of-concept studies investigating the efficacy of MRK adenovirus type 5 gag/pol/nef subtype B HIV vaccine. *Curr. Opin. HIV AIDS* 2010, 5:357-361.

159. McElrath MJ, De Rosa SC, Moodie Z, Dubey S, Kierstead L, Janes H, (...), Casimiro DR. HIV-1 vaccine-induced immunity in the test-of-concept Step Study: a case-cohort analysis. *Lancet* 2008, 372:1894-1905.

160. Buchbinder SP, Mehrotra DV, Duerr A, Fitzgerald DW, Mogg R, Li D, (...), Robertson MN. Efficacy assessment of a cell-mediated immunity HIV-1 vaccine (the Step Study): a double-blind, randomised, placebo-controlled, test-of-concept trial. *Lancet* 2008, 372:1881-1893.

161. Walker BD, Burton DR. Toward an AIDS vaccine. *Science* 2008, 320:760-764.

162. Rerks-Ngarm S, Pitisuttithum P, Nitayaphan S, Kaewkungwal J, Chiu J, Paris R, (...), Kim JH. Vaccination with ALVAC and AIDSVAX to prevent HIV-1 infection in Thailand. *New Engl. J. Med.* 2009, 361:2209-2220.

163. Haynes BF, Gilbert PB, McElrath MJ, Zolla-Pazner S, Tomaras GD, Alam SM, (...), Kim JH. Immune-correlates analysis of an HIV-1 vaccine efficacy trial. *New Engl. J. Med.* 2012, 366:1275-1286.

164. Gray GE, Laher F, Lazarus E, Ensoli B, Corey L. Approaches to preventative and therapeutic HIV vaccines. *Curr. Opin. Virol.* 2016, 17:104-109.

165. Hammer SM, Sobieszczyk ME, Janes H, Karuna ST, Mulligan MJ, Grove D, (...), Gilbert PB. Efficacy trial of a DNA/rAd5 HIV-1 preventive vaccine. *New Engl. J. Med.* 2013, 369:2083-2092.

166. McMichael A, Picker LJ, Moore JP, Burton DR. Another HIV vaccine failure: where to next? *Nat. Med.* 2013, 19:1576-1577.

167. D'Souza MP, Yang OO. Adenovirus vectors as HIV-1 vaccines: where are we? What next? *AIDS* 2015, 29:395-400.

168. Li Y, Luo L, Thomas DY, Kang CY. The HIV-1 Env protein signal sequence retards its cleavage and down-regulates the glycoprotein folding. *Virology* 2000, 272:417-428.

169. Li Y, Luo L, Thomas DY, Kang CY. Control of expression, glycosylation, and secretion of HIV-1 gp120 by homologous and heterologous signal sequences. *Virology* 1994, 204:266-278.

170. Haffar OK, Dowbenko DJ, Berman PW. Topogenic analysis of the human immunodeficiency virus type 1 envelope glycoprotein, gp160, in microsomal membranes. *J. Cell Biol.* 1988, 107:1677-1687.

171. Checkley MA, Luttge BG, Freed EO. HIV-1 envelope glycoprotein biosynthesis, trafficking, and incorporation. *J. Mol. Biol.* 2011, 410:582-608.

172. Kornfeld R, Kornfeld S. Assembly of asparagine-linked oligosaccharides. *Annu. Rev. Biochem.* 1985, 54:631-664.

173. Ware FE, Vassilakos A, Peterson PA, Jackson MR, Lehrman MA, Williams DB. The molecular chaperone calnexin binds Glc1Man9GlcNAc2 oligosaccharide as an initial step in recognizing unfolded glycoproteins. *J. Biol. Chem.* 1995, 270:4697-4704.

174. Helenius A, Aebi M. Roles of N-linked glycans in the endoplasmic reticulum. *Annu. Rev. Biochem.* 2004, 73:1019-1049.

175. Land A, Zonneveld D, Braakman I. Folding of HIV-1 envelope glycoprotein involves extensive isomerization of disulfide bonds and conformation-dependent leader peptide cleavage. *FASEB J.* 2003, 17:1058-1067.

176. Leonard CK, Spellman MW, Riddle L, Harris RJ, Thomas JN, Gregory TJ. Assignment of intrachain disulfide bonds and characterization of potential glycosylation sites of the type 1 recombinant human immunodeficiency virus envelope glycoprotein (gp120) expressed in Chinese hamster ovary cells. *J. Biol. Chem.* 1990, 265:10373-10382.

177. Pollock S, Dwek RA, Burton DR, Zitzmann N. N-butyldeoxynojirimycin is a broadly effective anti-HIV therapy significantly enhanced by targeted liposome delivery. *AIDS* 2008, 22:1961-1969.

178. Fischer PB, Collin M, Karlsson GB, James W, Butters TD, Davis SJ, (...), Platt FM. The alpha-glucosidase inhibitor N-butyldeoxynojirimycin inhibits human immunodeficiency virus entry at the level of post-CD4 binding. *J. Virol.* 1995, 69:5791-5797.

179. Fischer PB, Karlsson GB, Butters TD, Dwek RA, Platt FM. N-butyldeoxynojirimycin-mediated inhibition of human immunodeficiency virus entry correlates with changes in antibody recognition of the V1/V2 region of gp120. *J. Virol.* 1996, 70:7143-7152.

180. Dwek RA, Butters TD, Platt FM, Zitzmann N. Targeting glycosylation as a therapeutic approach. *Nat. Rev. Drug Discov.* 2002, 1:65-75.

181. Cutalo JM, Deterding LJ, Tomer KB. Characterization of glycopeptides from HIV-I(SF2) gp120 by liquid chromatography mass spectrometry. *J. Am. Soc. Mass Spectrom.* 2004, 15:1545-1555.

182. Bonomelli C, Doores KJ, Dunlop DC, Thaney V, Dwek Ra, Burton DR, (...), Scanlan CN. The glycan shield of HIV is predominantly oligomannose independently of production system or viral clade. *PLoS One* 2011, 6:e23521.

183. Doores KJ, Bonomelli C, Harvey DJ, Vasiljevic S, Dwek RA, Burton DR, (...), Scanlan CN. Envelope glycans of immunodeficiency virions are almost entirely oligomannose antigens. *Proc. Natl. Acad. Sci. USA* 2010, 107:13800-13805.

184. Pritchard LK, Vasiljevic S, Ozorowski G, Seabright GE, Cupo A, Ringe R, (...), Crispin M. Structural constraints determine the glycosylation of HIV-1 envelope trimers. *Cell Rep.* 2015, 11:1604-1613.

185. Rudd PM, Dwek RA. Glycosylation: heterogeneity and the 3D structure of proteins. *Crit. Rev. Biochem. Mol. Biol.* 1997, 32:1-100.

186. Bowden TA, Baruah K, Coles CH, Harvey DJ, Yu X, Song B-D, (...), Crispin M. Chemical and Structural Analysis of an Antibody Folding Intermediate Trapped during Glycan Biosynthesis. *J. Am. Chem. Soc.* 2012, 134:17554-17563.

187. Harvey DJ, Merry AH, Royle L, Campbell MP, Dwek RA, Rudd PM. Proposal for a standard system for drawing structural diagrams of N- and O-linked carbohydrates and related compounds. *Proteomics* 2009, 9:3796-3801.

188. Vliegenthart JFG, Dorland L, Halbeek Hv: High-Resolution, 1H-Nuclear Magnetic Resonance Spectroscopy as a Tool in the Structural Analysis of Carbohydrates Related to Glycoproteins. In *Advances in Carbohydrate Chemistry and Biochemistry*. Edited by Tipson RS, Derek H: Academic Press; 1983:209-374. vol 41.

189. Pinter A, Honnen WJ, Tilley SA, Bona C, Zaghouani H, Gorny MK, Zolla-Pazner S. Oligomeric structure of gp41, the transmembrane protein of human immunodeficiency virus type 1. *J. Virol.* 1989, 63:2674-2679.

190. Earl PL, Doms RW, Moss B. Oligomeric structure of the human immunodeficiency virus type 1 envelope glycoprotein. *Proc. Natl. Acad. Sci. USA* 1990, 87:648-652.

191. Vollenweider F, Benjannet S, Decroly E, Savaria D, Lazure C, Thomas G, (...), Seidah NG. Comparative cellular processing of the human immunodeficiency virus (HIV-1) envelope glycoprotein gp160 by the mammalian subtilisin/kexin-like convertases. *Biochem. J.* 1996, 314 (Pt 2):521-532.

192. Moulard M, Decroly E. Maturation of HIV envelope glycoprotein precursors by cellular endoproteases. *Biochim. Biophys. Acta* 2000, 1469:121-132.

193. Decroly E, Wouters S, Di Bello C, Lazure C, Ruysschaert JM, Seidah NG. Identification of the paired basic convertases implicated in HIV gp160 processing based on in vitro assays and expression in CD4(+) cell lines. *J. Biol. Chem.* 1996, 271:30442-30450.

194. Decroly E, Vandenbranden M, Ruysschaert JM, Cogniaux J, Jacob GS, Howard SC, (...), Seidah NG. The convertases furin and PC1 can both cleave the human immunodeficiency virus (HIV)-1 envelope glycoprotein gp160 into gp120 (HIV-1 SU) and gp41 (HIV-I TM). *J. Biol. Chem.* 1994, 269:12240-12247.

195. Franzusoff A, Volpe AM, Josse D, Pichuantes S, Wolf JR. Biochemical and genetic definition of the cellular protease required for HIV-1 gp160 processing. *J. Biol. Chem.* 1995, 270:3154-3159.

196. Hallenberger S, Bosch V, Angliker H, Shaw E, Klenk HD, Garten W. Inhibition of furin-mediated cleavage activation of HIV-1 glycoprotein gp160. *Nature* 1992, 360:358-361.

197. Thomas G. Furin at the cutting edge: from protein traffic to embryogenesis and disease. *Nat. Rev. Mol. Cell Biol.* 2002, 3:753-766.

198. Bass J, Turck C, Rouard M, Steiner DF. Furin-mediated processing in the early secretory pathway: sequential cleavage and degradation of misfolded insulin receptors. *Proc. Natl. Acad. Sci. USA* 2000, 97:11905-11909.

199. McCune JM, Rabin LB, Feinberg MB, Lieberman M, Kosek JC, Reyes GR, Weissman IL. Endoproteolytic cleavage of gp160 is required for the activation of human immunodeficiency virus. *Cell* 1988, 53:55-67.

200. Ringe RP, Sanders RW, Yasmeen A, Kim HJ, Lee JH, Cupo A, (...), Moore JP. Cleavage strongly influences whether soluble HIV-1 envelope glycoprotein trimers adopt a native-like conformation. *Proc. Natl. Acad. Sci. USA* 2013, 110:18256-18261.

201. Boge M, Wyss S, Bonifacino JS, Thali M. A membrane-proximal tyrosine-based signal mediates internalization of the HIV-1 envelope glycoprotein via interaction with the AP-2 clathrin adaptor. *J. Biol. Chem.* 1998, 273:15773-15778.

202. Yuste E, Reeves JD, Doms RW, Desrosiers RC. Modulation of Env content in virions of simian immunodeficiency virus: correlation with cell surface expression and virion infectivity. *J. Virol.* 2004, 78:6775-6785.

203. Schiller J, Chackerian B. Why HIV virions have low numbers of envelope spikes: implications for vaccine development. *PLoS Pathog.* 2014, 10:e1004254.

204. Klein JS, Bjorkman PJ. Few and far between: how HIV may be evading antibody avidity. *PLoS Pathog.* 2010, 6:e1000908.

205. Sanders RW, Derking R, Cupo A, Julien JP, Yasmeen A, de Val N, (...), Moore JP. A next-generation cleaved, soluble HIV-1 Env trimer, BG505 SOSIP.664 gp140, expresses multiple epitopes for broadly neutralizing but not non-neutralizing antibodies. *PLoS Pathog.* 2013, 9:e1003618.

206. Julien JP, Cupo A, Sok D, Stanfield RL, Lyumkis D, Deller MC, (...), Wilson IA. Crystal structure of a soluble cleaved HIV-1 envelope trimer. *Science* 2013, 342:1477-1483.

207. Lee JH, de Val N, Lyumkis D, Ward AB. Model building and refinement of a natively glycosylated HIV-1 Env protein by high-resolution cryoelectron microscopy. *Structure* 2015, 23:1943-1951.

208. Kwong PD, Wyatt R, Robinson J, Sweet RW, Sodroski J, Hendrickson WA. Structure of an HIV gp120 envelope glycoprotein in complex with the CD4 receptor and a neutralizing human antibody. *Nature* 1998, 393:648-659.

209. Huang CC, Tang M, Zhang MY, Majeed S, Montabana E, Stanfield RL, (...), Kwong PD. Structure of a V3-containing HIV-1 gp120 core. *Science* 2005, 310:1025-1028.

210. Zhou T, Xu L, Dey B, Hessell AJ, Van Ryk D, Xiang SH, (...), Kwong PD. Structural definition of a conserved neutralization epitope on HIV-1 gp120. *Nature* 2007, 445:732-737.

211. Pancera M, Majeed S, Ban YE, Chen L, Huang CC, Kong L, (...), Kwong PD. Structure of HIV-1 gp120 with gp41-interactive region reveals layered envelope architecture and basis of conformational mobility. *Proc. Natl. Acad. Sci. USA* 2010, 107:1166-1171.

212. Zhou T, Georgiev I, Wu X, Yang ZY, Dai K, Finzi A, (...), Kwong PD. Structural basis for broad and potent neutralization of HIV-1 by antibody VRC01. *Science* 2010, 329:811-817.

213. Kwon YD, Finzi A, Wu X, Dogo-Isonagie C, Lee LK, Moore LR, (...), Kwong PD. Unliganded HIV-1 gp120 core structures assume the CD4-bound conformation with regulation by quaternary interactions and variable loops. *Proc. Natl. Acad. Sci. USA* 2012, 109:5663-5668.

214. Ward AB, Wilson IA. Insights into the trimeric HIV-1 envelope glycoprotein structure. *Trends Biochem. Sci.* 2015, 40:101-107.

215. Stewart-Jones GBE, Soto C, Lemmin T, Chuang G-Y, Druz A, Kong R, (...), Kwong Peter D. Trimeric HIV-1-Env Structures Define Glycan Shields from Clades A, B, and G. *Cell* 2016, 165:1-14.

216. Lee JH, Ozorowski G, Ward AB. Cryo-EM structure of a native, fully glycosylated, cleaved HIV-1 envelope trimer. *Science* 2016, 351:1043-1048.

217. Lyumkis D, Julien JP, de Val N, Cupo A, Potter CS, Klasse PJ, (...), Ward AB. Cryo-EM structure of a fully glycosylated soluble cleaved HIV-1 envelope trimer. *Science* 2013, 342:1484-1490.

218. Pancera M, Zhou T, Druz A, Georgiev IS, Soto C, Gorman J, (...), Kwong PD. Structure and immune recognition of trimeric pre-fusion HIV-1 Env. *Nature* 2014, 514:455-461.

219. Wang H, Cohen AA, Galimidi RP, Gristick HB, Jensen GJ, Bjorkman PJ. Cryo-EM structure of a CD4-bound open HIV-1 envelope trimer reveals structural rearrangements of the gp120 V1V2 loop. *Proc. Acad. Nat. Sci. Phila.* 2016, 10.1073/pnas.1615939113.

220. Gristick HB, von Boehmer L, West AP, Jr., Schamber M, Gazumyan A, Golijanin J, (...), Bjorkman PJ. Natively glycosylated HIV-1 Env structure reveals new mode for antibody recognition of the CD4-binding site. *Nat. Struct. Mol. Biol.* 2016, 23:906-915.

221. Brandenberg OF, Magnus C, Regoes RR, Trkola A. The HIV-1 Entry Process: A Stoichiometric View. *Trends Microbiol.* 2015, 23:763-774.

222. Myszka DG, Sweet RW, Hensley P, Brigham-Burke M, Kwong PD, Hendrickson WA, (...), Doyle ML. Energetics of the HIV gp120-CD4 binding reaction. *Proc. Natl. Acad. Sci. USA* 2000, 97:9026-9031.

223. Kwong PD, Doyle ML, Casper DJ, Cicala C, Leavitt SA, Majeed S, (...), Arthos J. HIV-1 evades antibody-mediated neutralization through conformational masking of receptor-binding sites. *Nature* 2002, 420:678-682.

224. Hwang SS, Boyle TJ, Lyerly HK, Cullen BR. Identification of the envelope V3 loop as the primary determinant of cell tropism in HIV-1. *Science* 1991, 253:71-74.

225. Doms RW, Moore JP. HIV-1 membrane fusion: targets of opportunity. *J. Cell Biol.* 2000, 151:F9-14.

226. Binley JM, Sanders RW, Clas B, Schuelke N, Master A, Guo Y, (...), Moore JP. A recombinant human immunodeficiency virus type 1 envelope glycoprotein complex stabilized by an intermolecular disulfide bond between the gp120 and gp41 subunits is an antigenic mimic of the trimeric virion-associated structure. *J. Virol.* 2000, 74:627-643.

227. Sanders RW, Vesanen M, Schuelke N, Master A, Schiffner L, Kalyanaraman R, (...), Moore JP. Stabilization of the soluble, cleaved, trimeric form of the envelope glycoprotein complex of human immunodeficiency virus type 1. *J. Virol.* 2002, 76:8875-8889.

228. Khayat R, Lee JH, Julien J-P, Cupo A, Klasse PJ, Sanders RW, (...), Ward AB. Structural characterization of cleaved, soluble HIV-1 envelope glycoprotein trimers. *J. Virol.* 2013, 87:9865-9872.

229. Kwon YD, Pancera M, Acharya P, Georgiev IS, Crooks ET, Gorman J, (...), Kwong PD. Crystal structure, conformational fixation and entry-related interactions of mature ligand-free HIV-1 Env. *Nat. Struct. Mol. Biol.* 2015, 22:522-531.

230. Korber B, Gaschen B, Yusim K, Thakallapally R, Kesmir C, Detours V. Evolutionary and immunological implications of contemporary HIV-1 variation. *Br. Med. Bull.* 2001, 58:19-42.

231. Zhu X, Borchers C, Bienstock RJ, Tomer KB. Mass spectrometric characterization of the glycosylation pattern of HIV-gp120 expressed in CHO cells. *Biochemistry* 2000, 39:11194-11204.

232. Go EP, Liao H-X, Alam SM, Hua D, Haynes BF, Desaire H. Characterization of host-cell line specific glycosylation profiles of early transmitted/founder HIV-1 gp120 envelope proteins. *J. Proteome Res.* 2013, 12:1223-1234.

233. Alexandre KB, Gray ES, Lambson BE, Moore PL, Choge IA, Mlisana K, (...), Morris L. Mannose-rich glycosylation patterns on HIV-1 subtype C gp120 and sensitivity to the lectins, Griffithsin, Cyanovirin-N and Scytovirin. *Virology* 2010, 402:187-196.

234. Coss KP, Vasiljevic S, Pritchard LK, Krumm SA, Glaze M, Madzorera S, (...), Doores KJ. HIV-1 glycan density drives the persistence of the mannose patch within an infected individual. *J. Virol.* 2016, 90:11132-11144.

235. Go EP, Herschhorn A, Gu C, Castillo-Menendez L, Zhang S, Mao Y, (...), Desaire H. Comparative analysis of the glycosylation profiles of membrane-anchored HIV-1 envelope glycoprotein trimers and soluble gp140. *J. Virol.* 2015, 89:8245-8257.

236. Panico M, Bouche L, Binet D, O'Connor MJ, Rahman D, Pang PC, (...), Morris HR. Mapping the complete glycoproteome of virion-derived HIV-1 gp120 provides insights into broadly neutralizing antibody binding. *Sci. Rep.* 2016, 6:32956.

237. Crispin M, Doores KJ. Targeting host-derived glycans on enveloped viruses for antibody-based vaccine design. *Curr. Opin. Virol.* 2015, 11:63-69.

238. Ringe RP, Yasmeen A, Ozorowski G, Go EP, Pritchard LK, Guttman M, (...), Moore JP. Influences on the design and purification of soluble, recombinant native-like HIV-1 envelope glycoprotein trimers. *J. Virol.* 2015, 89:12189-12210.

239. Crocker PR, Paulson JC, Varki A. Siglecs and their roles in the immune system. *Nat. Rev. Immunol.* 2007, 7:255-266.

240. Anthony RM, Nimmerjahn F, Ashline DJ, Reinhold VN, Paulson JC, Ravetch JV. Recapitulation of IVIG anti-inflammatory activity with a recombinant IgG Fc. *Science* 2008, 320:373-376.

241. Pritchard LK, Harvey DJ, Bonomelli C, Crispin M, Doores KJ. Cell- and protein-directed glycosylation of native cleaved HIV-1 envelope. *J. Virol.* 2015, 89:8932-8944.

242. Stoiber H, Schneider R, Janatova J, Dierich MP. Human complement proteins C3b, C4b, factor H and properdin react with specific sites in gp120 and gp41, the envelope proteins of HIV-1. *Immunobiology* 1995, 193:98-113.

243. Ferreira VP, Pangburn MK, Cortes C. Complement control protein factor H: the good, the bad, and the inadequate. *Mol. Immunol.* 2010, 47:2187-2197.

244. Hirsch RL, Wolinsky JS, Winkelstein JA. Activation of the alternative complement pathway by mumps infected cells: relationship to viral neuraminidase activity. *Arch. Virol.* 1986, 87:181-190.

245. Fearon DT. Regulation by membrane sialic acid of beta1H-dependent decay-dissociation of amplification C3 convertase of the alternative complement pathway. *Proc. Natl. Acad. Sci. USA* 1978, 75:1971-1975.

246. Zou Z, Chastain A, Moir S, Ford J, Trandem K, Martinelli E, (...), Sun PD. Siglecs facilitate HIV-1 infection of macrophages through adhesion with viral sialic acids. *PLoS One* 2011, 6:e24559.

247. Hansen JE, Jansson B, Gram GJ, Clausen H, Nielsen JO, Olofsson S. Sensitivity of HIV-1 to neutralization by antibodies against O-linked carbohydrate epitopes despite deletion of O-glycosylation signals in the V3 loop. *Arch. Virol.* 1996, 141:291-300.

248. Go EP, Hua D, Desaire H. Glycosylation and disulfide bond analysis of transiently and stably expressed clade C HIV-1 gp140 trimers in 293T cells identifies disulfide heterogeneity present in both proteins and differences in O-linked glycosylation. *J. Proteome Res.* 2014, 13:4012-4027.

249. Stansell E, Panico M, Canis K, Pang PC, Bouche L, Binet D, (...), Dell A. Gp120 on HIV-1 virions lacks O-linked carbohydrate. *PLoS One* 2015, 10:e0124784.

250. Yang W, Shah P, Toghi Eshghi S, Yang S, Sun S, Ao M, (...), Zhang H. Glycoform analysis of recombinant and human immunodeficiency virus envelope protein gp120 via higher energy collisional dissociation and spectral-aligning strategy. *Anal. Chem.* 2014, 86:6959-6967.

251. Go EP, Chang Q, Liao H-X, Sutherland LL, Alam SM, Haynes BF, Desaire H. Glycosylation site-specific analysis of clade C HIV-1 envelope proteins. *J. Proteome Res.* 2009, 8:4231-4242.

252. Go EP, Hewawasam G, Liao H-X, Chen H, Ping L-H, Anderson JA, (...), Desaire H. Characterization of glycosylation profiles of HIV-1 transmitted/founder envelopes by mass spectrometry. *J. Virol.* 2011, 85:8270-8284.

253. Go EP, Irungu J, Zhang Y, Dalpathado DS, Liao H-X, Sutherland LL, (...), Desaire H. Glycosylation site-specific analysis of HIV envelope proteins (JR-FL and CON-S) reveals major differences in glycosylation site occupancy, glycoform profiles, and antigenic epitopes' accessibility. *J. Proteome Res.* 2008, 7:1660-1674.

254. Irungu J, Go EP, Zhang Y, Dalpathado DS, Liao H-X, Haynes BF, Desaire H. Comparison of HPLC/ESI-FTICR MS versus MALDI-TOF/TOF MS for glycopeptide analysis of a highly glycosylated HIV envelope glycoprotein. *J. Am. Soc. Mass Spectrom.* 2008, 19:1209-1220.

255. Pabst M, Chang M, Stadlmann J, Altmann F. Glycan profiles of the 27 N-glycosylation sites of the HIV envelope protein CN54gp140. *Biol. Chem.* 2012, 393:719-730.

256. Guttman M, Garcia NK, Cupo A, Matsui T, Julien JP, Sanders RW, (...), Lee KK. CD4-induced activation in a soluble HIV-1 Env trimer. *Structure* 2014, 22:974-984.

257. Zhang M, Gaschen B, Blay W, Foley B, Haigwood N, Kuiken C, Korber B. Tracking global patterns of N-linked glycosylation site variation in highly variable viral glycoproteins: HIV, SIV, and HCV envelopes and influenza hemagglutinin. *Glycobiology* 2004, 14:1229-1246.

258. Kong L, Stanfield RL, Wilson IA: Molecular recognition of HIV glycans by antibodies. In *HIV glycans in infection and immunity*. Edited by Pantophlet R; 2014. vol 1.

259. Moore PL, Gray ES, Wibmer CK, Bhiman JN, Nonyane M, Sheward DJ, (...), Morris L. Evolution of an HIV glycan-dependent broadly neutralizing antibody epitope through immune escape. *Nat. Med.* 2012, 18:1688-1692.

260. Pritchard LK, Spencer DI, Royle L, Bonomelli C, Seabright GE, Behrens AJ, (...), Crispin M. Glycan clustering stabilizes the mannose patch of HIV-1 and preserves vulnerability to broadly neutralizing antibodies. *Nat. Commun.* 2015, 6:7479.

261. Sok D, Doores KJ, Briney B, Le KM, Saye-Francisco KL, Ramos A, (...), Burton DR. Promiscuous glycan site recognition by antibodies to the high-mannose patch of gp120 broadens neutralization of HIV. *Sci. Transl. Med.* 2014, 6:236ra263.

262. Doyle-Cooper C, Hudson KE, Cooper AB, Ota T, Skog P, Dawson PE, (...), Nemazee D. Immune tolerance negatively regulates B cells in knock-in mice expressing broadly neutralizing HIV antibody 4E10. *J. Immunol.* 2013, 191:3186-3191.

263. Crispin M, Bowden TA. Antibodies expose multiple weaknesses in the glycan shield of HIV. *Nat. Struct. Mol. Biol.* 2013, 20:771-772.

264. Mikell I, Sather DN, Kalams SA, Altfeld M, Alter G, Stamatatos L. Characteristics of the earliest cross-neutralizing antibody response to HIV-1. *PLoS Pathog.* 2011, 7:e1001251.

265. Doria-Rose NA, Klein RM, Daniels MG, O'Dell S, Nason M, Lapedes A, (...), Connors M. Breadth of human immunodeficiency virus-specific neutralizing activity in sera: clustering analysis and association with clinical variables. *J. Virol.* 2010, 84:1631-1636.

266. Sather DN, Armann J, Ching LK, Mavrantoni A, Sellhorn G, Caldwell Z, (...), Stamatatos L. Factors associated with the development of cross-reactive neutralizing antibodies during human immunodeficiency virus type 1 infection. *J. Virol.* 2009, 83:757-769.

267. Euler Z, van Gils MJ, Bunnik EM, Phung P, Schweighardt B, Wrin T, Schuitemaker H. Cross-reactive neutralizing humoral immunity does not protect from HIV type 1 disease progression. *J. Infect. Dis.* 2010, 201:1045-1053.

268. bNAber on Web page URL: www.bnaber.org. accessed on 15/03/2016.

269. Haynes BF. New approaches to HIV vaccine development. *Curr. Opin. Immunol.* 2015, 35:39-47.

270. Burton DR, Mascola JR. Antibody responses to envelope glycoproteins in HIV-1 infection. *Nat. Immunol.* 2015, 16:571-576.

271. Trkola A, Purtscher M, Muster T, Ballaun C, Buchacher A, Sullivan N, (...), Katinger H. Human monoclonal antibody 2G12 defines a distinctive neutralization epitope on the gp120 glycoprotein of human immunodeficiency virus type 1. *J. Virol.* 1996, 70:1100-1108.

272. Murin CD, Julien J-P, Sok D, Stanfield RL, Khayat R, Cupo A, (...), Ward AB. Structure of 2G12 Fab2 in complex with soluble and fully glycosylated HIV-1 Env by negative-stain single-particle electron microscopy. *J. Virol.* 2014, 88:10177-10188.

273. Doores KJ. The HIV glycan shield as a target for broadly neutralizing antibodies. *FEBS J.* 2015, 282:4679-4691.

274. Julien J-P, Lee JH, Cupo A, Murin CD, Derking R, Hoffenberg S, (...), Ward AB. Asymmetric recognition of the HIV-1 trimer by broadly neutralizing antibody PG9. *Proc. Natl. Acad. Sci. USA* 2013, 110:4351-4356.

275. Klasse PJ, LaBranche CC, Ketas TJ, Ozorowski G, Cupo A, Pugach P, (...), Moore JP. Sequential and Simultaneous Immunization of Rabbits with HIV-1 Envelope Glycoprotein SOSIP.664 Trimers from Clades A, B and C. *PLoS Pathog.* 2016, 12:e1005864.

276. McCoy LE, van Gils MJ, Ozorowski G, Messmer T, Briney B, Voss JE, (...), Burton DR. Holes in the Glycan Shield of the Native HIV Envelope Are a Target of Trimer-Elicited Neutralizing Antibodies. *Cell Rep.* 2016, 16:1-12.

277. Yu L, Guan Y. Immunologic Basis for Long HCDR3s in Broadly Neutralizing Antibodies Against HIV-1. *Front. Immunol.* 2014, 5:250.

278. Wang F, Ekiert DC, Ahmad I, Yu W, Zhang Y, Bazirgan O, (...), Smider VV. Reshaping antibody diversity. *Cell* 2013, 153:1379-1393.

279. Pejchal R, Walker LM, Stanfield RL, Phogat SK, Koff WC, Poignard P, (...), Wilson IA. Structure and function of broadly reactive antibody PG16 reveal an H3 subdomain that mediates potent neutralization of HIV-1. *Proc. Natl. Acad. Sci. USA* 2010, 107:11483-11488.

280. West AP, Jr., Scharf L, Scheid JF, Klein F, Bjorkman PJ, Nussenzweig MC. Structural insights on the role of antibodies in HIV-1 vaccine and therapy. *Cell* 2014, 156:633-648.

281. Sok D, van Gils MJ, Pauthner M, Julien JP, Saye-Francisco KL, Hsueh J, (...), Burton DR. Recombinant HIV envelope trimer selects for quaternary-dependent antibodies targeting the trimer apex. *Proc. Natl. Acad. Sci. USA* 2014, 111:17624-17629.

282. Ofek G, McKee K, Yang Y, Yang ZY, Skinner J, Guenaga FJ, (...), Kwong PD. Relationship between antibody 2F5 neutralization of HIV-1 and hydrophobicity of its heavy chain third complementarity-determining region. *J. Virol.* 2010, 84:2955-2962.

283. Briney BS, Willis JR, Crowe JE, Jr. Human peripheral blood antibodies with long HCDR3s are established primarily at original recombination using a limited subset of germline genes. *PLoS One* 2012, 7:e36750.

284. Willis JR, Finn JA, Briney B, Sapparapu G, Singh V, King H, (...), Crowe JE, Jr. Long antibody HCDR3s from HIV-naive donors presented on a PG9 neutralizing antibody background mediate HIV neutralization. *Proc. Natl. Acad. Sci. USA* 2016, 113:6.

285. Pancera M, McLellan JS, Wu X, Zhu J, Changela A, Schmidt SD, (...), Kwong PD. Crystal structure of PG16 and chimeric dissection with somatically related PG9: structure-function analysis of two quaternary-specific antibodies that effectively neutralize HIV-1. *J. Virol.* 2010, 84:8098-8110.

286. Haynes BF, Moody MA, Verkoczy L, Kelsoe G, Alam SM. Antibody polyspecificity and neutralization of HIV-1: a hypothesis. *Hum. Antibodies* 2005, 14:59-67.

287. Mouquet H, Scheid JF, Zoller MJ, Krogsgaard M, Ott RG, Shukair S, (...), Nussenzweig MC. Polyreactivity increases the apparent affinity of anti-HIV antibodies by heteroligation. *Nature* 2010, 467:591-595.

288. Liu M, Yang G, Wiehe K, Nicely NI, Vandergrift NA, Rountree W, (...), Kelsoe G. Polyreactivity and autoreactivity among HIV-1 antibodies. *J. Virol.* 2015, 89:784-798.

289. Wardemann H, Yurasov S, Schaefer A, Young JW, Meffre E, Nussenzweig MC. Predominant autoantibody production by early human B cell precursors. *Science* 2003, 301:1374-1377.

290. Tsuiji M, Yurasov S, Velinzon K, Thomas S, Nussenzweig MC, Wardemann H. A checkpoint for autoreactivity in human IgM+ memory B cell development. *J. Exp. Med.* 2006, 203:393-400.

291. Tiller T, Tsuiji M, Yurasov S, Velinzon K, Nussenzweig MC, Wardemann H. Autoreactivity in human IgG+ memory B cells. *Immunity* 2007, 26:205-213.

292. Mouquet H, Nussenzweig MC. Polyreactive antibodies in adaptive immune responses to viruses. *Cell. Mol. Life Sci.* 2012, 69:1435-1445.

293. Dunlop DC, Ulrich A, Appelmelk BJ, Burton DR, Dwek RA, Zitzmann N, Scanlan CN. Antigenic mimicry of the HIV envelope by AIDS-associated pathogens. *AIDS* 2008, 22:2214-2217.

294. Yang G, Holl TM, Liu Y, Li Y, Lu X, Nicely NI, (...), Kelsoe G. Identification of autoantigens recognized by the 2F5 and 4E10 broadly neutralizing HIV-1 antibodies. *J. Exp. Med.* 2013, 210:241-256.

295. Chen Y, Zhang J, Hwang KK, Bouton-Verville H, Xia SM, Newman A, (...), Verkoczy L. Common tolerance mechanisms, but distinct cross-reactivities associated with gp41 and lipids, limit production of HIV-1 broad neutralizing antibodies 2F5 and 4E10. *J. Immunol.* 2013, 191:1260-1275.

296. Verkoczy L, Chen Y, Bouton-Verville H, Zhang J, Diaz M, Hutchinson J, (...), Haynes BF. Rescue of HIV-1 broad neutralizing antibody-expressing B cells in 2F5 VH x VL knockin mice reveals multiple tolerance controls. *J. Immunol.* 2011, 187:3785-3797.

297. Verkoczy L, Diaz M, Holl TM, Ouyang YB, Bouton-Verville H, Alam SM, (...), Haynes BF. Autoreactivity in an HIV-1 broadly reactive neutralizing antibody variable region heavy chain induces immunologic tolerance. *Proc. Natl. Acad. Sci. USA* 2010, 107:181-186.

298. Haynes BF, Kelsoe G, Harrison SC, Kepler TB. B-cell-lineage immunogen design in vaccine development with HIV-1 as a case study. *Nat. Biotechnol.* 2012, 30:423-433.

299. Scheid JF, Mouquet H, Ueberheide B, Diskin R, Klein F, Oliveira TYK, (...), Nussenzweig MC. Sequence and structural convergence of broad and potent HIV antibodies that mimic CD4 binding. *Science* 2011, 333:1633-1637.

300. Wu X, Zhou T, Zhu J, Zhang B, Georgiev I, Wang C, (...), Mascola JR. Focused evolution of HIV-1 neutralizing antibodies revealed by structures and deep sequencing. *Science* 2011, 333:1593-1602.

301. Xiao X, Chen W, Feng Y, Dimitrov DS. Maturation Pathways of Cross-Reactive HIV-1 Neutralizing Antibodies. *Viruses* 2009, 1:802-817.

302. Klein F, Diskin R, Scheid JF, Gaebler C, Mouquet H, Georgiev IS, (...), Nussenzweig MC. Somatic mutations of the immunoglobulin framework are generally required for broad and potent HIV-1 neutralization. *Cell* 2013, 153:126-138.

303. Sok D, Laserson U, Laserson J, Liu Y, Vigneault F, Julien JP, (...), Poignard P. The effects of somatic hypermutation on neutralization and binding in the PGT121 family of broadly neutralizing HIV antibodies. *PLoS Pathog.* 2013, 9:e1003754.

304. Georgiev IS, Rudicell RS, Saunders KO, Shi W, Kirys T, McKee K, (...), Kwong PD. Antibodies VRC01 and 10E8 neutralize HIV-1 with high breadth and potency even with Ig-framework regions substantially reverted to germline. *J. Immunol.* 2014, 192:1100-1106.

305. Sadanand S, Suscovich TJ, Alter G. Broadly Neutralizing Antibodies Against HIV: New Insights to Inform Vaccine Design. *Annu. Rev. Med.* 2015, 67:185-200.

306. MacLennan IC, Toellner KM, Cunningham AF, Serre K, Sze DM, Zuniga E, (...), Vinuesa CG. Extrafollicular antibody responses. *Immunol. Rev.* 2003, 194:8-18.

307. Muramatsu M, Kinoshita K, Fagarasan S, Yamada S, Shinkai Y, Honjo T. Class switch recombination and hypermutation require activation-induced cytidine deaminase (AID), a potential RNA editing enzyme. *Cell* 2000, 102:553-563.

308. Montezuma-Rusca JM, Moir S, Kardava L, Buckner CM, Louie A, Kim LJ, (...), Fauci AS. Bone marrow plasma cells are a primary source of serum HIV-1-specific antibodies in chronically infected individuals. *J. Immunol.* 2015, 194:2561-2568.

309. Aasa-Chapman MM, Hayman A, Newton P, Cornforth D, Williams I, Borrow P, (...), McKnight A. Development of the antibody response in acute HIV-1 infection. *AIDS* 2004, 18:371-381.

310. Gray ES, Moore PL, Choge IA, Decker JM, Bibollet-Ruche F, Li H, (...), Morris L. Neutralizing antibody responses in acute human immunodeficiency virus type 1 subtype C infection. *J. Virol.* 2007, 81:6187-6196.

311. Gray ES, Madiga MC, Hermanus T, Moore PL, Wibmer CK, Tumba NL, (...), Morris L. The neutralization breadth of HIV-1 develops incrementally over four years and is associated with CD4+ T cell decline and high viral load during acute infection. *J. Virol.* 2011, 85:4828-4840.

312. Piantadosi A, Panteleeff D, Blish CA, Baeten JM, Jaoko W, McClelland RS, Overbaugh J. Breadth of neutralizing antibody response to human immunodeficiency virus type 1 is affected by factors early in infection but does not influence disease progression. *J. Virol.* 2009, 83:10269-10274.

313. Doria-Rose NA, Schramm CA, Gorman J, Moore PL, Bhiman JN, DeKosky BJ, (...), Mascola JR. Developmental pathway for potent V1V2-directed HIV-neutralizing antibodies. *Nature* 2014, 509:55-62.

314. Liao HX, Lynch R, Zhou T, Gao F, Alam SM, Boyd SD, (...), Haynes BF. Co-evolution of a broadly neutralizing HIV-1 antibody and founder virus. *Nature* 2013, 496:469-476.

315. MacLeod DT, Choi NM, Briney B, Garces F, Ver LS, Landais E, (...), Poignard P. Early Antibody Lineage Diversification and Independent Limb Maturation Lead to Broad HIV-1 Neutralization Targeting the Env High-Mannose Patch. *Immunity* 2016, 44:1215-1226.

316. Mascola JR, Haynes BF. HIV-1 neutralizing antibodies: understanding nature's pathways. *Immunol. Rev.* 2013, 254:225-244.

317. Wu X, Zhang Z, Schramm CA, Joyce MG, Kwon YD, Zhou T, (...), Shapiro L. Maturation and Diversity of the VRC01-Antibody Lineage over 15 Years of Chronic HIV-1 Infection. *Cell* 2015, 161:470-485.

318. Li Y, O'Dell S, Walker LM, Wu X, Guenaga J, Feng Y, (...), Mascola JR. Mechanism of neutralization by the broadly neutralizing HIV-1 monoclonal antibody VRC01. *J. Virol.* 2011, 85:8954-8967.

319. Chen J, Frey G, Peng H, Rits-Volloch S, Garrity J, Seaman MS, Chen B. Mechanism of HIV-1 neutralization by antibodies targeting a membrane-proximal region of gp41. *J. Virol.* 2014, 88:1249-1258.

320. Halper-Stromberg A, Nussenzweig MC. Towards HIV-1 remission: potential roles for broadly neutralizing antibodies. *J. Clin. Invest.* 2016, 162:415-423.

321. Mouquet H. Antibody B cell responses in HIV-1 infection. *Trends Immunol.* 2014, 35:549-561.

322. Martin N, Welsch S, Jolly C, Briggs JA, Vaux D, Sattentau QJ. Virological synapse-mediated spread of human immunodeficiency virus type 1 between T cells is sensitive to entry inhibition. *J. Virol.* 2010, 84:3516-3527.

323. Malbec M, Porrot F, Rua R, Horwitz J, Klein F, Halper-Stromberg A, (...), Schwartz O. Broadly neutralizing antibodies that inhibit HIV-1 cell to cell transmission. *J. Exp. Med.* 2013, 210:2813-2821.

324. Su B, Xu K, Lederle A, Peressin M, Biedma ME, Laumond G, (...), Moog C. Neutralizing antibodies inhibit HIV-1 transfer from primary dendritic cells to autologous CD4 T lymphocytes. *Blood* 2012, 120:3708-3717.

325. Duncan CJ, Williams JP, Schiffner T, Gartner K, Ochsenbauer C, Kappes J, (...), Sattentau QJ. High-multiplicity HIV-1 infection and neutralizing antibody evasion mediated by the macrophage-T cell virological synapse. *J. Virol.* 2014, 88:2025-2034.

326. Euler Z, Alter G. Exploring the potential of monoclonal antibody therapeutics for HIV-1 eradication. *AIDS Res. Hum. Retroviruses* 2015, 31:13-24.

327. Barouch DH, Whitney JB, Moldt B, Klein F, Oliveira TY, Liu J, (...), Burton DR. Therapeutic efficacy of potent neutralizing HIV-1-specific monoclonal antibodies in SHIV-infected rhesus monkeys. *Nature* 2013, 503:224-228.

328. Shingai M, Nishimura Y, Klein F, Mouquet H, Donau OK, Plishka R, (...), Martin MA. Antibody-mediated immunotherapy of macaques chronically infected with SHIV suppresses viraemia. *Nature* 2013, 503:277-280.

329. Caskey M, Klein F, Lorenzi JC, Seaman MS, West AP, Jr., Buckley N, (...), Nussenzweig MC. Viraemia suppressed in HIV-1-infected humans by broadly neutralizing antibody 3BNC117. *Nature* 2015, 522:487-491.

330. Deeks SG. HIV: Shock and kill. *Nature* 2012, 487:439-440.

331. Moldt B, Shibata-Koyama M, Rakasz EG, Schultz N, Kanda Y, Dunlop DC, (...), Burton DR. A nonfucosylated variant of the anti-HIV-1 monoclonal antibody b12 has enhanced FcgammaRIIIa-mediated antiviral activity in vitro but does not improve protection against mucosal SHIV challenge in macaques. *J. Virol.* 2012, 86:6189-6196.

332. Sievers SA, Scharf L, West AP, Jr., Bjorkman PJ. Antibody engineering for increased potency, breadth and half-life. *Curr. Opin. HIV AIDS* 2015, 10:151-159.

333. Diskin R, Scheid JF, Marcovecchio PM, West AP, Jr., Klein F, Gao H, (...), Bjorkman PJ. Increasing the potency and breadth of an HIV antibody by using structure-based rational design. *Science* 2011, 334:1289-1293.

334. Asokan M, Rudicell RS, Louder M, McKee K, O'Dell S, Stewart-Jones G, (...), Mascola JR. Bispecific Antibodies Targeting Different Epitopes on the HIV-1 Envelope Exhibit Broad and Potent Neutralization. *J. Virol.* 2015, 89:12501-12512.

335. McMichael AJ, Koff WC. Vaccines that stimulate T cell immunity to HIV-1: the next step. *Nat. Immunol.* 2014, 15:319-322.

336. Scanlan CN, Offer J, Zitzmann N, Dwek RA. Exploiting the defensive sugars of HIV-1 for drug and vaccine design. *Nature* 2007, 446:1038-1045.

337. Mann JK, Ndung'u T. HIV-1 vaccine immunogen design strategies. *Virol. J.* 2015, 12:1-11.

338. Burton DR. Antibodies, viruses and vaccines. *Nat. Rev. Immunol.* 2002, 2:706-713.

339. Kulp DW, Schief WR. Advances in structure-based vaccine design. *Curr. Opin. Virol.* 2013, 3:322-331.

340. Javaherian K, Langlois AJ, LaRosa GJ, Profy AT, Bolognesi DP, Herlihy WC, (...), Matthews TJ. Broadly neutralizing antibodies elicited by the hypervariable neutralizing determinant of HIV-1. *Science* 1990, 250:1590-1593.

341. Sliepen K, Sanders RW. HIV-1 envelope glycoprotein immunogens to induce broadly neutralizing antibodies. *Expert Rev. Vaccines* 2015, 15:349-365.

342. Dennison SM, Sutherland LL, Jaeger FH, Anasti KM, Parks R, Stewart S, (...), Haynes BF. Induction of antibodies in rhesus macaques that recognize a fusion-intermediate conformation of HIV-1 gp41. *PLoS One* 2011, 6:e27824.

343. Zwick MB. The membrane-proximal external region of HIV-1 gp41: a vaccine target worth exploring. *AIDS* 2005, 19:1725-1737.

344. Hart MK, Palker TJ, Matthews TJ, Langlois AJ, Lerche NW, Martin ME, (...), Haynes BF. Synthetic peptides containing T and B cell epitopes from human immunodeficiency virus envelope gp120 induce anti-HIV proliferative responses and high titers of neutralizing antibodies in rhesus monkeys. *J. Immunol.* 1990, 145:2677-2685.

345. Zhou T, Zhu J, Yang Y, Gorman J, Ofek G, Srivatsan S, (...), Kwong PD. Transplanting supersites of HIV-1 vulnerability. *PLoS One* 2014, 9:e99881.

346. Ofek G, Guenaga FJ, Schief WR, Skinner J, Baker D, Wyatt R, Kwong PD. Elicitation of structure-specific antibodies by epitope scaffolds. *Proc. Natl. Acad. Sci. USA* 2010, 107:17880-17887.

347. Totrov M, Jiang X, Kong XP, Cohen S, Krachmarov C, Salomon A, (...), Zolla-Pazner S. Structure-guided design and immunological characterization of immunogens presenting the HIV-1 gp120 V3 loop on a CTB scaffold. *Virology* 2010, 405:513-523.

348. Stanfield RL, Julien JP, Pejchal R, Gach JS, Zwick MB, Wilson IA. Structure-based design of a protein immunogen that displays an HIV-1 gp41 neutralizing epitope. *J. Mol. Biol.* 2011, 414:460-476.

349. Chakraborty K, Durani V, Miranda ER, Citron M, Liang X, Schleif W, (...), Varadarajan R. Design of immunogens that present the crown of the HIV-1 V3 loop in a conformation competent to generate 447-52D-like antibodies. *Biochem. J.* 2006, 399:483-491.

350. Joyce MG, Kanekiyo M, Xu L, Biertumpfel C, Boyington JC, Moquin S, (...), Nabel GJ. Outer domain of HIV-1 gp120: antigenic optimization, structural malleability, and crystal structure with antibody VRC-PG04. *J. Virol.* 2013, 87:2294-2306.

351. Bhattacharyya S, Rajan RE, Swarupa Y, Rathore U, Verma A, Udaykumar R, Varadarajan R. Design of a non-glycosylated outer domain-derived HIV-1 gp120 immunogen that binds to CD4 and induces neutralizing antibodies. *J. Biol. Chem.* 2010, 285:27100-27110.

352. Qin Y, Banasik M, Kim S, Penn-Nicholson A, Habte HH, LaBranche C, (...), Cho MW. Eliciting neutralizing antibodies with gp120 outer domain constructs based on M-group consensus sequence. *Virology* 2014, 462-463:363-376.

353. Dosenovic P, von Boehmer L, Escolano A, Jardine J, Freund NT, Gitlin AD, (...), Nussenzweig MC. Immunization for HIV-1 Broadly Neutralizing Antibodies in Human Ig Knockin Mice. *Cell* 2015, 161:1505-1515.

354. Jardine J, Julien JP, Menis S, Ota T, Kalyuzhniy O, McGuire A, (...), Schief WR. Rational HIV immunogen design to target specific germline B cell receptors. *Science* 2013, 340:711-716.

355. Jardine JG, Ota T, Sok D, Pauthner M, Kulp DW, Kalyuzhniy O, (...), Nemazee D. Priming a broadly neutralizing antibody response to HIV-1 using a germline-targeting immunogen. *Science* 2015, 349:156-161.

356. Wu X, Yang Z-Y, Li Y, Hogerkorp C-M, Schief WR, Seaman MS, (...), Mascola JR. Rational design of envelope identifies broadly neutralizing human monoclonal antibodies to HIV-1. *Science* 2010, 329:856-861.

357. Ingale J, Tran K, Kong L, Dey B, McKee K, Schief W, (...), Wyatt RT. Hyperglycosylated stable core immunogens designed to present the CD4 binding site are preferentially recognized by broadly neutralizing antibodies. *J. Virol.* 2014, 88:14002-14016.

358. Dey B, Pancera M, Svehla K, Shu Y, Xiang SH, Vainshtein J, (...), Wyatt R. Characterization of human immunodeficiency virus type 1 monomeric and trimeric gp120 glycoproteins stabilized in the CD4-bound state: antigenicity, biophysics, and immunogenicity. *J. Virol.* 2007, 81:5579-5593.

359. Sanders RW, van Gils MJ, Derking R, Sok D, Ketas TJ, Burger JA, (...), Moore JP. HIV-1 neutralizing antibodies induced by native-like envelope trimers. *Science* 2015, 349:154-166.

360. Yasmeen A, Ringe R, Derking R, Cupo A, Julien JP, Burton DR, (...), Klasse PJ. Differential binding of neutralizing and non-neutralizing antibodies to native-like soluble HIV-1 Env trimers, uncleaved Env proteins, and monomeric subunits. *Retrovirology* 2014, 11:41.

361. Kovacs JM, Nkolola JP, Peng H, Cheung A, Perry J, Miller CA, (...), Chen B. HIV-1 envelope trimer elicits more potent neutralizing antibody responses than monomeric gp120. *Proc. Natl. Acad. Sci. USA* 2012, 109:12111-12116.

362. Pantophlet R, Wilson IA, Burton DR. Hyperglycosylated mutants of human immunodeficiency virus (HIV) type 1 monomeric gp120 as novel antigens for HIV vaccine design. *J. Virol.* 2003, 77:5889-5901.

363. Forsell MN, Schief WR, Wyatt RT. Immunogenicity of HIV-1 envelope glycoprotein oligomers. *Curr. Opin. HIV AIDS* 2009, 4:380-387.

364. Kovacs JM, Noeldeke E, Ha HJ, Peng H, Rits-Volloch S, Harrison SC, Chen B. Stable, uncleaved HIV-1 envelope glycoprotein gp140 forms a tightly folded trimer with a native-like structure. *Proc. Natl. Acad. Sci. USA* 2014, 111:18542-18547.

365. Yang X, Lee J, Mahony EM, Kwong PD, Wyatt R, Sodroski J. Highly stable trimers formed by human immunodeficiency virus type 1 envelope glycoproteins fused with the trimeric motif of T4 bacteriophage fibritin. *J. Virol.* 2002, 76:4634-4642.

366. Sharma SK, de Val N, Bale S, Guenaga J, Tran K, Feng Y, (...), Wyatt RT. Cleavage-Independent HIV-1 Env Trimers Engineered as Soluble Native Spike Mimetics for Vaccine Design. *Cell Rep.* 2015, 11:539-550.

367. Zhao L, Seth A, Wibowo N, Zhao CX, Mitter N, Yu C, Middelberg AP. Nanoparticle vaccines. *Vaccine* 2014, 32:327-337.

368. Sliepen K, Ozorowski G, Burger JA, van Montfort T, Stunnenberg M, LaBranche C, (...), Sanders RW. Presenting native-like HIV-1 envelope trimers on ferritin nanoparticles improves their immunogenicity. *Retrovirology* 2015, 12:82-82.

369. Pejawar-Gaddy S, Kovacs JM, Barouch DH, Chen B, Irvine DJ. Design of lipid nanocapsule delivery vehicles for multivalent display of recombinant Env trimers in HIV vaccination. *Bioconj. Chem.* 2014, 25:1470-1478.

370. Leaman DP, Lee JH, Ward AB, Zwick MB. Immunogenic Display of Purified Chemically Cross-Linked HIV-1 Spikes. *J. Virol.* 2015, 89:6725-6745.

371. Wang LX. Synthetic carbohydrate antigens for HIV vaccine design. *Curr. Opin. Chem. Biol.* 2013, 17:997-1005.

372. Clark BE, Auyeung K, Fregolino E, Parrilli M, Lanzetta R, De Castro C, Pantophlet R. A bacterial lipooligosaccharide that naturally mimics the epitope of the HIV-neutralizing antibody 2G12 as a template for vaccine design. *Chem. Biol.* 2012, 19:254-263.

373. Stanfield RL, De Castro C, Marzaioli AM, Wilson IA, Pantophlet R. Crystal structure of the HIV neutralizing antibody 2G12 in complex with a bacterial oligosaccharide analog of mammalian oligomannose. *Glycobiology* 2015, 25:412-419.

374. Dunlop DC, Bonomelli C, Mansab F, Vasiljevic S, Doores KJ, Wormald MR, (...), Scanlan CN. Polysaccharide mimicry of the epitope of the broadly neutralizing anti-HIV antibody, 2G12, induces enhanced antibody responses to self oligomannose glycans. *Glycobiology* 2010, 20:812-823.

375. Luallen RJ, Lin J, Fu H, Cai KK, Agrawal C, Mboudjeka I, (...), Geng Y. An engineered Saccharomyces cerevisiae strain binds the broadly neutralizing human immunodeficiency virus type 1 antibody 2G12 and elicits mannose-specific gp120-binding antibodies. *J. Virol.* 2008, 82:6447-6457.

376. Georgiev IS, Gordon Joyce M, Zhou T, Kwong PD. Elicitation of HIV-1-neutralizing antibodies against the CD4-binding site. *Curr. Opin. HIV AIDS* 2013, 8:382-392.

377. Tran K, Poulsen C, Guenaga J, de Val N, Wilson R, Sundling C, (...), Wyatt RT. Vaccine-elicited primate antibodies use a distinct approach to the HIV-1 primary receptor binding site informing vaccine redesign. *Proc. Natl. Acad. Sci. USA* 2014, 111:E738-747.

378. Hoffenberg S, Powell R, Carpov A, Wagner D, Wilson A, Kosakovsky Pond S, (...), Caulfield MJ. Identification of an HIV-1 clade A envelope that exhibits broad antigenicity and neutralization sensitivity and elicits antibodies targeting three distinct epitopes. *J. Virol.* 2013, 87:5372-5383.

379. Haynes BF, Shaw GM, Korber B, Kelsoe G, Sodroski J, Hahn BH, (...), McMichael AJ. HIV-Host Interactions: Implications for Vaccine Design. *Cell Host Microbe* 2016, 19:292-303.

380. Go EP, Zhang Y, Menon S, Desaire H. Analysis of the disulfide bond arrangement of the HIV-1 envelope protein CON-S gp140 DeltaCFI shows variability in the V1 and V2 regions. *J. Proteome Res.* 2011, 10:578-591.

381. Kim M, Qiao ZS, Montefiori DC, Haynes BF, Reinherz EL, Liao HX. Comparison of HIV Type 1 ADA gp120 monomers versus gp140 trimers as immunogens for the induction of neutralizing antibodies. *AIDS Res. Hum. Retroviruses* 2005, 21:58-67.

382. Hu JK, Crampton JC, Cupo A, Ketas T, van Gils MJ, Sliepen K, (...), Crotty S. Murine antibody responses to cleaved soluble HIV-1 envelope trimers are highly restricted in specificity. *J. Virol.* 2015, 89:10383-10398.

383. Feng Y, Tran K, Bale S, Kumar S, Guenaga J, Wilson R, (...), Wyatt RT. Thermostability of Well-Ordered HIV Spikes Correlates with the Elicitation of Autologous Tier 2 Neutralizing Antibodies. *PLoS Pathog.* 2016, 12:e1005767.

384. Bachmann MF, Jennings GT. Vaccine delivery: a matter of size, geometry, kinetics and molecular patterns. *Nat. Rev. Immunol.* 2010, 10:787-796.

385. Crooks ET, Tong T, Chakrabarti B, Narayan K, Georgiev IS, Menis S, (...), Binley JM. Vaccine-Elicited Tier 2 HIV-1 Neutralizing Antibodies Bind to Quaternary Epitopes Involving Glycan-Deficient Patches Proximal to the CD4 Binding Site. *PLoS Pathog.* 2015, 11:e1004932.

386. Sanders RW, Venturi M, Schiffner L, Kalyanaraman R, Katinger H, Lloyd KO, (...), Moore JP. The mannose-dependent epitope for neutralizing antibody 2G12 on human immunodeficiency virus type 1 glycoprotein gp120. *J. Virol.* 2002, 76:7293-7305.

387. Scanlan CN, Ritchie GE, Baruah K, Crispin M, Harvey DJ, Singer BB, (...), Dwek RA. Inhibition of mammalian glycan biosynthesis produces non-self antigens for a broadly neutralising, HIV-1 specific antibody. *J. Mol. Biol.* 2007, 372:16-22.

388. Agrawal-Gamse C, Luallen RJ, Liu B, Fu H, Lee FH, Geng Y, Doms RW. Yeast-elicited cross-reactive antibodies to HIV Env glycans efficiently neutralize virions expressing exclusively high-mannose N-linked glycans. *J. Virol.* 2011, 85:470-480.

389. Joyce JG, Krauss IJ, Song HC, Opalka DW, Grimm KM, Nahas DD, (...), Danishefsky SJ. An oligosaccharide-based HIV-1 2G12 mimotope vaccine induces carbohydrate-specific antibodies that fail to neutralize HIV-1 virions. *Proc. Natl. Acad. Sci. USA* 2008, 105:15684-15689.

390. Krauss IJ, Joyce JG, Finnefrock AC, Song HC, Dudkin VY, Geng X, (...), Danishefsky SJ. Fully synthetic carbohydrate HIV antigens designed on the logic of the 2G12 antibody. *J. Am. Chem. Soc.* 2007, 129:11042-11044.

391. Horiya S, Bailey JK, Temme JS, Guillen Schlippe YV, Krauss IJ. Directed evolution of multivalent glycopeptides tightly recognized by HIV antibody 2G12. *J. Am. Chem. Soc.* 2014, 136:5407-5415.

392. Wang SK, Liang PH, Astronomo RD, Hsu TL, Hsieh SL, Burton DR, Wong CH. Targeting the carbohydrates on HIV-1: Interaction of oligomannose dendrons with human monoclonal antibody 2G12 and DC-SIGN. *Proc. Natl. Acad. Sci. USA* 2008, 105:3690-3695.

393. Kabanova A, Adamo R, Proietti D, Berti F, Tontini M, Rappuoli R, Costantino P. Preparation, characterization and immunogenicity of HIV-1 related high-mannose oligosaccharides-CRM197 glycoconjugates. *Glycoconj. J.* 2010, 27:501-513.

394. Wang LX, Ni J, Singh S, Li H. Binding of high-mannose-type oligosaccharides and synthetic oligomannose clusters to human antibody 2G12: implications for HIV-1 vaccine design. *Chem. Biol.* 2004, 11:127-134.

395. Ni J, Song H, Wang Y, Stamatos NM, Wang LX. Toward a carbohydrate-based HIV-1 vaccine: synthesis and immunological studies of oligomannose-containing glycoconjugates. *Bioconj. Chem.* 2006, 17:493-500.

396. MacPherson IS, Temme JS, Habeshian S, Felczak K, Pankiewicz K, Hedstrom L, Krauss IJ. Multivalent glycocluster design through directed evolution. *Angew. Chem., Int. Ed. Engl.* 2011, 50:11238-11242.

397. Temme JS, Drzyzga MG, MacPherson IS, Krauss IJ. Directed evolution of 2G12-targeted nonamannose glycoclusters by SELMA. *Chemistry* 2013, 19:17291-17295.

398. Temme JS, MacPherson IS, DeCourcey JF, Krauss IJ. High temperature SELMA: evolution of DNA-supported oligomannose clusters which are tightly recognized by HIV bnAb 2G12. *J. Am. Chem. Soc.* 2014, 136:1726-1729.

399. Horiya S, MacPherson IS, Krauss IJ. Recent strategies targeting HIV glycans in vaccine design. *Nat. Chem. Biol.* 2014, 10:990-999.

400. Li H, Wang LX. Design and synthesis of a template-assembled oligomannose cluster as an epitope mimic for human HIV-neutralizing antibody 2G12. *Org. Biomol. Chem.* 2004, 2:483-488.

401. Marradi M, Di Gianvincenzo P, Enriquez-Navas PM, Martinez-Avila OM, Chiodo F, Yuste E, (...), Penades S. Gold nanoparticles coated with oligomannosides of HIV-1 glycoprotein gp120 mimic the carbohydrate epitope of antibody 2G12. *J. Mol. Biol.* 2011, 410:798-810.

402. Astronomo RD, Lee HK, Scanlan CN, Pantophlet R, Huang CY, Wilson IA, (...), Burton DR. A glycoconjugate antigen based on the recognition motif of a broadly neutralizing human immunodeficiency virus antibody, 2G12, is immunogenic but elicits antibodies unable to bind to the self glycans of gp120. *J. Virol.* 2008, 82:6359-6368.

403. Astronomo RD, Kaltgrad E, Udit AK, Wang SK, Doores KJ, Huang CY, (...), Burton DR. Defining criteria for oligomannose immunogens for HIV using icosahedral virus capsid scaffolds. *Chem. Biol.* 2010, 17:357-370.

404. Zhang H, Fu H, Luallen RJ, Liu B, Lee FH, Doms RW, Geng Y. Antibodies elicited by yeast glycoproteins recognize HIV-1 virions and potently neutralize virions with high mannose N-glycans. *Vaccine* 2015, 33:5140-5147.

405. Luallen RJ, Fu H, Agrawal-Gamse C, Mboudjeka I, Huang W, Lee FH, (...), Geng Y. A yeast glycoprotein shows high-affinity binding to the broadly neutralizing human immunodeficiency virus antibody 2G12 and inhibits gp120 interactions with 2G12 and DC-SIGN. *J. Virol.* 2009, 83:4861-4870.

406. Crispin M, Chang VT, Harvey DJ, Dwek RA, Evans EJ, Stuart DI, (...), Davis SJ. A human embryonic kidney 293T cell line mutated at the Golgi alpha-mannosidase II locus. *J. Biol. Chem.* 2009, 284:21684-21695.

407. Vliegenthart JF. Carbohydrate based vaccines. *FEBS Lett.* 2006, 580:2945-2950.

408. Slovin SF, Ragupathi G, Musselli C, Olkiewicz K, Verbel D, Kuduk SD, (...), Scher HI. Fully synthetic carbohydrate-based vaccines in biochemically relapsed prostate cancer: clinical trial results with alpha-N-acetylgalactosamine-O-serine/threonine conjugate vaccine. *J. Clin. Oncol.* 2003, 21:4292-4298.

409. Komagamine T, Yuki N. Ganglioside mimicry as a cause of Guillain-Barre syndrome. *CNS Neurol. Disord. Drug Targets* 2006, 5:391-400.

410. Willison HJ, Goodyear CS. Glycolipid antigens and autoantibodies in autoimmune neuropathies. *Trends Immunol.* 2013, 34:453-459.

411. Apostolico Jde S, Boscardin SB, Yamamoto MM, de Oliveira-Filho JN, Kalil J, Cunha-Neto E, Rosa DS. HIV Envelope Trimer Specific Immune Response Is Influenced by Different Adjuvant Formulations and Heterologous Prime-Boost. *PLoS One* 2016, 11:e0145637.

412. Morelli AB, Becher D, Koernig S, Silva A, Drane D, Maraskovsky E. ISCOMATRIX: a novel adjuvant for use in prophylactic and therapeutic vaccines against infectious diseases. *J. Med. Microbiol.* 2012, 61:935-943.

413. Garces F, Lee JH, de Val N, Torrents de la Pena A, Kong L, Puchades C, (...), Wilson IA. Affinity maturation of a potent family of HIV antibodies is primarily focused on accommodating or avoiding glycans. *Immunity* 2015, 43:1053-1063.

414. McGuire AT, Hoot S, Dreyer AM, Lippy A, Stuart A, Cohen KW, (...), Stamatatos L. Engineering HIV envelope protein to activate germline B cell receptors of broadly neutralizing anti-CD4 binding site antibodies. *J. Exp. Med.* 2013, 210:655-663.

415. McGuire AT, Glenn JA, Lippy A, Stamatatos L. Diverse recombinant HIV-1 Envs fail to activate B cells expressing the germline B cell receptors of the broadly neutralizing anti-HIV-1 antibodies PG9 and 447-52D. *J. Virol.* 2014, 88:2645-2657.

416. Sanders RW, Moore JP. Native-like Env trimers as a platform for HIV-1 vaccine design. *Immunol. Rev.* 2017, 275:161-182.

417. Medina-Ramirez M, Garces F, Escolano A, Skog P, de Taeye SW, Moral-Sanchez I, (...), Sanders RW. Design and crystal structure of a native-like HIV-1 envelope trimer that engages multiple broadly neutralizing antibody precursors in vivo. *J. Exp. Med.* 2017, in press.

418. Schiffner T, de Val N, Russell RA, de Taeye SW, de la Pena AT, Ozorowski G, (...), Sattentau QJ. Chemical Cross-Linking Stabilizes Native-Like HIV-1 Envelope Glycoprotein Trimer Antigens. *J. Virol.* 2015, 90:813-828.

419. Zotos D, Coquet JM, Zhang Y, Light A, D'Costa K, Kallies A, (...), Tarlinton DM. IL-21 regulates germinal center B cell differentiation and proliferation through a B cell-intrinsic mechanism. *J. Exp. Med.* 2010, 207:365-378.

420. Ma CS, Suryani S, Avery DT, Chan A, Nanan R, Santner-Nanan B, (...), Tangye SG. Early commitment of naive human CD4(+) T cells to the T follicular helper (T(FH)) cell lineage is induced by IL-12. *Immunol. Cell Biol.* 2009, 87:590-600.

421. Gupta S, Clark ES, Termini JM, Boucher J, Kanagavelu S, LeBranche CC, (...), Stone GW. DNA vaccine molecular adjuvants SP-D-BAFF and SP-D-APRIL enhance anti-gp120 immune response and increase HIV-1 neutralizing antibody titers. *J. Virol.* 2015, 89:4158-4169.

422. Schneider P. The role of APRIL and BAFF in lymphocyte activation. *Curr. Opin. Immunol.* 2005, 17:282-289.

423. Tiller T, Meffre E, Yurasov S, Tsuiji M, Nussenzweig MC, Wardemann H. Efficient generation of monoclonal antibodies from single human B cells by single cell RT-PCR and expression vector cloning. *J. Immunol. Methods* 2008, 329:112-124.

424. Chung NPY, Matthews K, Kim HJ, Ketas TJ, Golabek M, de Los Reyes K, (...), Cupo A. Stable 293 T and CHO cell lines expressing cleaved, stable HIV-1 envelope glycoprotein trimers for structural and vaccine studies. *Retrovirology* 2014, 11:33-33.

425. Neville DC, Dwek RA, Butters TD. Development of a single column method for the separation of lipid- and protein-derived oligosaccharides. *J. Proteome Res.* 2009, 8:681-687.

426. Börnsen KO, Mohr MD, Widmer HM. Ion exchange and purification of carbohydrates on a Nafion® membrane as a new sample pretreatment for matrix-assisted laser desorption/ionization mass spectrometry. *Rapid Commun. Mass Spectrom.* 1995, 9:1031-1034.

427. Harvey DJ. Fragmentation of negative ions from carbohydrates: part 2. Fragmentation of high-mannose N-linked glycans. *J. Am. Soc. Mass Spectrom.* 2005, 16:631-646.

428. Harvey DJ. Fragmentation of negative ions from carbohydrates: part 1. Use of nitrate and other anionic adducts for the production of negative ion electrospray spectra from N-linked carbohydrates. *J. Am. Soc. Mass Spectrom.* 2005, 16:622-630.

429. Harvey DJ. Fragmentation of negative ions from carbohydrates: part 3. Fragmentation of hybrid and complex N-linked glycans. *J. Am. Soc. Mass Spectrom.* 2005, 16:647-659.

430. Harvey DJ, Royle L, Radcliffe CM, Rudd PM, Dwek RA. Structural and quantitative analysis of N-linked glycans by matrix-assisted laser desorption ionization and negative ion nanospray mass spectrometry. *Anal. Biochem.* 2008, 376:44-60.

431. Geiger T, Clarke S. Deamidation, isomerization, and racemization at asparaginyl and aspartyl residues in peptides. Succinimide-linked reactions that contribute to protein degradation. *J. Biol. Chem.* 1987, 262:785-794.

432. Wuhrer M, Catalina MI, Deelder AM, Hokke CH. Glycoproteomics based on tandem mass spectrometry of glycopeptides. *J. Chromatogr. B Analyt. Technol. Biomed. Life Sci.* 2007, 849:115-128.

433. Cao L, Tolic N, Qu Y, Meng D, Zhao R, Zhang Q, (...), Wu S. Characterization of intact N- and O-linked glycopeptides using higher energy collisional dissociation. *Anal. Biochem.* 2014, 452:96-102.

434. Li M, Gao F, Mascola JR, Stamatatos L, Polonis VR, Koutsoukos M, (...), Montefiori DC. Human immunodeficiency virus type 1 env clones from acute and early subtype B infections for standardized assessments of vaccine-elicited neutralizing antibodies. *J. Virol.* 2005, 79:10108-10125.

435. Montefiori DC. Evaluating neutralizing antibodies against HIV, SIV, and SHIV in luciferase reporter gene assays. *Curr. Protoc. Immunol.* 2005, 12:11.11-11.17.

436. Pritchard LK, Spencer DI, Royle L, Vasiljevic S, Krumm SA, Doores KJ, Crispin M. Glycan microheterogeneity at the PGT135 antibody recognition site on HIV-1 gp120 reveals a molecular mechanism for neutralization resistance. *J. Virol.* 2015, 89:6952-6959.

437. Ongay S, Boichenko A, Govorukhina N, Bischoff R. Glycopeptide enrichment and separation for protein glycosylation analysis. *J. Sep. Sci.* 2012, 35:2341-2372.

438. Di Palma S, Boersema PJ, Heck AJR, Mohammed S. Zwitterionic hydrophilic interaction liquid chromatography (ZIC-HILIC and ZIC-cHILIC) provide high resolution separation and increase sensitivity in proteome analysis. *Anal. Chem.* 2011, 83:3440-3447.

439. Domon B, Costello CE. A systematic nomenclature for carbohydrate fragmentations in FAB-MS/MS spectra of glycoconjugates. *Glycoconj. J.* 1988, 5:397-409.

440. Wada Y. Glycan profiling: label-free analysis of glycoproteins. *Methods Mol. Biol.* 2013, 951:245-253.

441. Wada Y, Azadi P, Costello CE, Dell A, Dwek RA, Geyer H, (...), Taniguchi N. Comparison of the methods for profiling glycoprotein glycans--HUPO Human Disease Glycomics/Proteome Initiative multi-institutional study. *Glycobiology* 2007, 17:411-422.

442. Harvey DJ, Crispin M, Bonomelli C, Scrivens JH. Ion Mobility Mass Spectrometry for Ion Recovery and Clean-Up of MS and MS/MS Spectra Obtained from Low Abundance Viral Samples. *J. Am. Soc. Mass Spectrom.* 2015, 26:1754-1767.

443. Harvey DJ, Scarff CA, Edgeworth M, Struwe WB, Pagel K, Thalassinos K, (...), Scrivens J. Travelling-wave ion mobility and negative ion fragmentation of high-mannose N-glycans. *J. Mass Spectrom.* 2016, 51:219-235.

444. Harvey DJ. Collision-induced fragmentation of underivatized N-linked carbohydrates ionized by electrospray. *J. Mass Spectrom.* 2000, 35:1178-1190.

445. Harvey DJ. Matrix-assisted laser desorption/ionization mass spectrometry of carbohydrates. *Mass Spectrom. Rev.* 1999, 18:349-450.

446. Struwe WB, Stuckmann A, Behrens A-J, Pagel K, Crispin M. Global N-glycan site occupancy of HIV-1 gp120 by metabolic engineering and high-resolution intact mass spectrometry. *ACS Chem. Biol.* 2017, 12:357-361.

447. Cao L, Diedrich JK, Kulp DW, Pauthner M, He L, Park SR, (...), Paulson JC. Global site-specific N-glycosylation analysis of HIV envelope glycoprotein. *Nature communications* 2017, 8:14954.

448. Honarmand Ebrahimi K, West GM, Flefil R. Mass spectrometry approach and ELISA reveal the effect of codon optimization on N-linked glycosylation of HIV-1 gp120. *J. Proteome Res.* 2014, 13:5801-5811.

449. Travers SA. Conservation, compensation, and evolution of N-linked glycans in the HIV-1 group M subtypes and circulating recombinant forms. *ISRN AIDS* 2012, 2012:823605.

450. Doores KJ, Kong L, Krumm SA, Le KM, Sok D, Laserson U, (...), Burton DR. Two classes of broadly neutralizing antibodies within a single lineage directed to the high-mannose patch of HIV envelope. *J. Virol.* 2015, 89:1105-1118.

451. Klasse PJ, Depetris RS, Pejchal R, Julien J-P, Khayat R, Lee JH, (...), Moore JP. Influences on trimerization and aggregation of soluble, cleaved HIV-1 SOSIP envelope glycoprotein. *J. Virol.* 2013, 87:9873-9885.

452. Woods RJ, Pathiaseril A, Wormald MR, Edge CJ, Dwek RA. The high degree of internal flexibility observed for an oligomannose oligosaccharide does not alter the overall topology of the molecule. *Eur. J. Biochem.* 1998, 258:372-386.

453. Wu X, Parast AB, Richardson BA, Nduati R, John-Stewart G, Mbori-Ngacha D, (...), Overbaugh J. Neutralization escape variants of human immunodeficiency virus type 1 are transmitted from mother to infant. *J. Virol.* 2006, 80:835-844.

454. Chakrabarti BK, Feng Y, Sharma SK, McKee K, Karlsson Hedestam GB, Labranche CC, (...), Wyatt RT. Robust neutralizing antibodies elicited by HIV-1 JRFL envelope glycoprotein trimers in nonhuman primates. *J. Virol.* 2013, 87:13239-13251.

455. Mathys L, Francois KO, Quandte M, Braakman I, Balzarini J. Deletion of the highly conserved N-glycan at Asn260 of HIV-1 gp120 affects folding and lysosomal degradation of gp120, and results in loss of viral infectivity. *PLoS One* 2014, 9:e101181.

456. Moore JP, Willey RL, Lewis GK, Robinson J, Sodroski J. Immunological evidence for interactions between the first, second, and fifth conserved domains of the gp120 surface glycoprotein of human immunodeficiency virus type 1. *J. Virol.* 1994, 68:6836-6847.

457. Kong L, Torrents de la Pena A, Deller MC, Garces F, Sliepen K, Hua Y, (...), Wilson IA. Complete epitopes for vaccine design derived from a crystal structure of the broadly neutralizing antibodies PGT128 and 8ANC195 in complex with an HIV-1 Env trimer. *Acta Crystallogr. D Biol. Crystallogr.* 2015, 71:2099-2108.

458. Townsley S, Li Y, Kozyrev Y, Cleveland B, Hu SL. The conserved role of an N-linked glycan on the surface antigen of HIV-1 modulating virus sensitivity to broadly neutralizing antibodies against the receptor and coreceptor binding sites. *J. Virol.* 2015, 10.1128/jvi.02321-15.

459. Amin MN, McLellan JS, Huang W, Orwenyo J, Burton DR, Koff WC, (...), Wang L-X. Synthetic glycopeptides reveal the glycan specificity of HIV-neutralizing antibodies. *Nat. Chem. Biol.* 2013, 9:521-526.

460. Doores KJ, Burton DR. Variable loop glycan dependency of the broad and potent HIV-1-neutralizing antibodies PG9 and PG16. *J. Virol.* 2010, 84:10510-10521.

461. Binley JM, Sanders RW, Master A, Cayanan CS, Wiley CL, Schiffner L, (...), Moore JP. Enhancing the proteolytic maturation of human immunodeficiency virus type 1 envelope glycoproteins. *J. Virol.* 2002, 76:2606-2616.

462. Georgiev IS, Joyce MG, Yang Y, Sastry M, Zhang B, Baxa U, (...), Kwong PD. Single-chain soluble BG505.SOSIP gp140 trimers as structural and antigenic mimics of mature closed HIV-1 Env. *J. Virol.* 2015, 89:5318-5329.

463. Harvey DJ, Sobott F, Crispin M, Wrobel A, Bonomelli C, Vasiljevic S, (...), Scrivens JH. Ion mobility mass spectrometry for extracting spectra of N-glycans directly from incubation mixtures following glycan release: application to glycans from engineered glycoforms of intact, folded HIV gp120. *J. Am. Soc. Mass Spectrom.* 2011, 22:568-581.

464. Mathys L, Balzarini J. The role of N-glycans of HIV-1 gp41 in virus infectivity and susceptibility to the suppressive effects of carbohydrate-binding agents. *Retrovirology* 2014, 11:107.

465. Go EP, Cupo A, Ringe R, Pugach P, Moore JP, Desaire H. Native Conformation and Canonical Disulfide Bond Formation Are Interlinked Properties of HIV-1 Env Glycoproteins. *J. Virol.* 2016, 90:2884-2894.

466. AlSalmi W, Mahalingam M, Ananthaswamy N, Hamlin C, Flores D, Gao G, Rao VB. A New Approach to Produce HIV-1 Envelope Trimers: Both cleavage and proper glycosylation are essential to generate authentic trimers. *J. Biol. Chem.* 2015, 290:19780-19795.

467. Lynch RM, Wong P, Tran L, O'Dell S, Nason MC, Li Y, (...), Mascola JR. HIV-1 fitness cost associated with escape from the VRC01 class of CD4 binding site neutralizing antibodies. *J. Virol.* 2015, 89:4201-4213.

468. Wibmer CK, Gorman J, Anthony CS, Mkhize NN, Druz A, York T, (...), Morris L. Structure of an N276-Dependent HIV-1 Neutralizing Antibody Targeting a Rare V5 Glycan Hole Adjacent to the CD4 Binding Site. *J. Virol.* 2016, 90:10220-10235.

469. McGuire AT, Gray MD, Dosenovic P, Gitlin AD, Freund NT, Petersen J, (...), Stamatatos L. Specifically modified Env immunogens activate B-cell precursors of broadly neutralizing HIV-1 antibodies in transgenic mice. *Nat. Commun.* 2016, 7:10618.

470. Jardine JG, Kulp DW, Havenar-Daughton C, Sarkar A, Briney B, Sok D, (...), Schief WR. HIV-1 broadly neutralizing antibody precursor B cells revealed by germline-targeting immunogen. *Science* 2016, 351:1458-1463.

471. Scharf L, West AP, Sievers SA, Chen C, Jiang S, Gao H, (...), Bjorkman PJ. Structural basis for germline antibody recognition of HIV-1 immunogens. *eLife* 2016, 5.

472. Scharf L, Wang H, Gao H, Chen S, McDowall AW, Bjorkman PJ. Broadly Neutralizing Antibody 8ANC195 Recognizes Closed and Open States of HIV-1 Env. *Cell* 2015, 162:1379-1390.

473. de Taeye SW, Ozorowski G, Torrents de la Pena A, Guttman M, Julien JP, van den Kerkhof TL, (...), Sanders RW. Immunogenicity of stabilized HIV-1 envelope trimers with reduced exposure of non-neutralizing epitopes. *Cell* 2015, 163:1702-1715.

474. Doria-Rose NA, Mascola JR. HIV Immunology Goes Out On a Limb. *Immunity* 2016, 44:1088-1090.

475. Bonsignori M, Zhou T, Sheng Z, Chen L, Gao F, Joyce MG, (...), Haynes BF. Maturation Pathway from Germline to Broad HIV-1 Neutralizer of a CD4-Mimic Antibody. *Cell* 2016, 165:449-463.

476. Malherbe DC, Doria-Rose NA, Misher L, Beckett T, Puryear WB, Schuman JT, (...), Haigwood NL. Sequential immunization with a subtype B HIV-1 envelope quasispecies partially mimics the in vivo development of neutralizing antibodies. *J. Virol.* 2011, 85:5262-5274.

477. Ota T, Doyle-Cooper C, Cooper AB, Huber M, Falkowska E, Doores KJ, (...), Nemazee D. Anti-HIV B Cell lines as candidate vaccine biosensors. *J. Immunol.* 2012, 189:4816-4824.

478. Hossler P, Khattak SF, Li ZJ. Optimal and consistent protein glycosylation in mammalian cell culture. *Glycobiology* 2009, 19:936-949.

479. Croset A, Delafosse L, Gaudry JP, Arod C, Glez L, Losberger C, (...), Antonsson B. Differences in the glycosylation of recombinant proteins expressed in HEK and CHO cells. *J. Biotechnol.* 2012, 161:336-348.

480. Wheeler SF, Harvey DJ. Negative ion mass spectrometry of sialylated carbohydrates: discrimination of N-acetylneuraminic acid linkages by MALDI-TOF and ESI-TOF mass spectrometry. *Anal. Chem.* 2000, 72:5027-5039.

481. Kong L, Wilson IA, Kwong PD. Crystal structure of a fully glycosylated HIV-1 gp120 core reveals a stabilizing role for the glycan at Asn262. *Proteins* 2015, 83:590-596.

482. Wheeler SF, Rudd PM, Davis SJ, Dwek RA, Harvey DJ. Comparison of the N-linked glycans from soluble and GPI-anchored CD59 expressed in CHO cells. *Glycobiology* 2002, 12:261-271.

483. Crispin M, Harvey DJ, Bitto D, Halldorsson S, Bonomelli C, Edgeworth M, (...), Bowden TA. Uukuniemi Phlebovirus assembly and secretion leave a functional imprint on the virion glycome. *J. Virol.* 2014, 88:10244-10251.

484. Xiang Y, Karaveg K, Moremen KW. Substrate recognition and catalysis by GH47 alpha-mannosidases involved in Asn-linked glycan maturation in the mammalian secretory pathway. *Proc. Natl. Acad. Sci. USA* 2016, 113:E7890-7899.

485. Derdeyn CA, Decker JM, Bibollet-Ruche F, Mokili JL, Muldoon M, Denham SA, (...), Hunter E. Envelope-constrained neutralization-sensitive HIV-1 after heterosexual transmission. *Science* 2004, 303:2019-2022.

486. Chohan B, Lang D, Sagar M, Korber B, Lavreys L, Richardson B, Overbaugh J. Selection for human immunodeficiency virus type 1 envelope glycosylation variants with shorter V1-V2 loop sequences occurs during transmission of certain genetic subtypes and may impact viral RNA levels. *J. Virol.* 2005, 79:6528-6531.

487. Sagar M, Wu X, Lee S, Overbaugh J. Human immunodeficiency virus type 1 V1-V2 envelope loop sequences expand and add glycosylation sites over the course of infection, and these modifications affect antibody neutralization sensitivity. *J. Virol.* 2006, 80:9586-9598.

488. Cavrois M, Neidleman J, Santiago ML, Derdeyn CA, Hunter E, Greene WC. Enhanced fusion and virion incorporation for HIV-1 subtype C envelope glycoproteins with compact V1/V2 domains. *J. Virol.* 2014, 88:2083-2094.

489. Roepstorff P, Fohlman J. Proposal for a common nomenclature for sequence ions in mass spectra of peptides. *Biomed. Mass Spectrom.* 1984, 11:601.

490. Mechref Y. Use of CID/ETD mass spectrometry to analyze glycopeptides. *Current protocols in protein science* 2012, Chapter 12:Unit 12.11.11-11.

491. Behrens AJ, Harvey DJ, Milne E, Cupo A, Kumar A, Zitzmann N, (...), Crispin M. Molecular architecture of the cleavage-dependent mannose patch on a soluble HIV-1 envelope glycoprotein trimer. *J. Virol.* 2017, 91:e01894-01816.